NOVA SCHOOL OF SCIENCE & TECHNOLOGY

DEPARTAMENT OF CHEMISTRY

Microalgae Biomass Biorefinery: Development and Implementation of Processing Strategies in an Industrial Unit in Portugal

Cláudia Sofia Martins Ribeiro

Master in Chemical and Biochemical Engineering

DOCTORATE IN REFINING, PETROCHEMICAL AND CHEMICAL ENGINEEING

NOVA University Lisbon

September, 2022

DEPARTAMENT OF CHEMISTRY

Microalgae Biomass Biorefinery: Development and Implementation of Processing Strategies in an Industrial Unit in Portugal

Cláudia Sofia Martins Ribeiro

Master in Chemical and Biochemical Engineering

Advisor: João Paulo Serejo Goulão Crespo
Full Professor, NOVA University Lisbon

Co-advisors: Pedro Manuel Tavares Lopes de Andrade Saraiva
Full Professor, University of Coimbra

Edgar Tavares dos Santos
Executive Board Member, A4F – Algae for Future

Examination Committee:

Chair: Maria da Ascensão Carvalho Fernandes Miranda Reis,
Full Professor, NOVA University Lisbon

Rapporteurs: Nídia de Sá Caetano,
Coordinator Professor, Porto School of Engineering

Alberto José Delgado dos Reis,
Deputy Head Bioenergy and Biorefineries Unit, National Laboratory of Energy and Geology

Adviser: João Paulo Serejo Goulão Crespo,
Full Professor, NOVA University Lisbon

Members: Luís Filipe Amaro da Costa,
Executive Board Member, A4F – Algae for Future

Maria da Ascensão Carvalho Fernandes Miranda Reis,
Full Professor, NOVA University Lisbon

Isabel Maria Rôla Coelhoso,
Associate Professor with Aggregation, NOVA University Lisbon

DOCTORATE IN REFINING, PETROCHEMICAL AND CHEMICAL ENGINEERING

NOVA University Lisbon
September, 2022

Microalgae Biomass Biorefinery: Development and Implementation of Processing Strategies in an Industrial Unit in Portugal

Dedicada aos meus avós,

Alexandre e Dinória

ACKNOWLEDGEMENTS

Chega ao fim esta etapa da minha vida que contribuiu muito para o meu crescimento profissional e pessoal. Este percurso e a realização desta tese de doutoramento teria sido muito mais difícil sem o apoio de várias pessoas às quais gostaria de expressar o meu agradecimento.

Em primeiro lugar, gostaria de agradecer aos meus orientadores professores João Crespo e Pedro Saraiva por me acompanharem ao longo desta jornada e por todo o conhecimento transmitido durante o desenvolvimento deste projeto.

Gostaria de agradecer ao meu supervisor empresarial Doutor Edgar Santos pela sua disponibilidade e por todo o conhecimento transmitido. Obrigada por me dares a conhecer o mundo das microalgas!

Agradeço também ao Doutor Luís Costa por toda a disponibilidade demonstrada desde o início deste doutoramento. Obrigada por tudo o que me ensinaste nestes últimos anos.

Agradeço ainda Doutora Carla Brazinha pelo acompanhamento continuo ao longo do doutoramento. Obrigada por toda a disponibilidade e por todos os incentivos durante esta jornada.

Um agradecimento especial à A4F – Algae for Future, por me ter acolhido e me ter dado a oportunidade de realizar este trabalho de investigação nesta área tão interessante e tão desafiante como é a biorrefinaria de microalgas. Agradeço a todos os colaboradores com os quais tive a oportunidade de trabalhar, em especial ao Artur Lopes, à Celina Parreira, à Ana Catarina Ferreira, à Sara Pereira, à Ângela Peralta e à Margarida Duarte. Obrigada pela vossa colaboração durante a realização deste projeto.

Gostaria de agradecer também ao CoLAB BIOREF, ao Elson Gomes, ao Pedro Grilo, à Joana Araújo e ao João Bernardo por toda a disponibilidade e toda a simpatia demonstradas.

Agradeço também à Doutora Cristina Oliveira, Doutor Alberto Reis e ao professor Vitor Alves por toda a simpatia, disponibilidade e transmissão de conhecimento.

Obrigada a todo o grupo de membranas em especial à Mafalda Cadima, ao Jorge Bernardo e à Verónica Weng por toda a ajuda no desenvolvimento do trabalho. Obrigada por toda a vossa disponibilidade e simpatia.

Agradeço à D. Maria José e à D. Palminha por toda a sua disponibilidade, simpatia e boa disposição.

Agradeço também a todas as pessoas que tive a oportunidade de conhecer na A4F durante estes últimos anos, ao André Silva, à Daniela Vilhena, à Cláudia Duarte, à Ana Rita Serra, à Isabel Faustino, à Sara Cabral, ao Diogo Pinto e à Noreen Hiegle. Muito obrigada pela boa disposição e companheirismo!

Obrigada ao Diogo, à Mary, ao Casquilho, à Filipa, à Sofia, à Alexandra, à Ana Cláudia e à Vanessa pelo apoio e amizade.

Obrigada especial à Soraia, a minha irmã emprestada, por estar sempre presente em todos os momentos. Obrigada por toda a amizade e apoio incondicional durante toda esta etapa.

Muito obrigada à minha família por sempre me apoiarem incondicionalmente nesta jornada. Obrigada especial aos meus pais, Sabino e Maria Francisca pelo suporte emocional e por toda a força que me transmitiram durante este doutoramento. Obrigada ao meu irmão, Roberto, pela coragem transmitida nos momentos mais difíceis. Obrigada pelo apoio e pelo amor de todos vocês!

Por fim, não menos importante, obrigada ao Tiago por todo o apoio incondicional e por se recusar a deixar-me desistir. Obrigada por todo o amor, pela paciência e por todo o equilíbrio que transmitiste nestes últimos anos.

Muito obrigada!

ABSTRACT

Throughout the years, we have witnessed a disturbing increase in the consumption of resources provided by our planet as the world population increases. Microalgae have been receiving much interest as a promising feedstock for biorefinery products, such as nutraceuticals or protein for human food and animal feed applications, as these microorganisms are extremely competitive with other plant crops.

The ultimate goal of this thesis is to develop a sustainable and economically viable biorefinery for the co-production of several added-value products from *Nannochloropsis* sp. biomass, and compare its economic results with other solutions that attempt to set up a dedicated production facility to produce a single product (e.g., biodiesel). This work comprises the optimisation of several unit operations that are essential to the development of a refining process of *Nannochloropsis* sp. biomass.

Firstly, the *Nannochloropsis* sp. biomass stabilisation through heat treatment was performed. The stabilisation step aimed to minimise the lipid hydrolysis reactions by inactivating the enzymes responsible for catalysing those reactions. This step is of extreme importance as the main product of the proposed biorefinery is an EPA-rich lipid fraction. The optimised operating conditions (95 ºC for 3 min) were able to prevent the degradation of the lipids present in the wet biomass after the cellular disruption. The cellular disruption is also particularly important for *Nannochloropsis* sp. as this strain possesses a robust cell wall. Bead milling was proposed as a suitable technique and the operating conditions were optimised to enhance the cellular disruption. The optimised conditions for a pilot-scale bead mill revealed that it is possible to achieve almost 95% of cellular disruption with a single pass at a flow rate of 10 $L.h^{-1}$ and a tip speed of 14 $m.s^{-1}$.

Additionally, biomass fractionation steps were studied. Membrane technology was selected to produce a permeate enriched in soluble proteins, free from coloured chlorophyll *a*, insoluble proteins, and with low lipid content. Two different operating approaches were evaluated - controlled transmembrane pressure and controlled permeate flux – under concentration and diafiltration modes. Ultrafiltration operated in a diafiltration mode, under controlled permeate flux conditions, led to the highest soluble protein recovery (78%) with the highest constant permeate flux (12 $L.m^{-2}.h^{-1}$) and low membrane fouling.

On the other hand, a solvent extraction methodology was selected to produce an EPA-rich polar lipid extract. The solvent selected (ethanol) is considered a GRAS solvent (Generally Recognized as Safe), and a food grade solvent. The ethanol to biomass ratio was optimised, and a techno-

economic evaluation was performed. The extraction with a solvent to biomass ratio (v/w) of 5 $mL.g^{-1}$ allowed a final extraction efficiency of 71%, with the lowest production cost.

Finally, a biorefinery concept based on EPA-rich *Nannochloropsis* sp. is proposed, based on a downstream process where different value-added compounds are targeted. The techno-economic performance of a single product value chain and a multiproduct value chain biorefinery were compared. Also, a comparative analysis between five scenarios with different operational costs was performed. Therefore, the Net Present Value (NPV), the Internal Rate of Return (IRR), and the Payback Period were calculated and compared. The baseline designed multi-product biorefinery resulted in estimated economic performance indicators that correspond to an IRR of 20.3%, and a payback period of 4.7 years.

Keywords: *Nannochloropsis* sp. Microalgae biorefinery, Heat treatment, Cellular disruption, Ultrafiltration/ Diafiltration, Lipid extraction, Techno-economic assessment

RESUMO

Ao longo dos últimos anos, temos vindo a assistir ao aumento preocupante do consumo dos recursos fornecidos pelo nosso planeta, aumentando assim a busca por fontes que possam substituir esses recursos. As microalgas surgem como uma fonte promissora de vários produtos, como por exemplo suplementos alimentares ou proteína para alimentação humana e animal, uma vez que estes microrganismos são extremamente competitivos com outras culturas vegetais.

O objetivo principal desta tese de doutoramento é desenvolver uma biorrefinaria não só economicamente viável, mas também ambientalmente e socialmente sustentável, para a produção de diferentes produtos de valor acrescentado a partir da biomassa de *Nannochloropsis* sp.. A comparação dos resultados económicos da biorrefinaria proposta com os resultados de outras soluções que apostam na definição de unidades de produção dedicadas à produção de apenas um produto final (ex. biodiesel), será também um dos objetivos desta tese. Este trabalho será focado na otimização de diversas operações unitárias essenciais à biorrefinaria de *Nannochloropsis* sp..

Em primeiro lugar, foi realizada a estabilização da biomassa de *Nannochloropsis* sp. através de um tratamento térmico. O objetivo desta etapa foi minimizar as reações de hidrólise lipídica, através da inativação das enzimas responsáveis por catalisar essas mesmas reações. As condições de operação otimizadas (95 ºC por 3min) permitiram prevenir a degradação dos lípidos presentes na biomassa húmida, após a rutura celular. A rutura celular é também um passo particularmente importante no caso da *Nannochloropsis* sp., uma vez que esta espécie é conhecida por possuir uma parede celular robusta. A rutura celular em moinho de esferas foi proposta como a técnica mais adequada e as suas condições de operação foram otimizadas de forma a atingir o máximo de rutura celular. As condições otimizadas para um moinho de esferas em escala piloto revelaram que é possível atingir quase 95% de rutura celular com uma única passagem a um caudal de operação de 10 $L.h^{-1}$ e uma velocidade de rotação do veio de 14 $m.s^{-1}$.

Adicionalmente foi estudado o fracionamento da biomassa. A tecnologia de membranas foi selecionada para produzir um permeado enriquecido em proteínas solúveis, livre de clorofila *a* e de proteínas insolúveis e com baixo teor de lípidos. Foram avaliadas duas abordagens operacionais - pressão transmembranar controlada e fluxo de permeado controlado - nos modos de concentração e diafiltração. A ultrafiltração operada no modo de diafiltração, sob condições controladas de fluxo de permeado, resultou numa maior recuperação de proteína solúvel (78%) e permitiu manter um fluxo de permeado mais elevado (12 $L.m^{-2}.h^{-1}$).

Por outro lado, foi selecionada e testada uma metodologia de extração com solvente de forma a produzir um extrato de lípidos polares rico em EPA. O solvente selecionado (etanol) é um solvente considerado seguro e de grau alimentar. O rácio etanol/biomassa foi otimizado e uma avaliação técnico-económica foi realizada. A extração com uma razão (v/w) solvente/biomassa de 5 $mL.g^{-1}$ resultou numa eficiência final de extração de 71%, exibindo esta um custo de produção menor.

Finalmente, foi desenvolvido um processo de biorrefinaria de forma a fracionar e recuperar compostos de valor acrescentado. Foi realizada a comparação entre o desempenho técnico-económico de uma unidade produtiva para produção de um produto único e uma biorrefinaria multiproduto. Além disso, foi realizada uma análise comparativa entre cinco cenários cujos custos operacionais se diferenciam devido às disparidades existentes no preço de compra da biomassa. Foram calculados e comparados o valor presente líquido (VPL), a taxa interna de retorno (TIR) e o período de retorno. A biorrefinaria multiproduto projetada teve como resultados do seu desempenho económico uma TIR de 20.3% e um período de retorno de 4.7 anos.

Palavras-chave: *Nannochloropsis* sp., Biorrefinaria de microalgas, Tratamento térmico, Rutura celular, Ultrafiltração/ Diafiltração, Extração de lípidos, Avaliação técnico-económica

CONTENTS

LIST OF FIGURES

LIST OF TABLES

LIST OF ACRONYMS

Abbreviations

ALA – α-linolenic acid (all-cis-9,12,15-octadecatrienoic acid, C18:3 n-6)

ARA – Arachidonic acid (all-cis-5,8,11,14-eicosatetraenoic acid, C20:4 n-6)

BSA – Bovine serum albumin

CF – Concentration factor

CAPEX – Capital expenditure

DF – diafiltration

DHA – Docosahexaenoic acid (all-cis-docosa-4,7,10,13,16,19-hexaenoic acid, C22:6 n-3)

DW – Dry weight

EFSA – European Food and Safety Authority

EPA – Eicosapentaenoic acid (all-cis-eicosa-5,8,11,14,17-pentaenoic acid, C22:5 n-3)

FA – Fatty acids

FAME – Fatty acids methyl esters

FDA – Food and Drug Administration

FFAs – Free fatty acids

GC – Gas chromatography

GLs – Glycolipids

GRAS - Generally Recognized as Safe

HFR – Higher flow rate

HPH – High-pressure homogenisation

HT – Heat treatment

HTST – High-temperature short-time

IRR – Internal rate of return

LA – Linoleic acid (all-cis-9,12-Octadecadienoic acid, C18:2 n-6)

LC – Long chain

LFR – Lower flow rate

MUFA – Monounsaturated fatty acid

NL – Neutral lipids

NPV – Net present value

OPEX – Operational expenditure

PEF – Pulsed electric field

PES – Polyethersulfone

PBR – Photobioreactor

PhLs – Phospholipids

PL – Polar lipids

PS – Polysulfone

PUFA – Polyunsaturated fatty acid

SFA – Saturated fatty acids

SFDW – Salt-free dry weight

TAG – Triacylglycerols

TFA – Total fatty acids

TLS – Trilaminar structure

UF – Ultrafiltration

WS – Wet stored

Variables

A – Total membrane filtration area (m^2)

$C_{i,feed}$ – Concentration of a target compound in the feed ($g.L^{-1}$)

$C_{i,perm}$ – Concentration of a target compound in the permeate ($g.L^{-1}$)

$[Chl\ a]_{BM}$ – Chlorophyll *a* concentration after bead milling ($mg.\ g_{SFDW}^{-1}$)

$[Chl\ a]_{total}$ – Chlorophyll *a* concentration after total cellular disruption ($mg.\ g_{SFDW}^{-1}$)

Jv– Volumetric permeate flux ($L.m^{-2}.h^{-1}$)

m_0 – Initial mass (kg) or (g)

m_{perm} – Mass of permeate (kg) or (g)

$m_{s.protein,accum}$ – Mass of soluble protein adsorbed/ accumulated (kg) or (g)

$m_{s.protein,feed}$ – Mass of soluble protein in the feed (kg) or (g)

$m_{s.protein,perm}$ – Mass of soluble protein in the permeate (kg) or (g)

$m_{s.protein,reten}$ – Mass of soluble protein in the retentate (kg) or (g)

MWCO – Molecular weight cut-off (kDa)

Lp – Permeance ($L.m^{-2}.h^{-1}.bar^{-1}$)

$[Pheo\ a]_{BM}$ – Pheophytin *a* equivalents concentration after bead milling ($mg.g_{SFDW}^{-1}$)

$[Pheo\ a]_{total}$ – Pheophytin *a* equivalents concentration after total cellular disruption ($mg.g_{SFDW}^{-1}$)

pp – percentage points

R_i – Apparent rejection of a target compound (%)

R_{irrev} – Irreversible fouling resistance (m^{-1})

R_m – Intrinsic membrane resistance (m^{-1})

R_{rev} – Reversible fouling resistance (m^{-1})

R_{total} – Total resistance (m^{-1})

TMP – Transmembrane pressure (bar)

t – Time (h) or (min)

T – Temperature (ºC)

V_{feed} – Volume of the feed (L)

$V_{water\ added}$ – Volume of the water added during diafiltration (L)

$wTFA_{\ Ethanolic\ Extract}$ – Mass of total fatty acids extracted (g)

$wTFA_{SFDW\ Biomass}$ – Mass of total fatty acids in the initial biomass (g)

Greek symbols

ρ – Density ($kg.m^{-3}$)

η – Dynamic viscosity (Pa.s)

1. BACKGROUND AND MOTIVATION

1.1. Background and Motivation

Throughout history, humans have learned how to use different resources provided by nature for material, food and energy production. The needs have grown over time, both in diversity and quantity. The last century witnessed a massive growth of the world population and, consequently, an avid consumption of the limited resources produced by our planet [1]. Human interference with the climate system led to an unparalleled ecological debt that is growing every year: an increase in the global temperature, an increase in the ocean level and the increase in the number of natural disasters [1]. On the other hand, typical protein sources, such as meat, fish and soy, cannot be produced at this growth rate. This shortage in global fish stock [2] may also have a negative impact on food supplements attributed to several health benefits (e.g., omega-3), as the most commonly used omega-3 PUFA sources are fish oil, such as EPA omega-3 [3]. Thus, alternative measures are mandatory in the present scenario to provide solutions for a sustainable future.

Microalgae are a promising bio-based/ food feedstock with a unique lipid composition and a high protein and carbohydrate content [4]. Their interesting biochemical composition may contribute to addressing the problem of growing demand for alternative resources in response to the increase in world population and the need for sustainable sources of energy and food [5]. Microalgae biomass predominantly comprises proteins, lipids, carbohydrates, and pigments. In terms of its composition, under optimal cultivation conditions, protein is always the major organic constituent, followed by lipids and carbohydrates [5]:

(1) Proteins - Biologically active proteins are polymers consisting of amino acids linked by covalent peptide bonds [6]. The different properties of the amino acid side chains give proteins an amphipathic character [6]. The topic can be simplified by grouping the amino acids into five main classes based on the properties of their R groups, in particular, their polarity or tendency to interact with water at biological pH (near pH 7.0): nonpolar, aliphatic R groups (e.g., alanine, valine and leucine), aromatic R groups (e.g., tyrosine and tryptophan), polar, uncharged R groups (e.g., serine, glutamine and asparagine), and positively charged (e.g., lysine and arginine) or negatively charged (e.g., aspartate and glutamate) R groups. The R groups' polarity varies from nonpolar and hydrophobic to highly polar and hydrophilic. Some microalgae are a rich source of amino acids [7] essential to human beings [8].

(2) Lipids - The lipid content of microalgae usually varies from species to species [9], and frequently microalgae have an average lipid content of 5 - 20% when grown under nutrient-replete conditions [10].

Lipids are a heterogeneous group of molecules, defined by their limited solubility in water and their extractability into organic solvents [8]. Typically, lipids can be divided into two major classes: neutral lipids (storage lipids) [10], in which the entire molecule is hydrophobic and are commonly represented by tri-, di- and monoglycerides (a glycerol backbone with three, two or one fatty acid, respectively) [11]; and polar lipids (membrane lipids), with hydrophilic and hydrophobic regions within the same molecule, commonly represented by phospholipids (a glycerol molecule with an alcohol group esterified by a phosphoric acid molecule and two fatty acids) and glycolipids (a mono- or oligosaccharide group attached to a sphingolipid or a glycerol group with one or two fatty acids) [11]. As mentioned before, fatty acids are essential constituents of the majority of lipids, and microalgae are a recognised source of essential fatty acids such as omega-3 fatty acids (e.g., eicosapentaenoic acid, EPA C20:5w3) and omega-6 fatty acids (arachidonic acid, ARA C20:4w6).

A fatty acid is a simple structure based on a long hydrocarbon and one or more carboxylic groups (–COOH) at one end. Fatty acids are relatively uncommon in their free form in nature [6] but are an important component of most lipids [8]. If the carbon-to-carbon bonds are all single, the fatty acid is typically called saturated; however, if any of the bonds is double or triple, the fatty acid is named unsaturated and is more reactive. A single, double bond results in a monounsaturated fatty acid (MUFA) [12], and further desaturation results in a polyunsaturated fatty acid (PUFA) [13,14]. There are two main types of polyunsaturated fats: omega-3 fatty acids and omega-6 fatty acids [15]. A fatty acid is called omega-3 when the first double bond is located at the third carbon from the methyl group, and omega-6 when the double bond is at the sixth carbon of the chain from the same radical [16]. Both types provide health benefits and the most common are omega-6 linoleic acid (LA; 18:2 n-6) and omega-3 α-linolenic acid (ALA; 18:3 n-3) [15]. The most common are omega-6 linoleic acid (LA; 18:2 n-6) and omega-3 α-linolenic acid (ALA; 18:3 n-3), and they are the precursors to the longer chain n-6 and n-3 series of fatty acids, respectively [15]. **Figure 1.1**, shows how linoleic acid is converted to arachidonic acid, and α-linoleic acid can be converted to eicosapentaenoic acid, and docosahexaenoic acid [17].

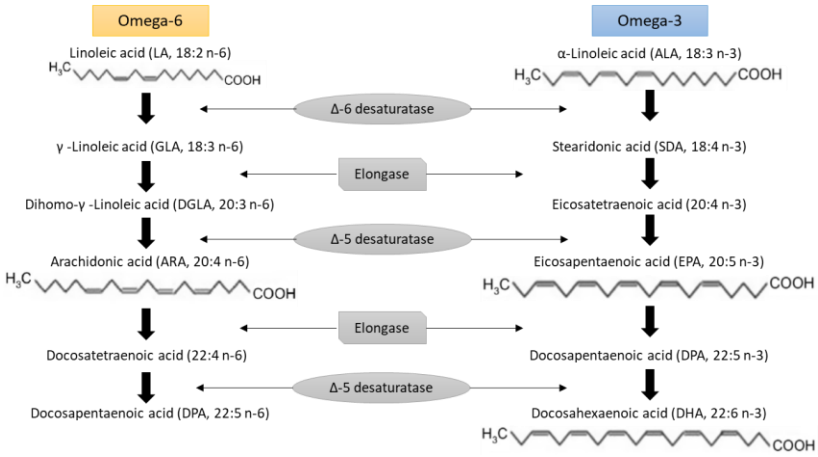

Figure 1.1. Metabolic pathways of linoleic acid and α-linolenic acid, which compete for the same enzymes biosynthetic pathways. Adapted from [15]

Microalgae are a known source of essential fatty acids such as omega-3 fatty acids, and omega-6 fatty acids. In the following table (**Table 1.1**) are presented the terms and symbols designating major fatty acids in food [18].

Table 1.1. Terms and symbols designating the majority of fatty acids found in nature. Adapted from [18]

Common Name	Chain Length	Double Bonds	Symbol I	Symbol II[a]	Symbol III[b]	Systematic Name
Caproic	6	0	$C_{5:0}$		6:0	n-Hexanoic
Caprylic	8	0	$C_{8:0}$		8:0	n-Octanoic
Capric	10	0	$C_{10:0}$		10:0	n-Decanoic
Lauric	12	0	$C_{12:0}$		12:0	n-Dodecanoic
Myristic	14	0	$C_{14:0}$		14:0	n-Tetradecanoic
Palmitic	16	0	$C_{16:0}$		16:0	n-Hexadecanoic
Palmitoleic	16	1	$C_{16:1}$	$C_{16:1w7}$	16:1 n-7	cis-9-Hexadecanoic
Stearic	18	0	$C_{18:0}$		18:0	n-Octadecanoic
Oleic	18	1	$C_{18:1}$	$C_{18:1w9}$	18:1 n-9	cis-9-Octadecanoic
Linoleic	18	2	$C_{18:2}$	$C_{18:2w6}$	18:2 n-6	cis, cis-9,12-Octadecadienoic
γ-Linoleic	18	3	$C_{18:3}$	$C_{18:3w6}$	18:3 n-6	All cis-6,9,12-octadecatrienoic
α-Linolenic	18	3	$C_{18:3}$	$C_{18:3w6}$	18:3 n-6	All cis-9,12,15-Octadecatrienoic
Gadoleic	20	1	$C_{20:1}$	$C_{20:1w9}$	20:1 n-9	n-11-Eicosenoic
Arachidonic	20	4	$C_{20:4}$	$C_{20:4w6}$	20:4 n-6	All cis-5,8,11,14-Eicosatetraenoic
EPA	20	5	$C_{20:5}$	$C_{20:5w3}$	20:5 n-3	cis-5.8.11.14.17-Eicosapentaenoic
DHA	22	6	$C_{22:6}$	$C_{22:6w3}$	22:6 n-3	cis-4,7,10,13,16,19-Docosahexaenoic

[a] carbon atoms are numbered from the methyl group, “w” indicates the first carbon where the point of unsaturation is found.

[b] carbon atoms are numbered from the methyl group, “n” indicates the first carbon where the point of unsaturation is found.

(3) Carbohydrates - The term "carbohydrates" refers to both monomers and polymers of sugars and sugar derivatives such as uronic acids and amino sugars [19]. Carbohydrates in microalgae can be found in the form of starch, glucose, sugars and other polysaccharides. The production of carbohydrates serves two main purposes for algae; they act as structural components in the cell walls, and as storage components inside the cell. Carbohydrates, as storage compounds, provide the energy needed for the metabolic processes of the organisms and allow, if needed, temporary survival in dark conditions, for example during the night-time [20].

(4) Pigments - Microalgae pigments are considered essential to the photosynthesis process since they are responsible for light harvesting and energy transfer to the reaction centres [21]. Pigments are typically aggregated into three major groups: chlorophylls, carotenoids and phycobiliproteins [22]. The phycobilins are linear tetrapyrroles present in cyanobacteria and red algae. These accessory pigments absorb blue-green, green, yellow, or orange light (500 - 560 nm) [22]. Carotenoids are a large group of biological chromophores with a known adsorption range between 400 and 550 nm [22]. The chlorophylls are characterized by having a tetrapyrrole ring that contains a central magnesium atom, and a long-chain terpenoid alcohol. The chlorophylls are known to adsorb blue or blue-green (450 - 475 nm), and red (630 - 675 nm) [22]. Besides the importance of the pigment's biological role, they have several properties highly attractive to the food, pharmaceutical, and cosmetic industries [21].

Over the last few years, the cultivation of microalgae has proved to be a pathway with high potential for replacement products such as food, pharmaceutical, cosmetic and nutraceutical applications [23]. Microalgal biotechnology is comparable to conventional agriculture, but it offers great sustainability due to the rapid growth rate of microalgae. As a consequence of the rapid growth rate of microalgae, higher productivity than traditional crops is achieved, and unlike traditional crops, microalgae can grow into areas and climates unsuitable for agricultural purposes (e.g., desert and seashore lands) [24].

The Food and Drug Administration (FDA) and the European Food and Safety Authority (EFSA), within the Novel Foods regulation [25], have recognised several microalgae as safe for food use (*Arthrospira* sp., *Chlorella* sp., *Tetraselmis chuii* and, *Odontella aurita*) [26]. Additionally, some microalgae are added to conventional foods aiming at the creation of functional foods. In Europe, functional foods for which a health claim is made must be in agreement with the EFSA's regulation within the Novel Foods regulation (e.g., *Ulkenia* sp. oil rich in DHA, *Schizochytrium* sp. oil rich in DHA and EPA) [25]. Numerous accepted health claims apply to molecules extracted from microalgae (e.g., fatty acids EPA and ARA) [27]. Pigments, which are part of the photosynthetic system of microalgae, are also great

additions to functional foods as, for example, carotenoids might be powerful biological antioxidants, protecting membranous phospholipids and other lipids against peroxidation [28].

There is a huge potential for the exploitation of eustigmatophyte microalgae *Nannochloropsis* sp., which is considered one of the most interesting marine microalgae to produce biofuels and food additives due to its high lipid accumulation [29] (up to 50% of salt-free dry weight, when produced under nitrogen-deplete conditions [30]) and rapid growth rate [31]. Nonetheless, *Nannochloropsis* sp. has a significant content in total protein [32], when produced under nitrogen-replete conditions (50% to 55% [33] of dry weight), both soluble (up to 20% dry weight) [34], and insoluble protein. The cells of *Nannochloropsis* sp. are small (3 - 5 μm) spherical or slightly ovoid [35], with a single chloroplast lodging a large volume of the cell [31]. *Nannochloropsis* genus has specific biochemical characteristics such as the lack of accessory chlorophylls *b* and *c*, and interesting xanthophyll pigments [36]. Also, when produced under optimal growth conditions, this species might present a relatively high content of eicosapentaenoic acid (3% [37] to 5% dry biomass [33]) [38]. EPA C20:5w3 is an essential fatty acid for human beings, and its market was estimated at US$ 582.4 million in 2020, and it is projected to reach US$ 1.1 billion in 2027 [39].

A refinery is known as a production plant that is composed of a group of unit processes that fractionate a raw material into different products of value, monetising the raw material. Petroleum refineries, where crude oil is converted into several products (e.g., gasoline, diesel and lubricating oil), are the most known type of refineries. The biorefinery concept arises from the original refinery concept, where the biomass can be fractionated to co-produce several products of interest. A biorefinery can use several kinds of biomass from agriculture, aquaculture, residues from industry, organic residues, forest rests, and aquatic biomass (algae and seaweeds) [40]. However, microalgae biomass brings real advantages as its metabolic flexibility offers the possibility to modify its biochemical pathways and cellular composition by varying culture conditions [41]. A typical microalgae biorefinery integrates the upstream, midstream, and downstream processing of biomass into a variety of products [40], and **Figure 1.2** shows a simplified scheme of the different steps within a microalgae biorefinery.

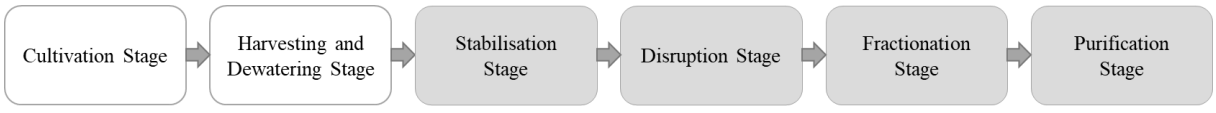

Figure 1.2. Simplified scheme of the different steps of a microalgae biorefinery. The boxes highlighted in grey represent the biorefinery steps within the main focus of this PhD project.

Although a microalgae biorefinery is typically known to include the six steps presented in **Figure 1.2**, this PhD project will only address the downstream processing of *Nannochloropsis* sp., which is widely known for its EPA-omega 3 accumulation capacity. Typically, the downstream is known to comprise:

(1) Cell harvesting/dewatering - This step is defined by the concentration of the previously cultivated microalgae culture. Usually, after the production stage, the cell concentration in the culture is around 0.1 to 10 $g.L^{-1}$. The main objective of this stage is to increase the cell concentration up to 100 - 200 $g.L^{-1}$, depending on the technique applied in the process [42]. The choice of the technology used in this step depends not only on the desired final cell concentration, as mentioned but also on the properties of the microalgae itself since some of the harvesting techniques might damage the microalgae cell wall, releasing the intracellular contents into the medium in a yearly stage of the downstream process. Common harvesting and dewatering techniques include centrifugation, membrane filtration, flocculation, and gravity sedimentation [43].

(2) Stabilization - The biomass stabilisation step is essential to a biorefinery whose raw material is wet biomass to avoid hydrolysis reactions that might affect the quality of the compounds. Hydrolysis is characterised by the cleavage of chemical bonds in the presence of water, which is generally catalysed by enzymes in biological systems [44]. In the particular case of a *Nannochloropsis* sp. biorefinery, one of the main concerns is lipid stability during wet biomass processing, as the fatty acids might be released from the backbone of neutral and polar lipids during lipid hydrolysis [44]. It is known that some external agents, such as high or low temperature, extreme pH, organic solvents, and high pressure, might be used to inactivate the enzymes responsible for hydrolysis reactions [45]. Heat treatments to inactivate lipases have been commonly used by food industries to enhance the stability and shelf-life of, for example, processed oats [46] or whole wheat flour [47].

(3) Cell disruption - For most algae strains, the value-added compounds are encapsulated within the cellular structures, including the cell membrane and cell wall. Most of the cell walls are mainly composed of complex carbohydrates and glycoproteins with high mechanical strength and chemical resistance, so the disruption step is often considered necessary [48]. In the particular case of *Nannochloropsis* sp., the cell wall is a robust structure composed of a cellulosic internal wall and a hydrophobic algaenan outer layer [49], which might affect the ease of rupture. Cell disruption methods can be classified into two groups: mechanical and non-mechanical (**Figure 1.3**).

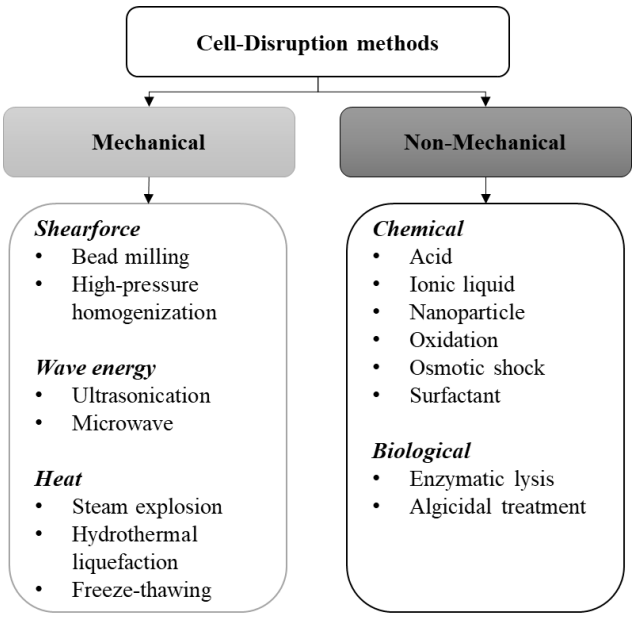

Figure 1.3. Cellular disruption methods, adapted [50]

Typically, mechanical methods are more energy-intensive than non-mechanical methods. However, non-mechanical, while not energy-intensive, might involve the use of harmful solvents, which may not assure cell rupture if a robust cell wall is present [51]. Also, the non-mechanical methods are not ideal for industrial-scale processing [51]. Mechanical cell disruption techniques using shear forces are the most conventional methods for cell rupture. Bead milling has a high potential for industrial implementations, and it is already used by some companies within the microalgae industry, given its practical scalability, repeatability and the fact that it could be used for concentrated suspensions (**Table 1.2**). Also, bead milling exhibits high disruption efficiency in single-pass operations [50].

Table 1.2. Comparison of cell mechanical disruption methods in terms of key aspects, adapted [52]

Disruption method	**Mildness**	**Optimum concentration**	**Energy consumption**	**Practical scalability**	**Repeatability***
Bead milling	Yes/No	Concentrated	High/Medium	Yes	+ + + +
High-pressure homogenization	Yes/No	Diluted/ Concentrated	High/Medium	Yes	+ + + +
Ultrasonication	Yes/No	Diluted	High/ Low	Yes/No	+ + +
Microwave	Yes/No	Diluted	High/Medium	Yes/No	+ + +

** + Low Repeatability; + + + Medium Repeatability; + + + + High Repeatability*

(4) Fractionation of target compounds - One of the most important steps within a biorefinery process is the fractionation step. The fractionation step will often include phase separations (e.g., separate the paste from the aqueous phase), and extractions which may include aqueous extractions or solvent extractions. Most extractions in biotechnology include the transfer of soluble bioproducts which have, at times, to be transferred between phases.

Supercritical extraction using CO_2 has been advanced as a green technology for recovering lipids from microalgae biomass. However, CO_2 has a low polarity; therefore, a polar co-solvent such as ethanol must be added to extract polar compounds such as polar lipids [53], which is a disadvantage. Also, the high-pressure requirements during the process are another disadvantage as the operation costs highly increase due to the safety requirements needed [54].

Conventional extraction techniques often select an organic solvent as the extracting liquid when the solute to be extracted is stable in the organic solvent. Therefore, the selection of proper solvents and the development of efficient extraction techniques for biomolecules are necessary [55]. Presently, hexane is the most used solvent for the extraction of neutral lipids, for its ideal functionalities in terms of lipid selectivity [56]. However, the research of greener and non-dangerous solvents has become a major concern for academic and industrial research. Terpenes, natural solvents existing both in citrus fruits and in many other plants [57], have been investigated as an alternative to organic solvent extraction [58] for the extraction of oil from oil-containing materials [59]. D-limonene has the chemical name (4R)-(1)-4-isopropenyl 1-methylcyclohexane and had been considered as GRAS (Generally Recognized as Safe) material by the U.S. Food and Drug Administration [59]. Limonene is not as abundant as hexane and the price of limonene is therefore higher. However, many health-promoting lipophilic nutraceuticals (e.g., carotenoids, lycopene) have been extracted with hexane, which is disturbing since these health products may contain residual hexane. Consumers would likely prefer those nutraceuticals processed with non-toxic and natural solvents [58]. D-limonene is completely miscible with oils and slightly more polar than hexane (considering their dielectric constant) as indicated in **Table 1.3**.

Table 1.3. Relevant properties of n-hexane and D-limonene

Solvent	**n-Hexane**	**D-Limonene**
Chemical Structure		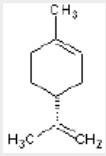
Molecular formula	C_6H_{14}	$C_{10}H_{16}$
Molecular weight (g.mol^{-1})	86.18	136.23
Density, 25 ºC (g.cm^{-3})	0.675	0.834
Flash point (ºC)	-23	48.3
Boiling point (ºC)	69	176
Viscosity, 25 (cP)	0.31	0.83
Enthalpy of vaporization (kJ.mol^{-1})	29.74	39.49
Surface tension, 25 ºC (dyne.cm^{-1})	20.3	25.8
Dielectric constant, 20 ºC	1.87	2.44
Hansen solubility parameters		
δ^a *(cal$^{1/2}$.cm$^{-3/2}$)*	7.3	8
δ_d	7.3	8
δ_p	0	0.1
δ_h	0	0.1

On the other hand, ethanol (cheap and safe solvent [60]) has been mentioned by several authors as the solvent selected for the polar lipid extraction from wet biomass [61].

(5) Purification - After fractionation, the added-value products must be purified. Membrane technology is very suitable for biological processes since it is usually operated at mild temperatures and pressures and requires no chemical additives or phase changes, thus diminishing the degree of denaturation, deactivation, and/or degradation of biological products [62]. In addition, the separation of components based on low energy consumption and mild operating conditions is a massive advantage [1].

However, in this specific PhD project, cell harvesting/dewatering will not be contemplated in the downstream processing of *Nannochloropsis* sp., since his stage has been extensively studied by A4F – Algae for Future in the past. Therefore, the main focus of this project will be on the last four stages of the downstream within a biorefinery concept: stabilisation, disruption, fractionation, and purification. From now on, whenever the term biorefinery is used in this document it will exclude the first two steps: the cultivation stage, and harvesting/ dewatering stage.

Microalgae biorefineries are emerging and there are numerous microalgae biomass refining processes described in the literature. Monte *et al.* [63] and Harvey *et al.* [64] proposed a biorefinery approach to produce carotenoids from *Dunaliella salina*. Ashokkumar *et al.* [65] described an *Haematococcus* sp, a biorefinery to produce astaxanthin. Koyande *et al.* [66] and Chia *et al.* [67] proposed different biorefinery approaches to produce value-added products from *Chlorella sorokiniana* and Spirulina, respectively.

The majority of *Nannochloropsis* sp. biorefineries approaches have been focused on the total lipid extraction for biodiesel production. Mendoza *et al.* [68] studied the effect of the lipid extraction used in biodiesel production on the integrated recovery of biodiesel from *Nannochloropsis gaditana*. Taher *et al.* [69] described the biodiesel production from *Nannochloropsis gaditana* using supercritical CO2 for lipid extraction. Turkkul *et al.* [70] studied biodiesel production from Spirulina and *Nannochloropsis oculata* microalgal lipids over alumina-calcium oxide catalyst.

Nevertheless, the recovery of microalgae proteins for food or feed [71], and the recovery of EPA omega-3 fatty acids for food supplements have also gained significant interest within the biorefinery concept [51]. For the development of a sustainable and economically feasible biorefinery, it is essential to focus on the compounds with added value that could be recovered at a relative abundance to overcome the production costs [72].

1.2. Research Strategy and Objectives

The research strategy of this PhD project was carried out within a business environment and, more particularly, within an industrial context. Therefore, the work developed during this PhD has a great component of optimisation of unit operations at a pilot scale that will allow an easy scale-up to an industrial scale. The aim was to produce added-value products such as EPA omega-3 and proteins to incorporate into aquaculture feeds and to replace the fish oil used in EPA omega-3 functional supplements.

The research strategy of this PhD comprises the optimisation of several unit operations essential to the development of a suitable refining process of *Nannochloropsis* sp. biomass. This strain is widely known for its capacity to accumulate lipids and, more specifically, to accumulate polyunsaturated fatty acids such as EPA omega-3.

Therefore, biomass stabilisation through heat treatment was studied to achieve the inactivation of the enzymes responsible for catalysing lipid hydrolysis reactions. The optimised operating conditions were able to prevent the degradation of the lipids present in the wet biomass after the cellular disruption.

After the optimisation of the operating conditions of the stabilisation step, the disruption step was also optimised. The cellular disruption is particularly important for *Nannochloropsis* sp. as this strain possesses a robust cell wall. High cellular disruption efficiencies lead to higher recovery rates of the targeted compounds.

The cellular disruption made all the added-value compounds available for the fractionation step and a solid-liquid separation step (centrifugation), where a supernatant (rich in soluble proteins) and a pellet/paste (rich in lipids and insoluble proteins) were obtained.

Consequently, the soluble protein-rich supernatant was processed via membrane filtration for the recovery of soluble proteins in the permeate (free from insoluble components, chlorophyll *a*, and other lipids). This process was studied in depth and optimised after the comparison of different operating conditions (controlled TMP or controlled permeate flux) and different operation modes (ultrafiltration under concentration or diafiltration mode).

Afterwards, the lipids extraction from the remaining pellet was also studied and optimised. Several scenarios and solvent (ethanol 99% v/v) to biomass ratios were proposed and evaluated in terms of lipids and EPA omega-3 extraction efficiency and economic sustainability.

Finally, a biorefinery concept based on EPA-rich *Nannochloropsis* sp. is proposed based on a downstream process where different value-added compounds are targeted. After biomass stabilisation and cellular disruption, two main routes were projected: an aqueous route and an ethanolic route. In the first one, through the combination of an aqueous extraction and membrane processing, a fraction rich in soluble protein was produced. Regarding the ethanolic route, an ethanolic extraction with an optimised solvent to biomass ratio was performed for the recovery of EPA-rich polar lipids fraction. Also, the defatted biomass was recovered to produce a fraction rich in insoluble proteins and carbohydrates.

This work demonstrates the potential of using *Nannochloropsis* sp. as a feedstock for the production of different compounds, improving the revenues of the microalgae industry.

The main objectives of this work are:

I. Study biomass stabilisation through heat treatment, to reduce the lipid degradation during a wet fractionation process, by inactivation of the enzymes responsible to catalyse lipid hydrolysis reactions.
II. Optimise the biomass pre-treatment aiming at increasing intracellular compounds extraction efficiencies. Particularly, optimise the operational parameters of the bead milling to increase the cellular disruption achieved.
III. Study and define a soluble proteins fractionation methodology involving membrane technology aiming at achieving the maximum soluble protein recovery in the permeate, and free from insoluble compounds.

Additionally, optimise the operation to minimise the fouling phenomenon and maximise the membrane life time.

IV. Evaluate and optimise the lipid extraction step to maximise the polar lipids extraction efficiency. Particularly, the assessment of the solvent to biomass ratio aiming for a higher lipid extraction efficiency with a lower production cost.

V. Design and propose a suitable biorefinery scheme, starting from EPA-rich *Nannochloropsis* sp., aiming at the recovery of three different fractions of compounds.

1.3. Thesis Outline

The studies and the work performed during this PhD project are ordered in the following way: a first chapter where the project background, motivation and outline are presented, five chapters that correspond to scientific work performed and the results attained during this PhD project, and a final chapter that presents the overall conclusions of the work and suggestions for future work. The fourth chapter, with the title "*Nannochloropsis* sp. Biorefinery: Recovery of soluble protein by membrane ultrafiltration/ diafiltration", corresponds to an original scientific paper accepted for publication.

A summary of the content of each section is presented below:

Chapter 1. Background and Motivation – Defines the background and the motivation for this PhD thesis, the fundamental objectives and the thesis outline.

Chapter 2. *Nannochloropsis* sp. Biorefinery: Biomass stabilisation through heat treatment – Reports a pilot-scale biomass stabilisation method ensuring that the lipids present in the biomass remain stable until the end of the process within the microalgae biorefinery concept. The biomass stabilisation was performed through heat treatment, and two different conditions were evaluated to optimise the biomass stabilisation methodology. The global efficiency of the heat treatment was mainly quantified by pigment content, the pH measurement (FFAs might decrease the pH of the biomass), and the fractionation of the lipids classes as an indicator of FFA formation due to lipid hydrolysis.

Chapter 3. *Nannochloropsis* sp. Biorefinery: Bead-milling optimisation for intracellular compounds extraction – Describes the optimisation of the cellular disruption step. Several processing parameters were optimised to increase the degree of disintegration of the cells, namely: flow rate, agitator tip speed, and the number of passes of the microalgae suspension through the grinding chamber. The global efficiency of the disruption step was qualitatively evaluated through microscopic observation and quantitatively evaluated by the extraction efficiency of total pigments from the disrupted *Nannochloropsis* sp. biomass.

Chapter 4. *Nannochloropsis* sp. Biorefinery: Recovery of soluble protein by membrane ultrafiltration/ diafiltration – Reports the soluble protein fractionation through membrane technology, producing a permeate enriched in uncoloured soluble proteins. Different operating conditions (controlled TMP or controlled permeate flux) and operation modes (ultrafiltration under concentration or diafiltration mode) were studied. The relevant parameters, namely: volumetric permeate flux, permeance, and soluble protein recovery, were assessed to select the optimal operating condition and the optimal operation mode. This chapter corresponds to an original scientific paper accepted for publication (Ribeiro *et al.*, Nannochloropsis sp. Biorefinery: Recovery of Soluble Protein by Membrane Ultrafiltration/ Diafiltration, Membranes 2022).

Chapter 5. *Nannochloropsis* sp. Biorefinery: Polar lipids extraction for omega-3 extract production – Describes the development and optimisation of an eco-friendly solvent methodology to carry out a polar lipid extraction from wet *Nannochloropsis* sp. biomass with high efficiency. Firstly, a neutral lipid extraction followed by a polar lipid extraction was evaluated. However, the results were not satisfactory. Therefore, the direct extraction of polar lipids with ethanol was studied and optimised. For the optimisation of the extraction step, several scenarios were proposed, and the lipid extraction efficiency, as well as the EPA omega-3 extraction efficiency, were evaluated. Additionally, a techno-economic analysis of the tested scenarios was performed, and a suitable scenario was selected.

Chapter 6. *Nannochloropsis* sp. Biorefinery: Process design and techno-economic assessment – Presents a suitable process for the production of three different fractions from *Nannochloropsis* sp. biomass, namely soluble protein-rich fraction, EPA omega-3 rich polar lipids fraction, and insoluble protein-rich fraction. The biorefinery scheme proposed integrates a biomass stabilisation step, a cellular disruption step, a soluble protein recovery step through membrane technology, and the solvent extraction (eco-friendly solvent) for the recovery of the EPA-rich polar lipids fraction and the defatted insoluble protein-rich fraction. Additionally, the techno-economic assessment of the biorefinery proposed was performed.

Chapter 7. Conclusions and Future Work – Describes the overall conclusions and results of this PhD project and suggestions for future work.

2. *NANNOCHLOROPSIS* SP. BIOREFINERY: BIOMASS STABILISATION THROUGH HEAT-TREATMENT

2.1. Abstract

Nannochloropsis sp. lipids have a massive potential in numerous applications such as biofuels, food and feed. However, during wet biomass storage, which is frequently needed between the different steps of the biorefinery, enzymatic lipolytic reactions can contribute to the formation of high amounts of free fatty acids (FFA). For the specific case of a *Nannochloropsis* sp. biorefinery for eicosapentaenoic acid (EPA) - omega-3 food supplements production is essential to avoid lipolysis not only because the bioavailability of omega-3 in the form of polar lipids is greater than that FFA but also because the presence of high amounts of free fatty acids can cause off-flavours. In this study, a heat treatment approach was suggested to achieve the inactivation of the endogenous enzymes that might catalyse hydrolysis reactions of the lipids present in the wet *Nannochloropsis* sp. biomass. A pilot-scale experiment using the pre-optimised conditions of the heat treatment concluded that the heat treatment at 95 ºC for 3 min was effective in preventing lipid degradation as well as pigment degradation in wet stored samples (4 ºC or -25 ºC for 7 days) after the heat treatment.

2.2. Introduction

Microalgae are considered one of the most relevant next-generation bio-based/ food feedstocks with a special lipid composition, high protein content, and an unlimited amount of other valuable compounds [73]. Furthermore, microalgae can grow in fresh or marine water, multiply rapidly, not compete with arable land, and have higher CO_2 fixation from waste gas emissions than terrestrial plants [74]. In addition, numerous microalgae species possess a high content of lipids (up to 50% of the biomass [44], when growth under stress conditions such as nutrient limitation). They are, therefore, promising lipid sources for biofuel, food and high-value applications such as dietary supplements or pharmaceuticals [75].

Microalgae can accumulate lipids in two different fractions [76], the polar lipids fraction (PL), mainly phospholipids (PhLs) and glycolipids (GLs); and the neutral lipid fraction (NL), mainly in the form of triacylglycerols (TAGs) [77]. Most microalgae biorefineries reported have been focused on total lipid extraction for biodiesel production [68]. Hereto, triacylglycerols are transformed to methyl esters by a transesterification reaction catalysed by acid or alkali catalysts or lipase enzymes [78].

However, it has great disadvantages compared with fossil fuel production costs, thus illustrating an economic need to obtain profitable microalgae biorefinery processes [79]. Besides neutral lipids for biodiesel production, microalgae have other products of interest within their lipid fraction (e.g., polar lipids and polyunsaturated fatty acids - PUFAs) [80]. Polar lipids have considerable interest in the food or pharmaceutical industry as they are excellent emulsifying agents [81]. Also, the lipid fraction of some marine species contains a substantial amount of PUFAs, predominantly docosahexaenoic acid (DHA C22:6n-3), and eicosapentaenoic acid (EPA C20:5n-3) [75], which have been established as health-promoting compounds [82].

Nannochloropsis sp. is one of the marine species that is widely known for the production of high-value oil containing omega-3 fatty acids, specifically EPA (up to 5% dry biomass when produced under optimal growth conditions) [33]. *Nannochloropsis* sp. can accumulate lipids up to 50% of the dry biomass when growing under environmental stress conditions (mostly TAGs) [30]; however, that is not reflected in EPA accumulation [83,84]. This long-chain (LC) PUFA is mostly accumulated in the cell membrane [85] in the form of polar lipids [84] (phospholipids and glycolipids [86]), which is considered a great advantage [87] as the bioavailability of omega-3 PUFAs in the form of polar lipids is greater than that of triacylglycerol or free fatty acids [88].

Nannochloropsis sp. photosynthetic apparatus is characterised by the presence of only chlorophyll *a* and lacking other accessory chlorophylls [89]. In the chloroplasts, chlorophylls are found attached to carotenoids, lipoproteins, and other lipids via noncovalent bonds.

When the wet microalgae biomass (5% to 25% of dry matter) is used as raw material for food, feed or the pharmaceutical industry, it is extremely important to preserve the biomass biochemical composition during the storage or during the transport from production to consumer [90]. Specifically, for applications of microalgae lipids, as mentioned before, their stability is of major importance.

One of the main difficulties in terms of lipid stability during wet biomass storage is lipid hydrolysis (lipolysis). Hydrolysis is characterised by the cleavage of chemical bonds in the presence of water, which is generally catalysed by enzymes in biological systems. During lipid hydrolysis, facilitated by endogenous enzymes (lipases), the fatty acids are released from the backbones of neutral lipids, glycolipids and phospholipids [44]. This process promotes the formation of high amounts of free fatty acids (FFA), which are disadvantageous for microalgae lipids applications. The presence of high amounts of FFA in food or high-value applications can cause off-flavours [91], and the consequential acidic conditions may result in the degradation of chlorophyll (bright green [92]) to pheophytin (olive-brown) [93]. Similarly, the chlorophyllase-generated chlorophyllide might be converted to pheophorbide under hight temperatures and acidic conditions [94]. Also, FFA are known to have a pro-

oxidative effect [95] and to be more readily oxidised by lipoxygenase enzymes [47], which may have a negative impact on the flavour (rancid off-flavour) and nutritional value of the final product [75]. Additionally, for specific applications, such as *Nannochloropsis* sp. omega-3 supplements, it is extremely important to avoid lipolytic reactions and to maintain the omega-3 PUFAs in the form of polar lipids since their bioavailability in this form is greater than that of triacylglycerol or free fatty acids, as mentioned before.

Several studies have indicated that lipolysis may be a serious problem not only during wet microalgae biomass storage but also during the wet stages of the production process (e.g., cell disruption, centrifugation or lipid extraction). Ryckebosh *et al.* [90] reported that lipolytic reactions occurred after two days of wet storage at 4 ºC of microalgae paste of *Phaeodactylum tricornutum.* Chen et al. [96] described an increase in FFA content from trace to 62% of FFA in the lipids extracted from the *Scenedesmus* sp. paste storage for 4 days at 4 ºC. Balduyck *et al.* [80] showed the temperature dependence of the lipolysis reactions in *T-Isochrysis lutea* biomass: a rapid increase of the FFA content was observed at 20 ºC and 4 ºC. In contrast, at - 20 ºC, almost no changes were observed.

Later, Balduyck *et al.* [44] concluded that cell wall strength plays a major role in lipolytic stability. The study showed no FFA formation in the non-disrupted *Nannochloropsis oculata* cells during 7 days of wet storage at 4 ºC, while in the previously disrupted cells, lipolysis starts very rapidly during and immediately after cell disruption. Thus, it is extremely important to inhibit lipid hydrolysis reactions before or immediately after the step that disrupts the cells, which may be the harvesting step for species with a weak cell structure or the cell disruption step (e.g., bead milling) for microalgae with a strong cell wall.

The most obvious solution is to remove the water present in the biomass, to avoid hydrolysis through drying processes such as spray dryer or freeze dryer. The removal of water through drying processes minimises microbial growth and deterioration by chemical reactions. However, drying is an expensive step with high energy consumption [90] and might be responsible for the biochemical decomposition and, thus, the nutritional value modification [97]. Therefore, the inactivation of lipolytic enzymes at an early stage is an alternative to avoid extensive FFA formation during the wet storage of the disrupted and non-disrupted biomass.

Enzymes are high compact globular proteins of more or less spherical shape [98], and a specific conformation is required (native state) to exhibit biological activity. The three-dimensional structure of globular proteins is stabilised by noncovalent forces, hydrogen bonding, van der Waals forces and hydrophobic interactions that are in a very delicate balance [45]. However, some external agents may

affect this subtle balance, such as high or low temperature, extreme pH, organic solvents, and high pressure, which will unfold the structure (denaturation) [45].

Heat treatments to inactivate lipases have been commonly used by food industries to enhance the stability and shelf-life of, for example, processed oats [46] or whole wheat flour [47]. Hereto, avoiding rancid off-flavours and the decrease of nutritional value related to FFA formation during lipolysis reactions. Several studies on lipolytic reactions occurring in microalgal biomass revealed that the optimum temperature for lipolytic enzymes is between 45 ºC [99] and 50 ºC [100], and the optimum pH is between 6.5 [99] and 10 [100].

However, it is also known that chlorophyll is susceptible to heat treatments, and long periods of heat treatment may cause the replacement of the central magnesium atom of the porphyrin ring by two hydrogen atoms and the formation of pheophytin [101]. On the other hand, it has been exposed that high-temperature short-time (HTST) treatments might be an effective approach to preserving chlorophyll [102]. Also, the chlorophyllase activity is seriously reduced when heated above 80 ºC, and its activity is completely lost when heated to 100 ºC [103]. Chlorophyllase is the only enzyme known to catalyse the degradation of chlorophyll. Characteristically, chlorophyllase catalyses the cleavage of phytol from chlorophyll and pheophytin, forming chlorophyllides and pheophorbides, respectively [94].

Several studies using a boiling water treatment of wet biomass of *Isochrysis galbana* [104], *Pseudo-nitzschia* [105], and *Skeletonema costatum* [106] have been reported. Balduyck *et al.* [75] studied the wet storage of *T-Isochrysis lutea* for a long term (7 days) at 4 ºC, after a heat treatment at 65 °C, 80 °C or 95 °C for 3, 8 or 13 min. The author reported that the heating to 65 ºC might have favoured the activity of the lipases as these temperatures were closer to the optimal temperature of the enzymes. However, a heat treatment at 95 ºC (minimum 3 min) prevented lipolytic reactions, and no FFA formation occurred during the wet storage (at 4 ºC for 7 days).

The main objective of this study is to define and optimise a heat treatment approach to achieve biomass stabilisation through the inactivation of endogenous enzymes that might catalyse the cleavage of lipids and pigments. The biomass stabilisation should avoid the degradation of the added value compounds and enable the wet storage of disrupted *Nannochloropsis* sp. biomass. Primarily, the optimisation of the heat treatment at a laboratory scale was accomplished. Then, the lab-scale optimised parameters were tested in pilot-scale heat treatment of *Nannochloropsis* sp. biomass, aiming at achieving wet stored biomass without lipid degradation and, consequently, no FFA formation. To our knowledge, pilot-scale heat treatment of *Nannochloropsis* sp. biomass has never been reported as a methodology for biomass stabilisation, allowing wet storage within the microalgae biorefinery concept. The global efficiency of the heat treatment was mainly quantified by pigments content (chlorophyll *a*, chlorophyll *a* degradation

products - pheophytin *a* equivalents, and carotenoids), the pH measurement (FFAs might decrease the pH of the biomass), and through the fractionation of the lipids classes as an indicator of FFA formation due to lipid hydrolysis.

2.3.Materials and Methods

2.3.1. Materials

The strain of *Nannochloropsis* sp. was grown in flat-panel photobioreactors (PBR) of A4F – Algae for Future (Portugal) in marine, N-replete culture medium and concentrated up to a 200 g_{SFDW}/L wet paste (between 30 to 35 g/L of salt), to facilitate the transport. For analytical procedures acetone 99.0% and methanol, 99.8% were purchased from JMGS (Odivelas, Portugal), chloroform and diethyl ether were obtained from Honeywell/ Riedel-de Haën (Seelze, Germany), n-hexane 99.0% was purchased from VWR Chemicals BDH® (Poole, United Kingdom), acetyl chloride 98% and 2,6-Di-tert-butyl-4-methylphenol (BHT) were obtained from Alfa Aesar (Karlsruhe, Germany), petroleum ether 60 - 80 ºC was purchased from Fisher Scientific (Leicestershire, United Kingdom), and the internal standard C17:0 was obtained from Dr. Ehrenstorfer GmbH (Augsburg, Germany).

2.3.2. Influence of different heat treatments at laboratory scale on pigments degradation during wet storage

In this first part of the experiment, the influence of different heat treatment conditions on pigment degradation immediately after heat treatment and during wet storage was studied. This first experiment was accomplished on a laboratory scale. The harvested *Nannochloropsis* sp. paste (approximately 200 $g_{SFDW}.L^{-1}$) was diluted with a culture medium to approximately 100 $g_{SFDW}.L^{-1}$. After homogenisation by stirring, the biomass at 20 ± 0.3 ºC and pH 7.3 ± 0.1 was divided in glass tubes (12 mL). The biomass was not disrupted, and the qualitative analysis was made through microscopic observation (data not shown). The glass tubes were put in a water bath (JP Selecta, Precisterm 6000138, Spain) at a certain temperature for a certain period, as summarised in **Table 2.1**. Balduyck *et al.* [75] reported that the heat-treatment at 95 ºC (minimum 3 min) of *T-Isochrysis lutea* prevented lipolytic reactions, and no FFA formation occurred during the wet storage (at 4 ºC for 7 days). Therefore, the heat treatment conditions for *Nannochloropsis* sp. were selected following the results reported.

After the heat treatment, the tubes were placed in an ice bath and kept there until they reached room temperature. The samples obtained after each heat treatment were divided into two portions so that one portion could be stored for 7 days at 4 ºC and the other for 7 days at -25 ºC (**Table 2.**1**)**.

Table 2.1. Scheme of the heat treatment experiments at a laboratory scale.

Experiment	HT Temperature (ºC)	HT Time (min)	Storage Temperature, after HT (ºC)	Storage Time, after HT (days)
HT.0.1	-	-	4	7
HT.0.2	-	-	-25	7
HT.1.1	80	8	4	7
HT.1.2	80	8	-25	7
HT.2.1	95	3	4	7
HT.2.2	95	3	-25	7

After the heat treatment, and previous to wet storage, samples were disrupted (about 90% of cell disruption) through bead beating (0.4 - 0.6 mm diameter). The heat treatment is conducted before cell disruption, as the enzyme's hydrolytic activity increases once they are released to the aqueous medium after cell disruption. A schematic representation of the different process steps to which the samples were submitted is presented in **Figure 2.1**.

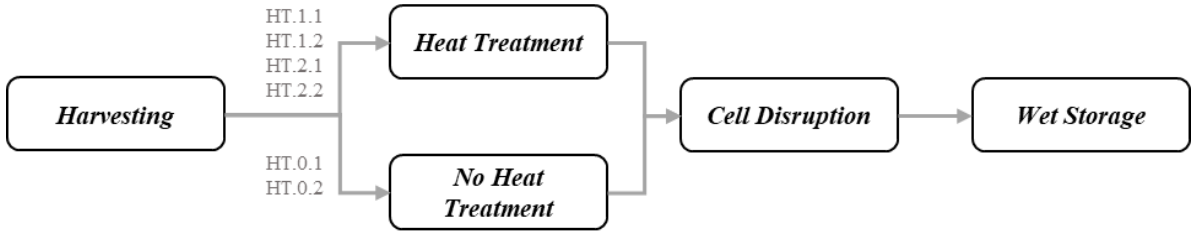

Figure 2.1. Schematic representation of the different steps of the first experiment.

After 7 days of wet storage, all the samples were analysed in terms of pigment content (chlorophyll *a*, chlorophyll *a* degradation products, and carotenoids). The control sample was not subjected to heat treatment and was analysed in terms of pigment content and pH immediately after the harvesting process. In addition to pigments analysis, the pH of all the heat-treated (HT) samples was measured as

an indicator of lipolysis, as the decrease of pH may be associated with FFA release from the glycerol backbone [107].

2.3.3. Influence of heat treatment at pilot scale on pigments and lipids degradation during wet storage

For the second part of the experiment, only one condition for the heat treatment was selected, based on the results of the experiment described in **section 2.3.2**: the selected condition was 3 min at 95 ºC. This second part of the experiment was accomplished at a pilot scale. The experiment started with the resuspension of 10 kg of fresh *Nannochloropsis* sp. paste (approximately 200 $g_{SFDW}.L^{-1}$) in 10 L of culture media to obtain 20 L of biomass with a concentration of approximately 100 $g_{SFDW}.L^{-1}$. Again, the biomass was not disrupted, and the qualitative analysis was made through microscopic observation (data not shown). After homogenisation by stirring, the biomass at 25 ± 0.2 ºC and pH 7.5 ± 0.1 was fed to the pilot-scale batch pasteuriser, and the heat treatment program was selected (3 min at 95 ºC), and the setpoint for the cooling process was 10 ºC. During the entire process of heat treatment, the biomass was stirred by the flat blade stirrer, which is shown in **Figure 2.2**. Also, the biomass is prevented from sticking to the pasteuriser walls and consequently heated to higher temperatures by the white scrapers exhibited in **Figure 2.2**.

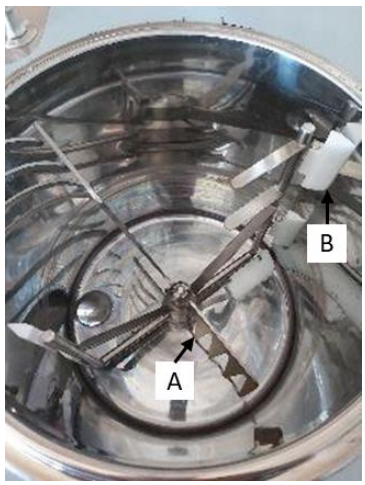

Figure 2.2. Image of the interior of the pasteuriser. A) flat blade stirrer, and B) scrapers.

After the heat treatment, two samples were collected, disrupted and stored in the same conditions described before (**section 2.3.2**), one for 7 days at 4 ºC, and the other for 7 days at -25 ºC as shown in **Table 2.2**.

Table 2.2. Scheme of the heat treatment experiments at a pilot scale.

Experiment	HT Temperature (ºC)	HT Time (min)	Storage Temperature, after HT (ºC)	Storage Time, after HT (days)
HT.0.3	-	-	4	7
HT.0.4	-	-	-25	7
HT.1.3	95	3	4	7
HT.1.4	95	3	-25	7

Previous to wet storage, the heat-treated samples were disrupted (about 90% of cell disruption) through bead beating (0.4 - 0.6 mm diameter), as the enzyme's activity increases once they are released to the aqueous medium after cell disruption. A schematic representation of the different process steps that the samples submitted is presented in **Figure 2.3**.

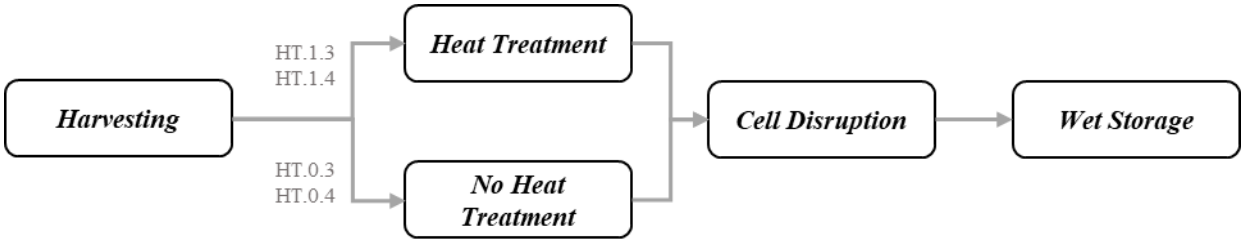

Figure 2.3. Schematic representation of the different steps of the pilot-scale experiment.

After 7 days of wet storage, all the samples were analysed in terms of pigments content, pH value and fractionated lipid classes content. The control sample was not subjected to heat treatment and was analysed in terms of pigments content, pH value and fractionated lipid class content immediately after the harvesting process.

2.3.4. Dry weight and salinity quantification

The dry weight was determined by weight variance after the water evaporation. The drying was run at 105 ºC until a constant weight was reached in a moisture analyser (Kern DBS 60-3, Kern, Germany). An amount of the previous dried sample (100 mg) was weighed into a glass tube, using an analytical balance (Kern, ABJ 220, Kern, Germany), and a knowing volume of demineralised water (1 mL) was added to the tube, to determine the sample salt-free dry weight (SFDW). The salt faction present in the demineralised water was measured through a salinity refractometer (Kern ORA 1SA, Kern, Germany).

2.3.5. Total lipids quantification

The total lipid content was quantified as described by Ryckebosch *et al.* [108]. Briefly, 500 mg of a fresh disrupted biomass paste (20% of salt-free dry weight) was mixed with 4 mL methanol. Subsequently, 2 mL of chloroform and 0.4 mL of water were added, and the sample was mixed in the vortex for 45 s. Then, 2 mL of chloroform and 2 mL of water were added, and the sample was mixed once again. Later, the sample was centrifuged (4,000 x g for 10 min), and the superior layer was kept in a glass tube. The cellular debris were re-extracted with a 4 mL methanol: chloroform 1:1. The centrifugation described before was repeated, and the collected solvent layers were filtered in a column filled with anhydrous sodium sulphate. After, the solvent was evaporated under a N_2 stream, and the lipid content was weighed.

2.3.6. Lipid Fractionation

After total lipid extraction, the lipids were separated into two distinct fractions: neutral lipids + free fatty acids (NL + FFA) and polar lipids (PL). Total lipids were extracted with a solvent mixture of 1:1 methanol: chloroform, as defined by Ryckebosch *et al.* [108]. The lipid fractionation was performed as proposed by Breuer *et al.* [109] and León-Saiki *et al.* [110], with some modifications. The methodology was validated as described in **Appendix A**. The lipids previously extracted were dissolved in a mixture of hexane: diethyl ether (7:1 v/v) to obtain a concentration of 25 ± 5 $mg.mL^{-1}$. The lipid extract was separated into neutral (+ FFA) and polar lipids using a Sep-Pak Silica Plus Long Cartridge (690 mg, Waters). The silica cartridge was prewashed with 10 mL of hexane before loading the sample onto the column. The neutral lipid fraction was eluted with 7 mL of hexane: diethyl ether (7:1 v/v). The polar lipid fraction was eluted with 7 mL of methanol: acetone: diethyl ether (2:2:1 v/v/v). Both extracts were evaporated under a N_2 stream and then weighed in the analytical balance (Kern, ABJ 220, Kern, Germany). Afterwards, both extracts were submitted to transesterification and the fatty acids were quantified using gas chromatography (GC). The gas chromatography required for the analysis was performed by an external supplier.

2.3.7. Total fatty acids transesterification

The total fatty acids transesterification was carried out after a lipid extraction process and/ or a lipid fractionation process, modifying Lepage and Roy [111]. Before total fatty acids transesterification, a known volume of the lipid extract sample (3 - 4 mL) was evaporated in a glass tube (12 mL) under a

nitrogen stream. The glass tube (12 mL) with the dried lipid fraction was strictly weighed (Kern, ABJ 220, Kern, Germany), and the weight of the empty glass tube was subtracted. The lipid fraction previously obtained was mixed with 200 µL of internal standard C17:0 (standard heptadecanoic acid dissolved in petroleum ether 60-80 ºC with a concentration of 5 $mg.mL^{-1}$) before the transesterification reaction. Finally, 4 mL of acetyl chloride/methanol solution with a 5:100 ratio was added to the tube and vortexed. The mixture was heated at 100 ºC for 1 hour in a water bath to conduct a transesterification reaction. The samples were thoroughly mixed during heating. The reaction tube was slowly cooled down to room temperature. Then, 2 mL of n-hexane was added to the tubes and mixed through a vortex stirrer. To aid in phase separation, 2 mL of demineralised water was added to the mixture and after centrifugation (for 3 min at 2,500 x g) the n-hexane layer that contained fatty acids methyl esters were collected and transferred to a glass vial passing through a cotton filter filled with sodium sulphate to prevent moisture and impurities. The gas chromatography (GC) required for the analysis was performed by an external supplier.

2.3.8. Pigments quantification

Chlorophyll *a*, chlorophyll *a* degradation products - pheophytin *a* equivalents, and carotenoids quantification was performed through spectrophotometric analysis. Briefly, 1 mL of a biomass sample with a concentration of 1 $g_{SFDW}.L^{-1}$ was centrifuged 4,000 x g (for 10 min, 5 ºC). The supernatant was rejected, and the remaining pellet (1 mg of salt-free dry weight) was mixed with 4 mL 99,0% acetone and vortex mixed for 60 s. After, the sample was once again centrifuged at 4,000 x g (for 10 min, 5 ºC). The extracted pigments, recovered in the supernatant, were analysed by spectrophotometry (Genesys 10S UV-VIS). After measuring the visible absorption spectrum of the pigment solution, each pigment concentration was determined by spectral decomposition: an iterative method that matched the sum of the absorbance spectra of each accounted pigment to the measured spectrum. The method was already implemented in the A4F laboratory for *Nannochloropsis* sp. pigments quantification.

2.4. Results and Discussion

2.4.1. Influence of different heat treatments at laboratory scale on pigments degradation during wet storage

The influence of two different heat treatments on pigment degradation, both before and after wet storage, was evaluated. The heat treatments at a laboratory scale were performed in a water bath at

80 ºC and 95 ºC for 8 and 3 minutes, respectively. The actual temperature in the *Nannochloropsis* sp. biomass during and immediately after the treatment was followed by a thermocouple (Gesa, DT-1, Spain), as shown in **Figure 2.4**. The temperature data acquisition revealed that the biomass sample temperature remained under the desired temperature for both experiments: 79 ºC and 93 ºC instead of 80 ºC and 95 ºC, respectively.

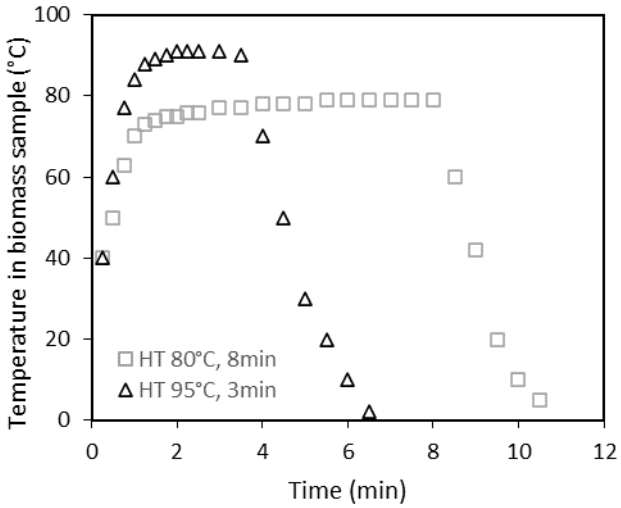

Figure 2.4. The actual temperature in *Nannochloropsis* sp. biomass (ºC) during heat treatment in the water bath at 80 ºC for 8 min (□ HT 80 ºC, 8 min) and in the water bath at 95 ºC for 3 min (Δ HT 95 ºC, 3 min) and subsequent cooling in an ice bath.

The *Nannochloropsis* sp. biomass control sample exhibit a total chlorophyll *a* content of 26.1 ± 0.5 $mg.g_{SFDW}^{-1}$, and a total carotenoids content of 7.9 ± 0.2 $mg.g_{SFDW}^{-1}$. The chlorophyll *a* degradation products content was non-existent, which suggests that the control sample was intact and didn't suffer any degradation during the harvesting step [94]. No noticeable decrease in the total chlorophyll content was detected from the control sample (26.1 ± 0.5 $mg.g_{SFDW}^{-1}$) to the heat-treated samples at 80 ºC for 8 min (25.4 ± 0.4 $mg.g_{SFDW}^{-1}$) and 95 ºC for 3 min (25.3 ± 0.6 $mg.g_{SFDW}^{-1}$). However, the high temperatures of both heat treatments (80 ºC, 8 min and 95 ºC, 3 min) might have favoured the formation of chlorophyll *a* degradation products - pheophytin *a* equivalents in the heat-treated samples, as reported by Schwartz *et al.* [101]. The pheophytin equivalents content slightly increased from non-existent content in the control sample to 0.672 ± 0.01 $mg.g_{SFDW}^{-1}$ and 0.661± 0.02 $mg.g_{SFDW}^{-1}$ in the heat-treated samples at 80 ºC for 8 min and 95 ºC for 3 min, respectively.

The effect of the different heat treatments (80 ºC, 8 min and 95 ºC, 3 min) on the pigments degradation during wet storage was studied through long-term wet storage (7 days) of samples refrigerated at 4 ºC and samples frozen at -25 ºC (**Figure 2.5 A and B**). The results suggest that the heat treatment at 95 ºC for 3 min might be somewhat better than the heat treatment at 80 ºC for 8 min. The chlorophyll *a* content decreased from 25.4 ± 0.4 mg.g_{SFDW}^{-1} in the sample immediately after the heat treatment at 80 ºC during 8min (T0), to 24.0 ± 0.2 mg.g_{SFDW}^{-1} in the sample after wet storage at 4 ºC during 7 days (Tws), while the chlorophyll *a* content remained practically constant in the sample wet stored in the same conditions after the heat treatment at 95 ºC during 3 min (**Figure 2.5 A**). These results might be related to the decrease of the chlorophyllase activity when heated above 80 ºC and its complete loss of activity when heated until 100 ºC [103].

However, such difference between the two different heat treatments was not noticed when the samples were stored at -25 ºC for 7 days, as the chlorophyll *a* remained almost constant before and after the wet storage for both heat treatments (**Figure 2.5 B**).

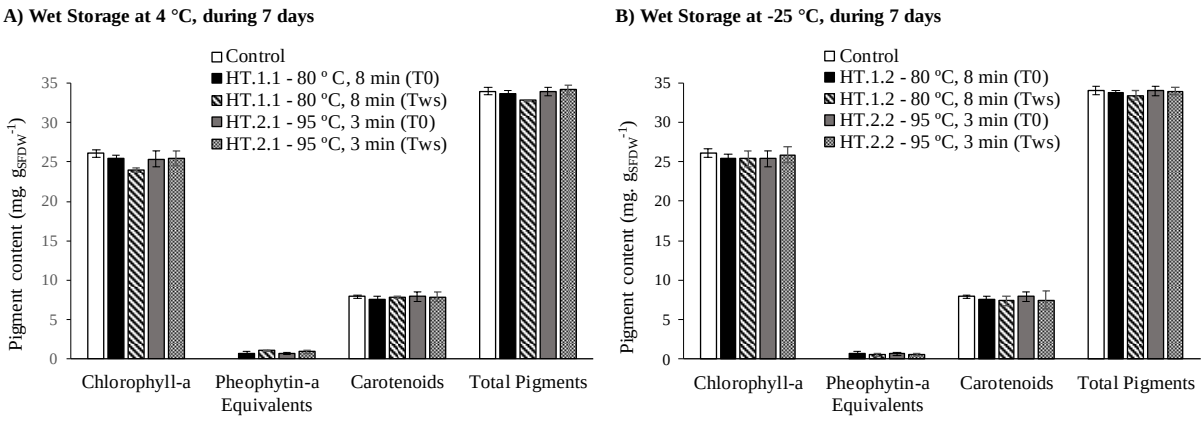

Figure 2.5. Pigment content in the disrupted *Nannochloropsis* sp. biomass, expressed as $mg_{pigment}$. g_{SFDW}^{-1}. A) Comparison of the heat-treated sample at 80 ºC for 8 min (HT.1.1) and heat-treated sample at 95 ºC for 3 min (HT.2.1), before (T0) and after (Tws) the wet storage at 4 ºC for 7 days. B) Comparison of the heat-treated sample at 80 ºC for 8 min (HT.1.2) and heat-treated sample at 95 ºC for 3 min (HT.2.2), before (T0) and after (Tws) the wet storage at -25 ºC for 7 days. The control sample was not heat-treated nor wet stored. Results are based on 3 replicates for each sample pigment analysis. The error bars represent the standard deviation calculated from the replicates.

The importance of heat treatment as a way to stabilise the biomass through the inactivation of endogenous enzymes previous to wet storage is shown in **Figure 2.6 A and B**. The non-heat-treated

sample wet stored for 7 days at 4 ºC suffered a severe degradation of the chlorophyll *a* and carotenoids. The chlorophyll *a* and carotenoids content decreased from 26.1 ± 0.5 $mg.g_{SFDW}^{-1}$ and 7.9 ± 0.2 $mg.g_{SFDW}^{-1}$ in the control sample, respectively, to 6.4 ± 0.8 mg. g_{SFDW}^{-1} and 3.8 ± 0.6 mg. $g_{SFDW}^{-1,}$ in the non-heat-treated sample after wet storage, respectively. That severe decrease after 7 days of wet storage at 4 ºC was not noticed in the heat-treated samples. However, as mentioned before, the sample heat-treated at 80 ºC for 8 min had a slightly higher decrease of the chlorophyll *a* content than the one heat-treated at 95 ºC for 3 min (**Figure 2.6 A**). Furthermore, **Figure 2.6 B** evidences the necessity of biomass stabilisation before the wet storage even when the samples are frozen at -25 ºC. The results showed that the wet storage for 7 days at -25 ºC of a non-heat-treated sample led to a significant decrease of chlorophyll *a* content from 26.1 ± 0.5 $mg.g_{SFDW}^{-1}$ in the control sample, to 20.5 ± 0.5 $mg.g_{SFDW}^{-1}$ in the non-heat-treated sample after wet storage. Contrarily, the total pigments content of heat-treated samples remained almost constant before and after the wet storage at -25 ºC for 7 days for both heat treatments (**Figure 2.6 B**).

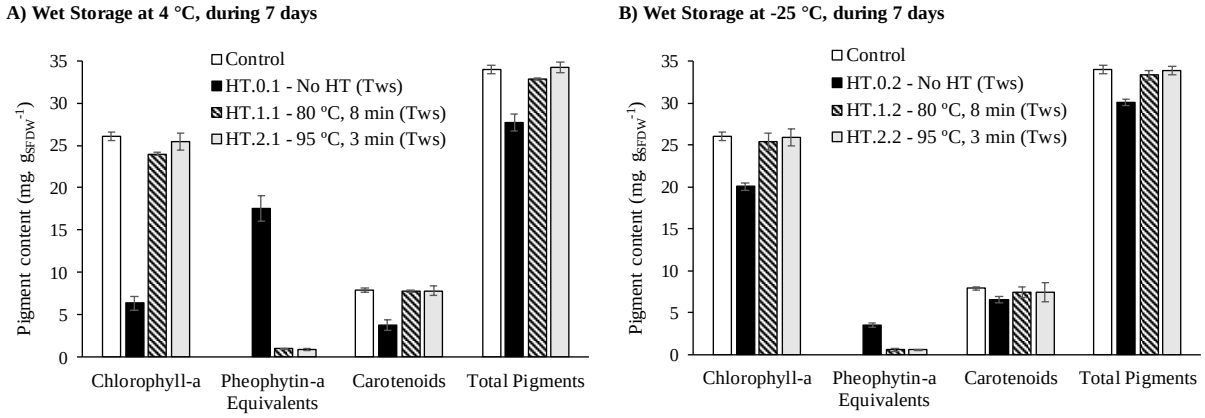

Figure 2.6. Pigment content in the disrupted *Nannochloropsis sp*. biomass, expressed as $mg_{pigment}\ g_{SFDW}^{-1}$. A) Comparison of a no heat-treated sample (HT.0.1), a heat-treated at 80 ºC for 8 min sample (HT.1.1), and a heat-treated at 95 ºC for 3 min sample (HT.2.1), wet stored (Tws) at 4 ºC for 7 days. B) Comparison of a not heat-treated sample (HT.0.2), a heat-treated at 80 ºC for 8 min sample (HT.1.2), and a heat-treated at 95 ºC for 3 min sample (HT.2.2), wet stored (Tws) at -25 ºC for 7 days. The control sample was not heat-treated nor wet stored. Results are based on 3 replicates for each sample pigment analysis. The error bars represent the standard deviation calculated from the replicates.

In addition to pigments degradation analysis, the pH of all the samples was measured, as an indicator of lipid hydrolysis, as mentioned in section **2.3.2**. The results of the pH measurements of heat-treated and non-heat samples after wet storage are shown in **Figure 2.7 A and B**. The non-heat-treated samples exhibit higher decreases in the pH value after 7 days of wet storage than the heat-treated samples, which

might suggest lipid degradation through lipolysis. After 7 days of wet storage at 4 ºC, the pH decreased from pH 7.0 ± 0.1 in the control sample to pH 5.9 ± 0.1 in non-heat-treated sample. Furthermore, after wet storage at 4 ºC for 7 days, the pH decreasing in the sample heat-treated at 95 ºC for 3 min (pH 6.9 ± 0.1) was smaller than in the sample heat-treated at 80 ºC for 8min (pH 6.5 ± 0.1), comparing to the control sample (pH 7.0 ± 0.1) (**Figure 2.7 A)**. The results are also following the previous results discussed regarding pigments degradation during wet storage and indicate that the heat treatment at 95 ºC for 3 min might be slightly better than the heat treatment at 80 ºC for 8 min.

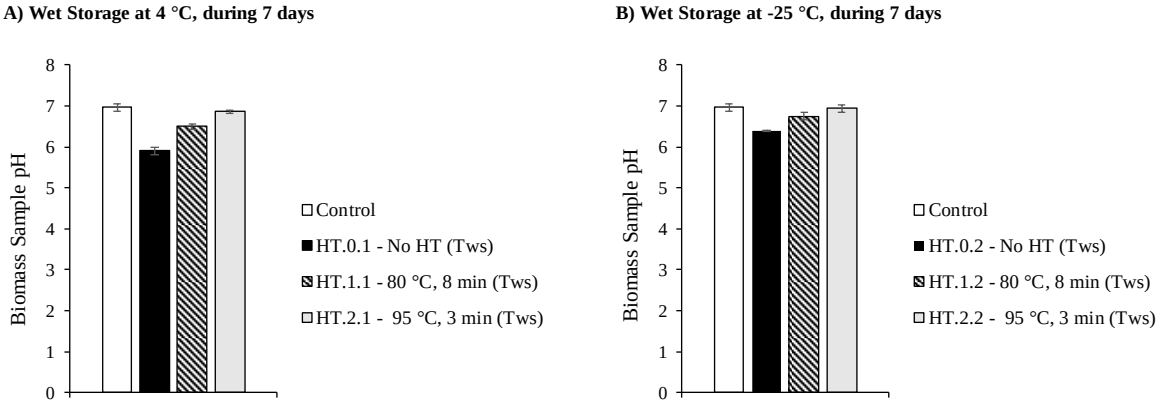

Figure 2.7. *Nannochloropsis sp.* biomass pH as an indicator of biomass degradation, specifically of lipids degradation through lipolysis. A) Comparison of a no heat-treated sample (HT.0.1), a heat-treated at 80 ºC for 8 min sample (HT.1.1), and a heat-treated at 95 ºC for 3 min sample (HT.2.1), wet stored (Tws) at 4 ºC for 7 days. B) Comparison of a no heat-treated sample (HT.0.2), a heat-treated at 80 ºC for 8 min sample (HT.1.2), and a heat-treated at 95 ºC for 3 min sample (HT.2.2), wet stored (Tws) at -25 ºC for 7 days. The control sample was not heat-treated nor wet stored. Results are based on 3 replicates for each sample pigment analysis. The error bars represent the standard deviation calculated from the replicates.

2.4.2. Influence of heat treatment at pilot scale on pigments and lipids degradation during wet storage

The previous study (section **2.4.1**) revealed that the heat treatment at 95 ºC for 3 min has better results in terms of reduction of pigments degradation during wet storage (4 ºC for 7 days or -25 ºC for 7 days) than the heat treatment at 80 ºC for 8 min. Therefore, the studies reported in the present section were performed with the previously selected heat treatment: 95 ºC for 3 min. The actual temperature in the *Nannochloropsis* sp. biomass during and immediately after the treatment was followed through the temperature sensor of the pilot-scale batch pasteuriser, as shown in **Figure 2.8**. The temperature data

acquisition revealed an overshoot of the setpoint (95 ºC) of 1.2 ± 0.2 ºC, and that is believed to be a limitation of the temperature controller of the pilot-scale batch pasteuriser.

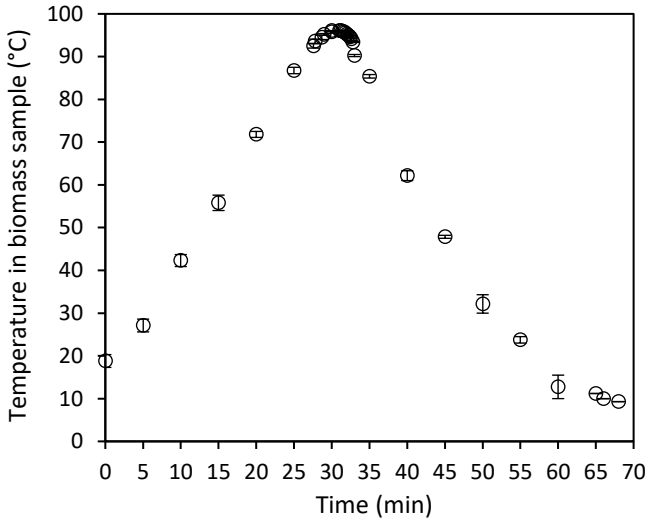

Figure 2.8. The actual temperature in *Nannochloropsis* sp. biomass (ºC) during heat treatment in the pilot-scale batch pasteuriser (95 ºC, 3 min). The experiment was performed two times, and the results are based on the 2 experiment replicates. The error bars represent the standard deviation calculated from the replicates.

The pigment degradation during the heat treatment program in the pilot-scale batch pasteuriser and after the wet storage was evaluated through the same methodology used in the study at the laboratory scale. The *Nannochloropsis* sp. biomass control sample exhibit a total chlorophyll *a* content of 29.2 ± 0.3 mg.g_{SFDW}^{-1}, and a total carotenoids content of 9.9 ± 0.1 mg.g_{SFDW}^{-1}. Again, the chlorophyll *a* degradation products content was non-existent. Comparing the control sample with the sample immediately after heat treatment, it is possible to notice a slight decrease in the total carotenoids content from 9.9 ± 0.1 mg.g_{SFDW}^{-1} in the control sample to 8.3 ± 0.4 mg.g_{SFDW}^{-1} in the heat-treated sample at 95 ºC for 3 min, which might be an effect of the high temperate of the heat treatment. The high temperatures of the heat treatment favoured the formation of chlorophyll *a* degradation products – pheophytin *a* equivalents in the heat-treated samples [101]. The pheophytin *a* equivalents content slightly increased from non-existent content in the control sample to 0.701 ± 0.02 mg.g_{SFDW}^{-1} in the heat-treated sample at 95 ºC for 3 min. This result suggests a slight degradation of chlorophyll *a* when the biomass is heat-treated at high temperatures, as reported by Schwartz *et al*. [101].

The effect of the heat treatment (95 ºC, 3 min), performed in the pilot-scale batch pasteuriser, on the inhibition of pigments degradation during wet storage was studied through long-term wet storage (7

days) of samples refrigerated at 4 ºC and samples that were frozen at -25 ºC, as showed in **Figure 2.9 A and B**. As seen before in the study at the laboratory scale, the heat treatment at 95 ºC for 3 min seems to exhibit the capacity to inactivate chlorophyllases [103]. The chlorophyll *a* content remained constant in the wet stored samples for 7 days (4 ºC and -25 ºC), after the heat treatment at 95 ºC for 3 min (**Figure 2.9 A and B**).

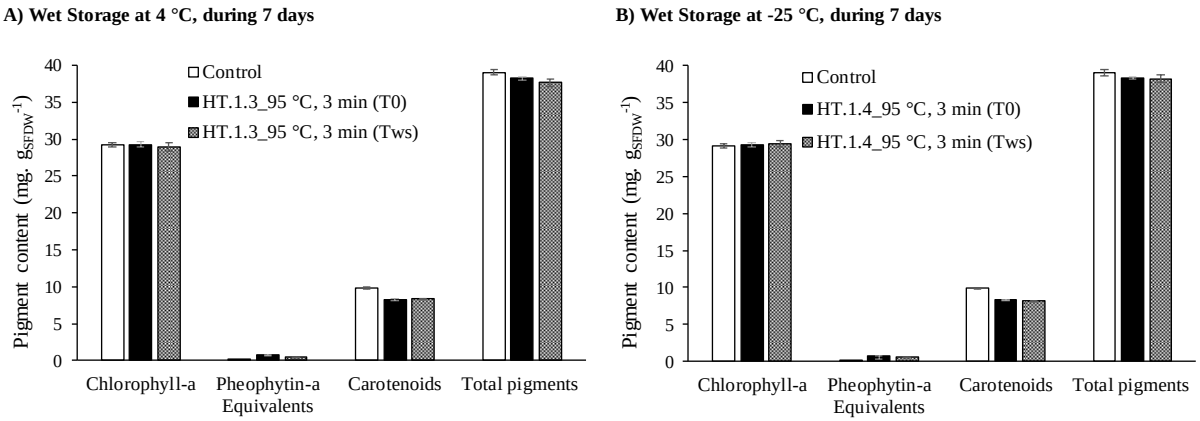

Figure 2.9. Pigment content in the disrupted *Nannochloropsis* sp. biomass, expressed as $mg_{pigment}.g_{SFDW}^{-1}$. A) Comparison of a heat-treated sample at 95 ºC for 3 min (HT.1.3) before (T0) and after (Tws) wet storage at 4 ºC for 7 days. B) Comparison of a heat-treated sample at 95 ºC for 3 min (HT.1.4) before (T0) and after wet (Tws) storage at -25 ºC for 7 days. The control sample was not heat-treated nor wet stored. Results are based on 3 replicates for each sample pigment analysis. The error bars represent the standard deviation calculated from the replicates.

Figure 2.10 A and B highlight the importance of heat treatment as a pre-treatment for biomass stabilisation. The results obtained on a pilot scale are in agreement with the previous results obtained on a laboratory scale. Again, the non-heat-treated samples wet stored for 7 days suffered a severe degradation of the chlorophyll *a* and carotenoids. As expected, the degradation was even more evident in the sample wet stored at 4 ºC for 7 days: the chlorophyll *a* and carotenoids content decreased from 29.2 ± 0.3 $mg.g_{SFDW}^{-1}$ and 9.9 ± 0.1 $mg.g_{SFDW}^{-1}$, respectively, in the control sample, to 4.4 ± 0.5 $mg.g_{SFDW}^{-1}$ and 3.8 ± 0.6 $mg.g_{SFDW}^{-1}$, respectively, in the non-heat-treated sample after wet storage. That severe decrease after 7 days of wet storage at 4 ºC was not noticed in the heat-treated samples (**Figure 2.10 A**). Also, the wet storage at -25 ºC for 7 days of a non-heat-treated sample led to a significant pigment degradation: the chlorophyll *a* and carotenoids content decreased from 29.2 ± 0.3 $mg.g_{SFDW}^{-1}$ and 9.9 ± 0.1 $mg.g_{SFDW}^{-1}$, respectively, in the control sample, to 14.2 ± 0.1 $mg.g_{SFDW}^{-1}$ and 5.0

± 0.1 mg.g_{SFDW}^{-1}, respectively, in the non-heat-treated sample after wet storage. Contrarily, the total pigments content of the heat-treated sample (95 ºC, 3 min) remained almost constant before and after the wet storage at -25 ºC for 7 days, for both heat treatments (**Figure 2.10 B**).

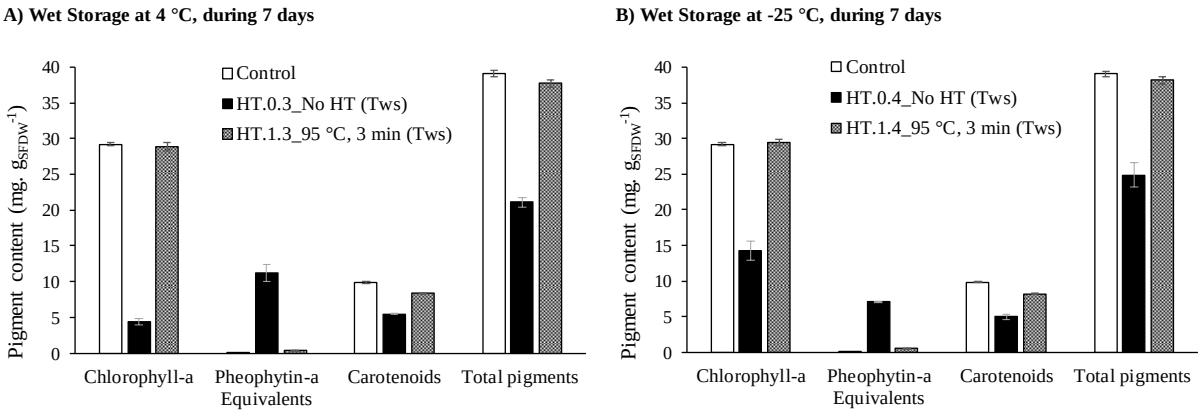

Figure 2.10. Pigment content in the disrupted *Nannochloropsis* sp. biomass, expressed as $mg_{pigment}/g_{SFDW}$. A) Comparison of a no heat-treated sample (HT.0.3), and a heat-treated at 95 ºC for 3 min sample (HT.1.3), wet stored (Tws) at 4 ºC for 7 days. B) Comparison of a no heat-treated sample (HT.0.4), heat-treated at 95 ºC for 3 min sample (HT.1.4), wet stored (Tws) at -25 ºC for 7 days. The control sample was not heat-treated nor wet stored. Results are based on 3 replicates for each sample pigment analysis. The error bars represent the standard deviation calculated from the replicates.

In addition to pigment degradation, the lipids degradation during wet storage of disrupted biomass samples (heat-treated and non-heat-treated) was evaluated. Primarily, the pH of all the samples was measured, as an indicator of lipid hydrolysis, as performed in the laboratory scale study. The results of the pH measurements of heat-treated and non-heat samples, after wet storage, are shown in **Figure 2.11 A and B**. Again, the results at a pilot scale are comparable with the results at a laboratory scale: the non-heat-treated sample exhibit a slightly higher decrease in the pH value after 7 days of wet storage than the heat-treated sample, which might suggest lipid degradation through lipolysis. After 7 days of wet storage at 4 ºC, the pH decreased from pH 7.6 ± 0.03 in the control sample to pH 6.8 ± 0.2 in the non-heat-treated sample, while the pH of the heat-treated sample remained constant (**Figure 2.11 A**). Additionally, after wet storage at -25 ºC for 7 days, the pH of the non-heat-treated sample decreased from pH 7.6 ± 0.03 in the control sample to pH 7.0 ± 0.05 in the non-heat-treated sample, while the pH of the heat-treated sample remained constant (**Figure 2.11 B**). The presented results may indicate the occurrence of lipid hydrolysis during wet storage of non-heat-treated samples, as the presence of free

fatty acids may decrease the pH of the biomass [44], and the stabilisation of the biomass through inactivation of endogenous enzymes by heat treatment at 95 ºC during 3 min.

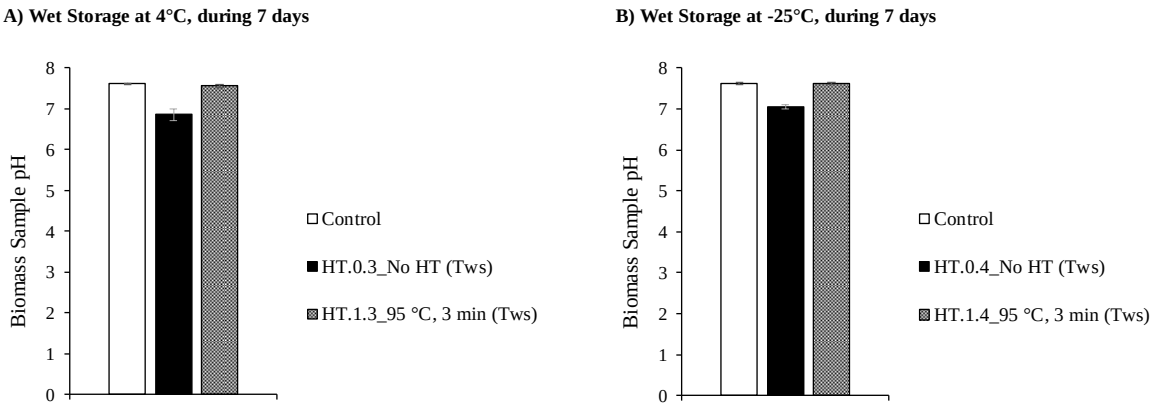

Figure 2.11. *Nannochloropsis* sp. biomass pH as an indicator of lipids degradation through lipolysis. A) Comparison of no heat-treated (HT.0.3) and heat-treated at 95 ºC for 3 min sample (HT.1.3), wet stored (Tws) at 4 ºC for 7 days. B) Comparison of no heat-treated (HT.0.4) and heat-treated at 95 ºC for 3 min sample (HT.1.4), wet stored (Tws) at -25 ºC for 7 days. The control sample was not heat-treated nor wet stored. Results are based on 3 replicates for each sample pigment analysis. The error bars represent the standard deviation calculated from the replicates.

As mentioned, in addition to pH measurement as an indicator of lipid hydrolysis, lipid degradation was evaluated in terms of the amount of free fatty acids (FFA) present in the heat-treated and non-heat samples. The results of the lipid fractionation of heat-treated and non-heat samples, after wet storage, are shown in **Figure 2.12 A** and **B**. The results presented are in agreement with all the results presented above. It was noticed an increase in the neutral lipids + FFA fraction from 6.9 ± 0.5% in the control sample to 8.6 ± 0.5% in the non-heat-treated sample after 7 days of wet storage at 4 ºC (**Figure 2.12 A)**. Also, a decrease in the polar lipid fraction from 26.9 ± 0.5% in the control sample to 23.0 ± 0.5% in the non-heat-treated sample after 7 days of wet storage at 4 ºC, was observed. This result might be explained by the occurrence of lipid hydrolysis during the wet storage as there was a significant decrease in the polar lipid fraction and a proportional increase in the fraction where the FFAs are found. After the hydrolysis reaction, the fatty acids that were previously attached to polar lipids change to their free form and were, therefore, fractionated and measured in the neutral lipids + FFA fraction. On the other hand, when comparing the control sample with the heat-treated sample (HT.1.3) after 7 days of wet storage at 4 ºC, no significant changes in the fraction neutral lipids + FFA were noticed, which might indicate that

the lipolytic enzymes were successfully inactivated through the heat treatment sat 95 ºC during 3 min. Similar results were described by Balduyck *et al.* [44], the author concluded that lipolysis occurrence in previously disrupted and non-heat treated *Nannochloropsis oculata* cells was very high during the wet storage (at 4 ºC for 7 days). Later, Balduyck *et al.* [75], reported that no FFA formation occurred during the wet storage (at 4 ºC for 7 days) of *T-Isochrysis lutea* (which possesses a much fragile cell wall), after a heat treatment at 95 ºC (minimum 3 min).

The results after the wet storage for 7 days at -25 ºC (**Figure 2.12 B**) were following the ones previously presented for the wet storage at 4 ºC for 7 days. Again, it was detected an increase in the neutral lipids + FFA fraction from 6.9 ± 0.5% in the control sample to 8.2 ± 0.4% in the non-heat-treated sample after 7 days of wet storage at -25 ºC. Correspondingly, a decrease of the polar lipid fraction from 26.9 ± 0.5% in the control sample to 23.6 ± 0.5% in the non-heat-treated sample after 7 days of wet storage at -25 ºC was observed.

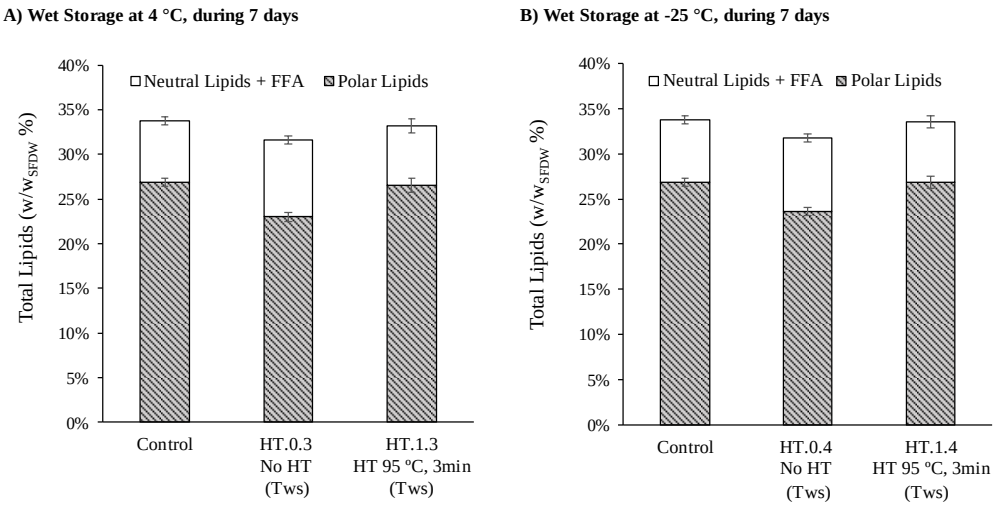

Figure 2.12. *Nannochloropsis* sp. lipid fractionation. A) Comparison of no heat-treated (HT.0.3) and heat-treated at 95 ºC for 3 min sample (HT.1.3), wet stored (Tws) at 4 ºC for 7 days. B) Comparison of no heat-treated (HT.0.4) and heat-treated at 95 ºC for 3 min sample (HT.1.4), wet stored (Tws) at -25 ºC for 7 days. The control sample was not heat-treated nor wet stored. Results are based on 3 replicates for each sample pigment analysis. The error bars represent the standard deviation calculated from the replicates.

The fatty acids present in both fractions (polar lipid fraction and neutral lipid + FFA fraction) were also analysed and the results are shown in **Figure 2.13 A** and **B**, and **Figure 2.14 A** and **B**. The fatty acids present in the polar lipid fraction exhibited a decrease from 9.8 ± 0.06% in the control sample to

7.7 ± 0.14% in the non-heat-treated sample after 7 days of wet storage at 4 ºC (**Figure 2.13 A)**. Also, when comparing the control sample with the heat-treated sample (HT.1.3) after 7 days of wet storage at 4 ºC, no significant variations in the amount of total fatty acids were noticed. The previously described behaviour was also observed in the samples after 7 days of wet storage at -25 ºC (**Figure 2.13 B)**. These results reinforce the hypothesis of the occurrence of lipid hydrolysis in the wet stored samples without prior heat-treatment, and the inactivation of the enzymes responsible for the hydrolysis reactions through a heat-treatment at 95 ºC for 3 min, as reported by Balduyck *et al.* [75].

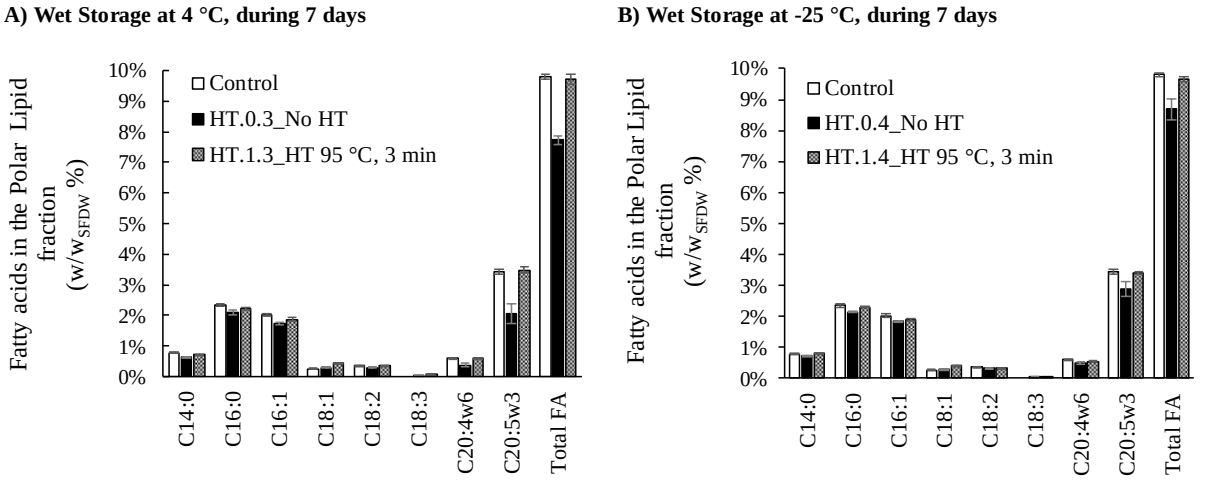

Figure 2.13. *Nannochloropsis* sp. fatty acids in the polar lipid fraction. A) Comparison of no heat-treated (HT.0.3) and heat-treated at 95 ºC for 3 min sample (HT.1.3), wet stored (Tws) at 4 ºC for 7 days. B) Comparison of no heat-treated (HT.0.4) and heat-treated at 95 ºC for 3 min sample (HT.1.4), wet stored (Tws) at -25 ºC for 7 days. The control sample was not heat-treated nor wet stored. Results are based on 3 replicates for each sample pigment analysis. The error bars represent the standard deviation calculated from the replicates.

On the other hand, the fatty acids present in the neutral lipid + FFA fraction exhibited an increase from 1.0 ± 0.06% in the control sample to 1.6 ± 0.07% in the non-heat-treated sample after 7 days of wet storage at 4 ºC (**Figure 2.14 A**). The results might indicate the formation of FFA due to lipid hydrolysis reactions on the non-heat-treated samples. Also, as expected, no significant variations in the amount of total fatty acids of the heat-treated sample (HT.1.3), after wet storage (7 days at 4 ºC), were noticed when compared with the control sample. This result highlights the prevention of FFA formation due to heat-treatment at 95 ºC for 3 min. Similarly, it was noticed an increase in the total fatty acids in the neutral lipid + FFA fraction of the non-heat-treated sample (1.3 ± 0.07%) stored at -25 ºC for 7 days, when compared with the control sample (1.0 ± 0.06%). The heat-treated sample, stored at -25 ºC for 7

days, did not show significant disparities from the control sample. Again, the results are in agreement with the results presented by Balduyck *et al.* [75].

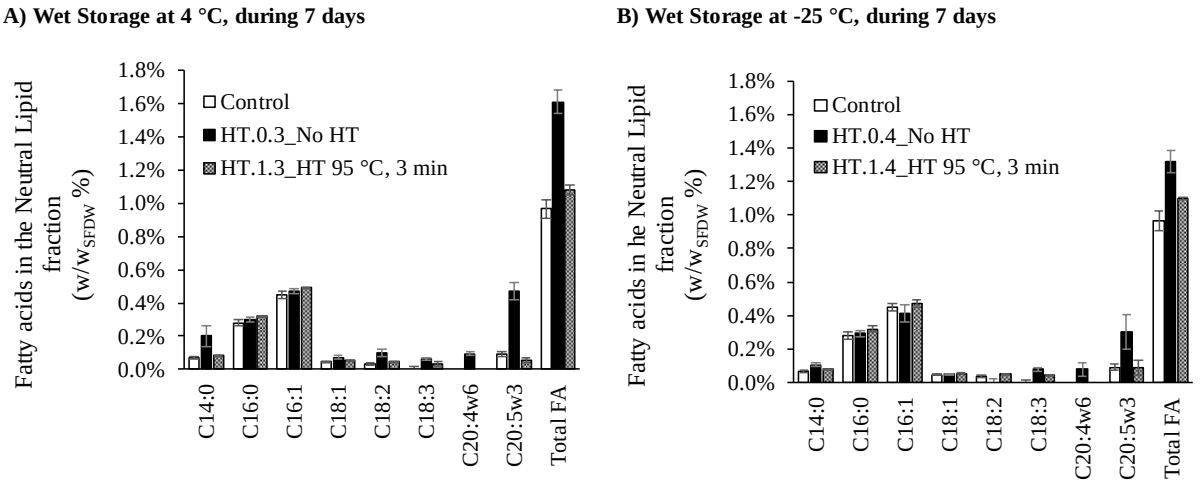

Figure 2.14. *Nannochloropsis* sp. fatty acids in the neutral lipid fraction. A) Comparison of no heat-treated (HT.0.3) and heat-treated at 95 ºC for 3 min sample (HT.1.3), wet stored (Tws) at 4 ºC for 7 days. B) Comparison of no heat-treated (HT.0.4) and heat-treated at 95 ºC for 3 min sample (HT.1.4), wet stored (Tws) at -25 ºC for 7 days. The control sample was not heat-treated nor wet stored. Results are based on 3 replicates for each sample pigment analysis. The error bars represent the standard deviation calculated from the replicates.

2.5. Conclusions

A heat treatment approach was suggested to achieve the inactivation of the endogenous enzymes that might catalyse hydrolysis reactions of the lipids present in the wet *Nannochloropsis* sp. biomass. The laboratory-scale experiment revealed that the pigment degradation during the wet storage was higher in the samples heat-treated at 80 ºC for 8 min than in the samples heat-treated at 95 ºC for 3 min. The chlorophyll *a* content decreased from 25.4 ± 0.4 $mg.g_{SFDW}^{-1}$ in the sample immediately after the heat treatment at 80 ºC for 8min, to 24.0 ± 0.2 $mg.g_{SFDW}^{-1}$ in the sample after wet storage at 4 ºC during 7 days, while the chlorophyll *a* content remained practically constant in the sample wet stored in the same conditions after the heat treatment at 95 ºC for 3 min. However, the high temperatures of both heat treatments (80 ºC, 8 min and 95 ºC, 3 min) favoured the formation of chlorophyll *a* degradation products – pheophytin *a* equivalents, after the heat treatment. The heat-treatment at 95 ºC for 3 min was selected to be tested in a pilot-scale experiment as it was the condition with better results in terms of avoiding pigment degradation during the wet storage. The pilot-scale experiment also concluded that the heat

treatment at 95 ºC for 3 min was effective in preventing lipid degradation, more specifically the polar lipid degradation, as no decrease in the polar lipids content was noticed in wet stored samples (4 ºC or -25 ºC for 7 days) after the heat treatment.

3. *NANNOCHLOROPSIS* SP. BIOREFINERY: BEAD MILLING OPTIMISATION FOR INTRACELLULAR COMPOUNDS EXTRACTION

3.1. Abstract

Microalgae are a promising source of pigments, lipids, proteins and carbohydrates for a variety of industries. However, the sturdiness of the microalgae cell wall might represent a drawback as it hinders the extraction of high-value biomolecules, such as pigments and lipids. Bead milling has been proposed several times as a way to improve the extraction of value-added compounds from *Nannochloropsis sp.*, which possesses a robust bilayer cell wall. This study reports the optimisation of the operating conditions to achieve a cellular disruption efficiency higher than 85 % on both a pilot scale and an industrial scale bead milling, with a single pass through the grinding chamber. The pilot-scale experiments revealed that it is possible to achieve almost 95 % of disruption efficiency for a single pass. A tendency to increase cellular disruption when the suspension is milled at a low flow rate and a high tip speed was observed. From the industrial scale experiments, it was concluded that it is possible to achieve 89.4% of cellular disruption with a single pass. This result is of extreme importance as it allows industrial microalgae biorefineries to achieve more than 85 % of cellular disruption.

3.2. Introduction

Microalgae are a promising source of several interesting compounds for a great variety of industries such as pharmaceuticals, nutraceuticals, chemicals, animal feed, and human food [38]. Examples of high-value products obtained from microalgae are pigments, lipids, proteins, lipids, and antioxidants [112]. Moreover, microalgae can grow in non-arable areas and brackish or saline water, resulting in a lower land and water footprint [52]. However, downstream processing still faces numerous challenges, and it should be taken into account that, in several biotechnology processes, the cost of downstream processing can be very influential on the total costs [113]. Therefore, the effort should be placed into minimizing the capital costs and energy requirements [114].

The microalgae biorefinery concept, analogous to petroleum refineries, reduces the typical cost of producing a single product and expands the economic feasibility of the microalgal bioindustry [115]. Microalgae biorefinery usually consists of a three-step concept including cell disruption, fractionation of the distinct main elements (including extraction), and purification of the high-value biomolecules [38]. Within this concept, cell disruption is a crucial step to achieving efficient extraction of high-value

compounds [116]. The cell disruption is often challenging as microalgae cells are small, several species are covered with a relatively stick cell wall, and the products of interest are usually located in globules or bonded to the cell membranes [52].

The cell disruption step has been extensively studied and the existing methods can be classified into non-mechanical and mechanical [52]. Mechanical methods are usually achieved by mechanical forces such as shear forces, energy transfer through waves, currents or heat. On the other hand, non-mechanical methods often involve cell lysis through osmotic shock, enzymes or chemical agents [52]. And even if these methods might provide higher selectivity than the mechanical ones, the costs of chemicals and enzymes have limited those methods to a laboratory scale [38]. Several cell disruption methods such as ultrasonication [117,118], pulsed electric field (PEF) [119,120], bead milling [121], microwave [122,123], high-pressure homogenisation (HPH) [124] and enzymatic treatment [125,126] have been already tested on microalgae at a laboratory scale. Mechanical treatments, such as bead milling, are preferable for industrial-scale applications due to their efficiency of disruption and the commercially available devices at a large scale [127]. Moreover, recent design improvements and the possibility to control the temperature of the microalgae suspension inside the grinding chamber, make bead milling an appropriate technology for microalgae cell disruption [121].

Bead mills are frequently used at an industrial scale for fine grinding of minerals, ceramics, paint pigments and other products [128]. In the field of biotechnology, bead milling has been successfully used in the disruption of cyanobacteria [129] and microalgae [121]. The principle of operation of a bead mill is based on the rapid stirring of a suspension in the presence of beads. Usually, the bead mill consists of a jacketed grinding chamber with a rotating shaft through its centre [130]. The shaft is fitted with discs that transfer kinetic energy to the small beads in the chamber, promoting collisions with the suspended cells [52]. The efficiency of cell disruption in bead mills depends on several parameters such as biomass concentration, chamber and agitator geometry, bead filling ratio, bead diameter, bead type, agitator tip speed, and biomass suspension flow rate [131]. Also, a bead mill can be operated under continuous operation (one single pass through the grinding chamber) or batch operation (two or more passes through the grinding chamber).

Nannochloropsis sp. is a strain that is perfectly able to grow in seawater and possesses small spherical cells (3-5 μm) [35], with a single chloroplast [31]. *Nannochloropsis* genus has a few specific biochemical characteristics such as the lack of accessory chlorophylls *b* and *c*, interesting xanthophyll pigments [36], and relatively high content of eicosapentaenoic acid (EPA) [38]. However, regarding the

ease of rupture, it should be taken into account that the *Nannochloropsis* sp. cell wall is a robust structure composed of cellulose and hydrophobic algaenan [49].

Algaenan is a resistant biopolymer, and the algaenan sheet has been reported to be composed of long, straight-chain, saturated aliphatics with ether cross-links [49]. Algaenan is one of the layers belonging to the called trilaminar layer structure (TLS) [132], two high electron density external layers sandwiching one layer with low electron density [133]. The resistance of the algaenan and their small radius confers a robust cell wall to *Nannochloropsis* sp. cells. Thus, an optimised cell disruption step before fractionation is essential. The operating conditions of bead milling and their impact on the cell disruption efficiency of various species of microalgae have been already studied by several authors. Montalescot *et al.* [38] optimised the bead milling parameters for the cellular disruption of *Prophyridium cruentum* and *Nannochloropsis oculata*. Postma *et al.* [121] proposed a mild disintegration of *Chlorella vulgaris* using bead milling. Günerken *et al.* [116] studied the effect of nitrogen reduction in the growth of *N. oleoabundans* on the release of intracellular components after bead milling.

Safi *et al.*, compared four different cell disruption methods for *Nannochloropsis gaditana* to release proteins: pulsed electric field, high-pressure homogenization, enzymatic treatment and bead milling (0.5 mm beads (ZrO2) at 65% filling ratio, and 8 $m.s^{-1}$ of tip speed). The authors reported similar results in terms of cellular disintegration for both high-pressure homogenization and the bead milling technologies (> 95% cellular disintegration) [124]. However, despite the higher energy consumption associated with bead milling, the scaling up of this disruption technology is easier than the other technologies studied by Safi et al. [124].

Quesada-Salas *et al.*, studied the effect of the flow rate and the bead size on the cell disruption efficiency of *Nannochloropsis gaditana* and *Nannochloropsis oceanica* through bead milling [134]. The author performed 3 grinding cycles to a 10 $g_{DW}.kg^{-1}$ microalgae suspension in a Dyno® - Mill Multi Lab (WAB) with a 600 mL grinding chamber, a bead filling percentage of 80%, and a tip speed of 10 $m.s^{-1}$. The results of this study revealed that a lower flow rate - LFR exhibits better results in terms of cell disruption percentage than a higher flow rate - HFR (93 ± 5% HFR and 99 ± 5% LFR). Also, the comparison between the diameter of zirconia beads (0.40 mm and 1.25 mm) revealed that the smaller beads lead to better results in terms of cell disruption efficiency (96 ± 5% 0.40 mm and 55 ± 5% 1.25 mm). However, the biomass that was used in these studies was initially frozen which might have contributed to cellular disintegration as freeze-thawing is a known mild cell disruption technique [135].

The main objective of this study is to optimise the extraction of intracellular compounds through the optimisation of the disruption step (bead milling). In this work, a pilot-scale bead milling was studied

to evaluate the influence of several processing parameters on the cell disintegration efficiency in thickened (100 $g_{SFDW}.L^{-1}$) *Nannochloropsis* sp. suspensions. The following processing parameters: flow rate, agitator tip speed, and the number of passes of the suspension through the grinding chamber were optimised to increase the cell disruption yield. The aim is to optimise the bead milling process to achieve more than 85% of cellular disruption with one single pass through the grinding mill. To our knowledge, the process optimisation of a pilot-scale bead milling to increase the cellular disruption efficiency of fresh biomass of *Nannochloropsis* sp. has never been reported. The global efficiency of the disruption step was qualitatively evaluated through microscopic observation and quantitatively evaluated by the extraction efficiency of total pigments (chlorophyll *a*, pheophytin *a* equivalents and carotenoids) from the disrupted *Nannochloropsis* sp. biomass. The number of stress events (SN), as well as the stress intensity (SI, Nm) and the energy consumption ($kWh.kg^{-1}_{biomass}$) of each experiment, were also calculated to characterize the bead milling process. Also, an industrial scale bead milling was studied to outline the optimal operating conditions to achieve 85% to 95% of cellular disruption for a biorefinery with a production capacity of 300 $L.h^{-1}$, as a requirement for industrial microalgae biorefineries. To the best of our knowledge, no optimisation process of industrial-scale bead milling has been reported.

3.3. Materials and Methods

3.3.1. Materials

The strain of *Nannochloropsis* sp. was grown in flat-panel photobioreactors (PBR) of A4F – Algae for Future (Portugal) in marine, N-replete culture medium and concentrated up to a 200 g_{SFDW}/L wet paste (between 30 to 35 g/L of salt), to facilitate the transport. For analytical procedures acetone, 99.0% purity, was purchased from JMGS (Odivelas, Portugal).

3.3.2. *Nannochloropsis* sp. bead milling at pilot scale

In this first part of the experimental work, bead mill experiments were performed with a Dyno®-Mill Multi Lab of WAB (Willy A Bachofen AG, Muttenz, Switzerland). This first part of the experiment was accomplished on a pilot scale. The harvested *Nannochloropsis* sp. paste obtained from A4F – Algae for Future was received with a concentration of approximately 200 $g_{SFDW}.L^{-1}$, which facilitated biomass transport. Then the paste was diluted with *Nannochloropsis* sp. culture media to approximately 100 $g_{SFDW}.L^{-1}$. After homogenisation by stirring, the *Nannochloropsis* sp. suspension (feed solution) at 100

$g_{SFDW}.L^{-1}$ was pumped by a peristaltic pump, from an agitated feed tank to a 1.4 L horizontal grinding chamber (**Figure 3.1**). A constant filling volume of 85 % $v.v^{-1}$ with grinding beads, was ensured and recommended by the supplier. The beads selected were 0.4-0.6 mm in diameter [136]. The suspension outlet temperature was maintained under 30 ºC with cold water (4 ºC) circulating in the cooling jacket of the grinding chamber. Samples of disrupted biomass were then collected at the outlet when steady-state was reached (constant flow rate and concentration obtained after 3 chamber volumes). The parameters tested in this study were: the number of passes through the grinding chamber (1 and 2), the rotational speed (10 and 14 $m.s^{-1}$), and the flow rate (10 and 13 $L.h^{-1}$). The operating conditions for each trial of bead milling are summarized in **Table 3.1**. The number of passes through the bead milling was assessed in the first two experiments (BM.1.1 and BM.1.2) with a flow rate fixed at 13 $L.h^{-1}$ and a tip speed fixed at 10 $m.s^{-1}$, as it was assumed that those were the most unfavourable operating conditions. As mentioned before, the aim was to optimise the bead milling process to achieve more than 85% of cellular disruption with one single pass through the grinding chamber, allowing to minimise of the number of mills in a biorefinery. Therefore, according to the results obtained in the first trial (87.7% ± 0.4% disruption efficiency, with a single pass), the number of passes through the bead milling was fixed at a single pass through the bead milling for the remaining trials.

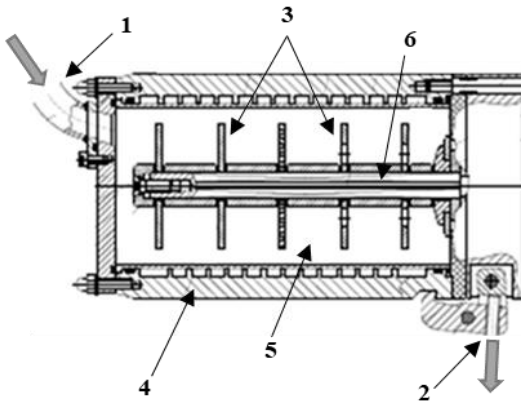

Figure 3.1. Bead milling inside view. (1) Input, (2) Output, (3) Agitator discs, (4) Cooling jacket, (5) Griding chamber, (6) Agitator shaft. Adapted [137]

Table 3.1. Scheme of the bead milling experiments at a pilot-scale

Experiment	Feed volume (L)	Number of passes (#)	Tip speed ($m.s^{-1}$)	Flow rate ($L.h^{-1}$)
BM.1.1	10	1	10	13
BM.1.2	10	2	10	13
BM.1.3	5	1	14	13
BM.1.4	10	1	10	10
BM.1.5	10	1	14	10

The global efficiency of the disruption step was quantitatively evaluated by the extraction efficiency of chlorophyll *a* (*Chl a*) and its degradation products - pheophytin *a* equivalents (*Pheo a*) [93,94,101], due to cell disruption of *Nannochloropsis* sp. biomass (**Eq. 3.1**). The behaviour of pigment extraction may also predict the behaviour of lipid extraction, as they may exhibit similar proprieties.

$$\text{Disruption Efficiency (\%)} = \frac{[Chl\ a]_{i_{BM}} + [Pheo\ a]_{i_{BM}}}{[Chl\ a]_{i_{total}} + [Pheo\ a]_{i_{total}}} \times 100 \quad \textbf{Eq. 3.1}$$

where $[Chl\ a]_{iBM}$ is the concentration of chlorophyll *a* (mg. g_{SFDW}^{-1}) in the sample (*i*), after the bead milling processing, $[Pheo\ a]_{iBM}$ is the concentration of pheophytin *a* equivalents (mg. g_{SFDW}^{-1}) in the sample (*i*), after the bead milling processing, $[Chl\ a]_{i\ total}$ is the concentration of chlorophyll *a* (mg. g_{SFDW}^{-1}) in the sample (*i*), after the bead milling processing plus further bead beating to achieve total cellular disruption (100% cell disruption), and $[Pheo\ a]_{itotal}$ is the concentration of pheophytin *a* equivalents (mg. g_{SFDW}^{-1}) in the sample (*i*), after the bead milling processing plus further bead beating to achieve total cellular disruption (100% cell disruption). In order to ensure that a complete rupture of the cells was achieved after the bead beating, the samples were re-extracted with fresh acetone (see **section 3.3.5**). The results (data not shown) revealed that no pigments were extracted during the last extraction, which means that the cells were 100% disputed after bead beating and all the pigments available for extraction were extracted during the first extraction.

The efficiency of cell disruption in bead mills depends on several parameters such as biomass type, biomass concentration, agitator speed, bead diameter, bead type, bead filling ratio, suspension flow rate, and residence time (t_r), calculated through **Eq. 3.2**:

$$t_r = \frac{V_{chamber,free}}{Q} \quad \textbf{Eq. 3.2}$$

with,

$$V_{chamber,free} = V_{chamber}\,\varepsilon\,\varphi_B + V_{chamber}(1 - \varphi_B) \quad \textbf{Eq. 3.3}$$

where $V_{chamber,\text{free}}$ represents the volume inside the chamber filled with *Nannochloropsis* sp. suspension (L), Q is the flow rate of the suspension (L.h^{-1}), $V_{chamber}$ represents the volume of the grinding chamber (L), ε is the bulk porosity (-), and φ_B is the bead filling ratio (-).

Bunge *et al*. [138], and Kwade and Schwedes [139] described the fragmentation of cells in a bead milling as a function of the number of stress events, *SN* (-), i.e., bead to bead collisions, and the stress intensity, *SI* (Nm), of each one of the stress events.

Accordingly, the stress number at deagglomeration and disintegration.

can be calculated through **4**,

$$\text{SN} \propto \frac{\varphi_B\,(1-\varepsilon)}{\{1-\varphi_B(1-\varepsilon)\}C_V} \cdot \frac{nt}{d_B} \cdot d_C \propto \text{C} \cdot SN_D$$

with,

$$\text{C} = \frac{\varphi_B\,(1-\varepsilon)}{\{1-\varphi_B(1-\varepsilon)\}C_V} \quad \textbf{Eq. 3.4}$$

where φ_B is the bead filling ratio (-), ε is the bulk porosity (-), C_V is the volume cell concentration (-), n number of revolutions of the stirrer per unit time (s^{-1}), t is the milling time (s), d_B is the bead diameter (m), and d_C is the microalgae cell diameter (m) [139]. For deagglomeration and disintegration, the reduced stress number (SN_D) is inversely proportional to the diameter of the grinding media [139].

In the case of deagglomeration/disintegration, i.e. cellular disruption, it is considered that the elasticity of the feed is much smaller than that of the grinding media [139]. Furthermore, the stress intensity *SI* (Nm), is approximately proportional to the intensity of the grinding media, SI_{GM}, and can be defined as the magnitude of the kinetic energy of a single bead [131], and can be calculated through **Eq. 3.5**,

$$\text{SI} \propto SI_{GM} = d_B^3 \rho_B u_s^2 \quad \textbf{Eq. 3.5}$$

where d_B is the bead diameter (m), ρ_B is the specific density of the beads (kg.m^{-3}), and u_s is the agitator tip speed (m.s^{-1}).

The specific energy consumption (kWh.kg$^{-1}_{\text{biomass}}$ or kWh.kg$^{-1}_{\text{DW}}$) was also calculated for each previously proposed scenario. This parameter translates the electric energy requirements as a function of the amount

of biomass processed. The electricity requirements for each bead milling experiment were estimated considering the average drive of the mill (3.3 kW) and the parameters described in **Table 3.1**.

3.3.3. *Nannochloropsis* sp. bead milling at industrial scale

In the second part of the experimental work, bead mill experiments were performed with a Dyno®-Mill UBM 20 of WAB (Willy A Bachofen AG, Muttenz, Switzerland). This second part of the experimental work was accomplished on an industrial scale. The harvested *Nannochloropsis* sp. paste (approximately 200 $g_{SFDW}.L^{-1}$) was diluted with culture media to approximately 100 $g_{SFDW}.L^{-1}$. After homogenisation by stirring, the *Nannochloropsis* sp. suspension (feed solution) at 100 $g_{SFDW}.L^{-1}$ was pumped by a peristaltic pump, from an agitated feed tank to a 19.6 L horizontal grinding chamber. The suspension outlet temperature was maintained under 30 ºC with cold water circulating in the cooling jacket of the grinding chamber. Samples of disrupted biomass were then collected at the outlet when steady-state was reached (constant flow rate and concentration obtained after 3 chamber volumes). The parameters studied were the flow rate (100, 200 and 300 $L.h^{-1}$), and the filling volume (70% and 85% $v.v^{-1}$) with grinding beads with 0.4-0.6 mm of diameter. The operating conditions for each trial of bead milling are summarized in **Table 3.2**.

Table 3.2. Scheme of the bead milling experiments at an industrial scale

Experiment	Feed volume (L)	Number of passes (#)	Bead filling volume (% $v.v^{-1}$)	Tip speed ($m.s^{-1}$)	Flow rate ($L.h^{-1}$)
BM.2.1	60	1	70	16	100
BM.2.2	60	1	85	16	100
BM.2.3	80	1	85	16	200
BM.2.4	80	1	85	16	300

As mentioned in section **3.3.2**, the global efficiency of the disruption step was quantitatively evaluated by the extraction efficiency of chlorophyll *a* (*Chl a*) and its degradation products presented as pheophytin *a* equivalents (*Pheo a*), through **Eq. 3.1**. Also, the residence time (t_r), the number of stress events (*SN*), and the stress intensity (*SI*) were calculated as demonstrated in section **3.3.2**. The specific energy consumption ($kWh.kg^{-1}_{biomass}$ or $kWh.kg^{-1}_{DW}$) was also calculated for each previously proposed scenario. The electricity requirements for each bead milling experiment were estimated considering the average drive of the mill (47.0 kW) and the parameters described in **Table 3.2**.

3.3.4. Dry weight and salinity quantification

The dry weight of the samples was determined as previously described in chapter **2.3.4**. The selected drying program was run at 105 ºC in a moisture analyser (Kern DBS 60-3, Kern, Germany). Afterwards, the concentration of salt in the sample was determined through a salinity refractometer (Kern ORA 1SA, Kern, Germany).

3.3.5. Pigments quantification

Chlorophyll *a*, chlorophyll *a* degradation products, and carotenoids quantification was performed as previously described in chapter 2.3.8. The extracted pigments were analysed by spectrophotometry (Genesys 10S UV-VIS). Each sample analysis was performed in triplicate.

3.4. Results and Discussion

The analysis of the results is focused on the cell disruption step, through bead milling, of a 100 $g_{SFDW}.L^{-1}$ *Nannochloropsis* sp. biomass suspension. The first subchapter presents the characterisation of biomass after the harvesting step. Subsequently, in the second and third subchapters, the results from the experimental work of bead milling on a pilot-scale and industrial scale, respectively, are presented and discussed.

3.4.1. *Nannochloropsis* sp. biomass characterisation

For each experiment, the harvested *Nannochloropsis* sp. paste (approximately 200 $g_{SFDW}.L^{-1}$) was diluted with culture media to approximately 100 $g_{SFDW}.L^{-1}$ and, after homogenization, a sample was collected and analysed in terms of salt-free dry weight, and total pigment content. The nine biomass suspension samples presented a 105.2 ± 8.1 $g.L^{-1}$ salt-free dry weight per volume, on average. The characterisation in terms of pigments revealed that, on average, the biomass was composed of 31.8 ± 2.6 $mg.g_{SFDW}^{-1}$ of chlorophyll *a*, 11.4 ± 1.1 $mg.g_{SFDW}^{-1}$ of carotenoids, and 3.0 ± 2.5 $mg.g_{SFDW}^{-1}$ of pheophytin *a* equivalents, which means that the biomass was in good conditions and with no significant degradation, as pheophytin *a* equivalents include all the degradation products of chlorophyll *a* [101]. Also, the initial characterisation of the biomass trough pigment analysis, shows that only 3.1% ± 1.6% of the cells were

initially compromised or sightly disrupted, and a microscopic image of *Nannochloropsis* sp. biomass before cell disruption is presented in **Figure 3.2**.

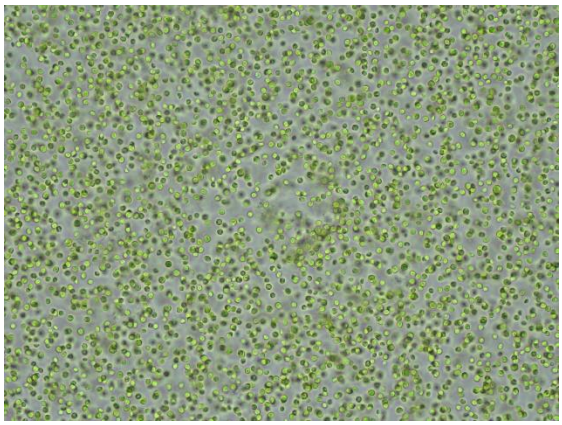

Figure 3.2. Microscopic image of *Nannochloropsis* sp. biomass before cell disruption (×40 magnification).

3.4.2. *Nannochloropsis* sp. bead milling at pilot scale

The first approach of the bead milling experiments aiming at the optimisation of the cell disruption was carried out in a pilot-scale bead mill. The results of the experiments are presented and discussed in terms of the effect of the number of passes through the bead mill, and the effect of flow rate and tip speed on the cellular disruption efficiency.

The results of the effect of the number of passes through the bead mill on the cell disruption efficiency, are presented in **Figure 3.3** and **Figure 3.4**. The microscopic image gives a piece of qualitative information, and it suggests that two passes (**Figure 3.3 B**) through the bead mill might be better than one single pass (**Figure 3.3 A**). A single pass through the bead mill seems to leave a few intact cells, while the two passes through the bead mill appear to shred all the cells.

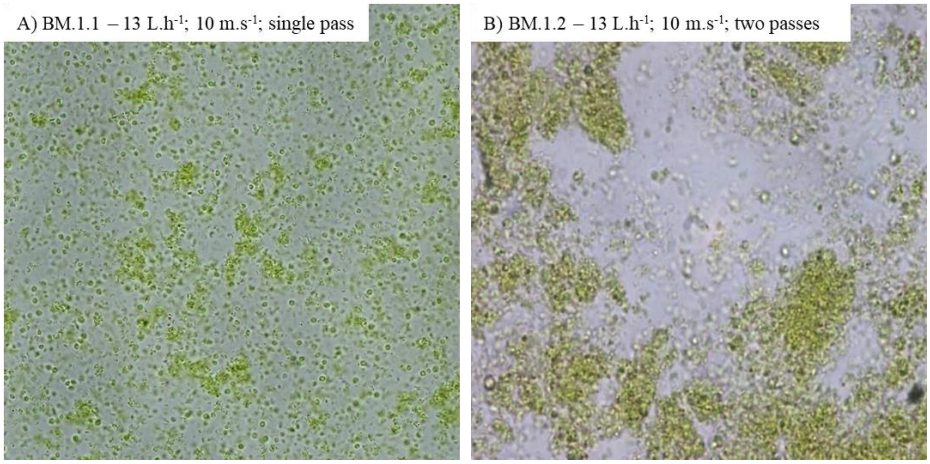

Figure 3.3. Microscopic image of *Nannochloropsis* sp. biomass after cell disruption in a pilot-scale bead mill (×40 magnification). A) Experiment BM.1.1 - bead milling through a single pass with a flow rate of 13 $L.h^{-1}$ and tip speed of 10 $m.s^{-1}$; B) Experiments BM.1.2 - bead milling through two passes with a flow rate of 13 $L.h^{-1}$ and tip speed of 10 $m.s^{-1}$.

These qualitative results are confirmed by the quantitative results presented in **Figure 3.4**. A single pass through the bead mill with a flow rate of 13 $L.h^{-1}$ and tip speed of 10 $m.s^{-1}$, leads to a disruption efficiency of 87.7% ± 0.4%, while the two passes achieve a disruption efficiency of 99.2% ± 0.6%. The results obtained through pigment quantification after cellular disruption, are in accordance with the ones reported by Safi *et al*. [124], of a cellular disintegration >95% in 1 hour of milling with 0.5 mm beads, and an agitation speed of 8 $m.s^{-1}$.

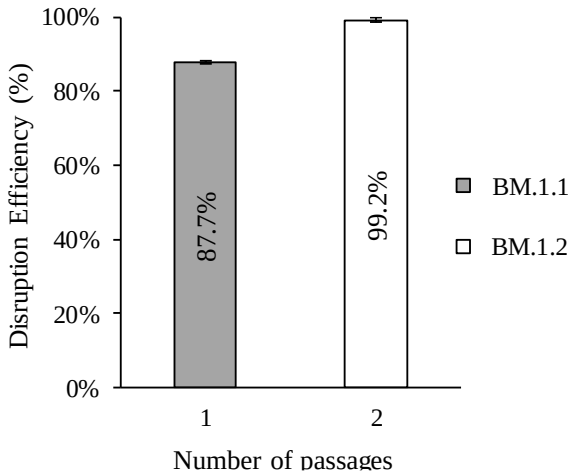

Figure 3.4. Pilot-scale bead milling. Disruption efficiency (%) as a function of the number of passages through the grinding chamber for *Nannochloropsis* sp. suspension, at a flow rate of 13 $L.h^{-1}$ and tip speed of 10 $m.s^{-1}$: BM.1.1 - one pass through the chamber, BM.1.2. Two passes through the chamber. The results are based on 3 replicates of the sample pigment analysis (one test for each condition). The error bars represent the standard deviation calculated from the replicates.

However, the main objective of this work was to outline and optimise the bead milling process, so that with one single pass through the grinding mill it should be possible to obtain > 85% of cellular rupture. Therefore, in the following studies, the effects of the flow rate and the tip speed were assessed for one single pass through the grinding chamber.

The microscopic images provide a qualitative result and suggest that a higher tip speed (**Figure 3.5 B and D**) promotes a higher disruption efficiency since there are fewer intact cells present in the microscopic images for a tip speed of 14 $m.s^{-1}$ (**Figure 3.5 B and D**) than in the ones for a tip speed of 10 $m.s^{-1}$ (**Figure 3.5 A and C)**. On the other hand, a lower flow rate (i.e., higher residence time in the grinding chamber) seems to lead to a higher disruption efficiency than a higher flow rate. Comparing **Figure 3.5 B** with **Figure 3.5 D** is possible to identify more intact cells in the microscopic image for the higher flow rate of 13 $L.h^{-1}$ (**Figure 3.5 B**) than in the microscopic image for the lower flow rate of 10 $L.h^{-1}$ (**Figure 3.5 D**).

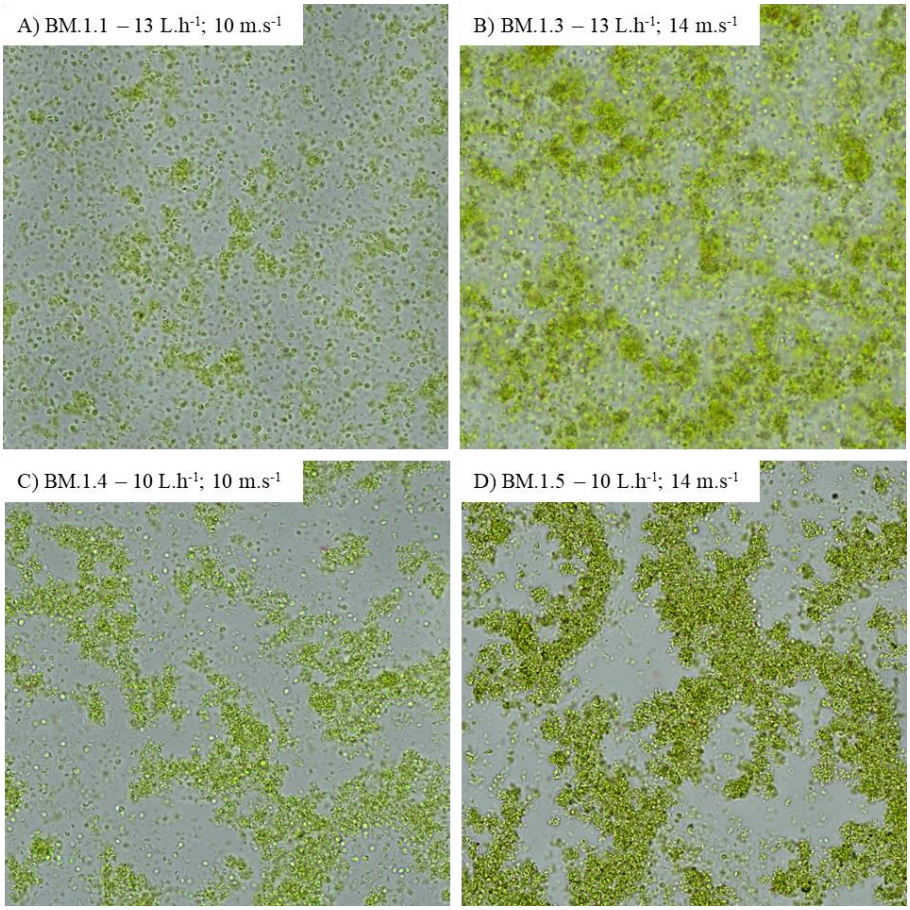

Figure 3.5. Microscopic images of *Nannochloropsis* sp. biomass after cell disruption in a pilot-scale bead mill (×40 magnification). A) BM.1.1 single pass, flow rate of 13 $L.h^{-1}$, and tip speed 10 $m.s^{-1}$; B) BM.1.3 single pass, flow rate of 13 $L.h^{-1}$ and tip speed 14 $m.s^{-1}$; C) BM.1.4 single pass, flow rate of 10 $L.h^{-1}$, and tip speed 10 $m.s^{-1}$; D) BM.1.5 single pass, flow rate of 13 $L.h^{-1}$, and tip speed 10 $m.s^{-1}$.

After the qualitative analysis through microscopic observation, a quantitative analysis was performed. The summary of the results of the effect of the flow rate ($L.h^{-1}$) and the tip speed ($m.s^{-1}$) on the cell disruption efficiency, as well as the number of stress events (Sn) and energy consumption, are presented in **Table 3.3**.

The intrinsic relation between the number of stress events and the disruption efficiency is shown in **Figure 3.6**. It is easily noticed that the higher the number of stress events, the higher the disruption efficiency. The number of stress events is directly influenced by the agitator tip speed and the residence time within the grinding chamber. Therefore, higher tip speeds, allied with higher residence times, lead to higher disruption efficiencies.

Table 3.3. Summary of the results of the effect of the flow rate and tip speed on the number of stress events (SN), energy consumption and disruption efficiency, for a bead milling with an 85% filling ratio.

Experiment	Flow rate ($L.h^{-1}$)	Tip speed ($m.s^{-1}$)	Residence Time (min)	*SN*	SI_{GM} (Nm)	Energy Consumption ($kWh.kg^{-1}_{biomass}$)	Disruption Efficiency (%)
BM.1.1	13	10	3.06	5.70×10^{7}	7.58×10^{-5}	0.152	87.70 %
BM.1.3	13	14	3.06	7.40×10^{7}	1.48×10^{-4}	0.254	90.80 %
BM.1.4	10	10	3.97	7.97×10^{7}	7.58×10^{-5}	0.198	88.00 %
BM.1.5	10	14	3.97	1.04×10^{8}	1.48×10^{-4}	0.330	94.4 %

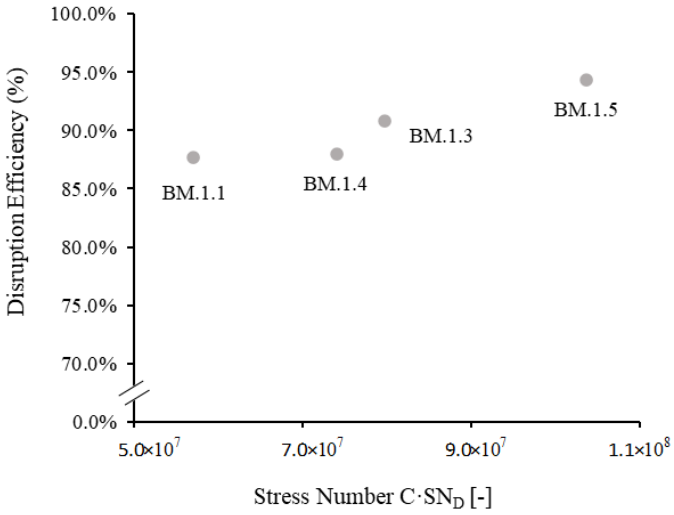

Figure 3.6. Disruption efficiency (%) against the number of stress events. BM.1.1 – Flow rate: 13 $L.h^{-1}$ and tip speed: 10 $m.s^{-1}$; BM.1.3 – Flow rate: 13 $L.h^{-1}$ and tip speed: 14 $m.s^{-1}$; BM.1.4 – Flow rate: 10 $L.h^{-1}$ and tip speed: 10 $m.s^{-1}$; BM.1.5 – Flow rate: 10 $L.h^{-1}$ and tip speed: 14 $m.s^{-1}$.

The cell disruption efficiency increased with the increase of the tip speed. For a flow rate of 13 $L.h^{-1}$ (**Figure 3.7 A)** the cell disruption was enhanced from 87.7% ± 0.4% to 90.8% ± 1.5%, when the tip speed was increased from 10 $m.s^{-1}$ (BM.1) to 14 $m.s^{-1}$ (BM.3) respectively. Also, for a flow rate of 10 $L.h^{-1}$ (**Figure 3.7 B)** the cell disruption was enhanced from 88.0% ± 0.2% to 94.4% ± 2.7% when the tip speed was increased from 10 $m.s^{-1}$ (BM.4) to 14 $m.s^{-1}$ (BM.5). A higher tip speed increases the number of collisions, as well as the energy in those collisions, between the beads and the cells. For example, for a flow rate of 10 $L.h^{-1}$, the number of stress events increased from 7.97×10^{7} to 1.04×10^{8}, when the tip speed was changed from 10 $m.s^{-1}$ to 14 $m.s^{-1}$ (**Table 3.3**).

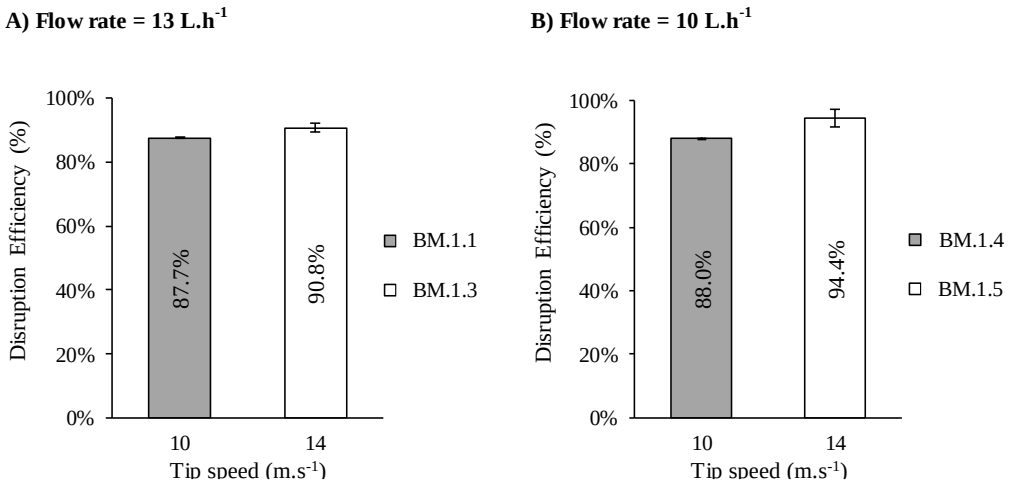

Figure 3.7. Pilot-scale bead milling. Disruption efficiency (%) as a function of the tip speed ($m.s^{-1}$) for *Nannochloropsis* sp. suspension. A) Flow rate fixed at 13 $L.h^{-1}$, single pass: BM.1.1 - tip speed 10 $m.s^{-1}$ and BM.1.3 - tip speed 14 $m.s^{-1}$, B) Flow rate fixed at 10 $L.h^{-1}$, single pass: BM.1.4 - tip speed 10 $m.s^{-1}$ and BM.1.5 - tip speed 14 $m.s^{-1}$. Results are based on 3 replicates for each sample pigment analysis (one test for each condition). The error bars represent the standard deviation calculated from the replicates.

The effect of the flow rate ($L.h^{-1}$), when the tip speed is fixed, was also evaluated (**Figure 3.8 A and B**). For a fixed tip speed, the cellular disruption efficiency decreased with the increase of the flow rate. **Figure 3.8 A**, shows that for a low tip speed (10 $m.s^{-1}$), the disruption efficiency slightly decreased with the increase of the flow rate from 10 $L.h^{-1}$ to 13 $L.h^{-1}$. However, for a high tip speed (14 $m.s^{-1}$), the cell disruption efficiency decreased from 94.4% ± 2.7% to 90.8% ± 1.5% when the flow rate increased from 10 $L.h^{-1}$ to 13 $L.h^{-1}$, respectively (**Figure 3.8 B)**. These results are following the results reported in the literature regarding the impact of the flow rate on cell disruption. Quesada-Salas *et al.*, reported a tendency to increase the cellular disruption when the suspension is milled at a lower flow rate [136].

These results are explained by the increase in the residence time when a lower flow rate is applied. For example, the residence time increased from 3.06 min to 3.97 min when the flow rate was changed from 13 $L.h^{-1}$ to 10 $L.h^{-1}$ (**Table 3.3**).

Increasing the residence time increases the number of collisions that every single cell suffers within the grinding chamber, which is justified by the increase in the number of stress events. However, higher residence times (i.e., a lower flow rate of the suspension) lead to an increase in energy consumption ($kWh.kg^{-1}_{biomass}$). For a fixed tip speed of 14 $m.s^{-1}$, the energy consumption increased from 0.254 $kWh.kg^{-1}_{biomass}$ to 0.330 $kWh.kg^{-1}_{biomass}$ (**Table 3.3**), when the flow rate decreased from 13 $L.h^{-1}$ (90.8%

of disruption efficiency) to 10 $L.h^{-1}$ (94.4% of disruption efficiency). These results are comparable with the results reported by Safi et al. [124]. The authors reported a specific energy input of 0.43 $kWh.kg^{-1}_{biomass}$ to achieve a cellular disruption efficiency of 95%.

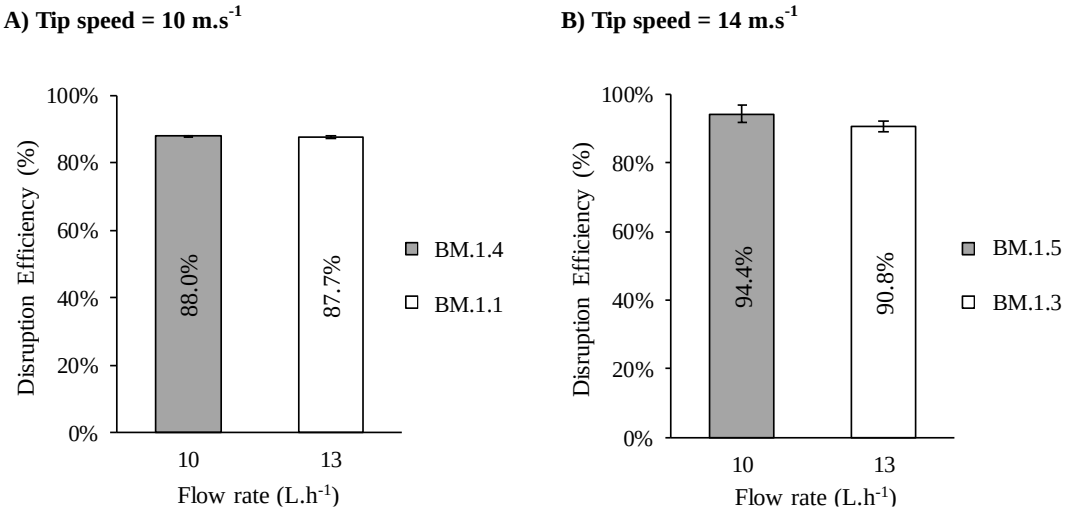

Figure 3.8. Pilot-scale bead milling. Disruption efficiency (%) as a function of the flow rate ($L.h^{-1}$) for *Nannochloropsis* sp. suspension. A) Tip speed fixed at 10 $m.s^{-1}$, single-pass: BM.1.4 - flow rate 10 $L.h^{-1}$ and BM.1.1 - flow rate 13 $L.h^{-1}$. B) Tip speed fixed at 14 $m.s^{-1}$, single-pass: BM.1.5 - flow rate 10 $L.h^{-1}$ and BM.1.3 - flow rate 13 $L.h^{-1}$. Results are based on 3 replicates for each sample pigment analysis (one test for each condition). The error bars represent the standard deviation calculated from the replicates.

Figure 3.9 represents the effect of the two combined variables (tip speed [$m.s^{-1}$] and flow rate [$m.s^{-1}$]) on the response variable (disruption efficiency %), for a target of 90% and a minimum value for disruption efficiency of 85%. It is possible to confirm that to achieve higher disruption efficiencies, high tip speeds and low flow rates are needed. The target performance can be reached when the experimental conditions fall in the upper left side of the figure, above the target line. The overall extraction efficiency of intracellular compounds increases as the cellular disruption rate increase. A higher cellular disruption efficiency enhances the contact between solvents and the target intracellular compounds, which is a great advantage within the biorefinery concept.

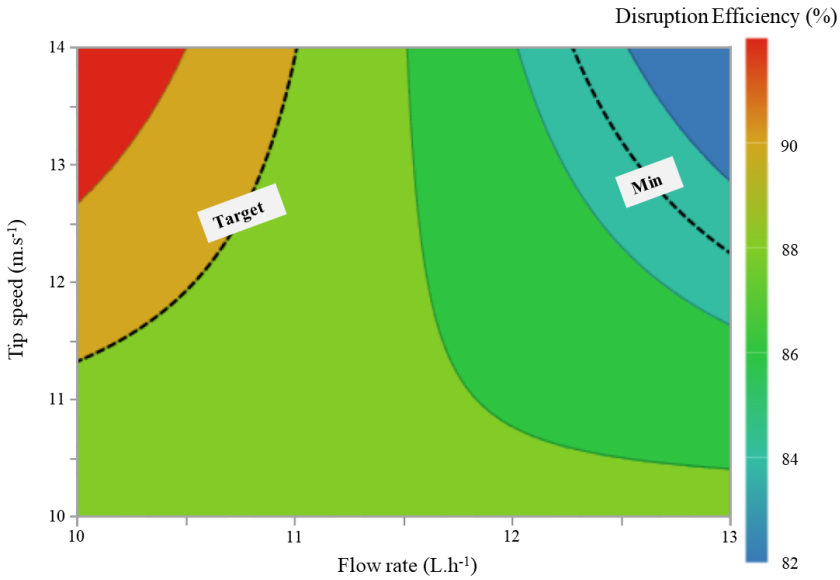

Figure 3.9. Pilot-scale bead milling. Effect of tip speed ($m.s^{-1}$) and flow rate ($L.h^{-1}$) in the disruption efficiency (%). The disruption efficiency target has been fixed at 90%, and the minimum has been fixed at 85%. The contour plot was built on Modde® 13.

3.4.3. *Nannochloropsis* sp. bead milling at industrial scale

The second part of the bead milling experiments aiming at the optimisation of the cell disruption was performed at an industrial-scale bead mill. The experiments at a pilot scale revealed that higher residence times (lower flow rates of the suspension), and higher tip speed lead to higher disruption efficiencies. Therefore, for the industrial scale experiments, the tip speed was fixed at 16 $m.s^{-1}$, which is the maximum allowed by the equipment. However, the main objective of this part of the study was to outline the optimal operating conditions to achieve 85% to 95% of cellular disruption for a biorefinery with a production capacity of 300 $L.h^{-1}$, as a requirement for industrial microalgae biorefineries.

The results of the experiments are presented and discussed in terms of the effect of the filling volume of the grinding chamber with beads (0.4 - 0.6 mm), and the effect of flow rate, on the cellular disruption efficiency. The summary of the results of the effect of the flow rate ($L.h^{-1}$) and the tip speed ($m.s^{-1}$) on the cell disruption efficiency, as well as the number of stress events and energy consumption, are presented in **Table 3.4**.

As previously observed for the pilot scale bead mill, the increase in the number of stress events lead to an increase in the disruption efficiency (**Figure 3.10**). The number of stress events, during these

industrial-scale trials, was affected by not only the residence time but also by the bead filling ratio inside the grinding chamber (**Table 3.4**).

Table 3.4. Summary of the results of the effect of the flow rate and the filling ratio on the number of stress events (SN), energy consumption and disruption efficiency, for a tip speed of 16 $m.s^{-1}$

Experiment	Flow rate ($L.h^{-1}$)	Filling ratio (%)	Residence Time (min)	*SN*	SI_{GM} (Nm)	Energy Consumption ($kWh.kg^{-1}_{biomass}$)	Disruption Efficiency (%)
BM.2.1	100	70	20.38	1.38×10^{8}	1.94×10^{-4}	0.470	89.9 %
BM.2.2	100	85	18.14	2.71×10^{8}	1.94×10^{-4}	0.470	95.7 %
BM.2.3	200	85	9.07	1.50×10^{8}	1.94×10^{-4}	0.235	93.0 %
BM.2.4	300	85	6.05	9.02×10^{7}	1.94×10^{-4}	0.157	89.4 %

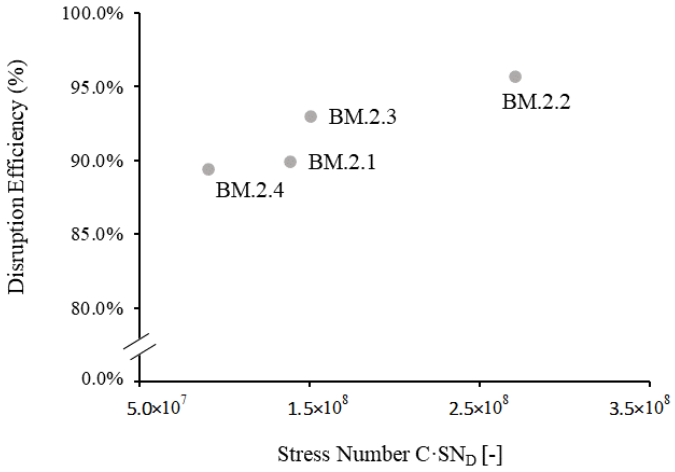

Figure 3.10. Disruption efficiency (%) against the number of stress events. BM.2.1 – Flow rate: 100 $L.h^{-1}$ and filling ratio: 70%; BM.2.2 – Flow rate: 100 $L.h^{-1}$ and filling ratio: 85%; BM.2.3 – Flow rate: 200 $L.h^{-1}$ and filling ratio: 85%; BM.2.4 – Flow rate: 300 $L.h^{-1}$ and filling ratio: 85%.

The results of the effect of the filling volume (% $v.v^{-1}$) of the chamber with beads on the cell disruption efficiency are presented in **Figure 3.11**. The experiments were performed with one single pass through the mill, at the maximum tip speed (16 $m.s^{-1}$) and with a flow rate of 100 $L.h^{-1}$, which means a residence time of 20.38 min in the experiment BM.2.1 (70% filling ratio), and 18.14 min in the experiment BM.2.2 (85% filling ratio). A significant enhancement of the disruption efficiency was observed when the percentage of filling with grinding beads increased. Cell disruption efficiencies of 89.9% ± 0.9% and

95.7% ± 1.4% were achieved, respectively, for 70% (BM.2.1) and 85% (BM2.2) of filling volume (% $v.v^{-1}$). A lower filling volume reduces the number of collisions that each cell suffers by creating higher void volumes (without beads) and, therefore, reducing the cellular disruption efficiency. The number of stress events achieved with a 70% filling ratio is lower (1.38×10^8) than the number of stress events with an 85% filling ratio (2.71×10^8).

For industrial-scale operations, the filling volume of the grinding chamber with beads (0.4 - 0.6 mm) should be fixed at 85% ($v.v^{-1}$), as previously used for the pilot scale tests, to achieve a cellular disruption efficiency higher than 90%. Therefore, further studies, on the effect of the flow rate, were performed with a filling volume of 85% ($v.v^{-1}$).

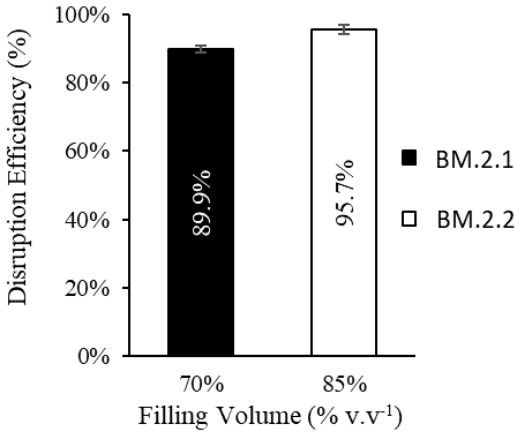

Figure 3.11. Industrial-scale bead milling. Disruption efficiency (%) as a function of the filling volume of the grinding chamber with beads (% $v.v^{-1}$), at a flow rate of 100 $L.h^{-1}$ and tip speed of 16 $m.s^{-1}$, for *Nannochloropsis* sp. suspension: BM.2.1 - 70% filling volume, BM.2.2 - 85% filling volume. Results are based on 3 replicates for each sample pigment analysis (one test for each condition). The error bars represent the standard deviation calculated from the replicates.

The effect of the flow rate, when a tip speed is fixed, was also studied for an industrial-scale bead milling operation, and the results are exhibited in **Figure 3.12**. The experiments were performed with one single pass through the bead mill, at the maximum tip speed (16 $m.s^{-1}$) and with a filling volume of 85% ($v.v^{-1}$). As previously observed for the pilot scale, as the flow rate increases and the residence time decreases, the cell disruption efficiency decreases. Cell disruption efficiencies of 95.7% ± 1.4%, 93.0% ± 0.2%, and 89.4% ± 2.2%, were achieved, respectively, for a flow rate of 100 $L.h^{-1}$ (residence time = 18.14 min), 200 $L.h^{-1}$ (residence time = 9.07 min), and 300 $L.h^{-1}$ (residence time = 6.05 min).

Again, the increase in residence time (for the same filling ratio) is reflected in the increasing number of stress events, i.e., the number of collisions between the beads and the cells (**Table 3.4**). For example, the increase of the residence time from 6.05 min in the experiment BM.2.4 (300 $L.h^{-1}$) to 9.07 min in the experiment BM.2.3 (200 $L.h^{-1}$) lead to an increase in the number of stress events from 9.02×10^{7} (experiment BM.2.4) to 1.50×10^{8} (experiment BM.2.3). As conclude in pilot scale experiments, the energy consumption is highly influenced by the residence time. The energy consumption increased, for example, from 0.157 $kWh.kg^{-1}_{biomass}$ to 0.235 $kWh.kg^{-1}_{biomass}$ (**Table 3.4**), when the flow rate decreased from 300 $L.h^{-1}$ (89.4% of disruption efficiency) to 200 $L.h^{-1}$ (93.0% of disruption efficiency).

Comparing the energy consumption results at an industrial scale with the results obtained at a pilot scale it was possible to conclude that for similar residence times, the experiments at an industrial scale revealed a lower energy consumption than the experiments at a pilot scale (0.157 $kWh.kg^{-1}_{biomss}$ at an industrial scale, and 0.330 $kWh.kg^{-1}_{biomss}$ at a pilot scale). However, contrarily as expected, for similar residence times, the disruption efficiency was higher in the pilot scale experiments (94.4%) than in the industrial scale experiments (89.4%). These results could be explained by the fact that some cells might be already compromised (not disrupted but fragilized, which was not seen in the microscopic observation) before the pilot scale experiment.

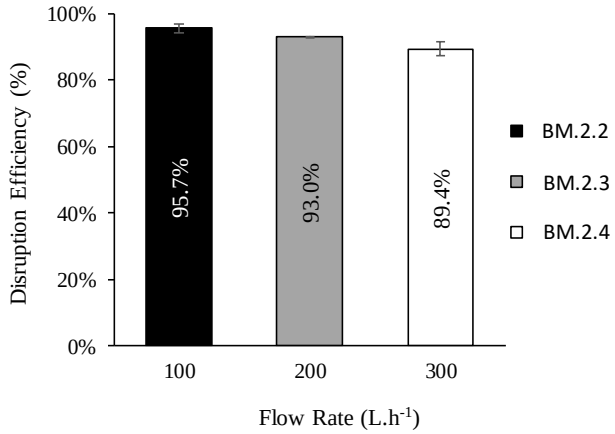

Figure 3.12. Industrial-scale bead milling. Disruption efficiency (%) as a function of the flow rate ($L.h^{-1}$) for *Nannochloropsis* sp. suspension, at a filling volume of 85% ($v.v^{-1}$) and a tip speed of 16 $m.s^{-1}$. BM.2.2 - flow rate 100 $L.h^{-1}$, BM.2.3 - flow rate 200 $L.h^{-1}$, BM.2.4 - flow rate 300 $L.h^{-1}$. Results are based on 3 replicates for each sample pigment analysis (one test for each condition). The error bars represent the standard deviation calculated from the replicates.

The main objective for the industrial scale was to outline the optimal operating conditions to achieve 85% to 95% of cellular disruption through bead milling. The biorefinery where this bead mill will be located will have a production capacity of 300 $L.h^{-1}$. Therefore, the results obtained revealed that it will be possible to achieve the main objective with a single bead mill (one single pass). This result is of extreme importance to microalgae industrial biorefineries.

3.5. Conclusion

In this work, the processing parameters of a pilot-scale bead milling were optimised to improve the extraction of intracellular compounds of *Nannochloropsis* sp. suspensions (100 $g_{SFDW}.L^{-1}$). The pilot-scale experiments revealed that it is possible to achieve 99% of cellular disruption, with two passes through the bead mill at a flow rate of 13 $L.h^{-1}$ and a tip speed of 10 $m.s^{-1}$. However, it was decided to optimise the bead milling process to achieve more than 85% of cellular disruption with one single pass through the grinding mill. It was observed a tendency to increase the cellular disruption with the decrease of the flow rate (i.e., with the increase of the residence time), and the increase of the tip speed. This tendency was concluded to be related to the increase in the number of stress events that each cell suffers during the disruption time. In fact, it was possible to achieve almost 95% of disruption efficiency for a single pass at a flow rate of 10 $L.h^{-1}$ and a tip speed of 14 $m.s^{-1}$ (maximum allowed by the equipment), with an energy consumption of 0.330 $kWh.kg^{-1}_{biomass}$. Similarly, the industrial-scale experiments revealed that lower flow rates, and consequently higher residence times, achieved higher disruption efficiencies at a fixed tip speed of 16 $m.s^{-1}$ (maximum allowed by the equipment). Comparing the energy consumption results at an industrial scale with the results obtained at a pilot scale it was possible to conclude that for similar residence times, the experiments at an industrial scale revealed a lower energy consumption than the experiments at a pilot scale (0.157 $kWh.kg^{-1}_{biomss}$ at an industrial scale, and 0.330 $kWh.kg^{-1}_{biomss}$ at a pilot scale). It was also concluded that it was possible to accomplish the main objective for the industrial-scale experiments (experiment BM.2.4), which was to achieve a cellular disruption efficiency higher than 85% with a single pass, and a flow rate required for an industrial microalgae biorefinery (300 $L.h^{-1}$).

4. *NANNOCHLOROPSIS* SP. BIOREFINERY: RECOVERY OF SOLUBLE PROTEIN BY MEMBRANE ULTRAFILTRATION/ DIAFILTRATION

Published as: Ribeiro, C.; Santos, E.T.; Costa, L.; Brazinha, C.; Saraiva, P.; Crespo, J.G., Nannochloropsis *sp. Biorefinery: Recovery of Soluble Protein by Membrane Ultrafiltration/ Diafiltration. Membranes 2022, 12, 401. https://doi.org/10.3390/membranes12040401*
The author was involved in planning and performing the experiments, as well as in the discussion and interpretation of the results and preparation of the manuscript.

4.1. Abstract

This work proposes a way to maximize the potential of a *Nannochloropsis* sp. biorefinery process, through membrane technology, producing an extract enriched in soluble proteins, free from the insoluble protein fraction, with a low lipid content and eliminating the coloured chlorophyll *a*. This procedure, following the principles of a circular economy approach, allows for the valorisation of a stream from the biorefining of *Nannochloropsis* sp. that, otherwise, would be considered a residue without commercial value. The process proposed minimizes fouling phenomena at the membrane surface, making it possible to achieve high permeate fluxes, thus reducing the need for membrane cleaning and, therefore, contributing to an extended membrane lifetime. The supernatant obtained after centrifugation of a suspension of ruptured *Nannochloropsis* sp. cells was processed by ultrafiltration using a membrane with a cut-off of 100 kDa MWCO. Two different operating approaches were evaluated—controlled transmembrane pressure and controlled permeate flux—under concentration and diafiltration modes. Ultrafiltration operated in a diafiltration mode, under controlled permeate flux conditions, led to the highest soluble protein recovery (78%) with the highest constant permeate flux (12 $L.m^{-2}.h^{-1}$) and low membrane fouling.

Keywords: *Nannochloropsis* sp.; protein recovery; circular economy; ultrafiltration; controlled transmembrane pressure; controlled permeate flux

4.2. Introduction

Microalgae Proteins are some of the microalgae products that have been receiving great attention from the research community. Microalgae proteins are a potential suitable source of high-quality protein not

only for human food [140], but also for animal feed [141], and in specific cases, such as the case of phycobiliproteins, for nutraceutical and pharmaceutical applications [142].

Several species of microalgae are known for their high protein contents [143], with nutritional values similar to other traditional protein sources, such as meat, egg, soybean and milk [144]. Fradique *et al.* [140], reported having successfully produced a high protein pasta product through the incorporation of *Chlorella vulgaris* and *Spirulina maxima* into semolina flour. The author also reported that the cooking quality of pasta was not compromised. Nevertheless, the incorporation of microalgae protein in food products faces several challenges, mostly those related to their organoleptic characteristics, such as odour, taste and colour [145]. Colour is the first parameter noticed by the consumer and the common green colour, linked to the presence of chlorophyll, leads to a very low sensorial acceptance by some consumers [146]. Qazi *et al.* [147], studied the impact on dough rheology and bread quality after the enrichment with an ethanol pre-treated *Tetraselmis chuii* protein fraction, in order to remove the green colour and improve the sensory properties. However, besides the clear improvement in dough rheology and bread quality, the author reported that the green pigmentation was not fully eliminated. For these reasons, microalgae coloured proteins are currently not regarded as valuable products with commercial value. Therefore, in line with the Circular Economy concept, it is important to find ways to reduce or eliminate the presence of chlorophyll in the microalgae protein.

Nannochloropsis sp., which is widely known for the production of omega-3 fatty acids, specifically eicosapentaenoic acid - EPA, has also an important content in total protein (up to 50% of dry weight) [33], both soluble (up to 20% dry weight) [34] and insoluble. *Nannochloropsis* sp. has a peculiar photosynthetic apparatus, characterized by the presence of only one type of chlorophyll (chlorophyll *a*), thus making its removal potentially simpler to address [89].

Nannochloropsis sp. is a small marine microalga (Eustigmatophyceae). The cells of *Nannochloropsis* sp. are small (3-5 µm) spherical or slightly ovoid [35], with a single chloroplast occupying a large volume of the cell [31], and with a strong cell wall composed of a bilayer structure consisting of a cellulosic inner wall and a hydrophobic algaenan outer layer [49]. Algaenan is a resistant biopolymer, and the algaenan layer has been described to be composed of long, straight-chain, saturated aliphatics with ether cross-links [83]. In numerous cases, algaenan is part of a layer called trilaminar layer structure (TLS), which exhibits two high electron density outside layers sandwiching one layer with low electron density [132]. The resistance of the algaenan and their small radius confers a robust cell wall to *Nannochloropsis* sp. cells.

The recovery of soluble proteins from aqueous supernatants, that result from the centrifugation of disrupted biomass, has attracted significant interest. In a microalgae biorefinery, besides the production of *Nannochloropsis* sp. extracts enriched in lipids, a soluble protein fraction can be produced for food applications, free from insoluble proteins and, ideally, without the presence of lipids and coloured chlorophyll *a*. Lipids tend to be attached to insoluble compounds [148] (e.g., insoluble proteins) that remain in suspension in the aqueous supernatant after centrifugation [149]. Thus, it is important to find a suitable process to recover the soluble protein fraction free from the insoluble compounds present (and the lipids attached to them) in the aqueous supernatant obtained by centrifugation.

Precipitation followed by centrifugation is one of the known methods for protein recovery from aqueous supernatants. Cavonius *et al*. used a pH-shift precipitation method to obtain a protein isolate from *Nannochloropsis oculata*, by lowering the pH to the protein's isoelectric point [71]. However, this method has significant limitations, such as the low selectivity for different proteins and, in some cases, the irreversible denaturation of proteins.

Alternatively, the use of membrane technologies for fractionation/concentration of proteins from microalgae offers the possibility of operating under mild conditions and thus prevents the denaturation of proteins [150]. Membrane processes, namely the commonly used ultrafiltration or nanofiltration are pressure-driven processes. The selective transport of the different compounds of a solution is mainly regulated by molecular size exclusion mechanisms, but also by the Coulombic and hydrophobic interactions between the compounds present and the membrane selective top layer [151]. Generally, membrane technologies are economic, easy to operate and to scale up, although not providing high product selectivity when compared e.g., with chromatography processes.

Ursu *et al*. [152], studied the concentration of *Chlorella vulgaris* proteins in the retentate, through ultrafiltration (using a membrane with a molecular weight cut-off (MWCO) of 300 kDa) in a concentration mode under fixed transmembrane pressure (fixed at 1.5 bar). The majority of the proteins remained in the retentate (87% w/w for pH 7). Safi *et al*. [1] focused on obtaining proteins in the permeate instead of the retentate, free from polysaccharides and chlorophyll. The author studied two-step ultrafiltration with a polyethersulfone (PES) membrane (concentration followed by diafiltration, using the same membrane). Three PES membranes with different molecular weight cut-offs were tested (300 kDa, 500 kDa and 1000 kDa) at fixed TMP (2.07 bar). The best performance was achieved with the 300 kDa membrane, and a protein recovery of 37% (w/w total proteins in the supernatant) was reported [1]. This low protein recovery could be explained by fouling phenomena, which reduce the permeate flow rate and increase the retention by the membrane.

The severe fouling observed at the start of the constant transmembrane pressure (TMP) ultrafiltration process, due to the often very high initial flux of the clean membrane [153], may be reduced by applying a milder operation, using a controlled permeate flux strategy, operated under subcritical/sustainable permeate flux conditions [154]. Monte *et al*. studied the harvesting of carotenoid-rich *Dunaliella salina* through ultrafiltration in a concentration mode under controlled flux conditions [155]. Similarly, Serra *et al*. combined ultrafiltration in a diafiltration mode with controlled flux conditions for the purification of viscous arabinoxylans from corn fibre through dia-ultrafiltration [156].

In the present work, membrane fouling occurring during protein filtration could be reduced by operating the ultrafiltration process in a diafiltration mode. The dia-ultrafiltration process enhances the removal of small proteins and carbohydrates, preventing the viscosity of the feed solution from rising over time.

The main objective of this study is to define a suitable methodology using membrane processing to obtain a high permeate flux with maximum soluble protein recovery (free from chlorophyll *a*, insoluble proteins and lipids). This work also aims to establish a process with minimum fouling, that could lead to easy membrane cleaning, therefore also contributing to maximising membrane lifetime. The global efficiency of the process under study was mainly quantified by the permeate volumetric flux, Jv ($L.m^{-2}.h^{-1}$) and by the percentage of soluble protein recovered in the permeate. To our knowledge, ultrafiltration in a diafiltration operation mode under controlled permeate flux has not been reported and evaluated as a methodology for the recovery of soluble proteins in microalgae biorefineries. Besides the study performed by dia-ultrafiltration, ultrafiltration in a concentration operation mode was also tested. In both cases, two different operating conditions were compared, corresponding to controlled transmembrane pressure and controlled permeate flux.

4.3.Materials and Methods

4.3.1. Materials

The *Nannochloropsis* sp. biomass used in this work was cultivated in photobioreactors (PBRs), mechanically disrupted and supplied by A4F – Algae for Future (Portugal). For the ultrafiltration studies, the *Nannochloropsis* sp. disrupted biomass (100 $g.L^{-1}$, on a salt-free dry weight basis - SFDW) was centrifuged at 11,000 × g (for 2 × 20 minutes, 5 °C) and the collected supernatant (30 $g_{SFDW}.L^{-1}$) was analysed in terms of salt-free dry weight, proteins, lipids, and chlorophyll *a* content.

Previous studies of ultrafiltration using a hydrophilic ceramic membrane with a nominal molecular weight cut-off (MWCO) of 300 kDa revealed a significant volumetric flux decrease during the process,

which may be related to high fouling, namely intrapore fouling (data not shown here). Also, *Nannochloropsis* sp. contains various proteins, which are associated with the light-harvesting complexes, with molecular masses ranging between 21-32 kDa [157]. Therefore, for optimization of soluble protein recovery, a hollow fibre module containing a tighter ultrafiltration membrane with an MWCO of 100 kDa was used (GE Healthcare, Chicago, IL, USA; Model: UFP-100-C-5A). It was composed of 520 hydrophilic polysulfone (PS) fibres, with an internal diameter of 0.5 mm, a length of 0.32 m, and a total filtration area of 0.2 m^2. The membrane selected is hydrophilic to enhance the permeation of the soluble proteins, as the extract is aqueous, and to avoid protein denaturation that is prone to occur at the surface of hydrophobic materials. The membrane cleaning products Ultrasil 110 and Ultrasil 75 were purchased from Ecolab (Mississauga, Ontario, Canada) and ethanol (97%) was obtained from Panreac (Barcelona, Spain). For analytical procedures acetone 99.0% and methanol 99.8% were purchased from JMGS (Odivelas, Portugal), chloroform was obtained from Honeywell/Riedel-de Haën (Seelze, Germany) and the Pierce ™ BCA Protein Assay Kit was acquired from Thermo Fisher Scientific (Waltham, Massachusetts, United States).

4.3.2. Membrane processing

In this work, the supernatant from the centrifugation of *Nannochloropsis* sp. disrupted biomass (30 $g_{SFDW}.L^{-1}$) and its dilution, with a dilution (1:3) corresponding to 10 $g_{SFDW}.L^{-1}$, were processed with the selected membrane system, as summarised in **Table 4.1**. The supernatant (30 $g_{SFDW}.L^{-1}$) from the centrifugation of *Nannochloropsis* sp. disrupted biomass was diluted with *Nannochloropsis* sp. culture media, which has a salt concentration similar to seawater (30 $g.L^{-1}$), to a dilution ratio of 1:3. After the dilution, the concentration of the diluted supernatant expressed in salt-free dry weight was 10 $g_{SFDW}.L^{-1}$.

Primarily, the membrane ultrafiltration experiments were conducted in a concentration operation mode, under controlled transmembrane pressure (TMP) conditions, as it is the most commonly reported in the literature (see the scheme of membrane set-up in **Figure 4.1 a**). The membrane filtration unit was constituted of a feed tank (1), a recirculation pump (2), pressure gauges (3), a membrane module (4) and a permeate tank (5). Additionally, the ultrafiltration experiments were also performed in a diafiltration operation mode followed by concentration, under controlled transmembrane pressure conditions (see the scheme of membrane set-up in **Figure 4.1 b**), where a water tank (6) and a peristaltic pump, for water feed, were added. The value of transmembrane pressure was set as 0.2 bar (see **Table 4.1**) to preserve mild operating conditions.

As shown in **Table 4.1**, three experiments were also performed under controlled permeate flux conditions, where the permeate flux was fixed and the TMP was allowed to vary. The membrane set-up for the controlled permeate flux experiments was similar to the preceding one (set-up for the controlled TMP experiments), both for concentration and diafiltration operation modes (see the scheme of membrane set-up in **Figure 4.1 c)** and **d)**, respectively). When operating under controlled permeate flux, its value was imposed by introducing a positive displacement pump (5) in the permeate circuit, which controls and defines the permeate flux, as presented in **Figure 4.1 c)** and **d)**. The value of permeate flux was set at 12 $L.m^{-2}.h^{-1}$ (see **Table 4.1**). This value was selected after preliminary experiments, which showed that at this flux no increase of transmembrane pressure occurs (sub-critical, sustainable flux conditions).

Table 4.1. Scheme of the ultrafiltration experimental studies conducted

Experiment	Feed total concentration ($g_{SFDW}.L^{-1}$)	Operation mode	Operating conditions	TMP (bar)	J_v ($L.m^{-2}.h^{-1}$)
Exp.1	30	Concentration	Controlled transmembrane pressure	0.2	
Exp.2	10	Concentration		0.2	
Exp.3	30	Diafiltration + Concentration		0.2	
Exp.4	30	Concentration	Controlled permeate flux		12
Exp.5	10	Concentration			12
Exp.6	30	Diafiltration + Concentration			12

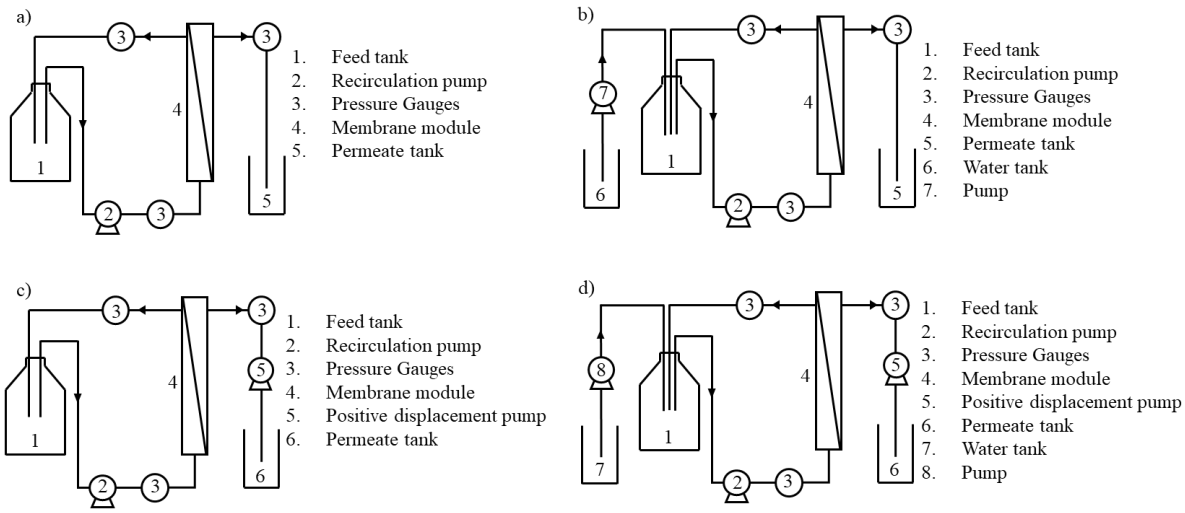

Figure 4.1. Representation of the ultrafiltration membrane unit during the experiments performed under different operating modes and conditions: (a) concentration operation mode, under controlled transmembrane pressure; (b) diafiltration operation mode followed by concentration, under controlled transmembrane pressure; (c) concentration operation mode, under controlled permeate flux; (d) diafiltration operation mode followed by concentration, under controlled permeate flux.

In each membrane experiment, the feed was pumped from the feed tank through the membrane module using a peristaltic pump and recirculated to the feed tank, with a cross-flow velocity of 0.25 $m.s^{-1}$. The feed reservoir was filled with 1.5 ± 0.5 L of protein aqueous extract at 20 °C and pH 6.7 ± 0.1. The permeate was collected in the permeate tank and the permeate flux was monitored by mass acquisition using an electronic balance (Kern 572, Kern, Germany). For the ultrafiltration in a diafiltration operation mode, the diafiltration volume D (-) was calculated through **Eq. 4.**1:

$$D = \frac{V_{water\ added}}{V_{feed}} \qquad \textbf{Eq. 4.1}$$

where $V_{water\ added}$ (L) is the volume of the water (diafiltration solvent) added and V_{feed} (L) is the volume of the feed. For the ultrafiltration process operated in a concentration operation mode, the concentration factor, CF (-), was determined according to **Eq. 4.**2:

$$CF = \frac{m_{t0}}{m_{t0} - m_{permeate}} \qquad \textbf{Eq. 4.2}$$

where m_{t0} (kg) represents the mass in the feed compartment at the beginning of the experiment and $m_{permeate}$ (kg) is the permeate mass collected during a given period.

The volumetric permeate flux, permeance, apparent rejection of soluble proteins, and percentage of soluble protein recovered in the permeate were calculated during the membrane ultrafiltration experiments.

The volumetric permeate flux *Jv* (L.m^{-2}.h^{-1}) was calculated according to **Eq. 4.**3:

$$J_v = \frac{m_{permeate}}{\rho . A . t} \quad \textbf{Eq. 4.3}$$

where $m_{permeate}$ (kg) is the mass of permeate, ρ (kg.m^{-3}) is the density of the permeate, A (m^2) is the total membrane filtration area, and t (h) is the time of permeation. The permeance L_p (L.m^{-2}.h^{-1}.bar^{-1}) was calculated through **Eq. 4.**4:

$$Lp = \frac{J_v}{TMP} \quad \textbf{Eq. 4.4}$$

where *Jv* (L.m^{-2}.h^{-1}) is the volumetric permeate flux and *TMP* (bar) is the transmembrane pressure. In each test (controlled transmembrane pressure concentration/diafiltration and controlled permeate flux concentration/diafiltration), the global apparent rejection of a target compound R_i (%) and the percentage of soluble protein recovered in the permeate were calculated during the filtration experiments through **Eq. 4.**5 and **Eq. 4.**6, respectively:

$$R_i(\%) = 1 - \frac{C_{i,perm}}{C_{i,feed}} \quad \textbf{Eq. 4.5}$$

$$\%\ Recover_{s.protein} = \frac{m_{s.protein,perm}\ (t)}{m_{s.protien,feed}\ (t0)} \quad \textbf{Eq. 4.6}$$

where in **Eq. 4.**5**,** $C_{i,perm}$ (g.L^{-1}) is the concentration of the target compound in the collected permeate and $C_{i,feed}$ (g.L^{-1}) is the concentration of the same compound in the feed (retentate) compartment, and in **Eq. 4.**6, $m_{s.protein,perm}$ (t) (g) is the mass of soluble protein in the permeate compartment at a defined time of the experiment (t) and $m_{s.protein,feed}$ (t_0) (g) is the mass of soluble protein in the feed compartment at the initial time of the experiment.

The soluble protein loss was defined as the soluble protein that is not recovered in the permeate for each experiment and was evaluated through a soluble protein mass balance, as shown in, **Eq. 4.**7:

$$m_{s.protein,feed}\ (t0) = m_{s.protein,perm}\ (t_F) + m_{s.protein,reten}\ (t_F) + m_{s.protein,accum}\ (t_F) \qquad \textbf{Eq. 4.7}$$

where $m_{s.protein,feed}\,(t_0)$ (g) is the mass of soluble protein in the feed compartment at the initial time of the experiment, $m_{s.protein,perm}\,(t_F)$ (g) is the mass of soluble protein recovered in the permeate at the end of the experiment, $m_{s.protein,reten}\,(t_F)$ (g) is the mass of soluble protein in the retentate at the end of the experiment, and $m_{s.protein,accum}\,(t_F)$ (g) is the soluble protein adsorbed/accumulated on the membrane surface and/or pores (surface intra-pore fouling).

The fouling phenomena, defined as the undesirable adsorption/deposition of dissolved solutes or suspended particles, was evaluated through the resistance-in-series model [158]:

$$J_v = \frac{TMP}{\eta . R_{total}} \ll\gg R_{total} = \frac{TMP}{\eta . J_v} \qquad \textbf{Eq. 4.8}$$

where in **Eq. 4.**8 Jv (m.s^{-1}) is the volumetric permeate flux, TMP (Pa) the transmembrane pressure, η (Pa.s) the dynamic viscosity of the permeate (we considered the water viscosity at 20 °C, 1.002 × 10^{-3} Pa.s, since we are dealing with an aqueous extract), and R_{total} (m^{-1}) represents the total resistance. We considered that the total resistance R_{total} (m^{-1}) results from a series of resistances introduced by the intrinsic membrane resistance R_m (m^{-1}) and the resistance caused by the fouling, which may comprise two distinct contributions: R_{rev} (m^{-1}), standing for the resistance that disappears when the pressure across the membrane is released and pure water is passed through the system at the end of the experiment, removing unbounded solutes from the membrane surface - i.e., reversible fouling resistance; R_{irrev} (m^{-1}), the resistance that is only removed when a cleaning cycle using chemical agents is applied, removing the compounds chemically bonded to the membrane - i.e., irreversible fouling resistance. Therefore, the total resistance was calculated through the following equation :

$$R_{total} = R_m + R_{rev} + R_{irrev} \qquad \textbf{Eq. 4.9}$$

The resistance that the membrane offers to the permeation of pure water, R_m (m^{-1}), was calculated through the hydraulic permeance measured at the beginning of each experiment:

$$R_m = \frac{1}{Lp_w . \eta_w} \qquad \textbf{Eq. 4.10}$$

where Lp_w (m.Pa^{-1}.s^{-1}) is the hydraulic permeance and η_w (Pa.s) is the viscosity of water at 20 °C (1.002 × 10^{-3} Pa.s).

To estimate the remaining resistances, as mentioned above (**Eq. 4.**9), the total resistance, R_{total} (m^{-1}) was calculated at the end of each *Nannochloropsis* sp. supernatant filtration experiment, using the last measured value of volumetric permeate flux, Jv ($m.s^{-1}$), and $R_m + R_{irrev}$ (m^{-1}) values were obtained through the volumetric flux of water, measured after a flush with pure water (20 °C) to eliminate reversible fouling. By subtracting $R_m + R_{irrev}$ (m^{-1}) from R_{total} (m^{-1}), it was then possible to calculate R_{rev} (m^{-1}) and compute R_{irrev} (m^{-1}), subtracting the known parameters, R_m (m^{-1}) and R_{rev} (m^{-1}), from the total resistance R_{total} (m^{-1}).

4.3.3. Membrane cleaning

In order to achieve reproducible membrane experiments, after membrane cleaning the hydraulic permeance was measured. The hydraulic permeance measured with deionized water at 20 °C before the experiments was 221 ± 3 L/ (m^2 h bar). After each trial, the membrane was cleaned, using a pre-established cleaning cycle to recover the initial hydraulic permeance. The cleaning procedure comprised the following steps: use of an alkaline solution (at 45 ± 2 °C) with a concentration of 0.5% (w/w) of Ultrasil 110 recirculated for 30 min, to remove organic fouling; then, an acid solution of Ultrasil 75 with a concentration of 0.03% (w/w) recirculated for 30 min (at 45 ± 2 °C), to remove the inorganic fouling; the last step consisted of circulating ethanol (at 45 ± 2 °C) for 20 min with a concentration of 70% (v/v), to recover the hydrophilicity of the membrane surface and restore the water permeability [159]. Between these different cleaning operations and steps, the membrane was flushed with deionized water until the pH was stabilized at 7 and a negligible conductivity was reached.

4.3.4. Dry weight and salinity quantification

The dry weight of each sample was determined by weight difference before and after water evaporation. The drying program was run at 105 °C until a constant weight was achieved in a moisture analyser (Kern DBS 60-3, Kern, Germany). To determine the salt present in the sample, a salinity refractometer (Kern ORA 1SA, Kern, Germany) was used.

4.3.5. Protein quantification

Total protein quantification of the different samples was performed using Pierce™ BCA Protein Assay Kit (Thermo Scientific) [160]. The calibration curves and quantification assays were performed

according to the supplier's instructions. Also, the soluble protein quantification was performed after centrifugation (14,000 x g for 15 min) of each sample to precipitate the membrane proteins that remain attached to cellular debris. The protein that remain in the supernatant after centrifugation was considered soluble protein and analysed through the Bicinchoninic Acid (BCA) assay [161].

4.3.6. Total lipids quantification

The total lipid content was extracted with a solvent mixture 1:1 methanol: chloroform, as described by Ryckebosch *et al.* [108]. Briefly, 100 mg of previously lyophilized samples were mixed with 4 mL of methanol. Chloroform (2 mL) and water (0.4 mL) were then added and the sample was vortex mixed for 45 s. Chloroform (2 mL) and water (2 mL) were added again and the sample was vortex mixed for another 45s. After that, the sample was centrifuged (4,000 × g for 10 min). The upper layer was reserved in a clear tube and the remaining pellet was re-extracted with 4 mL of methanol: chloroform 1:1. The centrifugation step was repeated and the solvent layers were passed through a layer of anhydrous sodium sulphate. Afterwards, the solvent was removed by rotary evaporation and the lipid content was determined gravimetrically.

4.3.7. Chlorophyll *a* quantification

The quantification of chlorophyll *a* was performed through spectrophotometric analysis. Briefly, 1 mg of a freeze-dried sample was mixed with 4 mL 99.0% acetone and vortex mixed for 60 s. Then, the sample was centrifuged at 4,000 x g (for 10 min, 5 °C). The extracted chlorophyll *a*, recovered in the supernatant, was analysed by spectrophotometry (Genesys 10S UV-VIS) and the chlorophyll *a* content was determined according to Eq. 4.11 proposed by Ritchie *et al.* [162] for two different wavelengths:

$$Chl\ a\ (\mu g.mL^{-1}) = -1.7858 \times A_{647} + 11.8668 \times A_{664} \quad \textbf{Eq. 4.11}$$

4.4. Results and Discussion

The analysis of the results obtained is focused here on the ultrafiltration process, after centrifugation of disrupted *Nannochloropsis* sp. biomass. In the first section, characterization of the supernatant from the centrifugation of disrupted *Nannochloropsis* sp. biomass is presented. Subsequently, in the second

section, results from the experimental work performed with ultrafiltration/diafiltration are presented and discussed.

4.4.1. *Nannochloropsis* sp. supernatant characterisation

The disrupted (> 90% disintegration) *Nannochloropsis* sp. biomass (100 $g_{SFDW}.L^{-1}$) was centrifuged and the supernatant was collected and analysed in terms of the salt-free dry weight, proteins, lipids, and chlorophyll *a*. The supernatant samples, used as feed solutions for filtration experiments without dilution, presented on average a salt-free dry weight of 30.2 ± 0.8 $g.L^{-1}$. The supernatant samples' characterization (**Table 4.2**) revealed that 83% of the proteins (*w/w* total proteins) present in the supernatant were soluble. The total lipids analysis revealed that the supernatant contains 4.37 ± 0.22 $g.L^{-1}$ of lipids, on average. The *Nannochloropsis* sp. used in the present study was grown under N-replete conditions; lipids were mainly present in the form of polar lipids (glycolipids and phospholipids), which are crucial to preserving cell-membrane integrity [149]. These lipid classes are expected to have interactions with cytoskeletal proteins [148] that are responsible for the structural organization of the cell and to ensure several cellular processes (e.g., cell division, motility, and contractility) [163]. Therefore, some of the polar lipids attached to cytoskeletal proteins might remain in the aqueous supernatant.

Table 4.2. Supernatant composition in terms of proteins, lipids, and chlorophyll *a*. Results are based on the average of six supernatant samples, used as feed solutions for each membrane experiment.

Total Protein ($g.L^{-1}$)	8.77 ± 0.37
Soluble Protein ($g.L^{-1}$)	7.28 ± 0.58
Insoluble Protein ($g.L^{-1}$)	1.48 ± 0.27
Total Lipids ($g.L^{-1}$)	4.37 ± 0.60
Chlorophyll *a* ($g.L^{-1}$)	0.08 ± 0.02

4.4.2. Ultrafiltration performance

During the ultrafiltration experiments, different operation modes (concentration and diafiltration) and operating conditions were compared (controlled transmembrane pressure, TMP, and controlled permeate flux). In an ultrafiltration process under controlled TMP, the transmembrane pressure is fixed and the flux is allowed to evolve, declining as the membrane fouls. On the other hand, ultrafiltration

under controlled permeate flux allows for the precise control of convective transport toward the membrane surface [164], making it possible to adjust the viscous force near the membrane [165]. If the controlled permeate flux is imposed assuring a sustainable flux (subcritical conditions), membrane fouling is avoided, or at least, minimized. In fact, unlike the controlled permeate flux operation, the controlled transmembrane pressure operation is more prone to causing severe fouling phenomena, with a typical trend for high initial permeate flux, followed by a drastic reduction [154].

The performance of the ultrafiltration/diafiltration process for both operating conditions is presented below.

4.4.2.1. Volumetric Flux and Permeance

The results of the volumetric flux (*Jv*) obtained while maintaining a controlled transmembrane pressure at 0.2 bar or a controlled permeate flux of around 12 $L.m^{-2}.h^{-1}$, are presented in **Figure 4.2**. The volumetric flux decreases rapidly at the beginning of the process for the ultrafiltration under controlled TMP, from higher than 8 $L.m^{-2}.h^{-1}$ (the permeate flux decline is extremely fast in the beginning and after 5 min, required to measure the permeate flux, this value is already significantly lower than its initial clean water flux) to 4 $L.m^{-2}.h^{-1}$. This behaviour is a consequence of the intensive fouling that occurs at the start of a constant TMP ultrafiltration operation [164]. These results are comparable with those obtained by Safi *et al*. [1], where the permeate flow rate decreases at the beginning of the ultrafiltration process, using a 300 kDa MWCO membrane under a constant TMP of 2.07 bar. The ultrafiltration process under controlled permeate flux (**Figure 4.2 B**) is known to provide milder operating conditions when compared to the ultrafiltration process under controlled TMP (**Figure 4.2 A**), allowing to maintain a higher value of volumetric flux, at around 12 $L.m^{-2}.h^{-1}$, during the entire process. When working under controlled permeate flux the operator determines the convective transport conditions of the feed stream towards the surface of the membrane. This means that the operator allows a defined mass flux of feed across the membrane, avoiding the situation that occurs during controlled transmembrane pressure operation where a very high mass flux of feed might occur during the initial period of operation (when the membrane is still clean and not fouled). As a consequence, a wise choice of permeate flux, imposed and controlled by the operator, allows for working under sub-critical (or sustainable) permeate flux conditions, minimizing fouling and thus extending operation under manageable permeate flux values. The value of 12 $L.m^{-2}.h^{-1}$, selected for the imposed permeate flux, was based on previous experience on the processing of biological media (data not shown here).

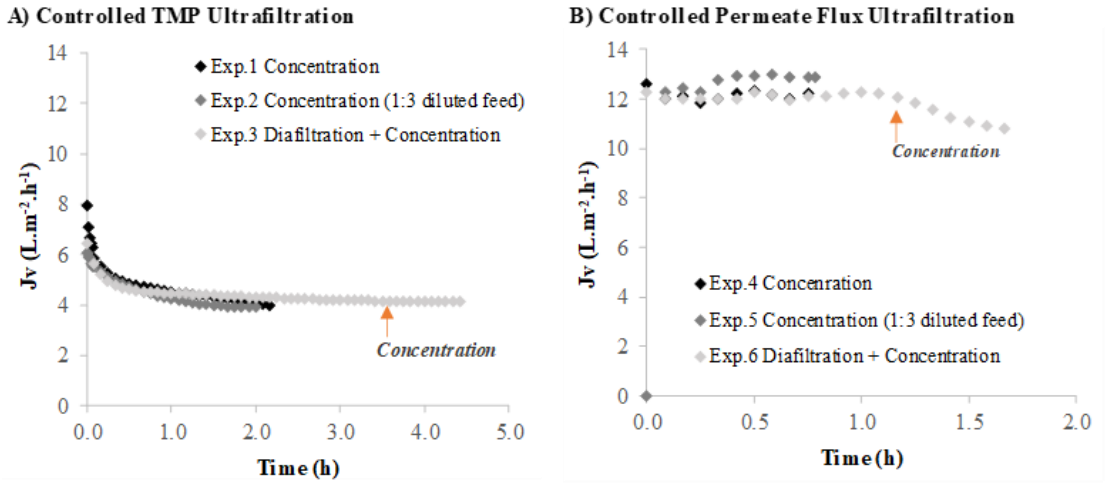

Figure 4.2. Volumetric flux plotted against operating time during *Nannochloropsis* sp. supernatant ultrafiltration. (A) Controlled TMP experiments: Exp.1 - ultrafiltration in a concentration operation mode; Exp.2 - ultrafiltration in a concentration operation mode using a diluted feed; Exp.3 - ultrafiltration in a diafiltration operation mode. (B) Controlled permeate flux experiments: Exp.4 - ultrafiltration in a concentration operation mode; Exp.5 - ultrafiltration in a concentration operation mode using a diluted feed; Exp.6 - Ultrafiltration in a diafiltration operation mode.

Similar to the volumetric flux (**Figure 4.2 A**), the membrane calculated permeance, considering the osmotic pressure difference as negligible, followed the same trends for the controlled TMP experiments (**Figure 4.3 A**). The selection of an ultrafiltration process under controlled permeate flux provides better results in terms of the process operating performance. Still, it should be noted that even with a gentle permeate flux of 12 $L.m^{-2}.h^{-1}$ (experiments 4 and 5), the transmembrane pressure increased due to some fouling, and consequently, the permeance decreased.

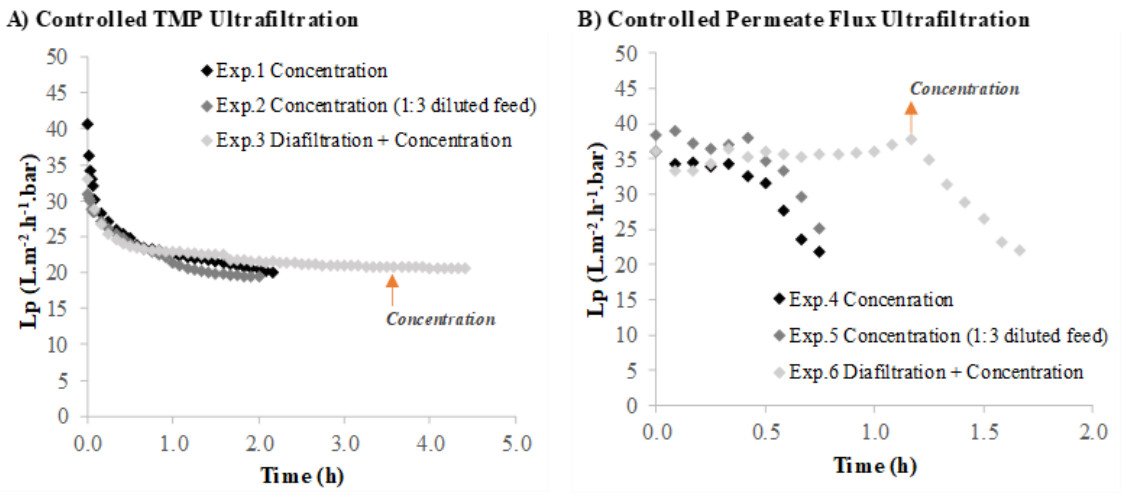

Figure 4.3. Membrane permeance plotted against operating time during *Nannochloropsis* sp. supernatant ultrafiltration. (A) Controlled TMP experiments: Exp.1 - ultrafiltration in a concentration operation mode; Exp.2 - ultrafiltration in a concentration operation mode using a diluted feed; Exp.3 - ultrafiltration in a diafiltration operation mode. (B) Controlled permeate flux experiments: Exp.4 - ultrafiltration in a concentration operation mode; Exp.5 - ultrafiltration in a concentration operation mode using a diluted feed; Exp.6 - ultrafiltration in a diafiltration operation mode.

4.4.2.2. Soluble protein recovery and permeate characterisation

The effects of different operation modes (concentration/diafiltration) and operating conditions (controlled TMP and controlled permeate flux) on the recovery of soluble protein in the permeate can be observed in **Table 4.3 A** and **B**, as calculated by **Eq. 4.6** (see **section 4.3**). The experiments under controlled permeate flux exhibit higher values of protein recovery in the permeate (between 44% and 62% for concentration mode and 78% for diafiltration mode) than the experiments conducted under controlled TMP (between 35% and 40% for concentration mode and 58% for diafiltration mode). The lower protein recovery obtained for controlled TMP experiments is related to the more severe fouling [164] associated with these process operating conditions, as it is known that fouling can act in the selectivity/rejection of solutes during the filtration process [154].

Table 4.3. Recovery of *Nannochloropsis* sp. soluble proteins in the permeate and soluble proteins rejection. A) Controlled TMP experiments: Exp.1 - ultrafiltration in a concentration operation mode; Exp.2 - ultrafiltration in a concentration operation mode of a diluted feed; Exp.3 - ultrafiltration in a diafiltration operation mode. B) Controlled permeate flux experiments: Exp.4 - ultrafiltration in a concentration operation mode; Exp.5 - ultrafiltration in a concentration operation mode of a diluted feed; Exp.6 - ultrafiltration in a diafiltration operation mode. Results are based on two replicates for each sample protein analysis. Note: the percentage of soluble protein recovered in the permeate plus the soluble protein rejected (in the retentate) does not reach 100%; this difference is attributed to protein adsorbed by the membrane.

(A) Controlled TMP Experiments

	Exp.1 Concentration	Exp.2 Concentration (1:3 diluted feed)	Exp.3 Diafiltration + Concentration
Soluble Protein Recovery (%)	35.0 ± 0.4	40.0 ± 1.5	58.0 ± 2.0
Soluble Protein Rejection (%)	57.0 ± 0.5	50.0 ± 1.8	37.0 ± 2.1

(B) Controlled Permeate Flux Experiments

	Exp.4 Concentration	Exp.5 Concentration (1:3 diluted feed)	Exp.6 Diafiltration + Concentration
Soluble Protein Recovery (%)	44.0 ± 4.1	66.0 ± 1.9	78.0 ± 0.4
Soluble Protein Rejection (%)	49.0 ± 4.2	26.0 ± 2.3	19.0 ± 0.4

The results obtained in terms of protein recovery during the diafiltration under controlled TMP are slightly lower than those obtained by Balti *et al*. [166], during the diafiltration of soluble proteins from Spirulina. The author reported a 64% recovery of soluble proteins in the permeate, using a 150 kDa ceramic membrane at a fixed TMP of 4 bar. It is also important to note that the author applied two more diavolumes (a total of five) than those applied during the diafiltration described in the present work (a total of three), which might have contributed to a slightly higher protein recovery.

The mass balance for soluble proteins (**Table 4.4**) also reinforces the association of lower soluble protein recovery with more severe fouling, due to soluble protein adsorption. The experiments under controlled TMP exhibit higher soluble protein losses due to adsorption ($OUT_{Adsorbed}/IN_{Feed}$) to the membrane during the filtration process (between 42 ± 0.4% and 35 ± 1.5% for concentration mode and 37 ± 2.0% for diafiltration mode), than the experiments under controlled permeate flux (between 37 ± 2.7% and 13 ± 2.6% for concentration mode and 7 ± 0.4% for diafiltration mode). These results also confirm that it is easier to clean a membrane after operation under controlled permeate flux than under controlled TMP.

Table 4.4. Mass balance of soluble proteins. (A) Controlled TMP experiments: Exp.1 - ultrafiltration in concentration mode; Exp.2 - ultrafiltration concentration mode of a diluted feed; Exp.3 - ultrafiltration in diafiltration + concentration mode. (B) Controlled permeate flux experiments: Exp.4 - ultrafiltration in concentration mode; Exp.5 - ultrafiltration in concentration mode of a diluted feed; Exp.6 - ultrafiltration in diafiltration + concentration mode. Results are based on 2 replicates for each sample protein analysis. (*) calculated through the subtraction of $\Sigma OUT_{Permeate+Retentate}$ (g) from IN_{Feed} (g).

(A) Controlled TMP Experiments

	Exp.1 Concentration	Exp.2 Concentration (1:3 diluted feed)	Exp.3 Diafiltration + Concentration
IN_{Feed} (g)	15.62 ± 0.20	5.40 ± 0.10	7.30 ± 0.06
$OUT_{Permeate}$ (g)	5.49 ± 0.13	2.16 ± 0.12	4.26 ± 0.18
$OUT_{Retentate}$ (g)	3.53 ± 0.05	1.33 ± 0.02	0.34 ± 0.02
$\Sigma OUT_{Permeate+Retentate}$ (g)	9.02 ± 0.18	3.49 ± 0.14	4.60 ± 0.20
$OUT_{Adsorbed}$ (g) (*)	6.60 ± 0.02	1.91 ± 0.04	2.71 ± 0.14
$OUT_{Adsorbed}$ (%)	42.27 ± 0.44	35.37 ± 1.47	37.05 ± 2.01

(B) Controlled Permeate Flux Experiments

	Exp.4 Concentration	Exp.5 Concentration (1:3 diluted feed)	Exp.6 Diafiltration + Concentration
IN_{Feed} (g)	12.80 ± 0.60	5.52 ± 0.18	10.35 ± 0.03
$OUT_{Permeate}$ (g)	5.62 ± 0.83	3.40 ± 0.01	7.96 ± 0.04
$OUT_{Retentate}$ (g)	2.45 ± 0.03	1.41 ± 0.01	1.40 ± 0.03
$\Sigma OUT_{Permeate+Retentate}$ (g)	8.07 ± 0.86	4.81 ± 0.01	9.58 ± 0.07
$OUT_{Adsorbed}$ (g) (*)	4.73 ± 0.26	0.71 ± 0.17	0.77 ± 0.04
$OUT_{Adsorbed}$ (%)	36.95 ± 2.71	12.93 ± 2.61	7.42± 0.40

The results presented in **Table 4.3 A** and **B** show that the diafiltration experiments lead to higher soluble protein recovery in the permeate. A comparison of the two diafiltration experiments (Exp.3 - under controlled TMP and Exp.6 - under controlled permeate flux) is shown in **Figure 4.4 A** and **B**. Comparison of these two experiments reveals that the soluble protein recovery is higher among all diafiltration volumes when the experiment is operated under controlled permeate flux (**Figure 4.4 A**). **Figure 4.4 B** shows that the diafiltration + concentration under controlled permeate flux presents clear advantages over the diafiltration + concentration under controlled TMP, not only in terms of soluble protein recovery in the permeate (58% for Exp.3 - under controlled TMP and 78% for Exp.6 - under controlled permeate flux) but also in the reduction of the overall process time.

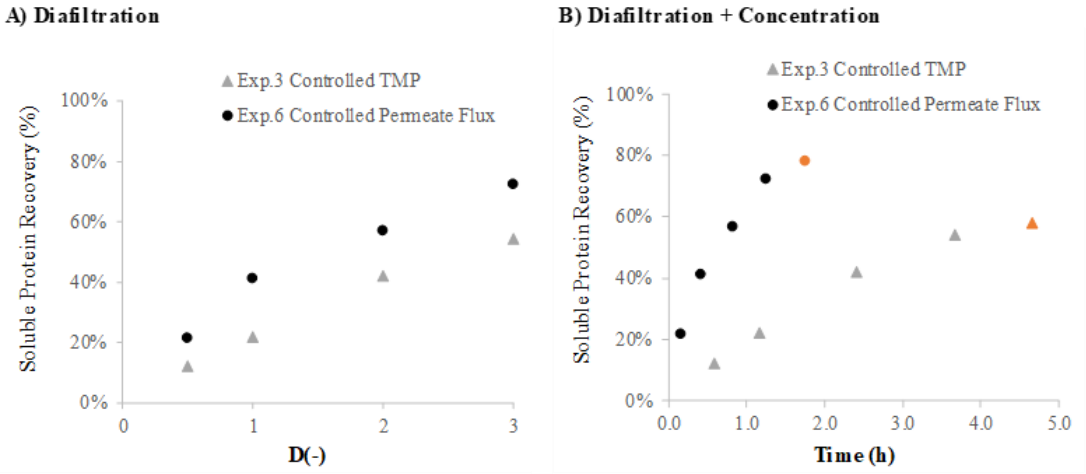

Figure 4.4. Recovery of *Nannochloropsis* sp. proteins in the permeate expressed as % (*w/w* soluble proteins in the permeate). (A) Ultrafiltration in diafiltration mode: protein recovery (%) against the D (-) diafiltration volume; Exp.3 - diafiltration under controlled TMP; Exp.6 - diafiltration under controlled permeate flux. (B) Ultrafiltration in diafiltration mode followed by a concentration step (Exp.3 concentration step (▲) and Exp.6 concentration step (●)) with protein recovery (%) against process time (h); Exp.3 - diafiltration under controlled TMP; Exp.6 - diafiltration under controlled permeate flux.

The characterization of the permeates after each trial shows that, for all the experiments, insoluble proteins, lipids, and chlorophyll *a* were retained in the retentate (**Table 4.5**), which is comparable with the results obtained in other ultrafiltration studies [1]. Polysaccharides may have been retained, according to other studies [167], as expected given their large molecular weights. Chlorophyll *a* retention may be explained by its adsorption to small hydrophobic cell debris that remained in the supernatant but are larger than the membrane pores. The results obtained in terms of chlorophyll *a* retention are comparable with those reported by Safi *et al.* [1], using a 300 kDa PES membrane, operated under a controlled TMP. The author reported that the chlorophyll present in a *Nannochloropsis gaditana* supernatant was fully retained, and associated the result with the fact that chlorophyll was present in lipid droplets that were larger than the membrane cut-off. The results presented in **Table 4.5** also show that the lipids present in the supernatant were highly retained which might have contributed to the retention of chlorophyll *a*.

Table 4.5. Feed and permeate compositions in terms of insoluble proteins, lipids, and chlorophyll *a*. (A) Non-diluted feed experiments: under controlled TMP (Exp.1 concentration mode and Exp.3 diafiltration + concentration mode), and under controlled permeate flux (Exp. 4 concentration mode and Exp.6 diafiltration + concentration mode). (B) Diluted feed experiments: under controlled TMP (Exp.2 concentration mode), and under controlled permeate flux (Exp.5 concentration mode). The results for the permeates from each experiment are based on two replicates for each sample analysis.

(A) Non-Diluted Feed Experiments

		Permeate			
		Controlled TMP		Controlled Permeate Flux	
	Feed	Exp.1 Concentration	Exp.3 Diafiltration + Concentration	Exp.4 Concentration	Exp.6 Diafiltration + Concentration
Insoluble Proteins ($g.L^{-1}$)	1.48 ± 0.27	ND (1)	ND (1)	ND (1)	ND (1)
Total Lipids ($g.L^{-1}$)	4.37 ± 0.61	0.47 ± 0.05	0.61 ± 0.05	0.47 ± 0.05	0.50 ± 0.05
Chlorophyll *a* ($g.L^{-1}$)	0.08 ± 0.02	ND (2)	ND (2)	ND (2)	ND (2)

(B) Diluted Feed (1:3) Experiments

		Permeate	
		Controlled TMP	Controlled Permeate Flux
	Feed	Exp.2 Concentration	Exp.5 Concentration
Insoluble Proteins ($g.L^{-1}$)	0.50 ± 0.13	ND (1)	ND (1)
Total Lipids ($g.L^{-1}$)	1.53 ± 0.13	0.20 ± 0.05	0.18 ± 0.05
Chlorophyll *a* ($g.L^{-1}$)	0.04 ± 0.01	ND (2)	ND (2)

This is a very interesting result since the green colour is a major drawback for certain food applications. These results are important not only for the soluble protein fraction enrichment but also for what concerns the overall performance of a *Nannochloropsis* biorefinery. The retention of more than 87% of the lipids present in the supernatant, in all the assays, is extremely significant for increasing the overall biorefinery efficiency as the membrane retentate can incorporate the feed stream for a lipid extraction process. The lipids retention can be related to the retention of the insoluble compounds, such as insoluble proteins, but also to the formation of aggregates between lipids and structural proteins [148] with a mass higher than the membrane molecular weight cut-off [167].

4.4.2.3. Fouling and membrane cleaning

Membrane fouling during membrane operation is inevitable, and therefore, the easiness and readiness of membrane cleaning is an important feature that needs to be taken into account for industrial membrane operation. The soluble protein mass balance (presented in **section 4.4.2.2**), hydraulic permeance decrease, and resistance (reversible and irreversible) for the different experiments were analysed to evaluate the possible relationships between the different operating conditions and the easiness/readiness of membrane cleaning. The initial hydraulic permeance $Lp_{w,i}$ (L/(h.m^2.bar)), experimentally determined before each of the ultrafiltration experiments, and the final hydraulic permeance $Lp_{w,f}$ (L/(h.m^2.bar)), determined at the end of each experiment, after a hydraulic flush to remove the layer deposited on the membrane surface (reversible fouling), were evaluated and the results are shown in **Table 4.6**. The experiments under controlled permeate flux exhibit slightly lower values of hydraulic permeance loss, % Lp_w *Loss* ($1 - Lp_{w,f}/ Lp_{w,i}$), than the experiments under controlled TMP. The last permeance values of each experiment with *Nannochloropsis* sp. supernatant Lp_f (L/(h.m^2.bar)) are shown in **Table 4.6**, confirming that experiments under controlled permeate flux can maintain a higher permeance value until the end of the experiment. On the other hand, comparing the diafiltration operation mode with the concentration operation mode (**Table 4.6**), it is notable that after a diafiltration step, the permeance value remains higher than after a concentration step. The difference between the two operation modes becomes even clearer when the operations are performed under controlled permeate flux.

These data indicate that fouling phenomena are more severe in ultrafiltration operated at a concentration mode under controlled TMP, and as a consequence, membrane cleaning might be harder under these conditions. Likewise, the membrane lifetime may be reduced when the ultrafiltration experiments are performed under controlled TMP. Severe fouling during ultrafiltration would occur if the operating conditions selected favoured a strong convective transport of foulant toward the membrane surface and the build-up of high local concentrations of these foulants near the membrane surface. In the particular case studied in this work, the presence of biological material, namely proteins and other biological compounds, represents a severe risk of fouling unless adequate operating strategies are adopted (operation under controlled permeate flux). Therefore, diafiltration followed by a concentration step under controlled permeate flux seems to be the best combination of operation conditions, allowing for lower membrane fouling and easier membrane cleaning.

Table 4.6. Initial hydraulic permeance $Lp_{w,i}$, hydraulic permeance after hydraulic flush at the end of each trial $Lp_{w,f}$, hydraulic permeance loss after each experiment Lp_w *Loss*, and the permeance at the end of each *Nannochloropsis* sp. supernatant filtration. (A) Controlled TMP experiments and (B) Controlled permeate flux experiments. * Permeance value at the end of the diafiltration step and before the concentration step.

(A) Controlled TMP Experiments

	Exp.1	Exp.2	Exp.3	
	Concentration	Concentration (1:3 diluted feed)	Diafiltration	Diafiltration + Concentration
$Lp_{w,i}$ [L/(h.m^2.bar)]	219.6	227.3	218.7	218.7
$Lp_{w,f}$ [L/(h.m^2.bar)]	53.1	49.2	-	53.8
Lp_w *Loss* (%)	76%	78%	-	75%
Lp_f [L/(h.m^2.bar)]	19.9	19.5	21.0 *	20.6

(B) Controlled Permeate Flux Experiments

	Exp.4	Exp.5	Exp.6	
	Concentration	Concentration (1:3 diluted feed)	Diafiltration	Diafiltration + Concentration
$Lp_{w,i}$ [L/(h.m^2.bar)]	221.8	219.8	221.7	221.7
$Lp_{w,f}$ [L/(h.m^2.bar)]	62.1	70.81	-	62.4
Lp_w *Loss* (%)	72%	68%	-	72%
Lp_f [L/(h.m^2.bar)]	21.8	25.2	37.0*	22.1

Furthermore, the results obtained for the calculated resistance due to reversible R_{rev} (m^{-1}) and irreversible fouling R_{irrev} (m^{-1}) for each experiment are shown in **Table 4.5**. Reversible resistance is slightly higher in the experiments under controlled TMP than in the experiments under controlled permeate flux, which is in accordance with other fouling studies [154,168]. This result suggests that it might be easier to clean a membrane, by hydraulic flushing, after ultrafiltration under controlled permeate flux than under controlled TMP. Such a result can be explained by the differences in the deposited layer's thickness. Vyas *et al.* [168] reported that the deposited layer formed on the membrane surface during constant permeate flux experiments was very thin. The experiments under controlled TMP exhibit higher values for the irreversible resistance, which might implicate the increase in frequency (and/or intensity) of chemical cleaning cycles, and consequently, the time devoted to cleaning protocols. The membrane lifetime may also be affected by the higher irreversible fouling experienced in the ultrafiltration process under controlled TMP.

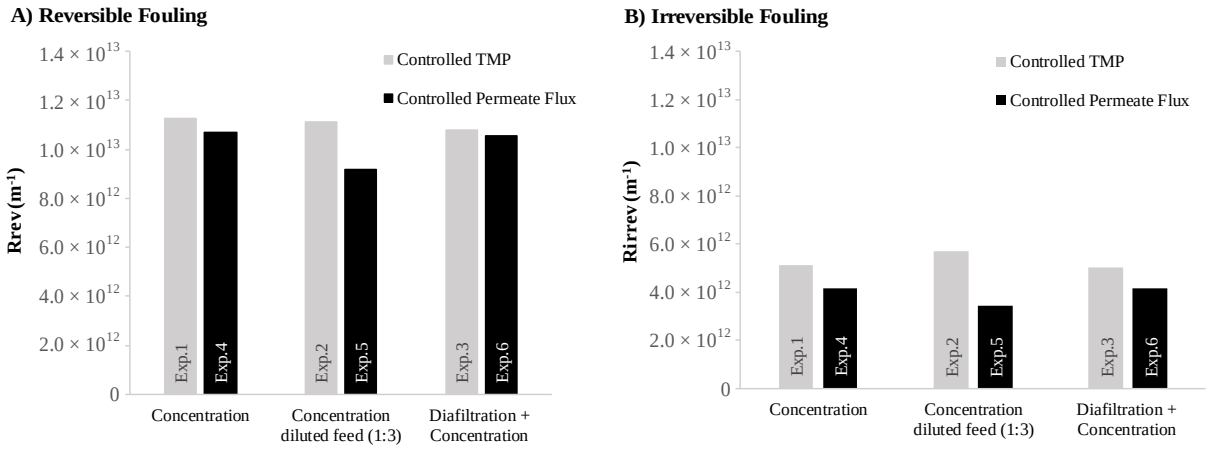

Figure 4.5. Calculated (A) reversible resistance (R_{rev}) and (B) irreversible resistance (R_{irrev}): Controlled TMP experiments compared with controlled permeate flux experiments. Exp.1/ Exp.4 - ultrafiltration in a concentration operation mode; Exp.2/ Exp.5 - ultrafiltration in a concentration operation mode of a diluted feed; Exp.3/ Exp.6 - ultrafiltration in a diafiltration operation mode.

4.5. Conclusions

The ultrafiltration process studied, using a 100 kDa MWCO membrane, resulted in obtaining an enriched protein fraction, free from potentially undesirable contaminants. The results show that the ultrafiltration process operated under controlled permeate flux presents significant advantages over operation under controlled transmembrane pressure: higher permeate flux (12 $L.m^{-2}.h^{-1}$), higher soluble protein recovery (78% in a diafiltration mode), and lower membrane fouling. This work shows that when working under controlled permeate flux, the operator determines the convective transport conditions of the feed stream toward the surface of the membrane. This means that the operator allows a defined mass flux of feed across the membrane, avoiding the situation that occurs during controlled transmembrane pressure operation where a very high-mass flux of feed might occur during the initial period of operation (when the membrane is still clean and not fouled). As a consequence, a wise choice of permeate flux, imposed and controlled by the operator, allows for working under subcritical (or sustainable) permeate flux conditions, minimizing fouling and thus extending the operation under manageable permeate flux values. The combination of ultrafiltration in a diafiltration mode followed by concentration under controlled permeate flux conditions enhances the soluble protein recovery in the permeate and allows a higher value of volumetric flux to be maintained for the entire diafiltration process. This strategy led to an increase in the average flux (3×) and soluble protein recovery (+34%),

along with a decrease in soluble protein rejection (to half of the initial value) and in soluble protein adsorbed to the membrane (to 17% of the initial value). This strategy may be applied to other microalgae in a very straightforward way. It may also apply to membrane processes that suffer from significant membrane fouling, e.g., when the feed solution has lipids and other potential foulants.

5. *NANNOCHLOROPSIS* SP. BIOREFINERY: POLAR LIPIDS EXTRACTION FOR OMEGA-3 EXTRACT PRODUCTION

5.1. Abstract

Nannochloropsis sp. has potential for numerous commercial applications, including producing long-chain omega-3 fatty acids (LC n-3 PUFA) such as eicosapentaenoic acid (EPA, $C_{20:5}$). This valuable fatty acid is vital for various nutraceutical purposes, and its market is continually growing. The bioavailability of n-3 PUFAs in the form of PLs is known to be greater than that of triacylglycerols and ethyl esters [169]. This work has developed and optimised a GRAS solvent methodology to perform a polar lipid extraction from wet *Nannochloropsis* sp. biomass with high efficiency. Firstly, a neutral lipidic fraction was obtained using D-limonene. However, D-limonene extracted almost 20% of the EPA present in the polar fraction, which was not anticipated. Next, in a cascading biorefinery approach, an EPA and polar lipids rich fraction was obtained using ethanol (99.8% *v*/*v*). The ethanol to wet biomass ratio was optimised, and the best results in terms of polar lipid extraction efficiency (81% $wFA_{extracted}/wFA_{available}$) were obtained with a solvent to biomass ratio of 10 $mL.g^{-1}$. Nevertheless, the economic assessment revealed that despite having a lower polar lipid extraction efficiency (71% $wFA_{extracted}/wFA_{available}$), the scenario with a solvent to biomass ratio of 5 $mL.g^{-1}$ was the one with a lower production cost (300 €/kg_{EPA}) for the EPA-rich polar lipid concentrate. A sensitivity analysis to assess the impact of the solvent recovery percentage and the price of the electric energy on the production cost of the EPA was performed and revealed that scenario C (scenario with a solvent to biomass ratio of 5 $mL.g^{-1}$) was the one with the lowest production cost even with an increase of 50% in the electrical energy price (301.5 €/kg_{EPA}) or with a decrease in the solvent recovery percentage to 70% (319.7 €/kg_{EPA}).

5.2. Introduction

Fatty acids are long aliphatic carbon chains, that might vary in the degree of unsaturation, structure, and length, with a terminal carboxylic acid moiety. Long-chain polyunsaturated fatty acids (LC-PUFAs) of C_{20} and C_{22} perform vital functions in the human body [170]. In the past few years, long-chain omega-3 polyunsaturated fatty acids (LC n-3 PUFA) have been associated with healthy lifestyles and attributed with several health benefits [171].

Omega-3 fatty acids such as eicosapentaenoic acid (EPA, $C_{20:5}$) have a significant role in the prevention of major diseases, such as cardiovascular diseases. In addition, they reduce blood pressure [172].

However, it can be challenging to obtain the recommended intake of EPA and DHA through a simple diet alone. The usual omega-3 fatty acid in the western diet is a shorter-chain omega-3 fatty acid (C_{18}), α-linolenic acid (ALA), which is the precursor of EPA and DHA [82]. Although it is possible for the human body to convert ALA to EPA and, consequently, to DHA through elongase and desaturase enzymes, several pieces of research suggest that only a tiny amount can be synthesized in the body through this process [82]. To that end, there is an increased interest in food/nutritional supplements from the general public and also an increased interest from the food industry to enrich the food with omega-3 FA.

Presently, the most commonly used omega-3 PUFA source is fish oil. However, the gradual shortage in global fish stocks and the presence of chemical contaminants (e.g., mercury) are some of the most significant risks associated with this source, which demands the search for other sustainable alternatives [3]. Photosynthetic organisms, including microalgae, are the primary producers of the aquatic ecosystem, and they can produce high amounts of omega-3 fatty acids. Therefore, they have been proposed as the most reliable alternative source to respond to the growing demand for omega-3 PUFA from the market [169].

Microalgae lipids can be classified as two major fractions: polar lipids such as glycolipids and phospholipids, and non-polar lipids (neutral lipids) such as triacylglycerols (TAGs). In most microalgae species, omega-3 PUFAs are present principally in the polar lipid fraction, claimed to be the most efficiently absorbed by the human body [169], which is a great advantage compared with the traditional sources (e.g., TAGs or free fatty acids). Kagan *et al.* [86], observed that within the polar lipids, omega-3 PUFAs are better absorbed in the form of glycolipids than phospholipids: possibly because GLs form smaller micelles than those of PLs during digestive hydrolysis [81]. In addition to the previously mentioned advantage, microalgae can be grown under controlled conditions, allowing the reproducibility of biomass with a pre-determined biochemical composition. Moreover, microalgae oleoresin can incorporate a considerable amount of carotenoids and other antioxidants, improving the nutritional value of the omega-3 PUFA rich microalgae oleoresin and naturally preventing its oxidation [3].

Nannochloropsis sp. (Eustigmatophyta) is a unicellular microalga, found mainly in marine sources, spherical (slightly to ovoid) with a cell diameter of 2-5 μm, and with a robust cell wall composed of a structure consisting of a cellulosic internal wall and a hydrophobic algaenan external layer [49]. Algaenan is a biopolymer, and the algaenan sheet has been defined to be composed of long, straight-chain, saturated aliphatics with ether cross-links [83]. In frequent cases, algaenan is part of a layer called trilaminar layer structure (TLS) [132], which exhibits two high electron density external layers

sandwiching one layer with low electron density [133]. The resistance of the algaenan and their small radius confers a robust cell wall to *Nannochloropsis* sp. cells.

This species is widely known for the production of omega-3 fatty acids, specifically EPA (up to 5% dry biomass, when produced under optimal growth conditions) [33]. *Nannochloropsis* sp. can accumulate lipids up to 50% of the dry biomass when grown under nitrogen deplete conditions (mainly TAGs) [30]; however, that is not reflected in EPA accumulation [83,84]. This long-chain n-3 PUFA is typically found in the cell membrane [85] in the form of polar lipids (phospholipids and glycolipids) [86], which is a great advantage as the human body more efficiently absorbs the polar lipids than triacylglycerides or free fatty acids [169]. Moreover, *Nannochloropsis* sp. has only violaxanthin and chlorophyll *a* as its primary pigments [83].

Although there is a great interest in extracting EPA from microalgal biomass, the methods currently used on a large scale for extraction of lipids, such as supercritical CO_2, are still not considered optimised methods. The drawbacks are mainly due to the great heterogeneity of microalgal lipids (e.g., different lipid class percentages according to the cultivation conditions), and the morphological variety (e.g., cell wall permeability) [81]. Over the last decades, chloroform/ methanol solvent mixture [173], as reported by the methods of Bligh & Dyer [174] and Folch [175], was the most commonly used solvent system to extract total lipids (TLs) from microalgal biomass with high efficiency [176]. However, the toxic nature of these solvents makes them unsuitable for large-scale lipid extraction processes targeting high-value applications [177].

Besides the safety issues (toxicity, flammability, etc.) of the solvents used in the mentioned methods, most of the studies regarding microalgae lipid extraction are often applied to dry biomass [178]. Unfortunately, the drying process is a process that requires high energy and may represent a significant percentage (about 85%) of the entire energy expended in the extraction step [179]. It is known that significant economic issues associated with the lipid extraction process are related to the high-water content of the harvested biomass (about 70-80% of water). The extraction process can be affected by the high-water content, as some organic solvents (especially non-polar) have difficulties penetrating the water barrier to extract intracellular lipids. To overcome this problem, pre-treatments such as bead milling can be applied to increase the accessibility of the solvent through cell disruption which is often called the wet route extraction [180]. The wet route extraction has been investigated in the past few years. Chen *et al*. [60] extracted lipids from wet *Nannochloropsis* sp. biomass at high temperature and pressure. Yang *et al*. [181] investigated lipid extraction with ethanol from wet *Picochlorum* sp. and *Chlorella* sp. biomass at room temperature, obtaining lipid extraction yields similar to those of the Bligh & Dyer method.

So far, several solvent mixtures of non-polar solvents and polar solvents have been studied for the extraction of lipids from microalgae, and some examples are: hexane/ methanol (3:2), hexane/ isopropanol (3:2), hexane/ ethanol (2:1), dichloromethane/ methanol (2:1). Balasubramanian *et al.* [182], reported that the extraction efficiency of dichloromethane/ methanol was almost as good as chloroform/ methanol. Ryckebosch *et al.*[183], studied different solvent systems, and reported that the best results were achieved with dichloromethane/ ethanol (92% $w/w_{total\ lipids}$), hexane/ isopropanol (58% $w/w_{total\ lipids}$) and ethanol systems (52% $w/w_{total\ lipids}$). Excluding the halogenated systems, extraction with ethanol gave the highest extraction yield, suggesting that it could be a good candidate for lipid extraction within a biorefinery concept. Additionally, being a polar solvent might allow focusing the extraction in the polar lipids, which is the product of interest for producing an EPA omega-3 oleoresin. However, direct extraction using polar solvents, such as ethanol or methanol, might involve the joint extraction of neutral lipids and polar lipids [81]. Ethanol is a polar solvent and it is considered a cheap and safe solvent and has a sturdy affinity to the lipid complex, which suggests that lipids can be removed efficiently [61]. Moreover, ethanol is accepted as a safe and eco-friendly solvent, therefore, the residual biomass could be used for feed or food ingredients after lipid extraction [184].

Aiming to achieve an EPA rich polar lipid fraction, Callejón *et al.* [81], studied the sequential extraction of saponifiable lipids from *Nannochloropsis* sp. biomass. The extraction of neutral lipids from the original biomass was performed with hexane and the extraction of EPA-rich polar lipids from the previously extracted biomass was performed with ethanol (96% *v*/*v*) [81]. However, n-hexane, which is one of the main constituents of the extraction grade hexane, is registered under REACH Regulation as category 2 reprotoxic and as category 2 aquatic chronic toxic. Therefore, the research for greener and safe solvents has become a major concern not only for academic but also for industrial research [56]. The replacement of n-hexane by bio-solvents such as terpenes has been investigated as an alternative to organic solvent extraction for the extraction of oil from oil-containing materials [58]. D-limonene is a low toxicity biodegradable terpene present in agricultural wastes derived from citrus peels, which have been investigated as an alternative to organic solvents in the extraction of neutral lipids [57].

The main objective of this study was to define an eco-friendly solvent methodology to perform a lipid extraction from wet microalgae biomass with high efficiency. In the first part of the study, a sequential extraction of lipids from *Nannochloropsis* sp. for the production of EPA-rich polar lipids concentrate was investigated. The sequential extraction of lipids was performed with low-toxicity solvents: (i) extraction of neutral lipids (NLs) from the original biomass using D-limonene and (ii) extraction of EPA-rich polar lipids (PLs) from the previously extracted biomass using ethanol. To the best of our knowledge, no studies about the application of D-limonene and ethanol in lipid extraction from wet

Nannochloropsis sp. biomass at room temperature and pressure have been reported. Also, the optimisation of the solvent to biomass ratio for the polar lipids extraction with ethanol was explored. Four different scenarios were compared not only in terms of lipids extraction efficiencies but also through a brief economic evaluation. The scenarios were simulated considering a *Nannochloropsis* sp. disrupted paste feed of 152 ton_{SFDW}/year). The mass balance, CAPEX (main equipment), OPEX and production cost of the EPA rich ethanolic concentrated extract (€/ kg $EPA_{extract}$) were calculated and compared.

5.3. Materials and Methods

5.3.1. Materials

The strain of *Nannochloropsis* sp. was grown in flat-panel photobioreactors (PBR) of A4F – Algae for Future (Portugal) in marine, N-replete culture medium and concentrated up to a 200 g_{SFDW}/L wet paste. The paste was diluted with a culture medium down to 100 g_{SFDW}/L to perform the heat treatment step (95 ºC for 3 min) when mentioned, and the cell disruption step (>90% cell disruption). The extraction solvent D-Limonene 96% was purchased from Acros Organics (Geel, Belgium), and ethanol 99.8% was obtained from Fisher Chemical (Merelbeke, Belgium). For analytical procedures acetone 99.0% and methanol 99.8% were purchased from JMGS (Odivelas, Portugal), n-hexane 99.0% was purchased from VWR Chemicals BDH® (Poole, United Kingdom), acetyl chloride 98% and 2,6-Di-tert-butyl-4-methylphenol (BHT) were obtained from Alfa Aesar (Karlsruhe, Germany), petroleum ether 60-80 ºC was purchased from Fisher Scientific (Leicestershire, United Kingdom), and the internal standard C17:0 was obtained from Dr. Ehrenstorfer GmbH (Augsburg, Germany).

5.3.2. Sequential lipid extraction from *Nannochloropsis* sp. biomass

In this first part of the experiment, to produce an EPA-rich polar lipid concentrate, a two-step extraction (non-polar solvent followed by the polar solvent) was investigated. Firstly, D-Limonene 96% was used to try to selectively extract the neutral lipids from the original disrupted *Nannochloropsis* sp. paste. Next, ethanol 99.8% was used to extract the EPA-rich polar lipid fraction from the residual biomass of the first step. **Figure 5.1** shows the laboratory-scale scheme for the fractionated lipids extraction.

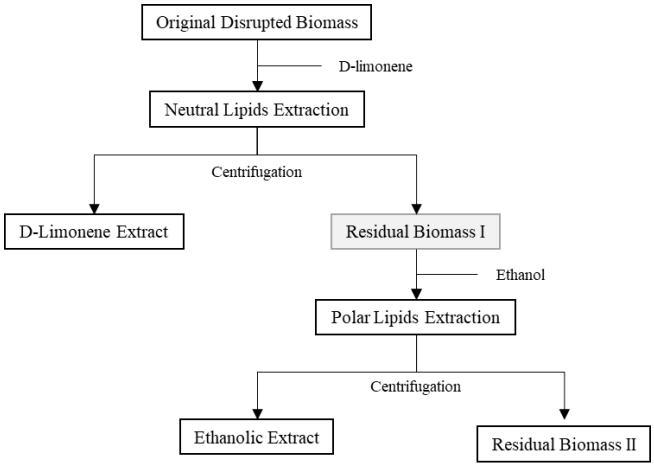

Figure 5.1. Scheme of the two-step lipid extraction from the original *Nannochloropsis* sp. disrupted biomass

Previously to the extraction, the disrupted biomass 100 g_{SFDW}/L was centrifuged at 11,000 x g (for 2 x 20 minutes, 5 ºC) and the collected pellet was analysed in terms of salt-free dry weight, total fatty acids (TFA) and pigments. The first extraction step was carried out by treating 50 g of paste (200 g_{SFDW}/L) with D-limonene and the non-polar solvent to biomass ratio selected was 10 $mL.g^{-1}$. The extraction was carried out at 20 ºC in a glass bottle with a screw cap (1 L) and placed on a magnetic stirrer plate. The mixture was left with magnetic stirring for 6 h, and samples were collected during the experiment. After this first step of extraction, the mixture was centrifuged at 11,000 x g (for 15 minutes, 5 ºC) and both supernatant (D-limonene Extract) and pellet (Residual Biomass I) were separated and collected. A sample of each fraction was collected and analysed in terms of salt-free dry weight, pigments, and total fatty acids. The pellet obtained from the centrifugation (Residual Biomass I) was then used in the second extraction step with ethanol 99.8% (% *v*/*v*). A polar solvent to biomass ratio of 10 $mL.g^{-1}$ was also tested in a glass bottle with a screw cap (1 L), placed on a magnetic stirrer plate. The second extraction step was carried out by treating the residual biomass with ethanol 99.8% for 6 h, and with a magnetic stirrer. Finally, the ethanolic mixture was centrifuged at 11,000 x g (for 15 minutes, 5 ºC), and again both supernatant (Ethanolic Extract) and pellet (Residual Biomass II) were separated and collected. A sample of each fraction was collected and analysed in terms of salt-free dry weight, pigments, and fatty acids profile. The extraction efficiency of the overall process was calculated through **Eq. 5.**1:

$$\text{Extraction Efficiency (\%)} = \frac{\text{wFA}_{extracted}}{w\text{FA}_{\ available}} \times 100 \qquad \textbf{Eq. 5.1}$$

where the $wFA_{extracted}$ (g) is the mass of total fatty acids that were extracted during the extraction step, and $wFA_{available}$ (g) is the mass of total fatty acids in the initial biomass.

5.3.3. Polar lipid extraction from *Nannochloropsis* sp. biomass

Taking into account the poor results of the first part of the experiment, the first extraction with a non-polar solvent was discontinued and the following research in terms of lipids extraction was focused on ethanol extraction of the original biomass and its optimisation.

5.3.3.1. Multi-step extraction with ethanol

In the second part of the experiment, to produce an EPA-rich polar lipid concentrate, a multi-step extraction with ethanol 99.8% was assayed. Previously to the extraction, the disrupted biomass at 100 g_{SFDW}/L was centrifuged at 11,000 x g (for 2 x 20 minutes, 5 ºC) and the collected pellet was analysed in terms of salt-free dry weight and fatty acids profile. Ethanol 99.8% was used to extract the EPA-rich polar lipid fraction from the disrupted biomass through a fifteen-step extraction as is shown in **Figure 5.2.**

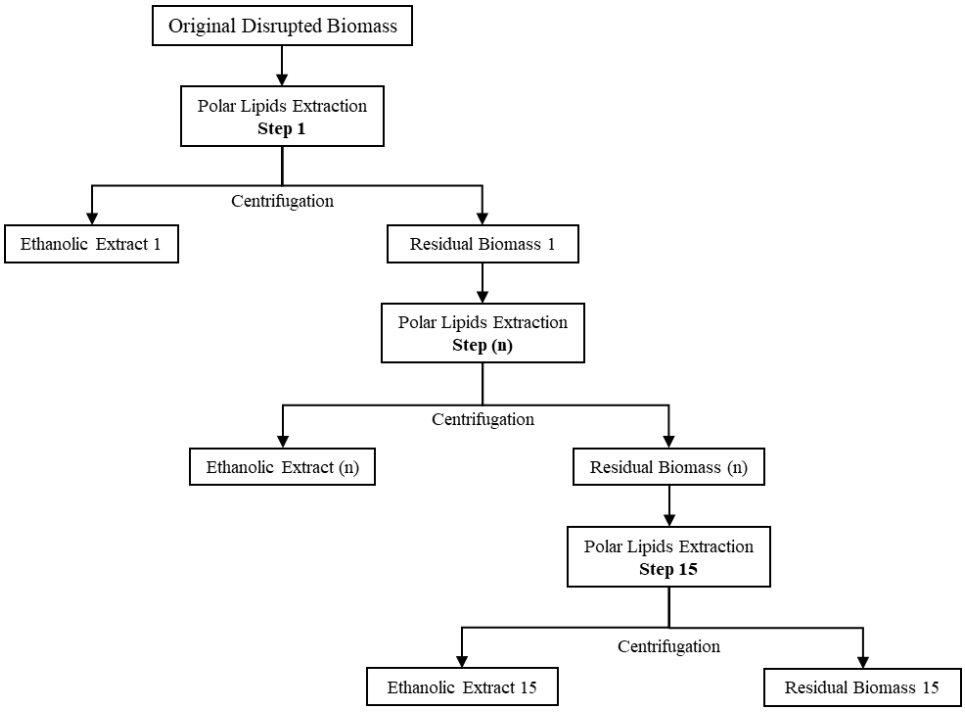

Figure 5.2. Scheme of the multi-step polar lipid extraction with ethanol from the original *Nannochloropsis* sp. disrupted biomass

The first extraction step was carried out by treating 4 g of paste (200 g_{SFDW}/L) with a solvent/ paste ratio of 1 $mL.g^{-1}$ paste. The extraction was carried out at 25 ºC in a plastic Falcon tube (50 mL). The mixture was vortex mixed for 5 min. After this first step of extraction, the mixture was centrifuged at 3,200 x g (for 10 minutes, 4 ºC) and both supernatant (Ethanolic Extract 1) and pellet (Residual Biomass 1) were separated and collected. The pellet obtained from the centrifugation (Residual Biomass 1) was extracted again with the same conditions described before. The extraction process was repeated until the fifteen steps of extraction were reached. A sample of the ethanolic extract from steps 1, 2, 3, 4, 5, 10 and 15 were collected and analysed in terms of salt-free dry weight and total fatty acids. The extraction efficiency was calculated through **Eq. 5.**1, previously described.

5.3.3.2. Ethanolic extraction: solvent/ biomass ratio optimisation

In the third part of the experiment, to produce an EPA-rich polar lipid concentrate, the optimisation of the solvent to biomass ratio ($mL.g^{-1}$) was investigated. Previously to the extraction, the heat-treated disrupted biomass 100 g_{SFDW}/L was centrifuged at 11,000 x g (for 2 x 20 minutes, 5 ºC) and the collected pellet was analysed in terms of salt-free dry weight and total fatty acids. Ethanol 99.8% was used to extract the EPA-rich polar lipid fraction from the disrupted biomass through different scenarios and different ratios of solvent/ biomass as shown in **Figure 5.3 A** to **D**. The first scenario (**Figure 5.3 A)** proposes a multi-step extraction with five steps of extraction, based on the results obtained before for a multi-step extraction with fifteen steps of extraction**.** The ethanolic extraction was carried out by treating 5 g of paste (about 200 g_{SFDW}/L) with a solvent/ paste ratio of 1 $mL.g^{-1}$ paste. The extraction was carried out at 25 ºC in a plastic Falcon tube (50 mL). The mixture was vortex mixed for 5 min. After this first step of extraction, the mixture was centrifuged at 3,200 x g (for 10 minutes, 4 ºC) and both supernatant and pellet were separated and collected. The pellet obtained from the centrifugation (Residual Biomass 1) was extracted again with the same conditions described before. The extraction process was repeated until the five steps of extraction were reached. A sample of the ethanolic extract from each step (step 1 to step 5), was collected and analysed in terms of salt-free dry weight total fatty acids. The second scenario (**Figure 5.3 B)** proposes a two-step extraction where the first extraction was performed by treating 5 g of paste (about 200 g_{SFDW}/L) with a solvent/ paste ratio of 1 $mL.g^{-1}$ paste, aiming the removal of the majority of the water present in the paste. The extraction was carried out at 25 ºC in a plastic Falcon tube (50 mL). The mixture was vortex mixed for 5 min. After this first step of extraction, the mixture was centrifuged at 3,200 x g (for 10 minutes, 4 ºC) and both supernatant and pellet were separated. The supernatant was discarded and the pellet obtained from the centrifugation (Residual Biomass 1) was extracted again. However, this time the solvent/ paste ratio was 5 $mL.g^{-1}$ paste. The

extraction process was repeated until the five steps of extraction were reached. A sample of the ethanolic fraction from each step was collected and analysed in terms of salt-free dry weight and total fatty acids. Finally, the third and fourth scenarios (**Figure 5.3 C** and **D)** propose only one step of extraction with a solvent/ paste ratio of 5 $mL.g^{-1}$ paste and 10 $mL.g^{-1}$ paste, respectively. Both extractions were performed as previously described. However, for scenario D, the extraction was performed by treating 4 g of paste (about 200 $g_{SFDW}.L^{-1}$) with a solvent to biomass ratio of 10 $mL.g^{-1}$ paste. A sample of the ethanolic extract from each scenario (C and D), was collected and analysed in terms of salt-free dry weight and total fatty acids. The extraction efficiency was calculated through **Eq. 5.**1, previously described.

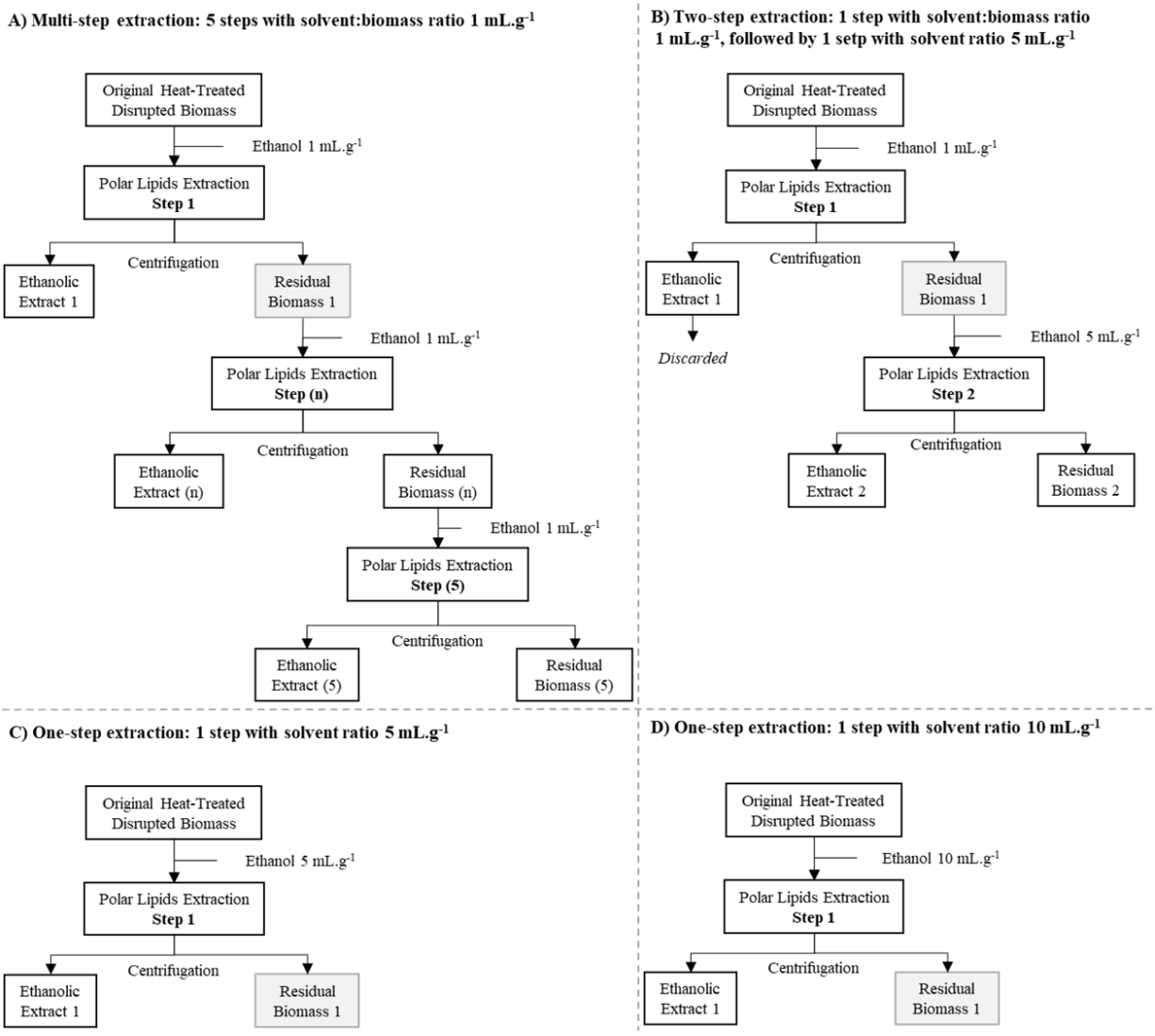

Figure 5.3. Scheme of the polar lipid extraction with ethanol from the original *Nannochloropsis* sp. disrupted biomass aiming the optimisation of the ethanolic extraction process.

5.3.4. Dry weight and salinity quantification

The dry weight was determined through a moisture analyser (Kern DBS 60-3, Kern, Germany), as previously described in chapter **2.3.4**. The sample was dried until a constant weigh was achieved. The sample salt fraction was determined through a salinity refractometer (Kern ORA 1SA, Kern, Germany).

5.3.5. Pigments quantification

Pigments were quantified as previously described in chapter **2.3.8**. Briefly, 1 mg of a biomass sample with a concentration of 200 g_{SFDW}/L was mixed with 4 mL 99,0% acetone and vortex mixed for 60 s. The extracted pigments, recovered in the supernatant after centrifugation, were analysed by spectrophotometry (Genesys 10S UV-VIS). The method was already implemented in the A4F laboratory for *Nannochloropsis* sp. pigments quantification.

5.3.6. Total fatty acids transesterification

The total fatty acid transesterification was carried out after a lipid extraction process, modifying Lepage and Roy [111], as previously mentioned in chapter **2.3.7**. The lipid sample obtained after the evaporation of the ethanol extract was mixed with 200 µL of internal standard C17:0 before the transesterification reaction. Afterwards, it was added 4 mL of acetyl chloride/methanol solution with a 5:100 ratio, and the sample was mixed. Then, the sample was heated at 100 ºC for 1 hour in a water bath. After the sample cool down, 2 mL of n-hexane were added to the tubes and mixed in a vortex. Finally, 2 mL of water were added and the mixture was centrifuged (for 3 min at 2,500 x g). The n-hexane layer was collected and passed through a column filled with anhydrous sodium sulphate (to absorb moisture and filter impurities). The gas chromatography (GC) was performed by an external supplier.

5.4. Results and Discussion

The analysis of the results is focused on the lipid extraction, through solvent extraction, of a 200 g/L *Nannochloropsis* sp. disrupted paste. In the first subchapter, the results from the sequential lipid extraction will be presented: neutral lipids extraction followed by polar lipids extraction from the disrupted paste. Subsequently, in the second subchapter, the results from the experimental work focused on the extraction of polar lipids will be presented and discussed.

5.4.1. Sequential lipid extraction from *Nannochloropsis* sp. biomass

The first part of the solvent extraction experiments was focused on sequential lipid extraction. The extraction process started with the extraction of neutral lipids, using a non-polar solvent (D-limonene), and it was followed by the extraction of polar lipids, through extraction with a polar solvent (ethanol 99.8% *v*/*v*).

The D-limonene to biomass ratio assayed in the first trial was 10 $mL.g^{-1}$ and the trial lasted for 6 hours. The evolution of the concentration of pigments in the D-limonene extract was monitored over the extraction time, and the results are exhibited in **Figure 5.4**. As predicted, the concentration of pigments in general increased at the beginning of the extraction. The evolution of the pigments extraction along the extraction time (h) seems to be heading towards a plateau, which could indicate that the extraction of the pigments available for extraction was complete, i.e., the extraction of all the pigments that were released from the chloroplast during the disruption step, or that the solvent reached a saturated state. To confirm if a saturated state of the solvent was reached a second trial was performed with a higher solvent to biomass ratio (16 mLg^{-1}). However, the results in terms of extraction (data not shown) were quite similar to the first extraction, which suggests that the solvent was not saturated in the first trial.

Although the extraction procedures were performed to prevent degradation of the pigments, the oxygen present in the atmosphere of the extractor might boost the degradation of chlorophyll *a*, as is noticeable in **Figure 5.4**. The concentration of pheophytin *a* equivalents (degradation product of chlorophyll *a*) increases with the course of the extraction. This result shows the importance of carrying out this kind of unit operation under inert atmospheres to prevent the degradation of biomass compounds.

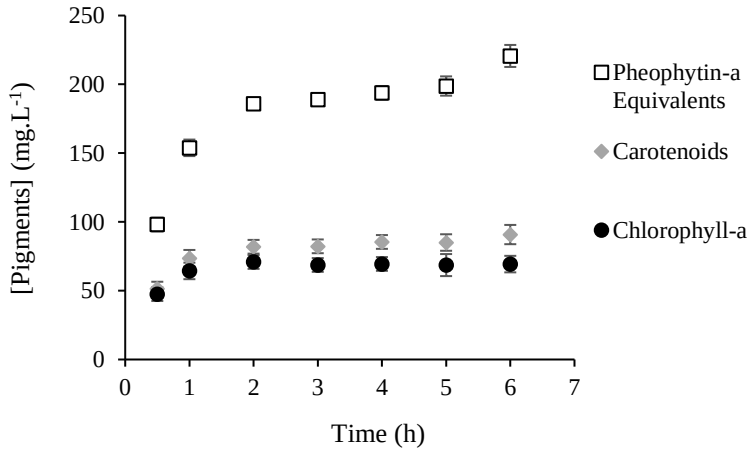

Figure 5.4. Evolution of pigments concentration ($mg.L^{-1}$) in the D-limonene extract against extraction time (h). The extraction was performed with a solvent to biomass ratio of 10 $mL.g^{-1}$. The results are based on 2 replicates for each sample analysis. The error bars represent the standard deviation calculated from the replicates.

The fatty acid profile analysis was also performed to evaluate the performance of this extraction step. The fatty acid profile of the disrupted paste, as well as the fatty acid profile of the neutral and polar fractions, are presented in **Table 5.1**. The first step of the experiment was performed by extracting the solid matrix (50 g of paste at 200 g_{SFDW}/L) with 500 mL of D-limonene (solvent to biomass ratio of 10 $mL.g^{-1}$). The fatty acid profile of the initially disrupted paste revealed that this biomass sample had 9.89% ± 0.24% of total fatty acids, and 2.50% ± 0.05% of C20:5n3 EPA omega-3 (the results are presented on a basis of the SFDW of the initially disrupted paste). The fatty acid profile of the neutral lipid fraction revealed that the biomass sample had 0.81% ± 0.07% of fatty acids in the neutral lipid fraction. Also, the presence of C20:5n3 EPA omega-3 in the neutral lipid fraction was not detected. The fatty acid profile of the D-limonene extract is also exhibited in **Table 5.1**. Different from expected, the D-limonene fraction contained 0.49% ± 0.02% of EPA omega-3, a high percentage considering that the biomass's neutral lipid fraction did not contain EPA. This result might indicate that an appreciable amount of polar lipids was extracted by the non-polar solvent. So, by using D-limonene, not only the fatty acids present in the neutral lipid fraction might be extracted from the initially disrupted paste but also a considerable amount of fatty acids present in the polar lipid fraction might be extracted. Similar results were obtained by Callejón *et al*. [81] and Ryckebosch *et al.* [183], testing the extraction of neutral lipids from *Nannochloropsis* sp. with hexane. The neutral lipids content in the hexane extracts was higher than the content in the original biomass. Ryckebosch *et al.* [183], reported that the hexane extract from *Nannochloropsis* sp. biomass contained 80% of neutral lipids, which was higher than the content

of the initial biomass (46.5%). Also, a considerable amount of polar lipids was found in the hexane extract (around 20% of polar lipids present in the biomass).

The results obtained were not very encouraging, as the present step of extraction extracted about 20% of the EPA present in the polar lipid fraction of the initial *Nannochloropsis* sp. biomass. This result might represent a 20% loss of EPA in the product of interest which is an oleoresin rich in polar lipids, and consequently in EPA omega-3 in a polar lipid form. As mentioned before, omega-3 PUFAs are better absorbed by consumers in the form of glycolipids and phospholipids [169].

Table 5.1. Fatty acid profile from the total fatty acids of the initially disrupted paste, from the neutral lipid fraction of the initially disrupted paste, and the D-Limonene extract. All results are provided on a basis of the SFDW of the initially disrupted paste. The extraction was performed with D-Limonene to biomass ratio of 10 $mL.g^{-1}$. The results are based on 2 replicates for each sample.

Fatty Acid	Initial Disrupted Paste (% w_{FA}/w_{SFDW})	Neutral Lipid Fraction (% w_{FA}/w_{SFDW})	Limonene Extract (% w_{FA}/w_{SFDW})
C14:0	0.87% ± 0.04%	0.09% ± 0.00%	0.20% ± 0.02%
C16:0	2.70% ± 0.05%	0.35% ± 0.02%	0.62% ± 0.06%
C18:0	0.10% ± 0.01%	0.01% ± 0.00%	0.03% ± 0.00%
ΣSFAs	3.57% ± 0.10%	0.45% ± 0.01%	0.85% ± 0.08%
C16:1	2.32% ± 0.07%	0.30% ± 0.05%	0.52% ± 0.05%
C18:1	0.30% ± 0.01%	0.05% ± 0.01%	0.10% ± 0.01%
ΣMUFAs	2.62% ± 0.08%	0.35% ± 0.06%	0.62% ± 0.06%
C18:2n6	0.60% ± 0.01%	0.01% ± 0.00%	0.04% ± 0.01%
C18:3	0.00% ± 0.00%	0.00% ± 0.00%	0.00% ± 0.00%
C20:4n6	0.50% ± 0.00%	0.00% ± 0.00%	0.02% ± 0.00%
C20:5n3	2.50% ± 0.05%	0.00% ± 0.00%	0.49% ± 0.02%
ΣPUFAs	3.60% ± 0.06%	0.01% ± 0.00%	0.55% ± 0.03%
Total FA	9.89% ± 0.24%	0.81% ± 0.07%	2.02% ± 0.17%

The same procedures of limonene extraction were adopted for the trial using ethanol (99.8% *v*/*v*), starting with the solvent to biomass ratio of 10 $mL.g^{-1}$. The evolution of the concentration of pigments in the ethanol extract was observed over the extraction time, and the results are presented in **Figure 5.5**. The concentration of pigments in general increased at the beginning of the extraction as occurred with the D-limonene extraction. Also, it was possible to detect carotenoids in the ethanolic extract, and it can be explained by the fact that *Nannochloropsis* sp. total carotenoids are constituted by predominantly xanthophylls, which exhibit a polar behaviour. The carotenoid family can be divided into two main

groups: the polar carotenoids (xanthophylls) and non-polar carotenoids (carotenes) [185]. Again, the evolution of the concentration of the pigments in the ethanolic extract along the extraction time (h) seems to be heading towards a plateau, which could indicate that the extraction of the pigments available for extraction was complete, i.e., the extraction of all the pigments that were released from the chloroplast during the disruption step was complete, or that the solvent reached a saturated state. Again, as performed for the limonene extraction, a second trial was performed with a higher solvent to biomass ratio (16 mLg^{-1}), to confirm if a saturated state of the solvent had been reached. Once more, the results in terms of extraction (data not shown) were quite similar to the first extraction, which suggests that the solvent was not saturated in the first trial.

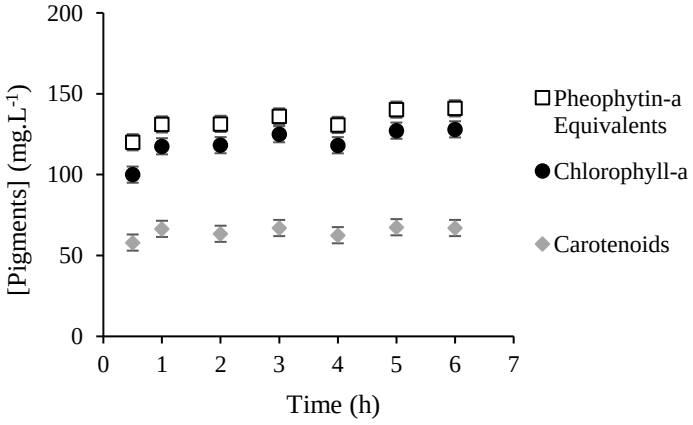

Figure 5.5. Evolution of pigments concentration ($mg.L^{-1}$) in the ethanol extract against extraction time (h). The extraction was performed with a solvent to biomass ratio of 10 $mL.g^{-1}$. The results are based on 2 replicates for each sample analysis. The error bars represent the standard deviation calculated from the replicates.

The fatty acid profile of the residual biomass I, as well as of the ethanolic extract, are presented in **Table 5.2**. The fatty acid profile of the residual biomass had 7.87% ± 0.07% of total fatty acids, and 2.01% ± 0.03% of C20:5n3 EPA omega-3 (the results are presented as % w_{FA}/ w_{SFDW}). The fatty acid profile of the ethanol extract is also exhibited in **Table 5.2**, and the ethanolic extract exhibited 5.59% ± 0.05% of total fatty acids, and 1.49% ± 0.02% of C20:5n3 EPA omega-3. The lipid extraction efficiency (**Table 5.2)** might be evaluated in terms of the total fatty acid present in the extract, and the results revealed an extraction efficiency of 71.83% ± 0.75% (% $wFA_{extracted}/wFA_{available}$). Also, it is possible to conclude that 74.56% ± 1.02% of the EPA present in the residual biomass was recovered in the ethanolic extract, which is similar to the percentage of recovery described by Callejón *et al*. [81].

Table 5.2. Fatty acid profile (residual biomass I after the neutral lipids extraction, and ethanolic extract), and extraction efficiency. The fatty acid profile results are provided on a basis of the SFDW of the initially disrupted paste. The extraction efficiency results are presented as % *w fatty acids extracted*/ *w fatty acids present in the residual biomass I*. The extraction was performed with an ethanol to biomass ratio of 10 $mL.g^{-1}$. The results are based on 2 replicates for each sample fatty acid analysis.

Fatty Acid	Fatty Acid Profile		Extraction Efficiency ($\%\ w_{FA_{extracted}}/w_{FA_{available}}$)
	Residual Biomass I ($\%\ w_{FA}/w_{SFDW}$)	Ethanol Extract ($\%\ w_{FA}/w_{SFDW}$)	
C14:0	0.67% ± 0.02%	0.44% ± 0.01%	65.00% ± 1.97%
C16:0	2.08% ± 0.01%	1.62% ± 0.01%	78.42% ± 0.51%
C18:0	0.07% ± 0.01%	0.05% ± 0.01%	65.00% ± 1.58%
ΣSFAs	2.82% ± 0.02%	2.06% ± 0.01%	73.94% ± 1.07%
C16:1	1.80% ± 0.02%	1.22% ± 0.01%	68.62% ± 0.65%
C18:1	0.20% ± 0.00%	0.15% ± 0.00%	75.74% ± 1.87%
ΣMUFAs	2.00% ± 0.02%	1.41% ± 0.01%	70.00% ± 0.78%
C18:2n6	0.56% ± 0.00%	0.42% ± 0.00%	75.68% ± 0.30%
C18:3	0.00% ± 0.00%	0.00% ± 0.00%	0.00% ± 0.00%
C20:4n6	0.48% ± 0.00%	0.10% ± 0.00%	21.02% ± 2.54%
C20:5n3	2.01% ± 0.03%	1.49% ± 0.02%	74.56% ± 1.02%
ΣPUFAs	3.05% ± 0.03%	2.14% ± 0.02%	74.40% ± 0.89%
Total FA	7.87% ± 0.07%	5.59% ± 0.05%	71.83% ± 0.75%

As mentioned before, the results obtained in the first extraction step (neutral extraction) were not very encouraging as the D-limonene might have the capacity to extract a considerable amount of polar lipids. However, the ethanolic extraction revealed that 71.83% ± 0.75% of the lipids present in the residual biomass were recovered in the ethanolic extract. Therefore, the following experiment was focused on ethanolic extraction and the optimisation of the ratio of solvent to biomass.

5.4.2. Polar lipid extraction from *Nannochloropsis* sp. biomass

The sequential lipid extraction hypothesis was abandoned, as mentioned before. Therefore, in this subchapter, the results from the experimental work focused on the extraction of polar lipids will be presented and discussed.

5.4.2.1. Multi-step extraction with ethanol

The first step towards an optimised ratio of extraction (solvent to biomass) was to perform a fifteen-step extraction with ethanol 99.8% (solvent to biomass ratio of 1:1 $mL.g^{-1}$) to promote the maximum lipid extraction, and to evaluate the lipid extraction efficiency of each step.

The fatty acid profile of the initially disrupted paste (**Table 5.3**) revealed that this biomass sample had 18.83% ± 0.47% of total fatty acids, and specifically 7.30% ± 0.12% of C20:5n3 EPA omega-3 (the results are presented as % w_{FA}/ w_{SFDW}). The fatty acid profiles of the ethanolic extracts from each of the analysed extraction steps are also exhibited in **Table 5.3**. Differently from expected, the first step only could extract 0.27 percentage points (pp) of the 18.83% of total fatty acids present in the initial biomass. In this first extraction step the water present in the paste might have negatively affected the extraction as the 4 mL of ethanol 99.8% was diluted 1.8 times with the 3.2 mL of water present in the initial 4 g of disrupted paste. This first step of extraction appears to be almost a pre-treatment step to reduce the amount of water present in the solid matrix. After the first extraction step and consequent centrifugation, the amount of water present in the pellet was reduced and replaced by ethanol. Therefore, the second extraction step could extract 7.54 pp of the 18.83% of total fatty acids present in the initial biomass. The extraction steps 1 to 5 appear to extract the majority of the fatty acids present in the initial disrupted biomass. Steps 10 and 15 only extracted 0.05 pp and 0.02 pp of the 18.83% of total fatty acids present in the initial biomass, respectively.

Table 5.3. Multi-step extraction of *Nannochloropsis* sp. disrupted biomass with ethanol. Fatty acid profile from the initially disrupted paste and from the ethanolic extracts resulting from the steps of extraction 1 to 5, 10 and 15; all the extraction steps were performed with a solvent to biomass ratio of 1:1 $mL.g^{-1}$, always reported to the initial biomass SFDW. The results are based on 2 replicates for each sample.

Fatty Acid	Initial Disrupted Paste (% w_{FA}/w_{SFDW})	Ethanolic Extract (% w_{FA}/w_{SFDW})			
		Step 1 Ratio 1:1 ($mL.g^{-1}$)	Step 2 Ratio 1:1 ($mL.g^{-1}$)	Step 3 Ratio 1:1 ($mL.g^{-1}$)	Step 4 Ratio 1:1 ($mL.g^{-1}$)
C14:0	0.91% ± 0.05%	0.02% ± 0.00%	0.39% ± 0.04%	0.16% ± 0.01%	0.07% ± 0.00%
C16:0	3.10% ± 0.15%	0.04% ± 0.00%	1.12% ± 0.09%	0.67% ± 0.10%	0.34% ± 0.06%
C18:0	0.01% ± 0.02%	0.00% ± 0.00%	0.01% ± 0.02%	0.00% ± 0.01%	0.00% ± 0.00%
ΣSFAs	4.02% ± 0.17%	0.06% ± 0.01%	1.52% ± 0.15%	0.83% ± 0.03%	0.41% ± 0.06%
C16:1	3.60% ± 0.08%	0.07% ± 0.01%	1.51% ± 0.04%	0.91% ± 0.02%	0.45% ± 0.03%
C18:1	1.07% ± 0.10%	0.01% ± 0.01%	0.57% ± 0.10%	0.20% ± 0.02%	0.09% ± 0.01%
ΣMUFAs	4.67% ± 0.08%	0.08% ± 0.02%	2.08% ± 0.22%	1.11% ± 0.00%	0.54% ± 0.04%
C18:2n6	0.80% ± 0.03%	0.01% ± 0.00%	0.29% ± 0.00%	0.17% ± 0.01%	0.08% ± 0.01%
C18:3	0.10% ± 0.05%	0.00% ± 0.00%	0.05% ± 0.01%	0.00% ± 0.01%	0.00% ± 0.00%
C20:3	0.10% ± 0.03%	0.00% ± 0.00%	0.01% ± 0.00%	0.00% ± 0.00%	0.00% ± 0.00%
C20:4n6	1.94% ± 0.17%	0.01% ± 0.01%	0.58% ± 0.10%	0.29% ± 0.01%	0.14% ± 0.01%
C20:5n3	7.30% ± 0.12%	0.11% ± 0.01%	3.06% ± 0.08%	1.56% ± 0.08%	0.70% ± 0.06%
ΣPUFAs	10.14% ± 0.25%	0.13% ± 0.02%	3.94% ± 0.21%	2.02% ± 0.10%	0.92% ± 0.08%
Total FA	18.83% ± 0.47%	0.27% ± 0.04%	7.54% ± 0.48%	3.96% ± 0.18%	1.87% ± 0.19%

Fatty Acid	Initial Disrupted Paste (% w_{FA}/w_{SFDW})	Ethanolic Extract (% w_{FA}/w_{SFDW})		
		Step 5 Ratio 1:1 ($mL.g^{-1}$)	Step 10 Ratio 1:1 ($mL.g^{-1}$)	Step 15 Ratio 1:1 ($mL.g^{-1}$)
C14:0	0.91% ± 0.05%	0.04% ± 0.00%	0.00% ± 0.00%	0.00% ± 0.00%
C16:0	3.10% ± 0.15%	0.17% ± 0.03%	0.02% ± 0.01%	0.01% ± 0.00%
C18:0	0.01% ± 0.02%	0.00% ± 0.00%	0.00% ± 0.00%	0.00% ± 0.00%
ΣSFAs	4.02% ± 0.17%	0.21% ± 0.03%	0.02% ± 0.01%	0.01% ± 0.01%
C16:1	3.60% ± 0.08%	0.22% ± 0.02%	0.02% ± 0.02%	0.01% ± 0.01%
C18:1	1.07% ± 0.10%	0.04% ± 0.00%	0.00% ± 0.01%	0.00% ± 0.01%
ΣMUFAs	4.67% ± 0.08%	0.26% ± 0.02%	0.02% ± 0.02%	0.01% ± 0.01%
C18:2n6	0.80% ± 0.03%	0.04% ± 0.00%	0.00% ± 0.02%	0.00% ± 0.00%
C18:3	0.10% ± 0.05%	0.00% ± 0.01%	0.00% ± 0.00%	0.00% ± 0.00%
C20:3	0.10% ± 0.03%	0.00% ± 0.00%	0.00% ± 0.00%	0.00% ± 0.00%
C20:4n6	1.94% ± 0.17%	0.05% ± 0.00%	0.00% ± 0.01%	0.00% ± 0.01%
C20:5n3	7.30% ± 0.12%	0.26% ± 0.01%	0.01% ± 0.01%	0.00% ± 0.01%
ΣPUFAs	10.14% ± 0.25%	0.35% ± 0.00%	0.01% ± 0.01%	0.00% ± 0.01%
Total FA	18.83% ± 0.47%	0.82% ± 0.07%	0.05% ± 0.01%	0.02% ± 0.02%

The lipid extraction efficiency was evaluated in terms of the total fatty acid content present in each extract. After the transesterification of the lipids present in each extract, the fatty acid methyl esters (FAME) were analysed through gas chromatography (GC). **Table 5.4** and **Figure 5.6 A** show the results and the evolution of the lipid extraction efficiency in steps 1 to 5, which are the most relevant as observed before. The first step only extracted 1.43% ± 0.18% of the total lipids present in the initial biomass, and it might be a step with a negatively large amount of water, as mentioned before. Also, as discussed before, the second step of the extraction is the one with the higher extraction efficiency; 40.02% ± 1.55% of the total lipids and 41.92% ± 0.41% of the EPA omega-3 present in the initial biomass were extracted in this step. From step 2 to step 3, a decrease of nearly 50% in the lipid extraction efficiency was noticed, from 40.02% ± 1.55% in step 2 to 21.03% ± 0.43% in step 3. The decreasing tendency revealed in **Figure 5.6 A** suggest that the five steps of extraction are a good compromise between the lipid extraction efficiency and the amount of solvent and energy needed to extract the remaining lipids present in the solid matrix.

Figure 5.6 B exhibits the lipid extraction efficiency along with the five steps of extraction and it is possible to conclude that the five steps of extraction reached a lipid extraction efficiency of 77% ± 3%. Ryckebosch *et al.* reported an extraction efficiency of 52% $w/w_{total\ lipids}$ for ethanol systems [183], which is lower than the extraction efficiency achieved in this experiment. This might be related to the cell disruption methods used by the author to disrupt the cells (bead-beating), which probably were not able to reach the same disruption efficiency as the bead milling used in this experiment. Also, the purity of the ethanol used by Ryckebosch *et al.* was lower (96% *v*/*v* instead of 99.8%), which could negatively affect the extraction efficiency. As mentioned before, the evolution of the lipid extraction efficiency along the 5 steps of extraction seems to be heading towards a plateau, which is also noticed in **Figure 5.6 B.** Therefore, it was concluded that the five steps of extraction (solvent to biomass ratio of 1:1 $mL.g^{-1}$) are sufficient to achieve a high lipid extraction efficiency.

Table 5.4. Multi-step extraction with ethanol. Extraction efficiency in each step of extraction 1 to 5; all the extraction steps were performed with a solvent ratio to the biomass of 1 mL.g^{-1}. The extraction efficiency results are presented as % *w fatty acids extracted/ w fatty acids present in the residual biomass I* The results are based on 2 replicates for each sample.

Fatty Acid	Extraction Efficiency ($wFA_{extracted}$/ $wFA_{available}$)				
	Step 1 Ratio 1:1 (mL.g^{-1})	**Step 2 Ratio 1:1 (mL.g^{-1})**	**Step 3 Ratio 1:1 (mL.g^{-1})**	**Step 4 Ratio 1:1 (mL.g^{-1})**	**Step 5 Ratio 1:1 (mL.g^{-1})**
C14:0	2.21% ± 0.12%	43.01% ± 2.05%	17.65% ± 0.13%	7.72% ± 0.43%	4.41% ± 0.24%
C16:0	1.29% ± 0.06%	36.13% ± 1.16%	21.61% ± 2.19%	10.97% ± 1.41%	5.48% ± 0.70%
C18:0	0.00% ± 0.00%	75.00% ± 0.00%	0.00% ± 0.00%	0.00% ± 0.00%	0.00% ± 0.00%
ΣSFAs	1.49% ± 0.19%	37.81% ± 2.14%	20.65% ± 0.13%	10.20% ± 1.06%	5.22% ± 0.53%
C16:1	1.94% ± 0.23%	41.94% ± 0.18%	25.28% ± 0.01%	12.50% ± 0.56%	6.11% ± 0.42%
C18:1	0.94% ± 0.86%	53.40% ± 4.40%	18.74% ± 0.12%	8.43% ± 0.15%	3.75% ± 0.35%
ΣMUFAs	1.71% ± 0.40%	44.56% ± 3.95%	23.78% ± 0.41%	11.57% ± 0.66%	5.57% ± 0.33%
C18:2n6	1.25% ± 0.05%	36.25% ± 1.36%	21.25% ± 0.45%	10.00% ± 0.88%	5.00% ± 0.19%
C18:3	0.00% ± 0.00%	54.00% ± 4.65%	0.00% ± 0.00%	0.00% ± 0.00%	0.00% ± 0.00%
C20:3	0.00% ± 0.00%	5.00% ± 1.65%	0.00% ± 0.00%	0.00% ± 0.00%	0.00% ± 0.00%
C20:4n6	0.52% ± 0.47%	29.90% ± 2.55%	14.95% ± 0.80%	7.22% ± 0.12%	2.58% ± 0.23%
C20:5n3	1.51% ± 0.11%	41.92% ± 0.41%	21.37% ± 0.74%	9.59% ± 0.66%	3.56% ± 0.08%
ΣPUFAs	1.28% ± 0.17%	38.81% ± 1.11%	19.92% ± 0.50%	9.07% ± 0.57%	3.45% ± 0.09%
Total FA	1.43% ± 0.18%	40.02% ± 1.55%	21.03% ± 0.43%	9.93% ± 0.76%	4.36% ± 0.26%

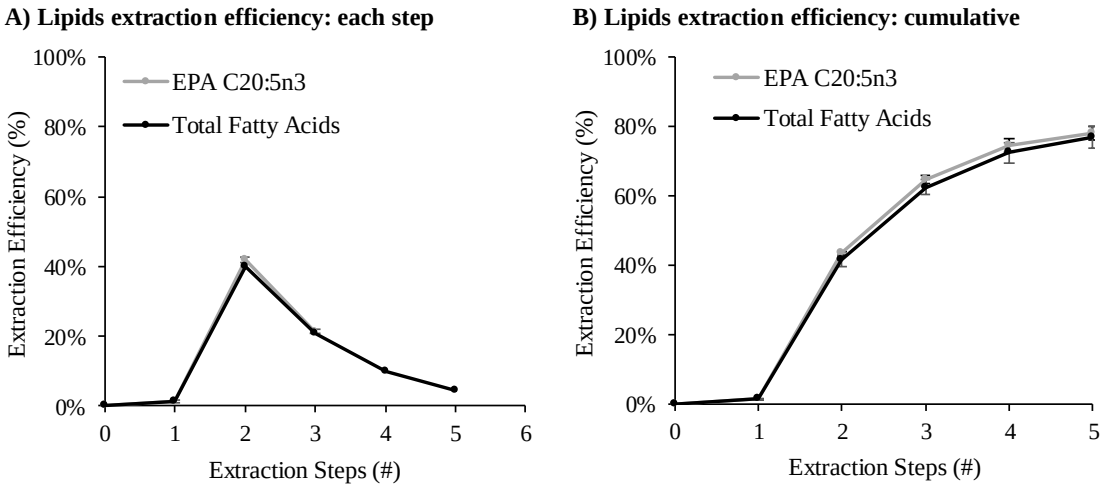

Figure 5.6. Multi-step extraction with ethanol. A) Lipid extraction efficiency in each step of extraction 1 to 5. B) Cumulative lipid extraction efficiency from step 1 to step 5. All the extraction steps were performed with a solvent to biomass ratio of 1 mL.g^{-1}. The results are presented as % $wFA_{extracted}$/ $wFA_{available}$ and are based on 2 replicates for each sample. The error bars represent the standard deviation calculated from the replicates.

5.4.2.2. Ethanolic extraction: solvent/ biomass ratio optimisation

The second part of the experiments was focused on the optimisation of the ratio of extraction (solvent to biomass) as well as the process of extraction itself. Four different scenarios were tested to maximize the lipid extraction efficiency: a 5-step extraction with solvent to biomass ratio of 1 $mL.g^{-1}$ (**scenario A**), a 2-step extraction with a solvent to biomass ratio of 1 $mL.g^{-1}$ in the first step, followed by the second step of extraction with a solvent to biomass ratio of 5 $mL.g^{-1}$ (**scenario B**), a 1-step extraction with a solvent to biomass ratio of 5 $mL.g^{-1}$ (**scenario C**), and a 1-step extraction with a solvent to biomass ratio of 10 $mL.g^{-1}$ (**scenario D**).

Scenario A) Five-step extraction with a solvent to biomass ratio of 1 $mL.g^{-1}$

The experiment was performed by extracting the solid matrix (5 g of paste at 200 g_{SFDW}/L) with 5 mL of ethanol 99.8% in each of the five steps of extraction (solvent to biomass ratio of 1 $mL.g^{-1}$).

The fatty acid profiles of the initial disrupted biomass and the ethanolic extracts from each of the extraction steps are exhibited in **Table 5.5**. Similar to the results presented in the previous subchapter for the 15-step extraction, the first extraction step could only extract 0.21 pp of the 17.30% of total fatty acids present in the initial biomass. The first step of extraction might be considered a pre-treatment to reduce the amount of water present in the solid matrix. Therefore, it might be discarded to reduce the amount of water remaining until the end of the biorefinery process. After the first extraction step and consequent centrifugation, the amount of water in the pellet was reduced and replaced by ethanol. Consequently, the second extraction step could extract 6.57 pp of the 17.30% of total fatty acids present in the initial biomass.

Table 5.5. Five-step extraction with ethanol. Fatty acid profile from the initially disrupted paste and from the ethanolic extracts resulting from the steps of extraction 1 to 5; all the extraction steps were performed with a solvent to biomass ratio of 1:1 $mL.g^{-1}$, always reported to the initial biomass SFDW. The results are based on 2 replicates for each sample

Fatty Acid	Initial Disrupted Paste (% w_{FA}/w_{SFDW})	Ethanolic Extract (% w_{FA}/w_{SFDW})				
		Step 1 Ratio 1:1 ($mL.g^{-1}$)	Step 2 Ratio 1:1 ($mL.g^{-1}$)	Step 3 Ratio 1:1 ($mL.g^{-1}$)	Step 4 Ratio 1:1 ($mL.g^{-1}$)	Step 5 Ratio 1:1 ($mL.g^{-1}$)
C14:0	0.80% ± 0.04%	0.01% ± 0.00%	0.33% ± 0.03%	0.18% ± 0.01%	0.07% ± 0.00%	0.03% ± 0.00%
C16:0	2.60% ± 0.05%	0.03% ± 0.00%	0.92% ± 0.10%	0.54% ± 0.07%	0.23% ± 0.05%	0.11% ± 0.03%
C18:0	0.10% ± 0.00%	0.00% ± 0.00%	0.05% ± 0.02%	0.03% ± 0.01%	0.00% ± 0.00%	0.01% ± 0.00%
ΣSFAs	3.50% ± 0.08%	0.04% ± 0.01%	1.30% ± 0.11%	0.74% ± 0.04%	0.31% ± 0.05%	0.15% ± 0.03%
C16:1	3.80% ± 0.06%	0.06% ± 0.01%	1.44% ± 0.04%	0.95% ± 0.02%	0.36% ± 0.04%	0.16% ± 0.03%
C18:1	0.70% ± 0.01%	0.00% ± 0.01%	0.24% ± 0.16%	0.15% ± 0.02%	0.07% ± 0.01%	0.03% ± 0.00%
ΣMUFAs	4.50% ± 0.07%	0.06% ± 0.01%	1.68% ± 0.20%	1.10% ± 0.00%	0.43% ± 0.06%	0.19% ± 0.03%
C18:2n6	0.70% ± 0.01%	0.01% ± 0.00%	0.28% ± 0.00%	0.16% ± 0.01%	0.07% ± 0.01%	0.03% ± 0.00%
C18:3	0.20% ± 0.04%	0.01% ± 0.00%	0.02% ± 0.02%	0.01% ± 0.01%	0.01% ± 0.00%	0.02% ± 0.01%
C20:3	0.20% ± 0.01%	0.00% ± 0.00%	0.01% ± 0.00%	0.00% ± 0.00%	0.00% ± 0.00%	0.00% ± 0.00%
C20:4n6	1.30% ± 0.01%	0.00% ± 0.01%	0.38% ± 0.10%	0.27% ± 0.01%	0.12% ± 0.01%	0.05% ± 0.00%
C20:5n3	6.90% ± 0.04%	0.10% ± 0.01%	2.89% ± 0.08%	1.38% ± 0.09%	0.58% ± 0.06%	0.25% ± 0.00%
ΣPUFAs	9.30% ± 0.07%	0.11% ± 0.01%	3.59% ± 0.17%	1.82% ± 0.10%	0.78% ± 0.07%	0.35% ± 0.00%
Total FA	17.30% ± 0.18%	0.21% ± 0.03%	6.57% ± 0.48%	3.66% ± 0.15%	1.51% ± 0.18%	0.69% ± 0.06%

The extraction efficiency results from step 1 to step 5 are presented in **Table 5.6**. The first step only extracted 1.21% ± 0.16 of the total lipids present in the initial biomass. The first extraction step had a significantly greater amount of water than the remaining steps, modifying the polarity of the extraction solvent and reducing the efficiency of the polar lipid extraction, as observed. It is again evidenced that lipid extraction is highly influenced by the dry weight of the initial disrupted biomass. Therefore, it is extremely important to optimise the centrifugation step previous to extraction to obtain a pellet (disrupted paste) with the higher dry weight possible. It could also be considered the possibility of carrying out the first extraction as a pre-treatment, to remove the water present in the pellet and enhance the extraction efficiency, since there is evidence that the extraction efficiency increases greatly in the second extraction step.

Table 5.6. Five-step extraction with ethanol. Extraction efficiency in each step of extraction 1 to 5. The extraction efficiency results are presented as % *w fatty acids extracted*/ *w fatty acids present in the initially disrupted paste*. All the extraction steps were performed with a solvent ratio to the biomass of 1:1 $mL.g^{-1}$. The results are based on 2 replicates for each sample.

Fatty Acid	Ethanolic Extract (% $wFA_{extracted}/wFA_{available}$)									
	Step 1 Ratio 1:1 ($mL.g^{-1}$)		**Step 2 Ratio 1:1 ($mL.g^{-1}$)**		**Step 3 Ratio 1:1 ($mL.g^{-1}$)**		**Step 4 Ratio 1:1 ($mL.g^{-1}$)**		**Step 5 Ratio 1:1 ($mL.g^{-1}$)**	
C14:0	1.80%	± 0.09%	41.65%	± 0.67%	21.94%	± 0.15%	9.23%	± 0.46%	4.19%	± 0.21%
C16:0	1.16%	± 0.02%	35.24%	± 3.17%	20.75%	± 2.29%	8.89%	± 1.75%	4.10%	± 1.08%
C18:0	0.00%	± 0.00%	50.00%	± 5.00%	28.15%	± 5.00%	4.00%	± 0.00%	6.51%	± 0.00%
ΣSFAs	1.28%	± 0.26%	37.12%	± 2.30%	21.23%	± 0.66%	8.83%	± 1.23%	4.19%	± 0.76%
C16:1	1.51%	± 0.24%	37.89%	± 0.45%	25.00%	± 0.13%	9.48%	± 0.90%	4.31%	± 0.72%
C18:1	0.00%	± 0.70%	34.71%	± 5.22%	21.92%	± 2.54%	9.44%	± 1.29%	4.36%	± 0.06%
ΣMUFAs	1.28%	± 0.20%	37.40%	± 3.86%	24.52%	± 0.38%	9.47%	± 1.19%	4.31%	± 0.60%
C18:2n6	0.93%	± 0.01%	40.63%	± 0.58%	22.25%	± 1.11%	9.65%	± 1.29%	4.31%	± 0.06%
C18:3	2.92%	± 0.61%	10.60%	± 1.95%	6.48%	± 3.86%	5.00%	± 1.04%	8.79%	± 2.38%
C20:3	0.00%	± 0.00%	5.00%	± 0.25%	0.00%	± 0.00%	0.00%	± 0.00%	0.00%	± 0.00%
C20:4n6	0.00%	± 0.38%	29.23%	± 5.16%	20.96%	± 0.61%	9.06%	± 0.70%	3.96%	± 0.03%
C20:5n3	1.38%	± 0.14%	41.90%	± 0.92%	19.94%	± 1.19%	8.46%	± 0.82%	3.64%	± 0.02%
ΣPUFAs	1.16%	± 0.10%	38.56%	± 1.54%	19.54%	± 0.93%	8.38%	± 0.69%	3.77%	± 0.03%
Total FA	1.21%	± 0.16%	37.97%	± 2.38%	21.18%	± 0.65%	8.75%	± 0.95%	4.00%	± 0.31%

Figure 5.7 B exhibits the cumulative lipid extraction efficiency along with the five steps of extraction. The five steps of extraction reached an overall lipid extraction efficiency of 73% ± 4%, which is very similar to the results obtained in the fifteen-step extraction experiment previously discussed. Again, the lipid extraction efficiency is higher than the result reported by Ryckebosch *et al.* for ethanol systems (52% $w/w_{total\ lipids}$) [183]. Also, the five steps of extraction reached an EPA omega-3 extraction efficiency of 75% ± 3%. The increase in the overall lipid extraction efficiency was very marked from step 1 to step 2, due to the removal of the water present in the paste in the first extraction step, as mentioned before. The evolution of the lipid extraction efficiency along the 5 steps of extraction seems to be heading towards a plateau, which indicates that the five steps of extraction are sufficient to achieve a high lipid extraction efficiency.

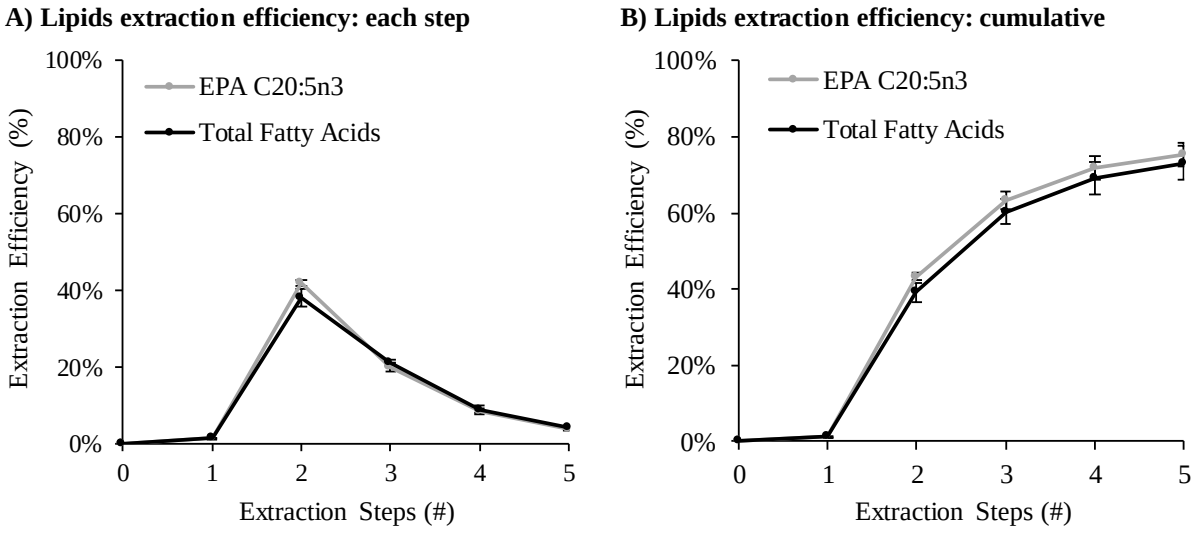

Figure 5.7. Five-step extraction with ethanol. A) Lipid extraction efficiency in each step of extraction 1 to 5. B) Cumulative lipid extraction efficiency from step 1 to step 5. All the extraction steps were performed with a solvent to biomass ratio of 1:1 mL.g^{-1}. The results are presented as % $wFA_{extracted}$/ $wFA_{available}$ and, they are based on 2 replicates for each sample. The error bars represent the standard deviation calculated from the replicates.

Scenario B) Two-steps extraction with a solvent to biomass ratio of 1 mL.g^{-1}in the first step and 5 mL.g^{-1}in the second step of extraction

In the previous extraction experiment (**scenario A**), it was hypothesized that the first extraction step might be a pre-treatment to reduce the amount of water that reaches the start of this step of the biorefinery process. Therefore, the premise of this second scenario was to reduce the amount of water in the process by discarding the extract originating in the first extraction step and then performing a second extraction step, with a solvent to biomass ratio of 5 mL.g^{-1}.

The fatty acid profiles (initial disrupted biomass and ethanolic extracts), as well as the extraction efficiency from each of the extraction steps, are presented in **Table 5.7**.

Table 5.7. Two-step extraction with ethanol. Fatty acid profile (initially disrupted paste and ethanolic extracts resulting from the steps of extraction 1 and 2), and extraction efficiency. The fatty acid profile results are provided on a basis of the SFDW of the initially disrupted paste. The extraction efficiency results are presented as % *w fatty acids extracted*/ *w fatty acids present in the initially disrupted paste*. The first extraction step was performed with a solvent to biomass ratio of 1 $mL.g^{-1}$, and the second extraction step was performed with a solvent to biomass ratio of 5 $mL.g^{-1}$. The results are based on 2 replicates for each sample.

Fatty Acid	Fatty Acid Profile			Extraction Efficiency (% $wFA_{extracted}/wFA_{available}$)	
	Initial Disrupted Paste (% w_{FA}/w_{SFDW})	Ethanolic Extract (% w_{FA}/w_{SFDW})			
		Step 1 Ratio 1:1 ($mL.g^{-1}$)	Step 2 Ratio 5:1 ($mL.g^{-1}$)	Step 1 Ratio 1:1 ($mL.g^{-1}$)	Step 2 Ratio 5:1 ($mL.g^{-1}$)
C14:0	0.80% ± 0.04%	0.01% ± 0.00%	0.60% ± 0.03%	1.40% ± 0.11%	75.00% ± 2.31%
C16:0	2.60% ± 0.05%	0.02% ± 0.00%	1.80% ± 0.10%	0.89% ± 0.04%	69.23% ± 2.24%
C18:0	0.10% ± 0.00%	0.00% ± 0.00%	0.04% ± 0.02%	0.00% ± 0.00%	40.00% ± 2.90%
ΣSFAs	3.50% ± 0.08%	0.03% ± 0.01%	2.44% ± 0.17%	0.98% ± 0.17%	69.71% ± 1.92%
C16:1	3.80% ± 0.06%	0.04% ± 0.01%	2.40% ± 0.12%	1.09% ± 0.14%	63.16% ± 3.00%
C18:1	0.70% ± 0.01%	0.01% ± 0.01%	0.40% ± 0.09%	0.79% ± 0.09%	57.14% ± 4.03%
ΣMUFAs	4.50% ± 0.07%	0.05% ± 0.02%	2.80% ± 0.23%	1.04% ± 0.36%	62.22% ± 3.13%
C18:2n6	0.70% ± 0.01%	0.01% ± 0.00%	0.58% ± 0.08%	1.14% ± 0.10%	82.86% ± 1.21%
C18:3	0.20% ± 0.04%	0.01% ± 0.00%	0.10% ± 0.01%	2.78% ± 0.31%	50.00% ± 3.36%
C20:3	0.20% ± 0.01%	0.00% ± 0.00%	0.10% ± 0.01%	0.00% ± 0.00%	50.00% ± 1.03%
C20:4n6	1.30% ± 0.01%	0.01% ± 0.01%	0.99% ± 0.06%	0.87% ± 0.23%	76.15% ± 3.26%
C20:5n3	6.90% ± 0.04%	0.08% ± 0.01%	5.48% ± 0.32%	1.15% ± 0.13%	79.42% ± 1.97%
ΣPUFAs	9.30% ± 0.07%	0.10% ± 0.02%	7.25% ± 0.34%	1.12% ± 0.20%	77.96% ± 1.56%
Total FA	17.30% ± 0.18%	0.19% ± 0.04%	12.49% ± 0.50%	1.07% ± 0.17%	72.20% ± 1.86%

As expected, the results from the first extraction step were similar to the ones described before for the fifteen-step extraction and five-step extractions. The first extraction step could only extract 0.19 pp of the 17.30% ± 0.18% of total fatty acids present in the initial biomass, which means that only 1.07% ± 0.17% of the total fatty acids present in the initial biomass were extracted in the first step. As assumed before, the first extraction step might have reduced the amount of water present in the residual pellet and consequently, it might have benefited the extraction efficiency of the second extraction step. On the other hand, the second step of extraction, with a solvent to biomass ratio of 5 $mL.g^{-1}$, reached an extraction efficiency of 72.20% ± 1.86% and an EPA extraction efficiency of 79.42% ± 1.97%. Again, the lipid extraction efficiency with ethanol 99.8% (% *v*/*v*) was higher than 70%.

Scenario C) One-step extraction with a solvent to biomass ratio of 5 mL.g^{-1}

The experiment was performed by extracting the solid matrix (5 g of paste at 200 g_{SFDW}/L) with 25 mL of ethanol 99.8% in only one extraction step. The solvent to biomass ratio of 5 mL.g^{-1} was selected based on the results of extraction efficiency from the previous experiments. All the previous extraction experiments demonstrated that it is possible to achieve extraction efficiencies above 70% with a volume of 5 mL of extraction solvent per gram of disrupted paste. The premise in this scenario was to achieve at least 70% of extraction efficiency in a single extraction step which could reduce the equipment required in a biorefinery and consequently the energy required in the extraction process.

Table 5.8 shows the results from the fatty acid profiles from the initial disrupted biomass, and ethanolic extract, as well as the extraction efficiency achieved with **scenario C**. The single-step extraction with a ratio of 5 mL.g^{-1} reached a lipid extraction efficiency of 70.98% ± 3.09% and an EPA extraction efficiency of 75.36% ± 3.48%. Compared with the previous scenario (**Scenario B**), where the extraction with a ratio of 5 mL.g^{-1} was performed after the first extraction with a ratio of 1 mL.g^{-1}, it is possible to conclude that **scenario C**, with a single extraction, extracted almost the same percentage of lipids from the initially disrupted paste as the scenario B (72.20% ± 1.86%). The same conclusion can be taken when comparing the percentage of EPA extracted in both scenarios. As mentioned before, Ryckebosch *et al.* reported an extraction efficiency of 52% $w/w_{total\ lipids}$ for ethanol systems (ethanol 96% *v*/*v*) [183], with a solvent to dry biomass ratio of 60 mL.g^{-1}. In the present experiment, the solvent to dry biomass ratio used was 25 mL.g^{-1}, which is almost 2.5 times lower than the ratio used by Ryckebosch *et al.* Nevertheless, it was possible to achieve a lipid extraction efficiency higher than 70%, with ethanol 99.8%. Again, this might be related to the cell disruption method selected by the author to disrupt the cells (bead beaten), which probably has a lower disruption efficiency when compared with the bead milling used in the present experiment (> 90% cellular disruption). Also, the purity of the ethanol used in the experiment might increase the lipid extraction efficiency.

Table 5.8. One-step extraction with ethanol. Fatty acid profile (initially disrupted paste and the ethanolic extract resulting from 1-step extraction), and extraction efficiency. The fatty acid profile results are provided on a basis of the SFDW of the initially disrupted paste. The extraction efficiency results are presented as % *w fatty acids extracted*/ w *fatty acids present in the initially disrupted paste*. The extraction step was performed with a solvent to biomass ratio of 5 $mL.g^{-1}$. The results are based on 2 replicates for each sample.

Fatty Acid	Fatty Acid Profile		Extraction Efficiency (% $wFA_{extracted}/wFA_{available}$)
	Initial Disrupted Paste (% w_{FA}/w_{SFDW})	Ethanolic Extract (% w_{FA}/w_{SFDW})	
		Ratio 5:1 ($mL.g^{-1}$)	Ratio 5:1 (mL.g-1)
C14:0	0.80% ± 0.04%	0.60% ± 0.05%	75.00% ± 2.51%
C16:0	2.60% ± 0.05%	2.10% ± 0.13%	80.77% ± 3.45%
C18:0	0.10% ± 0.00%	0.08% ± 0.08%	80.00% ± 2.00%
ΣSFAs	3.50% ± 0.08%	2.78% ± 0.20%	79.43% ± 3.16%
C16:1	3.80% ± 0.06%	2.70% ± 0.17%	71.05% ± 3.35%
C18:1	0.70% ± 0.01%	0.60% ± 0.19%	85.71% ± 3.06%
ΣMUFAs	4.50% ± 0.07%	3.30% ± 0.36%	73.33% ± 3.30%
C18:2n6	0.70% ± 0.01%	0.00% ± 0.02%	0.00% ± 1.41%
C18:3	0.20% ± 0.04%	0.10% ± 0.01%	50.00% ± 5.21%
C20:3	0.20% ± 0.01%	0.00% ± 0.01%	0.00% ± 1.38%
C20:4n6	1.30% ± 0.01%	0.90% ± 0.05%	69.23% ± 3.31%
C20:5n3	6.90% ± 0.04%	5.20% ± 0.27%	75.36% ± 3.48%
ΣPUFAs	9.30% ± 0.07%	6.20% ± 0.34%	66.67% ± 2.92%
Total FA	17.30% ± 0.18%	12.28% ± 0.50%	70.98% ± 3.09%

Scenario D) One-step extraction with a solvent to biomass ratio of 10 $mL.g^{-1}$

The experiment was performed by extracting the solid matrix (4 g of paste at 200 $g_{SFDW}.L^{-1}$) with 50 mL of ethanol 99.8% in only one extraction step. The solvent to biomass ratio of 10 $mL.g^{-1}$ was selected aiming at the maximization of the lipid extraction with ethanol 99.8%.

Table 5.9 shows the results of the lipid extraction efficiency for the single extraction with a solvent to biomass ratio of 10 $mL.g^{-1}$, as well as the results of the fatty acids profiles from the initially disrupted biomass and from the ethanolic extract obtained from **scenario D**. The single-step extraction with a ratio of 10 $mL.g^{-1}$ reached a lipid extraction efficiency of 80.81% ± 0.65% and an EPA extraction efficiency of 83.77% ± 1.11%. The difference in terms of extraction efficiency between the previous scenario (**scenario C**) and the present scenario (**scenario D**) is 9.83 percentage points. The results obtained in the present experiment demonstrate that the solvent to biomass ratio plays a major role in extraction efficiency. Also, the pre-treatments (e.g., mechanical disruption of the cells) before the extraction could

have a great influence on extraction efficiency. In the present experiment, the microalgae cells were disrupted through bead milling, achieving a cellular disruption higher than 90%, and allowing to reach a lipid extraction efficiency of 80.81% ± 0.65% with a solvent to dry biomass ratio of 50 $mL.g^{-1}$. Ryckebosch *et al.* disrupted the previously freeze-dried *Nannochloropsis gaditana* cells through bead beating and performed an extraction with ethanol (96% *v*/*v*) to dry biomass ratio of 60 $mL.g^{-1}$ [183]. However, the lipid extraction efficiency reported by the author was lower (52% $w/w_{total\ lipids}$) than the one achieved in the present experiment. The bead beating might not promote the same number of collisions (and with the same energy) between the beads and the cells, resulting in a lower number of disrupted cells. In the present experiment, it was achieved a cellular disruption higher than 90%, which indicates that almost the totality of the lipids were available to be extracted by the ethanol 99.8% (% *v*/*v*).

Table 5.9. One-step extraction with ethanol. Fatty acid profile (initially disrupted paste and the ethanolic extract resulting from 1-step extraction), and extraction efficiency. The fatty acid profile results are provided on a basis of the SFDW of the initially disrupted paste. The extraction efficiency results are presented as % *w fatty acids extracted*/ *w fatty acids present in the initially disrupted paste*. The extraction step was performed with a solvent to biomass ratio of 10 $mL.g^{-1}$. The results are based on 2 replicates for each sample fatty acid analysis.

Fatty Acid	Fatty Acid Profile		Extraction Efficiency (% $wFA_{extracted}/wFA_{available}$)
	Initial Disrupted Paste (% w_{FA}/w_{SFDW})	Ethanolic Extract (% w_{FA}/w_{SFDW})	
		Ratio 10:1 ($mL.g^{-1}$)	Ratio 10:1 ($mL.g^{-1}$)
C14:0	0.80% ± 0.04%	0.60% ± 0.01%	75.00% ± 2.51%
C16:0	2.60% ± 0.05%	2.30% ± 0.06%	88.46% ± 0.61%
C18:0	0.10% ± 0.00%	0.08% ± 0.00%	75.00% ± 1.67%
ΣSFAs	3.50% ± 0.08%	2.90% ± 0.08%	82.86% ± 1.25%
C16:1	3.80% ± 0.06%	3.00% ± 0.08%	78.95% ± 0.86%
C18:1	0.70% ± 0.01%	0.60% ± 0.02%	85.71% ± 1.63%
ΣMUFAs	4.50% ± 0.07%	3.60% ± 0.10%	80.00% ± 0.98%
C18:2n6	0.70% ± 0.01%	0.60% ± 0.01%	85.71% ± 0.20%
C18:3	0.20% ± 0.04%	0.05% ± 0.04%	25.00% ± 3.76%
C20:3	0.20% ± 0.01%	0.00% ± 0.00%	0.00% ± 1.19%
C20:4n6	1.30% ± 0.01%	1.10% ± 0.04%	84.62% ± 2.43%
C20:5n3	6.90% ± 0.04%	5.78% ± 0.11%	83.77% ± 1.11%
ΣPUFAs	9.30% ± 0.07%	7.48% ± 0.12%	80.43% ± 1.19%
Total FA	17.30% ± 0.18%	13.98% ± 0.29%	80.81% ± 0.65%

Scenarios comparison

The comparison in terms of extraction efficiency (**Table 5.10**) shows that scenario D (one-step extraction with a solvent to biomass ratio of 10 $mL.g^{-1}$) is the one with a higher lipid extraction efficiency (80.81 ± 0.65%). The other scenarios revealed that 71% to 73% of the lipids present in the initially disrupted paste were extracted during the ethanolic extraction. The results from these experiments suggest that the solvent to biomass ratio has an important role in the extraction process: with higher solvent to biomass ratios, higher lipid extraction efficiencies are achieved.

Table 5.10. Extraction efficiency in each proposed extraction scenario. The results are presented as % $wFA_{extracted}$/ $wFA_{available}$ and, they are based on 2 replicates for each sample.

Fatty Acid	Ethanolic Extract (% wTFA $_{ethanolic\ extract}$/wTFA $_{biomass\ SFDW}$)			
	Scenario A Ratio 1:1 × 5 ($mL.g^{-1}$)	**Scenario B Ratio 1:1 + 5:1 ($mL.g^{-1}$)**	**Scenario C Ratio 5:1 ($mL.g^{-1}$)**	**Scenario D Ratio 10:1 ($mL.g^{-1}$)**
C14:0	78.81% ± 1.91%	75.00% ± 2.31%	75.00% ± 2.51%	75.00% ± 2.51%
C16:0	70.14% ± 2.67%	69.23% ± 2.24%	80.77% ± 3.45%	88.46% ± 0.61%
C18:0	88.65% ± 5.03%	40.00% ± 2.90%	80.00% ± 2.00%	75.00% ± 1.67%
ΣSFAs	72.65% ± 1.36%	69.71% ± 1.92%	79.43% ± 3.16%	82.86% ± 1.25%
C16:1	78.19% ± 4.79%	63.16% ± 3.00%	71.05% ± 3.35%	78.95% ± 0.86%
C18:1	70.42% ± 7.41%	57.14% ± 4.03%	85.71% ± 3.06%	85.71% ± 1.63%
ΣMUFAs	76.98% ± 5.11%	62.22% ± 3.13%	73.33% ± 3.30%	80.00% ± 0.98%
C18:2n6	77.77% ± 2.01%	82.86% ± 1.21%	0.00% ± 1.41%	85.71% ± 0.20%
C18:3	33.79% ± 1.10%	50.00% ± 3.36%	50.00% ± 5.21%	25.00% ± 3.76%
C20:3	5.00% ± 0.52%	50.00% ± 1.03%	0.00% ± 1.38%	0.00% ± 1.19%
C20:4n6	63.21% ± 4.03%	76.15% ± 3.26%	69.23% ± 3.31%	84.62% ± 2.43%
C20:5n3	75.32% ± 1.31%	79.42% ± 1.97%	75.36% ± 3.48%	83.77% ± 1.11%
ΣPUFAs	71.41% ± 0.56%	77.96% ± 1.56%	66.67% ± 2.92%	80.43% ± 1.19%
Total FA	73.11% ± 1.83%	72.20% ± 1.86%	70.98% ± 3.09%	80.81% ± 0.65%

5.4.3. Techno-Economic evaluation

The four scenarios proposed and tested were compared against each other not only in terms of lipid extraction efficiency, as shown previously in **Table 5.10**, but also in terms of process complexity, EPA concentration in the final product, CAPEX, OPEX and production cost.

To evaluate the complexity of each one of the proposed scenarios, the flowcharts were designed and are presented below. Furthermore, all the scenarios were simulated considering a *Nannochloropsis* sp.

disrupted paste feed of 461 $kg_{SFDW}.day^{-1}$ (152 $ton_{SFDW}.year^{-1}$), for 330 $day.year^{-1}$ and 22 $h.day^{-1}$ of operation. The mass balance and consequently the economic parameters CAPEX (main equipment), OPEX and production cost of the EPA rich ethanolic concentrated extract (€.kg $EPA_{extract}^{-1}$) were calculated based on these assumptions. The average annual maintenance and consumables cost, for all the scenarios, has been assumed as a percentage of 5% and 2% of the investment cost, respectively. Regarding the solvent cost calculation, an 80% recovery ratio was assumed for all the scenarios.

The estimated values for the cost of each of the equipment were based on the supplier's price quotations and the scale-up factor [186]. The electric power and steam consumption for all the equipment were simulated and estimated in Super Pro Designer®.

Scenario A, which is five-step extraction with a solvent to biomass ratio of 1 $mL.g^{-1}$ is presented in **Figure 5.8** and includes 5 mixing tanks, 5 centrifuges, and 1 evaporator with an estimated total equipment investment of 1.127 M€.

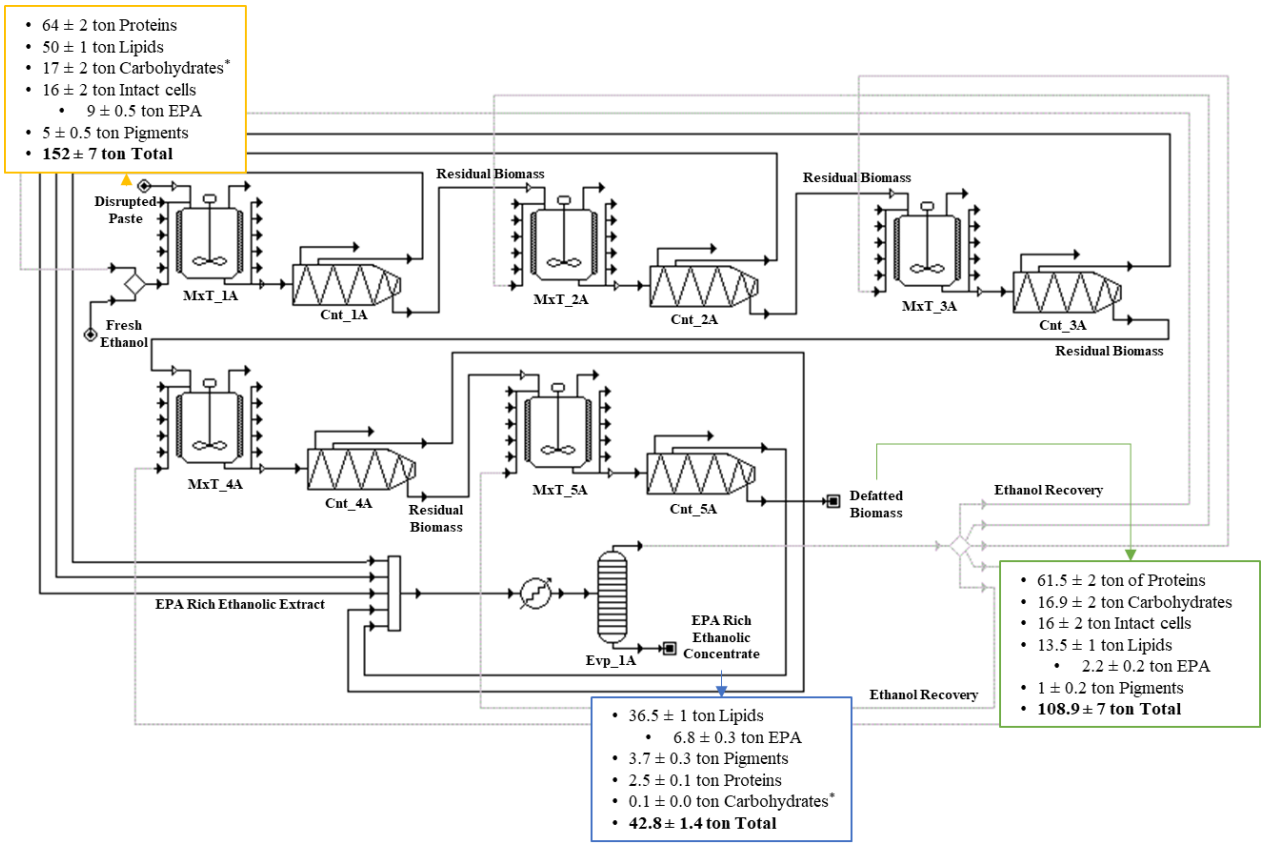

Figure 5.8. Flowchart and mass balance (salt-free dry weight) of the extraction process proposed for scenario A (five-step extraction with a solvent to biomass ratio of 1 $mL.g^{-1}$). The mixing tanks were named "MxT_xA", the

centrifuges "Cnt_xA", and the evaporator was named "Evp_xA". *The carbohydrates were estimated by the difference between the total salt-free dry weight and the sum of the analysed compounds.

Scenario A has a higher complexity in terms of operation and requires more equipment as well as a higher operational area for the installation of all the main equipment. The cost of the main equipment for **scenario A**, as well as the electrical energy consumption ($kWh.year^{-1}$), and the steam consumption ($ton.year^{-1}$) are presented in **Table 5.11**.

Table 5.11. Main equipment cost, electrical energy consumption, and steam consumption for scenario A (five-step extraction with a solvent to biomass ratio of 1 $mL.g^{-1}$). *The values were estimated in Super Pro Designer®.

	Name	Description	Equipment cost (€)	Electricity* (kWh/year)	Steam* (ton/year)
Main Equipment	**MxT_1A**	Mixing Tank 1	*74 000 €*	1900	-
	Cnt_1A	Centrifuge 1	*100 000 €*	36900	-
	MxT_2A	Mixing Tank 2	*58 000 €*	1200	-
	Cnt_2A	Centrifuge 2	*80 000 €*	30700	-
	MxT_3A	Mixing Tank 3	*50 000 €*	1100	-
	Cnt_3A	Centrifuge 3	*80 000 €*	31000	-
	MxT_4A	Mixing Tank 4	*50 000 €*	1100	-
	Cnt_4A	Centrifuge 4	*80 000 €*	29900	-
	MxT_5A	Mixing Tank 5	*50 000 €*	1100	-
	Cnt_5A	Centrifuge 5	*80 000 €*	29700	-
	Evp_1A	Evaporator	*425 000 €*	77500	2950
		Total	*1 127 000 €*	242100	2950

Scenario B (two-step extraction with a solvent to biomass ratio of 1 $mL.g^{-1}$ in the first step and 5 $mL.g^{-1}$ in the second step) is presented in **Figure 5.9** and includes 2 mixing tanks, 2 centrifuges, and 2 evaporators with an estimated total equipment investment of 1.101 M€. This scenario has two steps of extraction and requires only two mixing tanks and two centrifuges. However, this scenario involves the need for a second evaporator to recover the ethanol from the first step and additionally requires the waste treatment of the bottom phase of the evaporator.

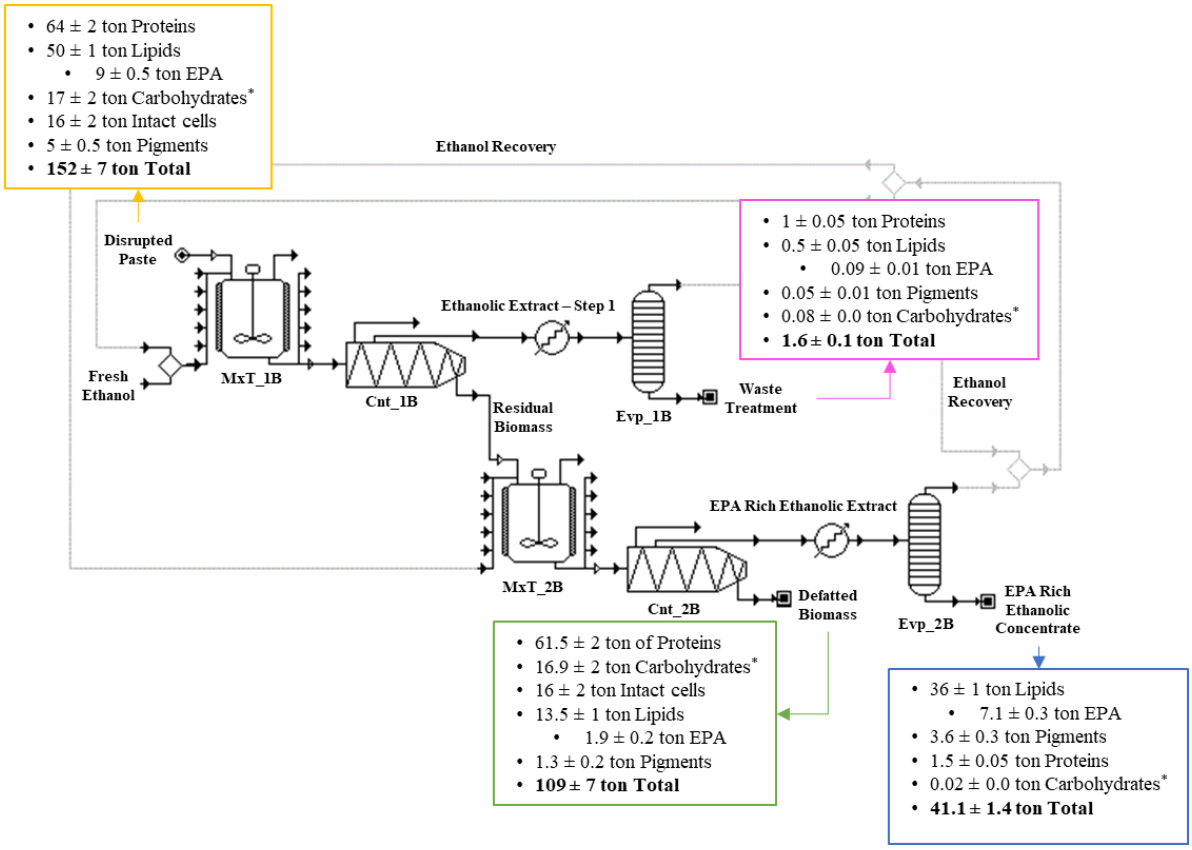

Figure 5.9. Flowchart and mass balance (salt-free dry weight) of the extraction process proposed for the scenario B (two-step extraction with a solvent to biomass ratio of 1 $mL.g^{-1}$ in the first step and 5 $mL.g^{-1}$ in the second step). The mixing tanks were named "MxT_xB", the centrifuges "Cnt_xB", and the evaporator was named "Evp_xB". *The carbohydrates were estimated by the difference between the total salt-free dry weight and the sum of the analysed compounds.

The cost of the main equipment for **scenario B**, as well as the electrical energy consumption ($kWh.year^{-1}$), and the steam consumption ($ton.year^{-1}$) are presented in **Table 5.12**.

Table 5.12. Main equipment, electrical energy consumption, and steam consumption for scenario B (two-step extraction with a solvent to biomass ratio of 1 mL.g^{-1} in the first step and 5 mL.g^{-1} in the second step). *The values were estimated in Super Pro Designer®.

	Name	Description	Equipment cost (€)	Electricity* (kWh/year)	Steam* (ton/year)
Main Equipment	**MxT_1B**	Mixing Tank 1	*74 000 €*	1900	-
	Cnt_1B	Centrifuge 1	*100 000 €*	36900	-
	Evp_1B	Evaporator 1	*270 000 €*	31800	1200
	MxT_2B	Mixing Tank 2	*112 000 €*	5000	-
	Cnt_2B	Centrifuge 2	*120 000 €*	56000	-
	Evp_2B	Evaporator 2	*425 000 €*	77327	2950
		Total	*1 101 000 €*	208927	4150

S**cenario C** (one-step extraction with a solvent to biomass ratio of 5 mL.g^{-1}) is presented in **Figure 5.10** and includes 1 mixing tank, 1 centrifuge, and 1 evaporator with an estimated total equipment investment of 662 k€.

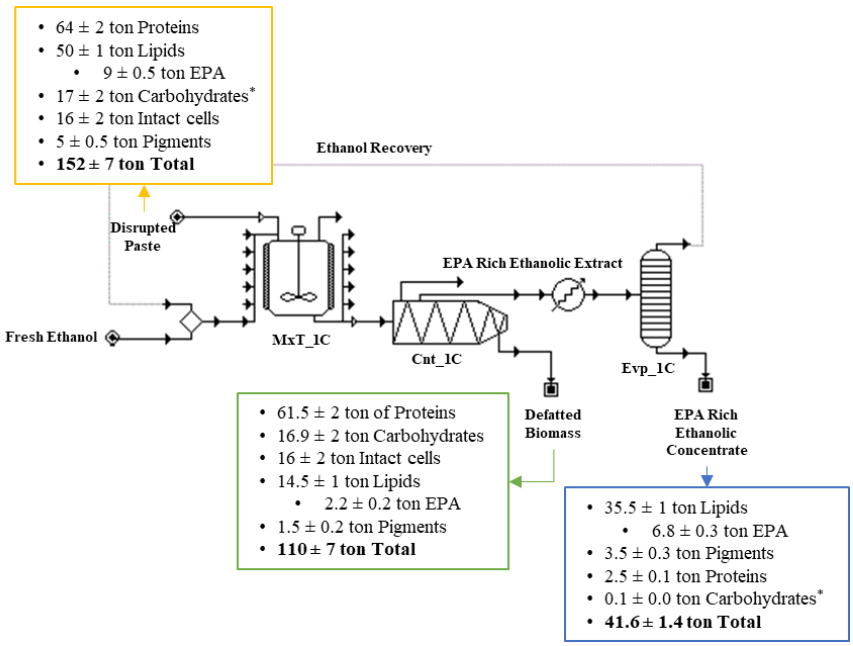

Figure 5.10. Flowchart and mass balance (salt-free dry weight) of the extraction process proposed for the scenario C (one-step extraction with a solvent to biomass ratio of 5 mL.g^{-1}). The mixing tanks were named "MxT_xC", the centrifuges "Cnt_xC", and the evaporator was named "Evp_xC". *The carbohydrates were estimated by the difference between the total salt-free dry weight and the sum of the analysed compounds.

Scenario C has only one step of extraction which decreases the number of equipment pieces as well as the area needed for their installation. **Table 5.13** shows the total equipment cost for **scenario C**. The electrical energy consumption (kWh.year^{-1}) and the steam consumption (ton.year^{-1}) are also presented in **Table 5.13**.

Table 5.13. Main equipment cost, electricity consumption, and steam consumption for scenario C (one-step extraction with a solvent to biomass ratio of 5 mL.g^{-1}). *The values were estimated in Super Pro Designer®.

	Name	Description	Equipment cost (€)	Electricity* (kWh/year)	Steam* (ton/year)
Main Equipment	**MxT_1C**	Mixing Tank 1	*117 000 €*	5000	-
	Cnt_1C	Centrifuge 1	*120 000 €*	57700	-
	Evp_1C	Evaporator 2	*425 000 €*	77400	2950
		Total	*662 000 €*	140100	2950

Scenario D (one-step extraction with a solvent to biomass ratio of 10 mL.g^{-1}) is presented in **Figure 5.11** and includes 1 mixing tank, 2 centrifuges, and 1 evaporator with an estimated total equipment investment of 1.055 M€. This scenario has also one step of extraction, however, the selected solvent to biomass ratio of 10 mL.g^{-1} implies the use of a higher volume of solvent than **scenario C**, and consequently requires equipment with higher volumes.

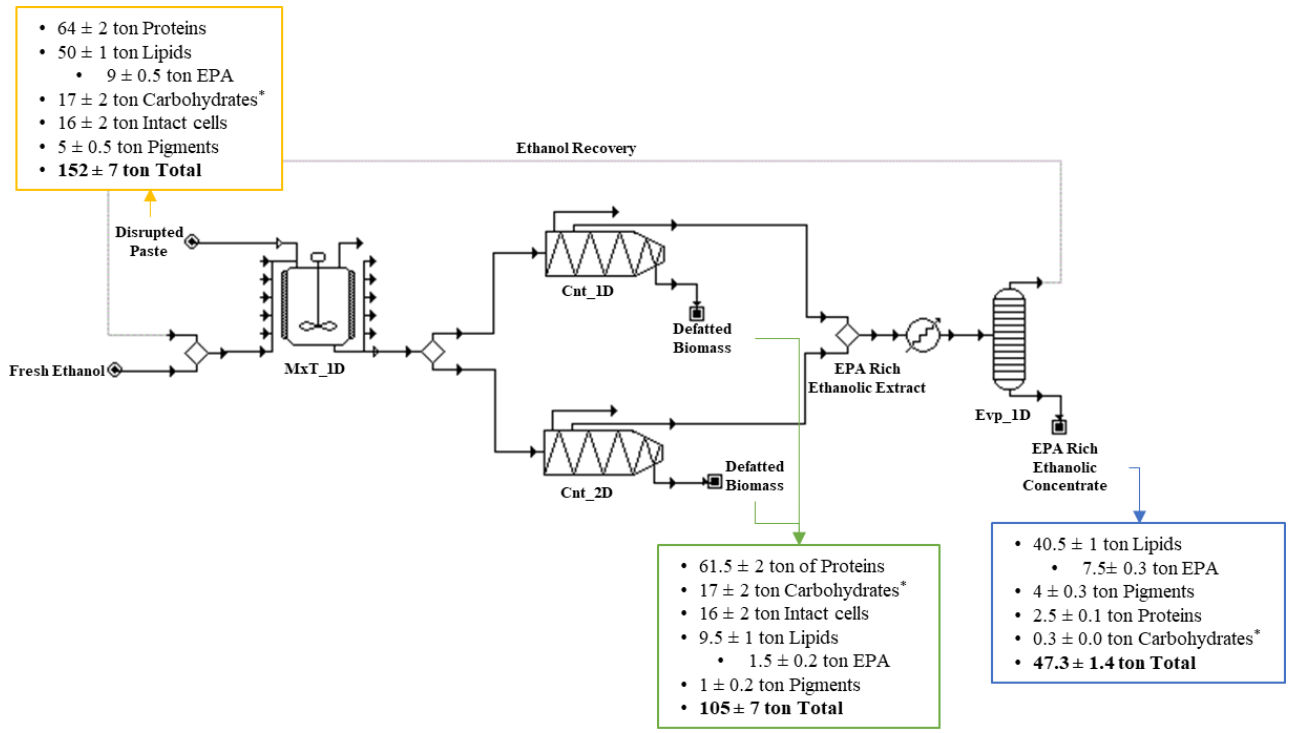

Figure 5.11. Flowchart and mass balance (salt-free dry weight) of the extraction process proposed for the scenario D (one-step extraction with a solvent to biomass ratio of 10 mL.g^{-1}). The mixing tanks were named "MxT_xD", the centrifuges "Cnt_xD", and the evaporator was named "Evp_xD". *The carbohydrates were estimated by the difference between the total salt-free dry weight and the sum of the analysed compounds.

The electrical energy consumption (kWh.year^{-1}), the steam consumption (ton.year^{-1}), and the total equipment cost for **scenario D** are presented in **Table 5.14**.

Table 5.14. Main equipment cost, electricity consumption, and steam consumption for scenario D (one-step extraction with a solvent to biomass ratio of 10 mL.g^{-1}). *The values were estimated in Super Pro Designer®.

	Name	Description	Equipment cost (€)	Electricity* (kWh/year)	Steam* (ton/year)
Main Equipment	**MxT_1D**	Mixing Tank 1	*190 000 €*	9500	-
	Cnt_1D	Centrifuge 1	*120 000 €*	57700	-
	Cnt_2D	Centrifuge 2	*120 000 €*	57700	-
	Evp_1D	Evaporator 1	*625 000 €*	146500	5700
		Total	*1 055 000 €*	271400	5700

Regarding the four scenarios proposed for the ethanolic extraction, which were previously presented, a techno-economic evaluation of each scenario was performed and the results are exhibited in **Table 5.15**. The assessment was based on the flowcharts and mass balances proposed for each scenario as well as the estimated values of main equipment cost, energy consumption, and steam consumption for each scenario, as exhibited before.

Table 5.15. Techno-economic evaluation of each scenario proposed for the ethanolic extraction process. The economic evaluation was based on 330 day.year^{-1} and 22 h.day^{-1} of operation. The capacity of each scenario was fixed in 152 ton$_{SFDW}$.year^{-1} of disrupted microalgae paste.

	Scenario A Ratio 1:1 x5 (mL.g^{-1})	Scenario B Ratio 1:1 + 5:1 (mL.g^{-1})	Scenario C Ratio 5:1 (mL.g^{-1})	Scenario D Ratio 10:1 (mL.g^{-1})
CAPEX				
Total equipment cost (€)	*1,127,000*	*1,101,000*	*662,000*	*1,055,000*
Capital costs (€.year^{-1}) *depreciation over 10 years	*112,700*	*110,100*	*66,200*	*105,500*
OPEX				
Human Resources (€.year^{-1})*1	*300,000*	*120,000*	*70,000*	*140,000*
Operational Electricity (kWh.year^{-1})	242100	208927	140100	271400
Electricity price (€.year^{-1}) (0.13 €/kWh) *2	*31,328*	*27,035*	*18,129*	*35,119*
Operational Steam (ton.year^{-1})	2950	4150	2950	5700
Steam price (€.year^{-1}) (20.0 €.ton^{-1}) [187]	*59,000*	*83,000*	*59,000*	*114,000*
Maintenance (€.year^{-1})	*56,350*	*55,050*	*33,100*	*52,750*
Consumables (€.year^{-1})	*22,540*	*22,020*	*13,240*	*21,100*
Solvents/Reagents (€.year^{-1})	*265,331*	*318,398*	*265,331*	*530,663*
Disrupted Paste Purchase Cost (€.year^{-1}) (10.0 €.kg$_{SFDW}^{-1}$)[188]	*1,516,342*	*1,516,342*	*1,516,342*	*1,516,342*
Total OPEX (€.year^{-1})	*2,250,892*	*2,141,845*	*1,975,143*	*2,409,974*
Total Cost of Ownership (€.year^{-1})	***2,363,592***	***2,251,945***	***2,041,343***	***2,515,474***
Total Disrupted Paste processed (ton.year^{-1})	691	691	691	691
Lipid Extraction Efficiency (%)	**73.1%**	**72.2%**	**71.0%**	**80.8%**
Total EPA Rich Extract production (ton.year^{-1})	**91**	**89**	**90**	**96**
Total EPA production (ton.year^{-1})	6.8	7.1	6.8	7.5
% Lipids/ EPA Rich Extract (w/w)	**40.0%**	**40.3%**	**39.4%**	**44.2%**
% Lipids/ EPA Rich Extract (w/w$_{SFDW}$)	85.3%	87.5%	85.3%	85.6%
% EPA/ EPA Rich Extract (w/w)	**7.5%**	**8.0%**	**7.6%**	**7.8%**
% EPA/ EPA Rich Extract (w/w$_{SFDW}$)	15.9%	17.3%	16.3%	15.9%
Production Cost EPA rich extract (€.kg$_{Extract}^{-1}$)	**25.9**	**25.2**	**22.7**	**26.2**
Production Cost EPA rich extract (€.kg$_{EPA}^{-1}$)	**347.6**	**317.2**	**300.2**	**335.4**
Electricity Consumption (kWh.kg$_{Extract}^{-1}$)	2.7	2.3	1.6	2.8
Electricity Consumption (kWh.kg$_{EPA}^{-1}$)	35.6	29.4	20.6	36.2

*1 HR = 2 x number centrifuges x 2500 €/mo/employee
*2 source: www.pordata.pt

The comparison between the four different scenarios concerning the technical assessment (**Table 5.15)**, revealed that **scenario D** has the higher lipid extraction efficiency (80.8% *w*/*w*), and the higher production capacity in terms of EPA rich extract – 96 ton.year^{-1}. However, the final product from this scenario is not the product with the highest concentration of EPA (15.9% *w*/w_{SFDW}). A higher solvent to biomass ratio (10 mL.g^{-1}) might have led to higher extraction efficiencies of other compounds besides lipids, such as chlorophyll *a* or ethanol-soluble proteins / amino acids, which dilutes the final product. On the other hand, **Scenario B** (two-step extraction with a solvent to biomass ratio of 1 mL.g^{-1} in the first step and 5 mL.g^{-1} in the second step) has the lowest production capacity – 89 ton.year^{-1} EPA rich extract. However, the final product of this scenario is the one with the highest concentration of EPA (17.3% *w*/w_{SFDW}). **Scenario B** has a higher complexity in terms of operation than scenario D, as it comprises the need for a second evaporator to recover the ethanol from the first step. However, this first step of extraction removes some of the compounds responsible for the final product dilution.

The CAPEX analysis revealed that **scenario A** (five-step extraction with a solvent to biomass ratio of 1 mL.g^{-1}) is the one that requires a higher investment in terms of main equipment (1.127 M€). Contrarily, **scenario C** (one-step extraction with a solvent to biomass ratio of 5 mL.g^{-1}) is the one that needs a lower investment (662 k€). Furthermore, among the four scenarios, **scenario C** has the lower value of OPEX per year (1.975 M€), which means that this scenario has the lowest total cost of ownership per year (2.041 M€). However, as mentioned before, **scenario C** (one-step extraction with a solvent to biomass ratio of 5 mL.g^{-1}) revealed the lowest lipid extraction efficiency (71% *w*/*w*), which can interfere with the decision of which one of the scenarios is the most advantageous one.

Two different indicators for the production of the EPA rich ethanolic extract (production cost, €/kg$_{EPA}$ and electricity consumption, kWh/kg$_{EPA}$) were calculated for each one of the proposed scenarios to choose the most suitable scenario. The results **Table 5.15**, revealed that scenario C (one-step extraction with a solvent to biomass ratio of 5 mL.g^{-1}) was the one with the lowest production cost (302 €/kg$_{EPA}$) and the lowest electricity consumption for the production of the EPA rich extract (22.7 kWh/kg$_{EPA}$). Therefore, the one-step extraction with a solvent to biomass ratio of 5 mL.g^{-1} scenario should be considered the most advantageous for an industrial application in terms of production costs. However, to achieve a more complete techno-economic analysis, the different scenarios should be also analysed from the point of view of the sales market. Also, as most of the techno-economic analysis parameters results for the 4 scenarios fall within a range of only 10-20% distance from one another, other business plan variables are likely to have a determinant weight in the choice of the scenario by an investor.

5.4.3.1. Sensitivity analysis

The parameters and assumptions used in this economic analysis have an intrinsic degree of uncertainty and are subject to change. To assess the impact of certain parameters, such as the solvent recovery percentage and the electricity cost (€/kWh), on the production cost of the EPA rich extract, a sensitivity analysis was conducted. Also, a sensitivity analysis regarding the extraction efficiency itself was performed, safeguarding any differences that may exist between the extraction efficiency on a laboratory scale (which has been tested) and the efficiency on an industrial scale. The main research questions that are answered are:

i. How does the total operation costs vary with the solvent recovery percentage?
ii. How does the production cost of EPA rich extract vary with the solvent recovery percentage?
iii. How does the total operation costs vary with the electrical energy price?
iv. How does the production cost of EPA rich extract vary with the electrical energy price?
v. How does the total operation costs vary with the extraction efficiency?
vi. How does the production cost of EPA rich extract vary with the extraction efficiency?

The sensitivity analysis based on the variation of the solvent recovery percentage (**Table 5.16**) demonstrates that an increase of 10 pp in the solvent recovery percentage leads to a decrease in the total operating costs of 5.8% in **scenario A**, 7.5% in **scenario B**, 6.6% in **scenario C**, and 11.2% in **scenario D**. The same tendency is observed in terms of production cost of EPA rich extract. The present sensitivity analysis also revealed that **scenario C** remained as the scenario with a lower production cost of EPA rich extract, even when the solvent recovery percentage decreased 10 percentage points.

Table 5.16. Economic sensitivity analysis for total operation cost and EPA rich extract production cost based on the variation of the solvent recovery percentage. The baseline was considered to be 80% of solvent recovery.

	Scenario A Ratio 1:1 x5 ($mL.g^{-1}$)			Scenario B Ratio 1:1 + 5:1 ($mL.g^{-1}$)			Scenario C Ratio 5:1 ($mL.g^{-1}$)			Scenario D Ratio 10:1 ($mL.g^{-1}$)		
Solvent Recovery (%)	70%	80%	90%	70%	80%	90%	70%	80%	90%	70%	80%	90%
Total OPEX (€.year^{-1})	*2.38M*	*2.25M*	*2.12M*	*2.30M*	*2.14M*	*1.98M*	*2.11M*	*1.97M*	*1.84M*	*2.68M*	*2.41M*	*2.14M*
Production Cost EPA rich extract (€.kg$_{Extract}^{-1}$)	27.4	25.9	24.5	27.0	25.2	23.4	24.2	22.7	21.2	29.0	26.2	23.5
Production Cost EPA rich extract (€.kg$_{EPA}^{-1}$)	367.1	347.6	328.1	339.6	317.2	294.8	319.7	300.2	280.7	370.8	335.4	300.0

On the other hand, the sensitivity analysis based on the variation of the electrical energy price (**Table 5.17**) revealed lower variations in the total operating costs than the variation of the solvent recovery percentage. Again, the sensitivity analysis revealed that **scenario C** remained as the scenario with a lower production cost of EPA rich extract, even when the electrical energy price decreased 50%, from 0.129 €/kWh to 0.065 €/kWh.

Table 5.17. Economic sensitivity analysis for total operation cost and EPA rich extract production cost based on the variation of the electrical energy price. The baseline was considered to be 0.129 €/kWh.

	Scenario A Ratio 1:1 x5 ($mL.g^{-1}$)			Scenario B Ratio 1:1 + 5:1 ($mL.g^{-1}$)			Scenario C Ratio 5:1 ($mL.g^{-1}$)			Scenario D Ratio 10:1 ($mL.g^{-1}$)		
Electricity price (€/kWh)	0.065	0.129	0.194	0.065	0.129	0.194	0.065	0.129	0.194	0.065	0.129	0.194
Total OPEX ($€.year^{-1}$)	*2.24M*	*2.25M*	*2.27M*	*2.13M*	*2.14M*	*2.16M*	*1.96M*	*1.97M*	*1.98M*	*2.43M*	*2.41M*	*2.39M*
Production Cost EPA rich extract ($€.kg_{Extract}^{-1}$)	25.7	25.9	26.1	25.1	25.2	25.4	22.6	22.7	22.8	26.0	26.2	26.4
Production Cost EPA rich extract ($€.kg_{EPA}^{-1}$)	345.3	347.6	349.9	315.3	317.2	319.1	298.9	300.2	301.5	333.1	335.4	337.7

Finally, the sensitivity analysis based on the variation of extraction efficiency is presented in **Table 5.18**. This sensitive analysis revealed that maintaining the total operating costs and variating the extraction efficiency within 5%, results in a relevant variation in the production cost in each one of the scenarios. Once again, the sensitivity analysis revealed that **scenario C** remained as the scenario with a lower production cost of EPA rich extract, even when the extraction efficiency decreases by 5%.

Table 5.18. Economic sensitivity analysis for total operation cost and EPA rich extract production cost based on the variation of the extraction efficiency. The baseline for each scenario was considered to be the extraction efficiency obtained in the experimental trials

	Scenario A Ratio 1:1 x5 ($mL.g^{-1}$)			Scenario B Ratio 1:1 + 5:1 ($mL.g^{-1}$)			Scenario C Ratio 5:1 ($mL.g^{-1}$)			Scenario D Ratio 10:1 ($mL.g^{-1}$)		
Extraction Efficiency (%)	69%	73%	77%	69%	72%	76%	67%	71%	75%	77%	81%	85%
Total OPEX (€.year^{-1})	*2.25M*	*2.25M*	*2.25M*	*2.14M*	*2.14M*	*2.14M*	*1.97M*	*1.97M*	*1.97M*	*2.41M*	*2.41M*	*2.41M*
Production Cost EPA rich extract (€.kg$_{Extract}^{-1}$)	27.3	25.9	24.7	26.5	25.2	24.0	23.9	22.7	21.6	27.6	26.2	25.0
Production Cost EPA rich extract (€.kg$_{EPA}^{-1}$)	365.9	347.6	331.0	333.9	317.2	302.1	316.0	300.2	285.9	353.1	335.4	319.4

5.5. Conclusions

An eco-friendly solvent methodology to perform a polar lipid extraction from wet *Nannochloropsis* sp. biomass with high efficiency was developed and optimised. Firstly, simultaneous extraction and fractionation of lipid from *Nannochloropsis* sp. for the production of EPA-rich polar lipid concentrate was attempted. However, the first extraction (neutral lipid extraction) with D-limonene extracted almost 20% of the EPA present in the polar fraction, which was not anticipated and represented a major loss of EPA to the neutral fraction. Therefore, this route was abandoned and the focus of the study turned to the extraction of polar lipids with ethanol. The results of the optimisation of the ethanol to biomass ratio revealed that the ratio of 10 $mL.g^{-1}$ was capable of achieving high polar lipid extraction efficiency (81% $w_{TFAextracted}/w_{TFAbiomass}$). However, the techno-economic assessment revealed that scenario B (two-step extraction with a solvent to biomass ratio of 1 $mL.g^{-1}$ in the first step and 5 $mL.g^{-1}$ in the second step of extraction) was able to produce a final product with the highest EPA concentration (17.3% w/w_{SFDW}). On the other hand, a sensitivity analysis to assess the impact of the solvent recovery percentage and the price of the electric energy on the production cost of the EPA revealed that scenario C (one-step extraction with a solvent to biomass ratio of 5 $mL.g^{-1}$) was the most advantageous one. Despite having a lower polar lipid extraction efficiency (71% $w_{TFAextract}/w_{TFAbiomass}$), scenario C was the one with the lowest production cost even with an increase of 50% in the electrical energy price (301.5 €/kg_{EPA}), or with a decrease in the solvent recovery percentage to 70% (319.7 €/kg_{EPA}).

6. *NANNOCHLOROPSIS* SP. BIOREFINERY: PROCESSING STRATEGIES AND TECHNO-ECONOMIC ASSESSMENT

6.1. Abstract

Nannochloropsis sp. is well-known for its high content in eicosapentaenoic acid which is one of the several omega-3 fatty acids, and it is commonly known as EPA. Nevertheless, *Nannochloropsis* sp. has also a high content of proteins, which are suitable for human food and feed applications. This work proposes a suitable process to maximise the potential of *Nannochloropsis* sp. for the production of distinct fractions of polar lipids rich in EPA omega-3 for supplements, colourless soluble protein for human food, and insoluble protein for animal feed, which may contribute to improving the viability of the microalgae industry. The proposed biorefinery with a production capacity of 218 $ton_{SFDW}.year^{-1}$ was designed and the mass and energy flow model were simulated. To evaluate the profitability of the proposed biorefinery, a detailed techno-economic evaluation was achieved.

A comparative analysis between three different scenarios with different operational costs, as well as a comparative analysis between three different scenarios with different operational scales of production was performed. Also, the techno-economic performance of a single product value chain and a multiproduct value chain biorefinery were compared. The net present value (NPV), the internal rate of return (IRR), and the payback periods were calculated and compared for the different conditions considered, pointing out the major drivers and bottlenecks concerning the plant's economic performance and profitability. The baseline designed multi-product biorefinery resulted in estimated economic performance indicators that correspond to an IRR of 20.3%, and a payback period of 4.7 years.

6.2. Introduction

A biorefinery is an installation that integrates biomass conversion processes to produce biofuels, energy, and high-value products from several kinds of biomass (e.g., organic residues, forest residues, and aquatic biomass such as algae and seaweeds) [189]. A biorefinery includes the pre-treatment and the fractionation of the biomass components and the subsequent conversion to generate a variety of different products. By producing multiple products, a biorefinery can take advantage of the different components present in the biomass, taking full advantage of the value of the biomass feedstock [189].

Microalgae are often referred to as a highly advantageous feedstock for the production of biofuels in response to the increase of the world population and the consequent uprising energy crisis. This is mainly

because several microalgae species have superior biomass production potentials and photosynthetic efficiencies than terrestrial crops [190]. However, the high production cost, when compared with fossil fuel, represents a major drawback and shows an economic need to find profitable microalgae solutions and processes [1,79]. High-value products have been produced through the fractionation of microalgae extracts to improve the economic performance achieved, by applying the concept of microalgae biorefinery [191]. There are several such microalgae biorefineries described in the literature. Chua *et al.* [83] proposed a *Nannochloropsis* biorefinery to produce EPA-rich oil and high-value protein. Nobre *et al.* [192] studied a biorefinery from *Nannochloropsis* sp. to extract oils and pigments and produce biohydrogen from the leftover biomass. Bongiovani *et al.* [193] described a biorefinery approach from *Nannochloropsis oceanica* CCALA 978, to produce neutral lipids and carotenoids. Cui *et al.* [194] developed a biorefinery approach to produce omega-3 fatty acids and protein from *Phaeodactylum tricornutum*.

In the present work, *Nannochloropsis* sp. was selected as a promising microalgae for a biorefinery concept as this strain global market is predictable to record a compound annual growth rate (CAGR) of 8.5% from 2021 to 2028, reaching a market value of US$ 15.8 million by 2028. The increasing demand for microalgae protein with functionality for human food or animal feed, the growing demand for omega-3 fatty acids for food supplements, and the protein- and carbohydrates-rich fraction for animal feed, are driving the growth of the global *Nannochloropsis* market [195]. Also, this strain has a particular interest for A4F – Algae for Future since the product with the higher added-value (EPA-rich lipid extract) obtained from it is soluble in polar solvents, and therefore *Nannochloropsis* sp. can be stated as a model for future work with other microalgae strains in which the compounds of interest are also soluble in polar solvents.

Nannochloropsis sp. is one of the unicellular marine species that is widely known for its capacity to accumulate high amounts of omega-3 fatty acids, specifically EPA (up to 5% of dry biomass, when produced under optimal growth conditions) [33]. In most microalgae species, omega-3 PUFAs are present principally in the polar lipid fraction, appealing to be the most efficiently absorbed by the human body [169].

The *Nannochloropsis*-derived lipids market is expected to record a CAGR of 8.5% from 2021 to 2028 to reach a market value of US $ 4.2 million by 2028, according to the Research and Markets 2021 report [196]. Also, it is important to notice that the EPA-rich lipid fraction could be a substitute for fish oil whose global market size was valued at US$ 1,905.77 million in 2019, and it is estimated to reach US$ 2,844.12 million by 2027 with a CARG of 5.8% from 2021 to 2027 [197].

Nannochloropsis sp. cells are spherical with a diameter of 2-5 μm, and with a robust cell wall composed of a structure consisting of a cellulosic internal wall and a hydrophobic algaenan outer layer [83]. This microalga presents specific biochemical characteristics such as the lack of accessory chlorophylls *b* and *c*, the presence of interesting xanthophyll pigments [36], and its ability to accumulate lipids up to 50% of the dry biomass when grown under Nitrogen-deplete conditions (mainly TAGs) [30], but this is not reflected on EPA accumulation [84]. When the cells are grown under Nitrogen-replete conditions, the lipid content represents 20%-30% of the total dry weight [198,199], and the polar lipid fraction represents 80-90% of the total lipids [200].

This strain has also an important content in total protein, when produced under Nitrogen-replete conditions (up to 50% of dry weight) [32], both soluble (up to 20% salt-free dry weight) [34], and insoluble protein. The carbohydrates present in the *Nannochloropsis* sp. cells may represent 20-30% of the total dry weight [198,199] and are commonly used in animal feed applications [201]. The soluble protein fraction may be introduced on the market as a substitute for plant-based protein hydrolysates, whose market was valued at US$ 1197.13 million in 2020 and is expected to reach US$ 1755.89 million by the end of 2027, growing at a CARG of 4.8% from 2021 to 2027 [202]. On the other hand, the insoluble protein and carbohydrates mix fraction is commonly used in animal feed applications, as mentioned before, and might be a suitable substitute for fishmeal, whose market was valued at US$ 8,153.6 million in 2020 and is projected to reach US$ 15,264.6 million by the end of 2028, with expected growth at a CARG 8.3% from 2021 to 2028 [203].

Therefore, this proposed *Nannochloropsis* sp. biorefinery seems to be related to products that have large market potential and interesting expected growth rates, provided that competitive, feasible and profitable solutions can be identified, as will be further explored below.

The overall biorefinery costs are known to strongly depend on the biomass composition and the selected downstream processing technologies [190]. The first stage of biorefinery processing is the pre-treatment of the biomass, which might be composed of a biomass stabilisation step, to avoid the degradation of the intracellular compounds, and a cell disruption step, to release intracellular compounds. The most obvious solution to avoid biomass deterioration is to remove the water present in the biomass through drying processes (e.g., spray drying or freeze-drying). However, drying has typically high energy consumption [90], and therefore, the inactivation of the enzymes responsible for the chemical reactions that degrade the biomass at an early stage is an alternative [45]. The most common external agents to inactivate the enzymes are high or low temperature, extreme pH, and organic solvents [45]. After biomass stabilisation, there is a need to release the intracellular compounds to the media and make them accessible for further extraction and fractionation steps. The most common cell disruption techniques

are bead mill, high-pressure homogenisation and ultrasonication [204]. *Nannochloropsis* sp. has a strong cell, as mentioned before, and for that reason, bead milling is the disruption technique usually chosen [38].

After cell disruption, the fractionation step is typically composed of extraction steps where the target compounds are extracted from the disrupted biomass. The selected solvents should exhibit hydrophobicity/hydrophilicity properties similar to the compounds to be recovered. The most reported techniques are water-based extraction for water-soluble compounds (e.g., soluble proteins and carbohydrates), and solvent extractions for insoluble compounds (e.g., lipids and pigments). Accordingly, in a biorefinery aiming at the production of water-soluble compounds such as soluble protein, the target compounds are extracted by the aqueous media itself after the cell disruption step, as reported by Safi *et al.* [1]. On the other hand, when the target compounds are water-insoluble, such as polar lipids, the extraction might be carried out with a polar solvent or a mixture of solvents, as reported by Callejón *et al.* [81], and Ryckebosch *et al.*[183].

Finally, the compounds of interest are fractionated and purified from the previous extracts produced. The recovery of protein has gained a lot of attention, and different studies have been reported aiming at a suitable protein recovery technique. Membrane processing is an emerging technology in microalgae biorefinery processes, offering the possibility of operating under mild conditions and preventing the denaturation of proteins [150]. On the other hand, the purification of lipids extracts and the recovery of the organic solvents used in lipid extractions are mainly carried out through rotary evaporation [205] or vacuum distillation [184].

So far, *Nannochloropsis* sp. biorefineries strategies have been focused on the total lipid extraction for biodiesel production [68]. Nobre *et al.* [192] developed a *Nannochloropsis* sp. biorefinery for the production of oil (for biodiesel), carotenoids (for food supplements) and biohydrogen using the defatted biomass. Bongiovani *et al.* [193] also proposed a biorefinery approach from *Nannochloropsis oceanica* CCALA 978, under nutritional stress conditions, for the production of neutral lipids (for biodiesel) and carotenoids as a value-added bioproduct to increase the profitability of the process. Nevertheless, the recovery of microalgae proteins from aqueous supernatants has also gained a lot of interest. Safi *et al.* [1] reported the recovery of *Nannochloropsis gaditana* proteins by ultrafiltration/ diafiltration (UF/DF). Cavonius *et al.* [71] described a pH-shift precipitation technique to find a protein isolate from *Nannochloropsis oculata.* More recent studies within the biorefinery concept have been focused on the extraction of an EPA rich polar lipid fraction, which is a value-added bioproduct, to increase the profitability of the process. Callejón *et al.* [81] studied the sequential extraction of saponifiable lipids

from *Nannochloropsis* sp. biomass, for the production of an EPA omega-3 rich fraction (for food supplements).

This work aims to propose and discuss the development of a process scheme to maximise the potential of *Nannochloropsis* sp. as a feedstock, focusing on the production of distinct fractions: EPA rich polar lipids fraction (for food supplements) as a substitute for fish oil, soluble protein rich fraction (for human food) as a substitute for plant-based protein hydrolysates, and insoluble protein rich fraction (for animal feed) as a substitute for fishmeal. To the best of our knowledge, a biorefinery for the production of such a portfolio of compounds from *Nannochloropsis* sp. has not been proposed or studied. Therefore, here we will study the techno-economic performance of a single product value chain as compared to a multiproduct value chain biorefinery. The ultimate goal is to assess if the biorefinery process proposed in this work is profitable and economically more appealing than a single product value chain biorefinery. Also, a comparative analysis between different scenarios, with different operational and investment costs, was performed. This includes, for each possibility, the computation and comparison of net present value (NPV), internal rate of return (IRR), and payback values.

6.3. Materials and Methods

For the sake of the economic analysis, standard project investment tools were employed and applied to the several scenarios of the multi-product biorefinery proposed, where the cash flows connected with the major streams of the flowsheet, as well as the corresponding equipment investments, are accounted for, as illustrated in the coming sections presented next.

6.3.1. *Nannochloropsis* sp. biorefinery

For the multi-product biorefinery proposed, a specific technical process model has been designed and will now be linked to its techno-economic evaluation. The scheme of the selected processing steps, within a biorefinery concept, is presented in **Figure 6.1** where two different downstream routes are proposed: an aqueous route, and an ethanolic route. Within the biorefinery concept, the downstream processing is initiated with a set of pre-treatments. The first one is a biomass stabilisation step, aiming at the inactivation of enzymes responsible for the degradation of intracellular compounds. Then, the cellular disruption step will release the intracellular compounds to the aqueous media, enabling the following fractionation steps. Finally, the phase separation step will create the two different routes proposed: an aqueous route, and an ethanolic route. The aqueous route is composed of aqueous membrane processes, aiming for maximum recovery of soluble proteins. On the other hand, the main

objective of the ethanolic route is the extraction of an EPA-rich polar lipid fraction. Nevertheless, the ethanolic route also comprises the downstream steps to recover an insoluble protein fraction.

The detailed sequence of unit operations involved was already discussed before, and therefore for the sake of this economic assessment **Figure 6.1** provides an appropriate summary of the plant's main building blocks for such an analysis to be performed and studied.

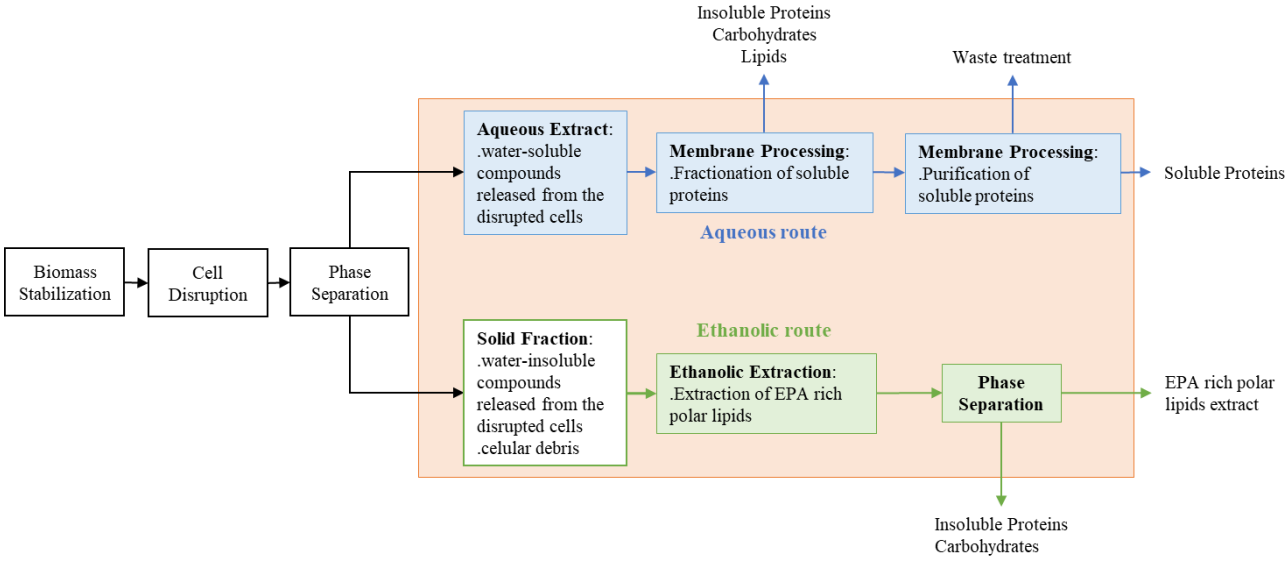

Figure 6.1. Scheme of the main downstream steps of the *Nannochloropsis* sp., considering the biorefinery scheme proposed in this work

The biomass stabilisation within the *Nannochloropsis* sp. biorefinery proposed is performed through heat treatment, as demonstrated and optimised in **chapter 2**. The selected operational condition for the heat treatment is 95 ºC for 3 minutes, for a 100 $g_{SDW}.L^{-1}$ *Nannochloropsis* sp. suspension The described process for a *Nannochloropsis* sp. biorefinery with a production capacity of 300 $L.h^{-1}$, was modelled using SuperPro Designer®.

The cellular disruption proposed is performed through bead milling, as demonstrated and optimised in **chapter 3**. The selected operational conditions for the cellular disruption through bead milling are the maximum tip speed (16 $m.s^{-1}$), a filling volume of 85% ($v.v^{-1}$), and a flow rate of around 300 $L.h^{-1}$. The described process was also modelled using SuperPro Designer®. The phase separation after the cellular disruption to separate cell debris from the aqueous fraction is described in **Appendix B**.

The membrane processing within the *Nannochloropsis* sp. biorefinery was divided into two different steps. The first step is performed using a 100 kDa MWCO membrane as demonstrated and optimised in

chapter 4. The mixture of ultrafiltration in a diafiltration mode followed by concentration under controlled permeate flux conditions enhances the soluble protein recovery in the permeate and allows to maintain a higher value of volumetric flux (12 $L.m^{-2}.h^{-1}$), during the entire diafiltration process. The second step of the membrane processing aims to purify the soluble protein present in the permeate resulting from the first step of the membrane processing. The removal of the salt present in the permeate is performed through ultrafiltration in a concentration mode followed by diafiltration, using a 1 kDa MWCO membrane. Details of the second step are provided in **Appendix B**.

The ethanolic extraction proposed is performed as demonstrated and optimised in **chapter 5**. The eco-friendly solvent (ethanol) step to perform the polar lipid extraction from wet *Nannochloropsis* sp. biomass is performed in one-step extraction with a solvent to biomass ratio of 5 $mL.g^{-1}$. The phase separation after the ethanolic extraction that separates the defatted pellet from the ethanolic extract and the following steps are described in **Appendix B**.

To support the economic performance analysis, a simplified process diagram was defined and considered for the recovery of the three different target fractions, defined previously: soluble protein fraction (with functionality for human food), insoluble protein fraction (for animal feed), and EPA-rich polar lipids fraction (for food supplements). All economic indicators and values were computed from the mass balances and the chemical characterisation of each process stream that was conducted before.

As a baseline, the mass balances were conducted considering a *Nannochloropsis* sp. biomass feed of 660 $kg_{SFDW}.day^{-1}$ (218 $ton_{SFDW}.year^{-1}$), for 330 $day.year^{-1}$ and 22$h.day^{-1}$ of operation. This reference production capacity of the biorefinery was fixed at 218 $ton_{SFDW}.year^{-1}$ as a value suggested by A4F – Algae for Future since it corresponds to what the company believes to be an appropriate scale for building and running such a plant.

6.3.2. Techno-economic analysis

The cost calculations covered both total capital investment (CAPEX) and total operational expenditures (OPEX), computed for a biorefinery to be located in Póvoa de Santa Iria, Portugal, next to the A4F – Algae for Future microalgae production facility.

The biorefinery capital investment was calculated from the purchase costs of the main equipment needed. The estimated values for the cost of each of the main pieces of equipment were based on the supplier's price quotations, combined, when needed, with a scale-up factor [186].

Furthermore, it is assumed that the construction period is one year, the start-up period is 3 years, and the plant lifetime is 10 years, with a linear depreciation of the CAPEX over these 10 years.

Operating expenditures are calculated as the sum of the cost of utilities (electricity and steam), raw materials (*Nannochloropsis* sp. biomass), solvents, membrane replacement, waste-water treatment, labour, additional consumables and maintenance costs. Such costs for utilities and raw materials are specified in **Appendix B**.

The biomass production cost is highly dependent upon biomass production scale, the production system selected, and the location where the biomass is produced, as demonstrated by the Public Output report of the EnAlgae project [188]. In the referred report, the production cost for algae produced in a flat panel PBR, located in the south of Spain (similar climate conditions to Portugal), and at a scale of 100 ha was reported to be between 4 €.kg_{SFDW}^{-1} and 5 €.kg_{SFDW}^{-1} [188]. On the other hand, for a microalgae production facility at a 10 ha scale level, the biomass production cost was reported to be between 7 €.kg_{SFDW}^{-1} and 10 €.kg_{SFDW}^{-1} [188]. Later, Ruiz et al. [206], and Branco-Vieira et al. [207] reported values of biomass production cost between 2 €.kg_{SFDW}^{-1} and 3 €.kg_{SFDW}^{-1}, at a 100 ha scale level and with production closed systems installed. Although microalgae production closed systems, such as flat panel reactors, need higher investments, they offer greater productivities, normally between 34 [206] and 38 $ton_{SFDW}.ha^{-1}.year^{-1}$ [208]. Therefore, even a microalgae production facility at a 10 ha scale level, with production closed systems, would have the capacity to feed the proposed biorefinery, whose annual biomass needs are assumed to have as a baseline a total of 218 $ton.ha^{-1}.year^{-1}$.

This techno-economic evaluation of the biorefinery proposed will assume that the biorefinery will be constructed next to an existing microalgae production facility, at a 100 ha scale level and with flat panel PBRs installed. Hence, the biomass cost will not include additional delivery costs, and therefore based on the reported values, and considering the 25% of profit margin for the production facility, the biomass market price that will be assumed as the reference point is 5 €.kg_{SFDW}^{-1}.

The average annual maintenance and consumables costs were assumed to be a percentage of 5% and 2% of the investment costs [63], respectively. The wastewater treatment cost was assumed to be constant and valued a 0.45 €.m^{-3}, as presented by Slegers *et.al* [209]. For location-dependent costs, Portugal was assumed as a reference.

The EPA-rich polar lipids fraction price is highly influenced by the concentration of omega-3 PUFAs, and for a final product with 15% to 17% of EPA, as validated by A4F – Algae for Future, the final price might vary between 40 €.kg^{-1} [210] and 70 €.kg^{-1} of EPA-rich polar lipids oleoresin [211]. In the present assessment, the final price of EPA-rich polar lipids oleoresin was assumed to be 55 €.kg^{-1}, based on the reported market values. The soluble proteins with functionality for food applications price was

foreseeable by Slegers to range between 5 €.kg^{-1} and 8 €.kg^{-1} [209]. On the other hand, the price of insoluble proteins and carbohydrates mix for feed applications was predicted as varying between 1 €.kg^{-1} and 3 €.kg^{-1} [209]. Therefore, in the present study, the average price for the soluble protein fraction with functionality for food applications was assumed to be 6.5 €.kg^{-1}, and the price of insoluble protein and carbohydrates mix for feed applications was assumed to be 2 €.kg^{-1}, also based on the reported values.

6.4. Results and Discussion

Taking into account the assumptions mentioned before, and the biorefinery design, including its main blocks, as summarized below, different alternatives and scenarios were considered, leading to economic performance results and comparisons that will be described next.

6.4.1. *Nannochloropsis* sp. biorefinery

Regarding the development of a biorefinery based on EPA-rich *Nannochloropsis* sp., for the sake of its economic analysis a simplified process diagram, as shown in **Figure 6.2**, is proposed for the recovery of the three different target fractions, defined previously: soluble protein fraction (with functionality for human food), insoluble protein fraction (for animal feed), and EPA-rich polar lipids fraction (for food supplements).

Briefly, the proposed biorefinery scheme uses EPA-rich *Nannochloropsis* sp. wet biomass that is first submitted to an aqueous extraction for the recovery of water-soluble compounds (e.g., soluble proteins), and then to an ethanolic extraction for the recovery of EPA-rich polar lipids. From the second extraction, it is also possible to recover a co-product mainly composed of water-insoluble compounds (e.g., insoluble proteins).

The first step of the proposed scheme comprises a heat treatment to stabilise the wet biomass before the cellular disruption. Heat treatment has been proven to be extremely helpful in the inactivation of the enzymes responsible for the degradation of intracellular compounds (e.g., lipid degradation through hydrolysis reactions catalysed by lipases). Then, bead milling was selected for cellular disruption, allowing to enhance the extraction of water-soluble compounds. Afterwards, the two main routes were established through phase separation by centrifugation: the aqueous route and the ethanolic route (**Figure 6.2**).

In the aqueous route, membrane processing (cut-offs of 100 kDa and 1 kDa) is used not only for the recovery of a soluble protein fraction but also for the reduction of lipid loss in this route. In the ethanolic route, an ethanolic extraction with a solvent to biomass ratio of 5 $mL.g^{-1}$ is performed to extract the EPA-rich polar lipids. After the ethanolic extraction, ethanolic centrifugation is performed to separate the ethanolic extract (EPA-rich polar lipids) from the defatted pellet (insoluble proteins), with more specific details provided in **Appendix B**.

Targeting the optimisation of the EPA recovery, it is proposed to have ethanol washing of the defatted pellet as the first operation of the first cycle performed in the *Nutsche* filter. The ethanol resulting from the defatted pellet washing is fed to the ethanolic extraction, as represented in the process diagram (**Figure 6.2**). The first cycle of the *Nutsche* filter ends with a drying step of the defatted pellet and solvent recovery (**Appendix B**).

The ethanolic extract obtained from the previously mentioned ethanolic centrifugation is fed to a microfiltration process aiming at the removal of the possible remaining particles, which could interfere with the concentration of EPA-rich polar lipids in the final product (**Appendix B**). Pointing to the decrease of viscosity and the stabilisation of the extracted lipid emulsion, it is also proposed to include the addition of an excipient – polysorbate 80 (Tween-80, non-ionic surfactant and emulsifier). Finally, the second cycle of the *Nutsche* filter is proposed to concentrate the EPA-rich polar lipid oleoresin and recover ethanol (**Appendix B**).

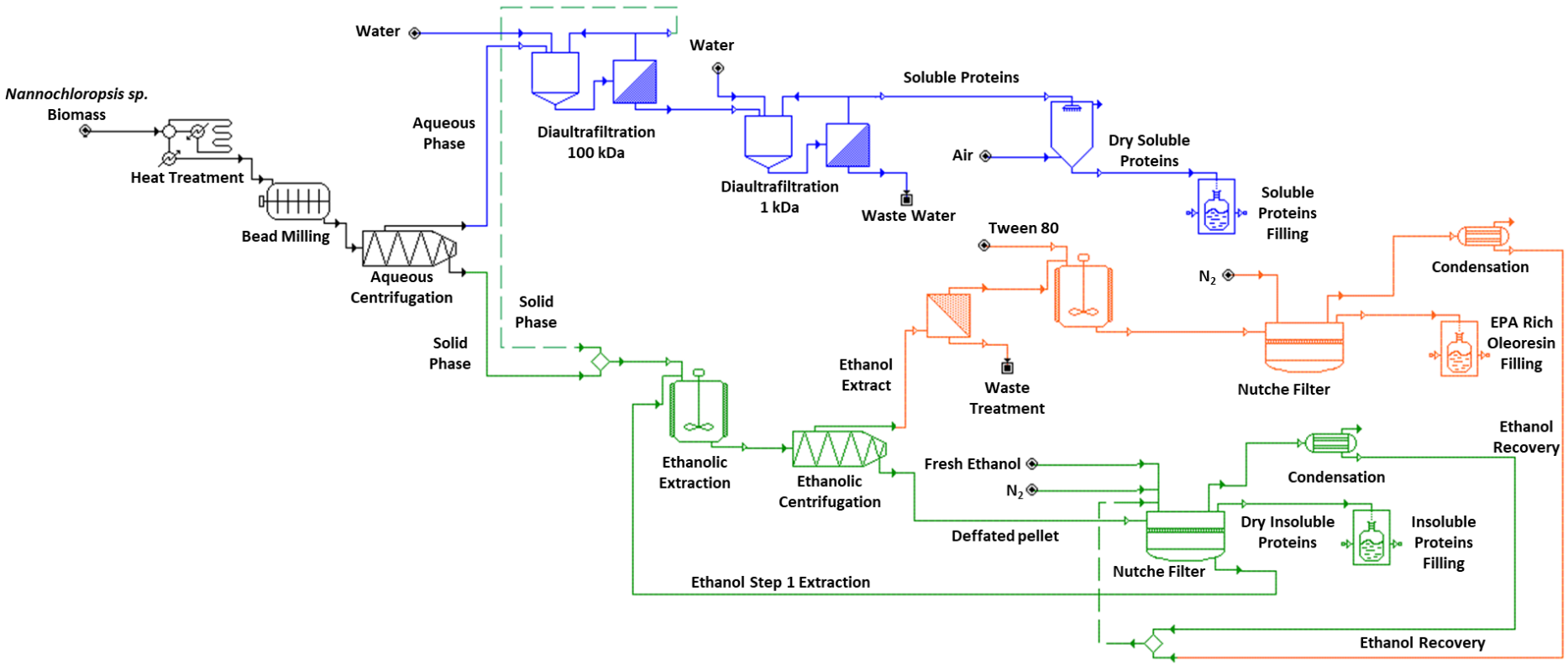

Figure 6.2. Simplified flow chart of the biorefinery proposed for the production of a target compound from *Nannochloropsis* sp. biomass.

After having completed the process design and the definition of the biorefinery major processes, mass balances and the chemical characterisation of each process stream were performed. This proposed biorefinery was simulated considering a *Nannochloropsis* sp. biomass feed of 660 $kg_{SFDW}.day^{-1}$ (218 $ton_{SFDW}.year^{-1}$), with 330 $day.year^{-1}$ and 22$h.day^{-1}$ of operation, according to guidelines provided by A4F – Algae for Future, based upon its experience.

The characterisation in a salt-free dry weight basis for each process stream of the stabilisation and biomass disruption is presented in **Figure 6.3**.

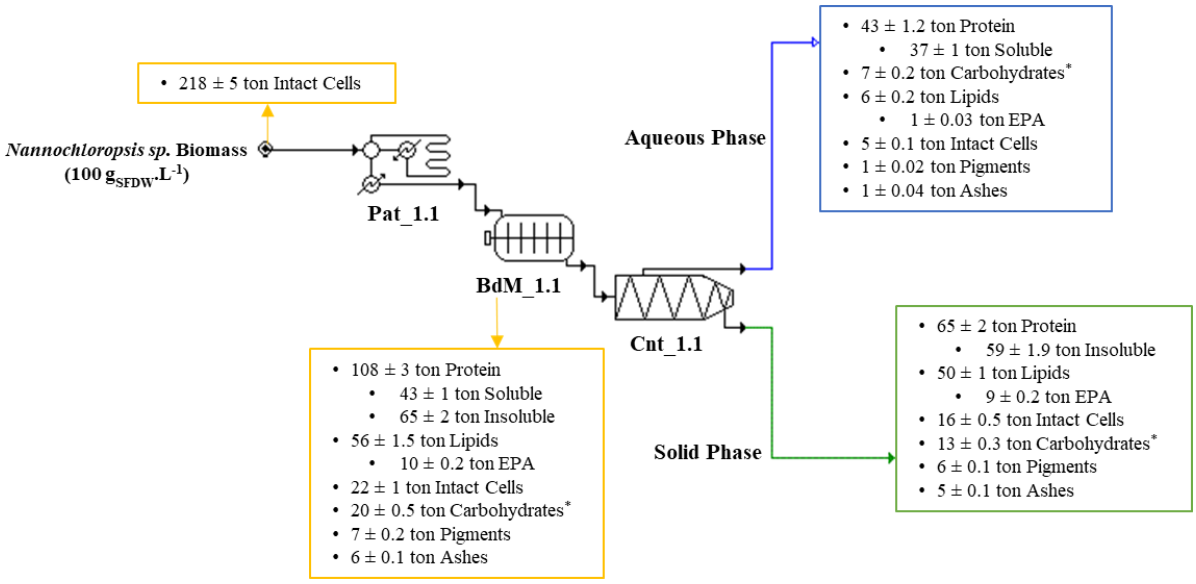

Figure 6.3. Scheme of the proposed biomass stabilization and disruption steps within the biorefinery concept, including the characterisation of the process streams on a salt-free dry weight basis. The pasteurizer was named "Pat_1.1", the bead mill was called "BdM_1.1", and the centrifuge was named "Cnt_1.1". *The carbohydrates were estimated by the difference between the total salt-free dry weight and the sum of the other compounds.

The stabilisation step through a heat treatment at 95 ºC for 3min was able to successfully avoid the degradation of the value-added compounds such as lipids and pigments, as demonstrated in **chapter 2**. It was considered that no cells were damaged during this process and stabilised intact cells were, therefore, fed to a disruption step through bead milling. As reported in **chapter 3**, it was possible to achieve around 90% of cellular disruption with a single pass through the grinding chamber at a flow rate of 300 $L.h^{-1}$ and a tip speed of 16 m/s. Hence, from the 218 ± 5 ton of intact cells that are fed to the bead milling, only 22 ± 1 ton remained intact after the cellular disruption step. The disrupted biomass was separated into two different phases, the aqueous phase and the solid phase through a centrifugation step

as mentioned before. Therefore, 85% of the soluble proteins were recovered in the aqueous phase. However, 11% of the lipids were also recovered in this stream which might represent a significant loss of lipids, which may be attached to cytoskeletal proteins [22]. On the other hand, in the solid phase, it was possible to recover 89% of the insoluble proteins as well as 89% of the lipids present in the initial biomass.

The characterisation in a salt-free dry weight basis of the main process stream of the aqueous route is presented in **Figure 6.4**.

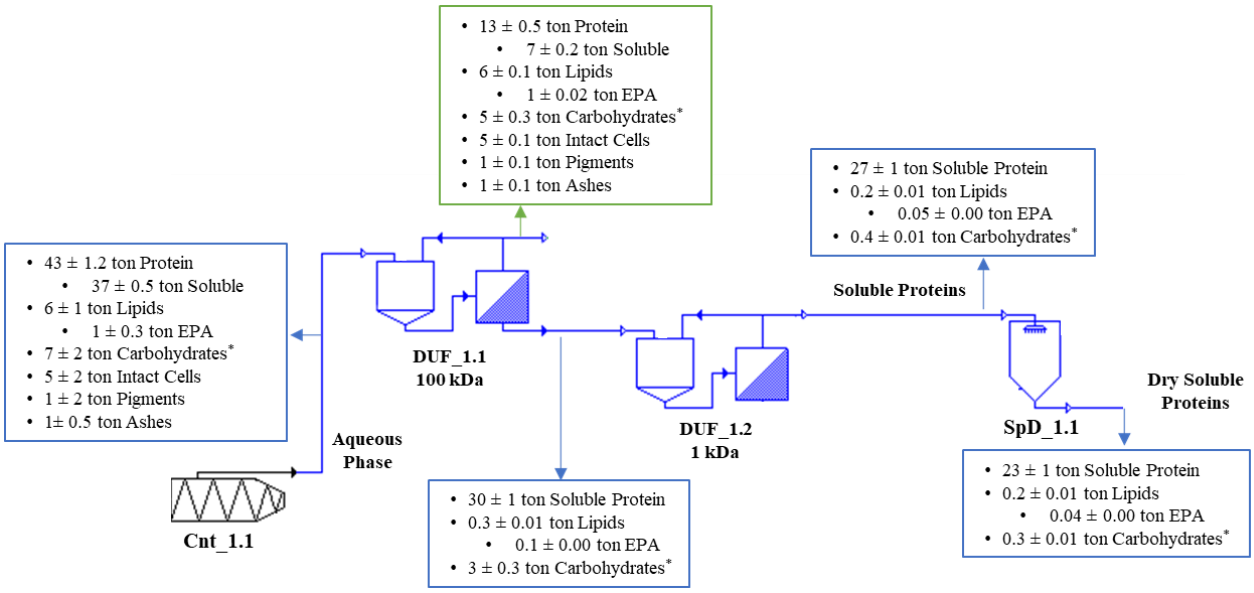

Figure 6.4. Scheme of the proposed aqueous route within the biorefinery concept, including the characterisation of the process streams on a salt-free dry weight basis. The centrifuge was named "Cnt_1.1", the dia-ultrafiltrations were called "DUF_1.1" and "DUF_1.2", and the spray dryer was named "SpD_1.1". *The carbohydrates were estimated by the difference between the total salt-free dry weight and the sum of the other analysed compounds.

Regarding the aqueous route, it is possible to recover 80% of the soluble protein present in the supernatant through a dia-ultrafiltration (MWCO 100 kDa), as reported in **chapter 4**. The protein recovered in the permeate is free from pigments and 95% of the lipids present in the supernatant are retained in the concentrate. The second dia-ultrafiltration (MWCO 1 kDa) step is performed to remove the low molecular weight compounds present in this fraction, such as salt and sugars. However, 10% of the soluble protein is lost during the diafiltration process. The final step of the aqueous route is the spray drying of the soluble protein aqueous fraction, and an efficiency of 85% was admitted for this step.

Therefore, from the 28 ± 1 ton of soluble protein fed to the spray dryer, only 28 ± 1 ton are recovered at the end of the process.

The characterisation in a salt-free dry weight basis of the main process stream of the solid (ethanolic) router is presented in **Figure 6.5**.

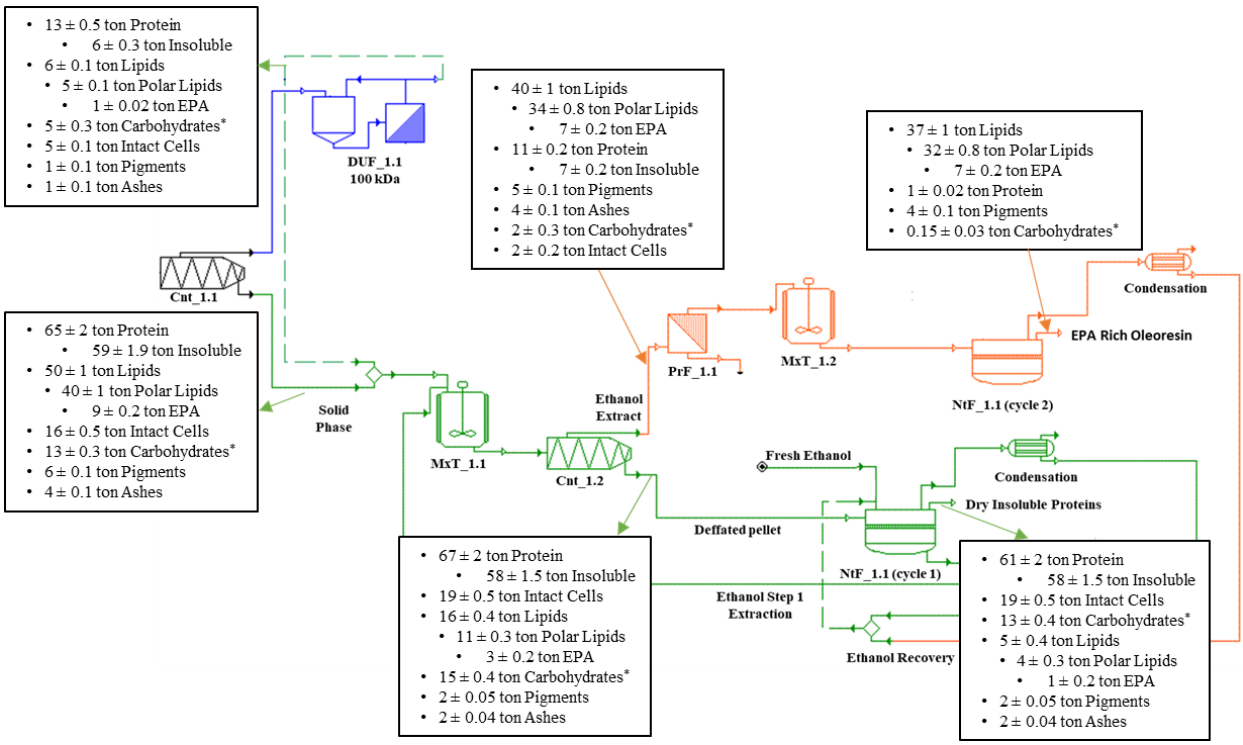

Figure 6.5. Scheme of the proposed aqueous route within the biorefinery concept, including the characterisation of the process streams on a salt-free dry weight basis. The centrifuges were named "Cnt_1.1" and "Cnt_1.2", the dia-ultrafiltration called "DUF_1.1", the mixing tanks named "MxT_1.1" and "MxT_1.2", the pre-filter called "PrF_1.1" and the *Nutsche* filter named "NtF_1.1". *The carbohydrates were estimated by the difference between the total salt-free dry weight and the sum of the other analysed compounds.

Concerning the ethanolic route represented in **Figure 6.5**, 95% of the lipids previously lost to the aqueous fraction, after the centrifugation, are recovered in the concentrate of the first dia-ultrafiltration step. The concentrate is fed to the ethanolic extraction along with the pellet recovered from the aqueous centrifugation, which means that 56 ± 1 ton of lipids (45 ± 1 ton of polar lipids) were fed to the ethanolic extraction step. After the ethanolic extraction, it was possible to recover around 71% of the lipids as reported in **chapter 5**, which means that 32 ± 0.8 ton of polar lipids and 7 ± 0.2 ton of EPA might be recovered annually. On the other hand, 90% of the insoluble protein was recovered in the defatted pellet

(58 ± 1.5 ton/year of insoluble protein), and 28% of the lipids remained in the defatted pellet. However, as mentioned before, an ethanol washing of the defatted pellet is performed inside the *Nutsche* filter, and only 11% of the lipids remained in the defatted pellet after washing (5 ± 0.4 ton/year of lipids).

A brief preliminary assessment of the economic potential of the process was performed after carrying out the mass balances, by identifying the economic values of the main input stream (*Nannochloropsis* sp. biomass) and the output streams (final products). The biomass cost is assumed to be 5 €.kg_{SFDW}^{-1}, based on the reported values for a production facility at the 100 ha scale level and with flat panel, PBRs installed [188,206], as previously justified in **section 6.3**. The price of the final products was also justified in **section 6.3**, and they are presented in **Table 6.1** as well as the corresponding annual revenues (€.year-1) coming from each one of the final biorefinery products considered. The values obtained do show, as expected, that revenues are mostly connected with the EPA-rich oleoresin stream, with marginal additional economic value attached to the proteins, that should be seen as complementary by-products with no major profitability impacts attached to them.

Table 6.1. Annual production, price, and annual revenue of the final products from the *Nannochloropsis* sp. biorefinery.

Biorefinery Products	**Production (kg.year^{-1})**	**Price (€.kg^{-1})**	**Revenue (€.year^{-1})**
Main Product			
EPA-rich oleoresin	44 621	*55.00* [210,211]	*2,454,164*
By-products			
Soluble protein	23 730	*6.50* [209]	*154,244*
Insoluble protein	105 710	*2.00* [209]	*211,420*

A concise summary of the economic potential of this process is presented in **Figure 6.6**. The 218 ton.year^{-1} of *Nannochloropsis* sp. biomass that are needed to feed the proposed biorefinery represents an annual cost of 1.09 M€. However, the revenue generated by the sales of the final products can cover the cost of *Nannochloropsis* sp. biomass and still create a positive cash flow of 1.73 M€, which one needs to assure that is large enough to cover other operating costs, as well as the depreciation of equipment, together with a remaining positive profit.

This brief preliminary assessment, therefore, reveals the economic potential of the proposed biorefinery, but in the next subchapter, a more detailed techno-economic evaluation will be presented and discussed,

to verify it the positive economic potential is large enough to cover other costs and generate interesting profitability.

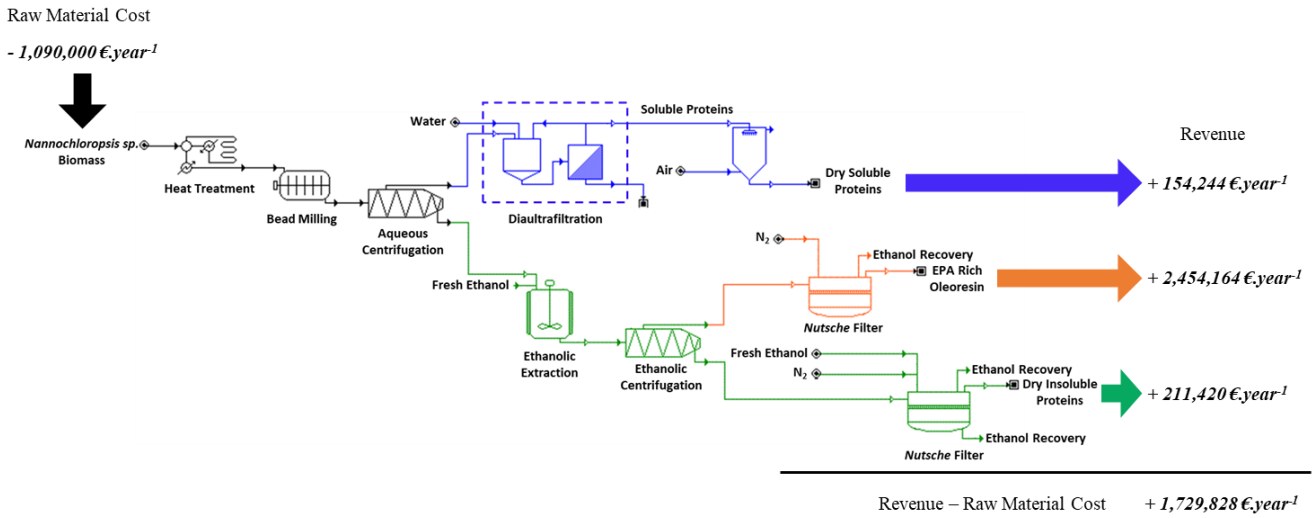

Figure 6.6. Simplified economic flows related to the main raw material (*Nannochloropsis* sp. biomass) cost outflow and the final product revenue inflows.

6.4.2. Techno-Economic Assessment of a biorefinery based on EPA-rich *Nannochloropsis* sp.

As stated before, this process was simulated considering a *Nannochloropsis* concentrated biomass (100 $g_{SFDW}.L^{-1}$) feed of 660 $kg_{SFDW}.day^{-1}$ (218 $ton_{SFDW}.year^{-1}$). The *Nannochloropsis* sp. biorefinery flow chart and mass balance were presented before (**section 6.4.1**), and the designed plant includes the following main pieces of equipment: 1 pasteurizer, 1 bead milling, 2 centrifuges (aqueous and ethanolic), 2 mixing tanks, 2 ultrafiltration modules (100 kDa and 1kDa), 1 filter, 1 spray drier, and 1 *Nutsche* filter (2 different cycles). The corresponding total equipment cost (CAPEX) was estimated at 1.61 M€, with the estimated values for the cost of each of the relevant pieces of equipment being based on the supplier's price quotations and the application of a scale-up factor [186]. The cost of the main equipment is presented in more detail in **Table 6.2**.

Table 6.2. Capital Expenditures (CAPEX) regarding the main equipment of the proposed *Nannochloropsis* sp. biorefinery.

	Name	Description	Equipment cost (€)
Main Equipment	Pat_1.1	Pasteurizer 1	*112,000*
	BdM_1.1	Bead Mill 1	*184,500*
	Cnt_1.1	Centrifuge 1	*241,000*
	DUF_1.1	Dia-ultrafiltration 1 (100 kDa)	*110,000*
	DUF_1.2	Dia-ultrafiltration 2 (1 kDa)	*110,000*
	SpD_1.1	Spray Dryer 1	*165,000*
	MxT_1.1	Mixing Tank 1	*80,000*
	Cnt_1.2	ATEX Centrifuge 2	*260,000*
	PrF_1.1	Pre-filter 1	*10,000*
	MxT_1.2	Mixing Tank 2	*40,000*
	NtF_1.1	Nutsche Filter 1	*295,200*
	Total Equipment Cost (€)		*1,607,700*
	Depreciation costs (€.year^{-1}) ***depreciation over 10 years**		*160,770*

A graphical representation of the capital expenditures (CAPEX) is presented in **Figure 6.7** for easier comprehension of the capital expenditures associated with each section of the proposed biorefinery. As illustrated, the ethanolic section represents 43% of the total capital expenditure, while the pre-treatment section represents 33%, and the aqueous section represents 24% of the overall CAPEX.

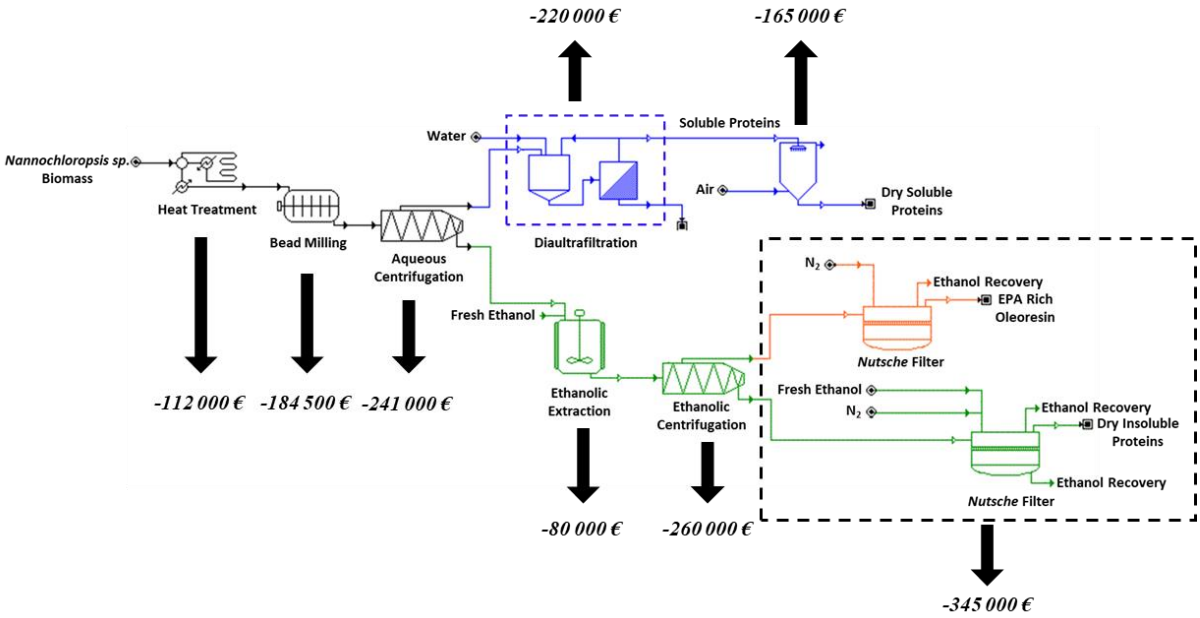

Figure 6.7. Graphical representation of the Capital Expenditures (CAPEX) associated with each section of the proposed *Nannochloropsis* sp. biorefinery.

Regarding the biorefinery that was designed, the main operating costs were also estimated. These estimates were based on the flowchart and mass balances presented before, with the energy and the steam consumption for all the equipment (**Table 6.3**) simulated and estimated in Super Pro Designer®.

Table 6.3. Energy and steam consumption for the designed biorefinery. *Values were estimated with Super Pro Designer®.

	Name	Description	Electrical Energy* (kWh.year^{-1})	Steam* (ton.year^{-1})
Main Equipment	**Pat_1.1**	Pasteurizer 1	70 700	1500
	BdM_1.1	Bead Mill 1	268 000	
	Cnt_1.1	Centrifuge 1	101 000	
	DUF_1.1	Dia-ultrafiltration 1 (100 kDa)	30 000	
	DUF_1.2	Dia-ultrafiltration 2 (1 kDa)	48 000	
	SpD_1.1	Spray Dryer 1	197 401	
	MxT_1.1	Mixing Tank 1	30 000	
	Cnt_1.2	ATEX Centrifuge 2	120 000	
	PrF_1.1	Pre-filter 1	15 000	
	MxT_1.2	Mixing Tank 2	28 000	
	NtF_1.1	Nutsche Filter 1	933 687	
	Total		1 841 789	1500

As for the costs of raw materials, and regarding the solvent cost calculation, a 90% recovery ratio was assumed. The average annual maintenance and consumables cost, for all the scenarios to be considered, was assumed as a percentage of 5% and 2% of the investment, respectively, as mentioned in **section 6.3.2**. Also, in this techno-economic evaluation, it was assumed, as mentioned in **section 6.3.2,** that the biorefinery will be constructed next to the microalgae production facility, with 100 ha of scale and flat panel PBRs installed, so that the biomass cost does not need to include additional logistic costs. Therefore, in the present work, and based on the reported values, and considering 25% of the profit margin for the production facility, the biomass cost was assumed to be 5 €.kg_{SFDW}^{-1} as a baseline scenario [188,206], and it represents a significant part of the total operating costs of the *Nannochloropsis* sp. biorefinery proposed. The estimated total operational cost (OPEX) per year for the designed *Nannochloropsis* sp. biorefinery is presented in **Table 6.4**.

Table 6.4. Estimated total operational cost (OPEX) for the designed *Nannochloropsis* sp. biorefinery.

OPEX	
Human Resources (€.$year^{-1}$) [*1]	*300,000*
Operational Energy Consumption (kWh.$year^{-1}$)	1 841 789
Energy Cost (€.$year^{-1}$) (0.129 €.kWh^{-1}) [*2]	*237,591*
Operational Steam Consumption (ton.$year^{-1}$)	1 500
Steam Cost (€.$year^{-1}$) (20.0 €.ton^{-1}) [187]	*30 000*
Membrane Replacement Cost (€.$year^{-1}$)	*10,000*
Maintenance (€.$year^{-1}$)	*80,385*
Consumables (€.$year^{-1}$)	*32,154*
Solvents/Reactants (€.$year^{-1}$)	*362,310*
Waste Water Treatment (m^3.$year^{-1}$)	6 536
Waste Water Treatment (€.$year^{-1}$) (0.45 €.m^{-3}) [209]	*2,941*
Biomass Cost (€.$year^{-1}$) (5.00 €.kg_{SFDW}^{-1}) [188,206]	*1,090,000*
Total OPEX (€.$year^{-1}$)	*2,145,381*

[*1] HR = (number equipment -1) x 2500 €/employee
[*2] source: www.pordata.pt

As shown above, the biomass cost represents a major portion of the total operating costs of the biorefinery. **Figure 6.8 A) and B)** show the contribution of each utility to the total operating costs of the biorefinery of *Nannochloropsis* sp.: **Figure 6.8 A)** presents the total operation costs including biomass costs and **Figure 6.8 B)** exhibits the total operation costs excluding biomass costs. It is possible to easily conclude that the biomass cost is the one that contributes a higher percentage (51.1%) to the total operating costs of the proposed biorefinery. The solvents used in the biorefinery contribute 17.0%, human resources represent 14.1% and electric power corresponds to 11.1% of the total operating costs

of the biorefinery. The sum of the remaining utilities represents 6.9% of the total operating costs. Therefore, it is clear that biomass cost has a great impact on the proposed biorefinery's economic profitability. It is thus extremely important to reduce the microalgae biomass cultivation and harvesting operation costs to also reduce the global costs of a microalgae biorefinery, such as the one designed here, and to have it next to the biomass production facilities, in order to avoid additional biomass transportation costs.

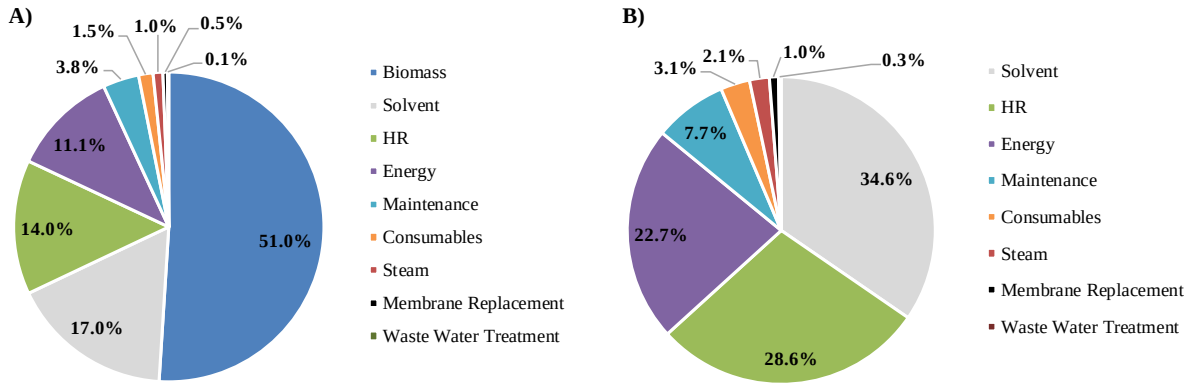

Figure 6.8. Contribution of each category of costs to the total operating costs of the biorefinery proposed: A) Operation costs including biomass costs; B) Operation costs excluding biomass costs.

To get an easier view of the remaining operation costs, if we ignore for a moment the biomass costs and remove them from the total operation costs (**Figure 6.8 B**), one can see that the solvents used in the biorefinery represent the larger remaining cost (34.7%), followed by human resources costs (28.7%) and electric energy consumption (22.8%).

A graphical representation of the operating expenses (OPEX) associated with each section of the proposed biorefinery was also made, as illustrated in **Figure 6.9**. This illustration facilitates the identification of the plant sections that contribute the most to the annual operating expenses. As was also observed for the graphical representation of CAPEX, the ethanolic section is also the one which contributes the most to the annual biorefinery OPEX. The high OPEX value associated with the ethanolic section is mostly related to solvent and energy needs in this part of the process, and therefore this section, in particular, may be considered as an opportunity for further process optimisation, for example, with regards to the solvent to biomass ratio in the extraction step. A reduction in the quantity of ethanol that is processed in the ethanolic section may reduce both solvent (less ethanol used in the extraction) and energy needs (less energy to process and recover ethanol).

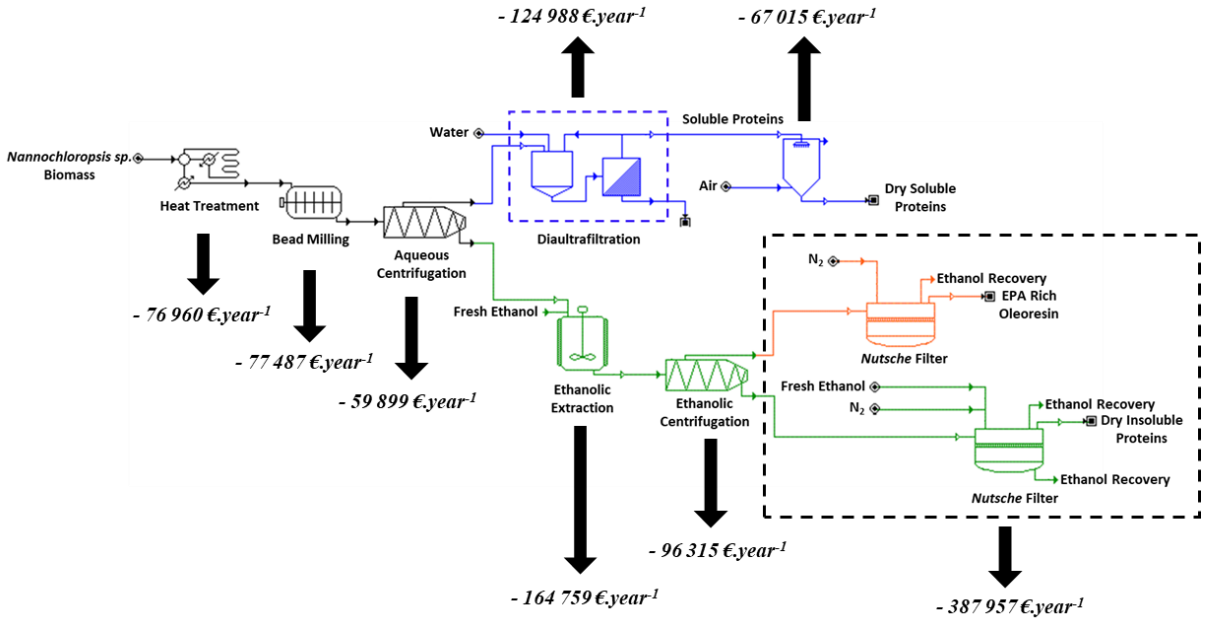

Figure 6.9. Graphical representation of the annual Operating Expenses (OPEX), excluding biomass costs, associated with each section of the proposed *Nannochloropsis* sp. biorefinery.

Taking now into account all of the previous information and data, a full economic analysis of the biorefinery was performed. The capital expenditure and the operating expenses of the proposed biorefinery are summarized and presented in **Table 6.5**. All of the major investment is assumed to take place in the construction stage (100% of CAPEX in year 0), with no final economic value attached to the plant by then, given the specific nature of the equipment considered and the need to preserve the ecology of the surrounding environment if the plant is discontinued after a decade of operation. Revenues were calculated based on the prices previously presented in **Table 6.1**. The ramp-up of operations is assumed to last for some years, with full capacity reached only in year 4, due to the need to continuously learn and adjust operating conditions, to optimize productivity levels and avoid for instance possible contaminations, failures or errors. The equipment residual value at the end of the project (10 years) was not taken into account in the values presented in **Table 6.5**. The discount selected to calculate the Net Present Value (NPV) of the biorefinery project was 5%. This discount rate was chosen because the interest rates currently practised are considered low, and also because the risk associated with this type of technology is not considered very high risk.

Table 6.5. Biorefinery estimated Costs, Revenues and Cash Flows over 10 years of the project lifetime. [*1] Considering a 5% discount rate.

Year	Action	Investment	Production Capacity	CAPEX (€.year^{-1})	OPEX (€.year^{-1})	Revenue (€.year^{-1})	Cash Flow (€.year^{-1})	NPV[*1] (€.year^{-1})
0	Construction	100%	0%	-1,607,700			-1,607,700	-1,607,700
1	Start-up	0%	65%		-2,145,381	1,832,888	-312,493	-297,612
2	Start-up	0%	85%		-2,145,381	2,396,854	251,473	228,093
3	Start-up	0%	95%		-2,145,381	2,678,837	533,456	460,819
4	Production	0%	100%		-2,145,381	2,819,828	674,447	554,869
5	Production	0%	100%		-2,145,381	2,819,828	674,447	528,447
6	Production	0%	100%		-2,145,381	2,819,828	674,447	503,283
7	Production	0%	100%		-2,145,381	2,819,828	674,447	479,317
8	Production	0%	100%		-2,145,381	2,819,828	674,447	456,492
9	Production	0%	100%		-2,145,381	2,819,828	674,447	434,755
10	Production	0%	100%		-2,145,381	2,819,828	674,447	414,052

The economic performance measures presented in **Table 6.5** and **Table 6.6** show that positive cash flows are reached on and after year 2, leading to an estimated Internal Rate of Return (IRR) of 20.3% and a Net Present Value (NPV), with a discount rate of 5%, of 2,154,815 €, seen as promising investment indicators.

Table 6.6 Summary of biorefinery estimated main economic performance indicators: Net present value (NPV), Internal Rate of Return (IRR), and Payback.

NPV[* 5% discount rate]	2,154,815 €
IRR	20.3%
Payback Period (year)	4.7

Taking this as our baseline for the biorefinery economic analysis, next we will present additional results obtained for several alternative scenarios that were also considered. The first comparative analysis conducted will be focused on different biomass purchase costs and the influence that they have on the production costs of the biorefinery and the general economic performance of the project. The second comparative analysis will study the influence of different production scales on the economic performance of the plant. The third and last comparative analysis will be performed aiming to test if the proposed multi-product biorefinery is a more viable option than a single product biorefinery, in which only EPA oleoresin is produced.

6.4.2.1. First comparative analysis: impact of the biomass purchase cost on the biorefinery economic performance

In this subchapter, we will study the impact of biomass purchase costs on the economic viability of the proposed biorefinery. For that purpose, the proposed biorefinery (scenario A) was compared with two different alternative scenarios (scenarios B and C). As discussed before (**section 6.3.2)**, in scenario A it was assumed that the biorefinery is built next to a microalgae production facility, at the 100 ha scale level and with flat-panel PBRs installed, and hence the corresponding biomass costs do not include any additional transportation or processing costs. Consequently, based on reported values and considering 25% of the profit margin for the production facility, the biomass market price has been settled at 5 €.kg_{SFDW}^{-1} [188,206].

Regarding the two additional scenarios here considered (B and C), a microalgae production facility at a 10 ha scale level and a biomass market price of 8 €.kg_{SFDW}^{-1} was considered for scenario B, and a microalgae production facility at a 100 ha scale level and a biomass market price of 3 €.$kg_{SFDW}^{-1}$was considered for scenario C. The market prices are based on the reported values of production cost as presented in section **6.3.2**, and on a 25% profit margin for the production facility.

The influence of biomass purchase costs over the biorefinery total operational costs was already identified and can be easily seen also from **Figure 6.10**, and therefore, the biorefinery profitability will always depend considerably on the operational costs associated with biomass cultivation and harvesting.

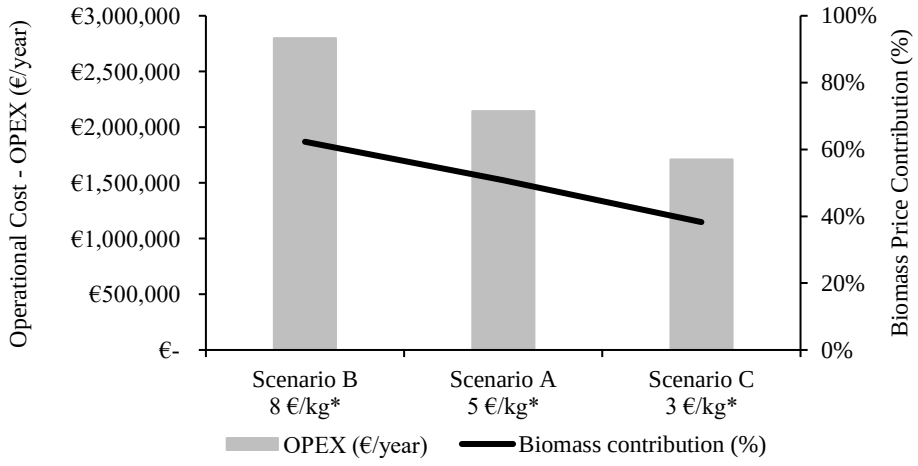

Figure 6.10. Estimated total operational costs of five different scenarios assuming five different values for the biomass purchasing prices, and the contribution of the biomass purchasing costs for the total operational costs of the biorefinery under each scenario considered. *The biomass purchase price is presented in €.kg_{SFDW}^{-1}

To further assess the economic feasibility of each scenario, and also to emphasize the importance of the biomass purchasing prices over each scenario, the main project economic performance measures were calculated, with the corresponding results presented in **Table 6.7**. As expected, scenario B, which considers a higher biomass price, was the one that consequently presented the highest value of operating expenses and the lowest values of cash flows over the years of the project. The revenues of all the scenarios considered were calculated based on the values previously presented in **Table 6.1**

Table 6.7. Costs, Revenues, Cash Flows and NPV variation for different scenarios of the biorefinery project. **Scenario A** considers a biomass cost of **5 €.kg^{-1}**, **scenario B** considers **8 €.kg^{-1}**, and scenario C considers **3 €.kg^{-1}**. Biomass purchasing costs are considered in €.kg$^{-1}_{SFDW}$. [*1] Considering a 5% discount rate.

Year	CAPEX (M€.year^{-1})	OPEX (M€.year^{-1})			Revenue (M€.year^{-1})	Cash Flow (M€.year^{-1})			NPV[*1] (M€.year^{-1})		
		Scenario				Scenario			Scenario		
	All scenarios	B	A	C	All scenarios	B	A	C	B	A	C
0	-1.608					-1.608	-1.608	-1.608	-1.608	-1.608	-1.608
1		-2.799	-2.145	-1.709	1.833	-0.966	-0.312	0.124	-0.920	-0.298	0.118
2		-2.799	-2.145	-1.709	2.397	-0.403	0.251	0.687	-0.365	0.228	0.624
3		-2.799	-2.145	-1.709	2.679	0.020	0.533	1.110	0.018	0.461	0.959
4		-2.799	-2.145	-1.709	2.820	0.020	0.674	1.110	0.017	0.555	0.914
5		-2.799	-2.145	-1.709	2.820	0.020	0.674	1.110	0.016	0.528	0.870
6		-2.799	-2.145	-1.709	2.820	0.020	0.674	1.110	0.015	0.503	0.829
7		-2.799	-2.145	-1.709	2.820	0.020	0.674	1.110	0.015	0.479	0.789
8		-2.799	-2.145	-1.709	2.820	0.020	0.674	1.110	0.014	0.456	0.752
9		-2.799	-2.145	-1.709	2.820	0.020	0.674	1.110	0.013	0.435	0.716
10		-2.799	-2.145	-1.709	2.820	0.020	0.674	1.110	0.013	0.414	0.682

In terms of overall economic project performance, the metrics presented in **Table 6.8** show that scenario B is the least attractive scenario, with a negative NPV and a negative IRR. Scenario A, which corresponds to the biorefinery previously proposed, exhibits an IRR of 20.3%, and a payback period of 4.7 years, as mentioned before. On the other hand, scenario C exhibits an IRR of 43.1%, which is higher than the IRR calculated under scenario A. In conclusion, the influence of biomass purchasing prices is once again notorious and it is extremely important to optimise the cultivation as well as the harvesting steps, to diminish the biomass production costs, and consequently the biomass purchasing prices. For the designed biorefinery to be profitable, it needs to have access to biomass with a purchasing price that should not exceed 3€.kg$^{-1}_{\mathbf{SFDW}}$.

Table 6.8 Summary of main project economic performance indicators for the three different scenarios considered: Net present value (NPV), Internal Rate of Return (IRR), and Payback. Scenario A considers a biomass cost of 5 €.kg^{-1}, scenario B considers 8 €.kg^{-1}, and scenario C considers 3 €.kg^{-1}. Biomass purchasing costs are considered in €.kg$^{-1}_{SFDW}$ *1 Considering a 5% discount rate.

	Scenario B	Scenario A	Scenario C
Biomass purchase cost (€.kg$_{SFDW}^{-1}$)	*8.00*	*5.00*	*3.00*
NPV*1	-2,773,406 €	2,154,815 €	5,643,285 €
IRR	-	20.3%	43.1%
Payback Period (year)	Never Achieved	4.7	2.7

These three different scenarios are compared again in **Table 6.9**, to assess the influence of the biomass purchasing costs on the production costs of the main product of the *Nannochloropsis* sp. biorefinery. The impact of the biomass purchasing costs on the production cost (€.kg$^{-1}_{final\ product}$) of the EPA oleoresin is obvious and for example a decrease of 40% of the biomass purchasing cost (from 5 €.kg$_{SFDW}^{-1}$ to 3 €.kg$_{SFDW}^{-1}$), leads to a reduction of 22% in the EPA oleoresin production cost (from 43.97 €.kg^{-1} to 34.20 €.kg^{-1}). For the sake of comparison, a reduction of 40% in the solvent costs, which are the second largest expense that contributes to operational costs, leads to a reduction of only 6% in the EPA oleoresin overall production costs. Therefore, as stated above, it is rather important to optimise the biomass cultivation and harvesting steps, to diminish the biomass costs, and consequently the production costs of the biorefinery products, to assure its economic feasibility.

Table 6.9. EPA oleoresin production costs (€.kg^{-1}) for each scenario (A, B and C), with different biomass purchasing prices (€.kg$^{-1}_{SFDW}$). Scenario A considers a biomass cost of 5 €.kg^{-1}, scenario B considers 8 €.kg^{-1}, and scenario C considers 3 €.kg^{-1}. Biomass purchasing costs are considered in €.kg$^{-1}_{SFDW}$.

	Scenario B	Scenario A	Scenario C
Biomass purchase cost (€.kg$_{SFDW}^{-1}$)	*7.00*	*5.00*	*3.00*
EPA oleoresin annual production (kg.year^{-1})	44 621	44 621	44 621
Total EPA oleoresin production Cost (€.year^{-1})	*2,397,928*	*1,961,928*	*1,525,928*
EPA oleoresin Production Cost (€.kg $_{final\ product}^{-1}$)	*53.74*	*43.97*	*34.20*
EPA oleoresin Production Cost (€.kg $_{EPA}^{-1}$)	*346.79*	*283.74*	*220.68*

6.4.2.2. Second comparative analysis: impact of production scale capacity on the biorefinery economic performance

The impact of the biorefinery production scale capacity on its economic performance was also evaluated. For that purpose, the proposed biorefinery (scenario A) was compared with two different alternative scenarios (scenarios D and E). Scenario D represents a biorefinery with a production capacity of 109 $ton_{SFDW}.year^{-1}$, which is 50% less than the capacity of the biorefinery proposed as baseline (scenario A – 218 $ton_{SFDW}.year^{-1}$). On the other hand, scenario E represents a biorefinery with a production capacity of 327 $ton_{SFDW}.year^{-1}$, which is 50% higher than the capacity of scenario A.

A full economic analysis of both scenarios D and E was performed to compare these results with the economic analysis previously performed (scenario A), presented in section **6.4.2**. The corresponding capital expenditures and operating expenses for scenarios D and E are summarized and presented in **Table 6.10** and **Table 6.11**

Table 6.10. Costs, Revenues and Cash Flows for scenario D biorefinery .[*1] Considering a 5% discount rate

A) Scenario D: Production capacity of 109 $ton_{SFDW}.year^{-1}$

Year	Action	Investment	Production Capacity	CAPEX (€.year^{-1})	OPEX (€.year^{-1})	Revenue (€.year^{-1})	Cash Flow (€.year^{-1})	NPV[*1] (€.year^{-1})
0	Construction	100%	0%	-1,060,686			-1,060,686	-1,060,686
1	Start-up	0%	65%		-1,305,242	1,023,760	-281,482	-268,078
2	Start-up	0%	85%		-1,305,242	1,338,763	33,521	30,405
3	Start-up	0%	95%		-1,305,242	1,496,265	191,023	165,013
4	Production	0%	100%		-1,305,242	1,575,016	269,774	221,943
5	Production	0%	100%		-1,305,242	1,575,016	269,774	211,375
6	Production	0%	100%		-1,305,242	1,575,016	269,774	201,309
7	Production	0%	100%		-1,305,242	1,575,016	269,774	191,723
8	Production	0%	100%		-1,305,242	1,575,016	269,774	182,593
9	Production	0%	100%		-1,305,242	1,575,016	269,774	173,898
10	Production	0%	100%		-1,305,242	1,575,016	269,774	165,618

Table 6.11. Costs, Revenues and Cash Flows for scenario E biorefinery. [*1] Considering a 5% discount rate

B) Scenario E: Production capacity of 327 $ton_{SFDW}.year^{-1}$

Year	Action	Investment	Production Capacity	CAPEX (€.year^{-1})	OPEX (€.year^{-1})	Revenue (€.year^{-1})	Cash Flow (€.year^{-1})	NPV[*1] (€.year^{-1})
0	Construction	100%	0%	-2,050,500			-2,050,500	-2,050,500
1	Start-up	0%	65%		-2,979,813	2,642,016	-337,797	-321,712
2	Start-up	0%	85%		-2,979,813	3,454,944	475,131	430,958
3	Start-up	0%	95%		-2,979,813	3,861,408	881,595	761,555
4	Production	0%	100%		-2,979,813	4,064,640	1,084,827	892,490
5	Production	0%	100%		-2,979,813	4,064,640	1,084,827	849,990
6	Production	0%	100%		-2,979,813	4,064,640	1,084,827	809,515
7	Production	0%	100%		-2,979,813	4,064,640	1,084,827	770,966
8	Production	0%	100%		-2,979,813	4,064,640	1,084,827	734,254
9	Production	0%	100%		-2,979,813	4,064,640	1,084,827	699,289
10	Production	0%	100%		-2,979,813	4,064,640	1,084,827	665,990

Regarding the economic performance measures presented in **Table 6.12**, it was possible to conclude that scenario D, with a lower production capacity, is the least attractive one, as expected. Scenario D has an IRR of 7.6%, values which are considerably worse when compared with scenario A (20.3%) and scenario E (27.0%). On the other hand, scenario E corresponds to a more appealing investment, when compared with scenario A. These results highlight the importance of economies of scale, and this indicates that it might be possible to improve the financial results of the proposed biorefinery by increasing the corresponding production capacity and that at least the capacity predicted under Scenario A is needed to assure the biorefinery economic feasibility.

Table 6.12. Summary of main economic performance indicators for the three different scenarios: Net present value (NPV), Internal Rate of Return (IRR), and Payback. The baseline was considered

	Scenario D	Scenario A	Scenario E
Production Capacity ($ton_{SFDW}.year^{-1}$)	109	218	327
NPV[*1]	*215,112 €*	*2,154,815 €*	*4,242,794 €*
IRR	7.6%	20.3%	27.0%
Payback Period (year)	7.2	4.7	3.9

6.4.2.3. Third comparative analysis of a single product and multi-product biorefinery

The economic performance of three different biorefinery scenarios was also compared: the multi-product biorefinery previously proposed and studied versus a two-product biorefinery, and a single product biorefinery. These three scenarios will be compared to test if the biorefinery with multiple products (EPA oleoresin, soluble protein and insoluble protein) proposed in this work is economically more attractive than a productive process with two final products (EPA oleoresin, and insoluble protein), or a scenario with a single final product (EPA oleoresin). The flow chart of the previously proposed multi-product biorefinery is presented in **Figure 6.2**. The flow chart of the proposed scenario with two final products is presented in **Figure 6.11**, and the single product scenario is presented in **Figure 6.12**. In the scenario with two final products, the aqueous fraction (soluble protein) is discarded. On the other hand, in the single-product biorefinery, the aqueous fraction (soluble protein), as well as the defatted pellet (insoluble protein), are discarded, and therefore less equipment is needed.

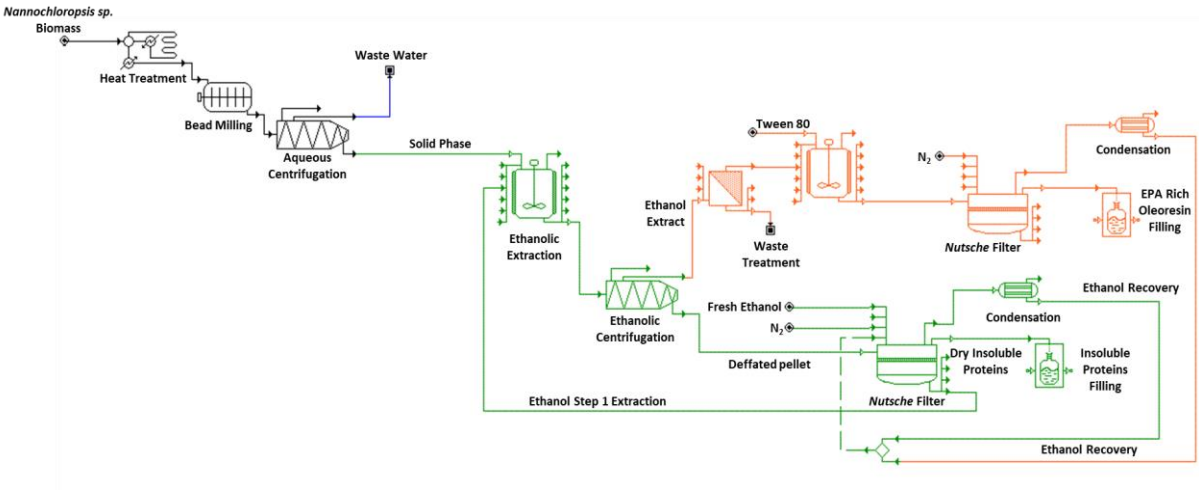

Figure 6.11. Flow chart for the biorefinery scenario with two final products.

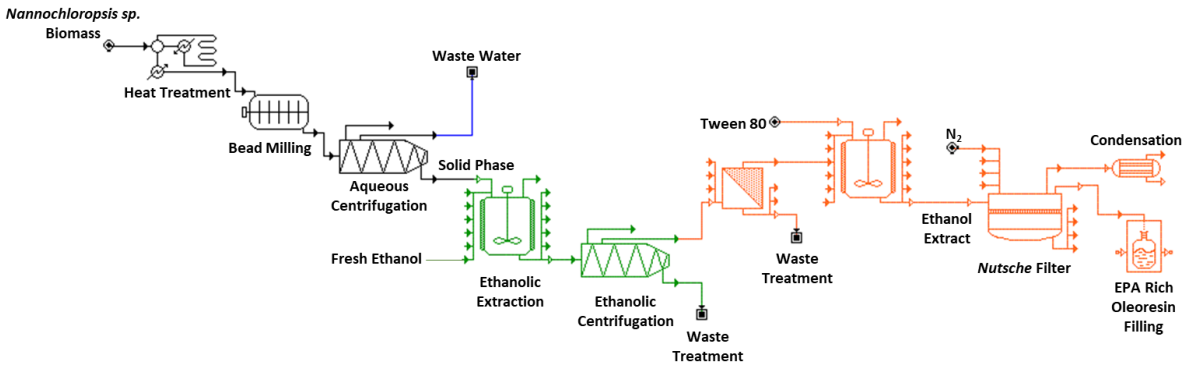

Figure 6.12. Flow chart for a single product biorefinery

The detailed capital expenditure (CAPEX), as well as the corresponding operating expenses (OPEX) of both scenarios, the two final products scenario, and single product biorefinery scenario are presented in **Appendix B**. Since these two scenarios require less equipment than the multi-product biorefinery, the CAPEX and the OPEX of these two scenarios are lower than the CAPEX and the OPEX of the multi-product biorefinery, which was previously discussed in **section 6.4.2**. The proposed multi-product biorefinery has an estimated CAPEX value of 1,61 M€ and an estimated OPEX value of 2,15 M€, as mentioned before. On the other hand, the estimated total equipment cost (CAPEX) of a single product biorefinery is 1,22 M€ and the estimated total operational cost (OPEX) per year is 1.99 M€. In the two different proposed scenarios, the aqueous fraction (for both scenarios) as well as the defatted pellet (for the single product scenario) are discarded, as shown in **Figure 6.11** and **Figure 6.12**, and therefore the corresponding waste treatment costs were added to the plant.

Taking into account all of this information and data, a full economic analysis of the two-product biorefinery scenario and the single product biorefinery scenario was performed.

The capital expenditure and operating expenses of the proposed scenarios are summarized and presented in **Table 6.13** and **Table 6.14**.

Table 6.13. Costs, Revenues and Cash Flows variation for the two products biorefinery scenario. [*1] Considering a 5% discount rate.

Year	Action	Investment	Production Capacity	CAPEX (€.year^{-1})	OPEX (€.year^{-1})	Revenue (€.year^{-1})	Cash Flow (€.year^{-1})	NPV[*1] (€.year^{-1})
0	Construction	100%	0%	-1,222,700			-1,222,700	-1,222,700
1	Start-up	0%	65%		-1,823,589	1,485,415	-338,173	-322,070
2	Start-up	0%	85%		-1,823,589	1,942,466	118,878	107,825
3	Start-up	0%	95%		-1,823,589	2,170,992	347,403	300,100
4	Production	0%	100%		-1,823,589	2,285,254	461,666	379,814
5	Production	0%	100%		-1,823,589	2,285,254	461,666	361,727
6	Production	0%	100%		-1,823,589	2,285,254	461,666	344,502
7	Production	0%	100%		-1,823,589	2,285,254	461,666	328,097
8	Production	0%	100%		-1,823,589	2,285,254	461,666	312,474
9	Production	0%	100%		-1,823,589	2,285,254	461,666	297,594
10	Production	0%	100%		-1,823,589	2,285,254	461,666	283,423

Table 6.14. Costs, Revenues and Cash Flows variation for the single product biorefinery scenario. [*1] Considering a 5% discount rate.

Year	Action	Investment	Production Capacity	CAPEX (€.year^{-1})	OPEX (€.year^{-1})	Revenue (€.year^{-1})	Cash Flow (€.year^{-1})	NPV[*1] (€.year^{-1})
0	Construction	100%	0%	-1,222,700			-1,222,700	-1,222,700
1	Start-up	0%	65%		-1,986,084	1,370,035	-616,049	-586,714
2	Start-up	0%	85%		-1,986,084	1,791,584	-194,500	-176,418
3	Start-up	0%	95%		-1,986,084	2,002,358	16,274	14,058
4	Production	0%	100%		-1,986,084	2,107,746	121,661	100,091
5	Production	0%	100%		-1,986,084	2,107,746	121,661	95,325
6	Production	0%	100%		-1,986,084	2,107,746	121,661	90,786
7	Production	0%	100%		-1,986,084	2,107,746	121,661	86,463
8	Production	0%	100%		-1,986,084	2,107,746	121,661	82,345
9	Production	0%	100%		-1,986,084	2,107,746	121,661	78,424
10	Production	0%	100%		-1,986,084	2,107,746	121,661	74,690

In terms of economic performance and investment, the main indicators obtained are presented in **Table 6.15** revealing that the single product biorefinery scenario has a negative NPV and a negative IRR. The biorefinery scenario with two products (EPA oleoresin and insoluble protein) is also less viable than the initially proposed multi-product biorefinery. In addition, the aqueous fraction that is eliminated in this

scenario is responsible for the production of a soluble protein fraction with functionality for food applications which has currently a high interest from the food industry. The multi-product biorefinery is therefore much more attractive, from an economic perspective, with an NPV (5% discount rate) of 2,154,815 €, and an IRR of 20.3%. In general, the performance measures indicate that the proposed biorefinery is an economically feasible project, with a reasonable investment return, with the proposed multi-product biorefinery being a much better choice than a single product biorefinery.

Table 6.15. Summary of the main economic performance metrics of the three different scenarios, for a multiproduct, two products, and single product biorefinery: Net present value (NPV), Internal Rate of Return (IRR), and Payback. [*1] Considering a 5% discount rate.

	Multi Product	***Two Products***	***Single Product***
NPV[*1]	2,154,815 €	1,152,288	-1,363,650 €
IRR	20.3%	15.9%	-12.0%
Payback Period (year)	4.7	5.4	Never Achieved

6.5. Conclusions

A suitable process to maximise the potential of *Nannochloropsis* sp. for the production of distinct fractions and products was proposed. The production of polar lipids rich in EPA omega-3 for supplements, colourless soluble protein for human food, and insoluble protein for animal feed, may contribute to improving the economic feasibility of the biorefinery concept. The proposed biorefinery, with a production capacity of 218 $ton_{SFDW}.year^{-1}$, was designed and the corresponding mass and energy flows were simulated. In order to evaluate the profitability of the proposed biorefinery, a detailed techno-economic evaluation was conducted.

Early in this study was concluded that the most expensive section of the biorefinery, both from an investment as well as operating cost perspective, is the ethanolic route, which should deserve further attention for fine-tuning and optimisation purposes. On the other hand, the biomass price was found to have a great impact on the economic profitability of the biorefinery, and the comparative analysis conducted revealed that a reduction of 40% in the biomass price, from 5.0 $€.kg_{SFDW}^{-1}$ (scenario A) to 3.0 $€.kg_{SFDW}^{-1}$ (scenario C), increases the project IRR from 20.3% (scenario A) to 43.1% (scenario C). From an economy of scale perspective, a comparative analysis between scenarios with different scales of production highlighted the importance of economies of scale for biorefinery profitability. The comparison carried out revealed that it is possible to improve profitability results from an IRR of 20.3% (scenario A) to an IRR of 27.0% (scenario E), by increasing the production capacity by 50%. Finally,

the ultimate goal of studying if the proposed multi-product biorefinery is economically more attractive than a single product value chain biorefinery was also taken into account. The multi-product biorefinery was found to reach higher profitability levels, with an IRR of 20.3%, which stands clearly above the single-product biorefinery approach, for which a negative IRR was obtained.

7. *CONCLUSIONS AND FUTURE WORK*

Taking into account the results and outcomes presented in the previous chapters, some conclusions reached and possible future research directions and work are presented next.

7.1. General Conclusions

The research work conducted in this thesis provides an integrated study, design and analysis of a multi-product biorefinery, i.e., a biorefinery capable of producing a wide range of final products (pigments and lipids for nutraceutical applications, and proteins for food and feed applications).

The microalgae strain selected as a role model for the development of such a biorefinery was *Nannochloropsis* sp. This strain was selected and studied, but some of the conclusions reached can also apply to other microalgae strains that possess the same type of morphological characteristics as *Nannochloropsis* sp. (e.g., tough cell wall), and whose products of interest have similar chemical proprieties (e.g., molecular polarity). Also, *Nannochloropsis* sp. was chosen as a microalga of interest due to its high productivity under climate conditions like the ones found in Portugal, and also due to its ability to accumulate high amounts of EPA – omega 3, thus competing with omega-3 supplements from fish sources.

Downstream processing operations were studied not only on a laboratory scale but also at pilot scales for different steps, namely biomass stabilisation after harvesting, biomass disruption, extraction and fractionation/purification of value-added compounds. A biomass stabilisation process through heat treatment was developed and optimized, to avoid degradation of the value-added compounds (mainly EPA-omega 3) during the wet storage or other sections of the biorefinery. The disruption of *Nannochloropsis* sp. was also optimised, aiming to improve the extraction of intracellular compounds, such as lipids, proteins and pigments. A strategy using ultrafiltration/diafiltration to recover the maximum of soluble proteins from an aqueous supernatant, obtained after the centrifugation of *Nannochloropsis* sp. disrupted biomass, was proposed. Also, a solvent extraction methodology was designed in order to enhance the EPA-rich polar lipid recovery. Finally, an overall integrated *Nannochloropsis* sp. biorefinery was designed combining all the optimised steps described before, and its techno-economic assessment was also conducted.

Given these overall main conclusions, directly related to the research questions and goals for this thesis, next, somewhat more detailed information is provided about the process design work conducted and corresponding outcomes. Initially, heat treatment was assessed as a way to inactivate the endogenous enzymes that catalyse hydrolysis reactions of the lipids present in the wet *Nannochloropsis* sp. biomass. Experiments were performed on both laboratory and pilot scales, and the pigment degradation, as well as the lipid degradation, were evaluated. The laboratory scale experiments revealed that the chlorophyll *a* content remained practically constant in the samples that were wet stored (at 4 ºC and -25 ºC) after a heat treatment at 95 ºC for 3 min. The pilot scale experiment also concluded that the heat treatment at 95 ºC for 3 min was effective in preventing lipid degradation, more specifically the polar lipid degradation, as no decrease in the polar lipids content was noticed in wet stored samples (4 ºC or -25 ºC for 7 days) after the heat treatment.

In what concerns the cellular disruption to increase the accessibility of value-added compounds, processing parameters of the bead milling were optimised. The pilot scale experiments revealed that it is expectable to achieve almost 95% of disruption efficiency for a single pass at a flow rate of 10 $L.h^{-1}$ and a tip speed of 14 $m.s^{-1}$. An increase in the cellular disruption rate was identified when the suspension was milled at a lower flow rate. Also, it was observed that higher tip speeds led to higher disruption efficiencies during the experiments. Similarly, the industrial scale experiments revealed that lower flow rates achieve higher disruption efficiencies at a fixed tip speed of 16 $m.s^{-1}$. It was possible to conclude that the cellular disruption rate might be higher than 89% with a single pass through the bead mill within a biorefinery with a production capacity of 300 $L.h^{-1}$.

After the cellular disruption of *Nannochloropsis* sp., two different routes were pursued: the aqueous fraction route and the solid fraction route. In the aqueous fraction route, a membrane ultrafiltration strategy was proposed to recover the maximum of soluble proteins in the permeate stream, free from insoluble proteins, lipids, and chlorophyll *a*. The corresponding results show that the membrane ultrafiltration process ran under controlled permeate flux presents significant advantages over operation under controlled transmembrane pressure: higher permeate flux during the entire operation period (12 $L.m^{-2}.h^{-1}$), higher soluble protein recovery in the permeate (between 44% and 62% in a concentration mode and 78% in a diafiltration mode) and lower membrane fouling, both reversible and irreversible. It was also concluded that the mixture of ultrafiltration in a diafiltration mode followed by concentration under controlled permeate flux conditions enhances the soluble protein recovery in the permeate and allows to maintain a higher value of volumetric flux, during the entire diafiltration process.

Regarding the solid fraction route, an eco-friendly solvent methodology to perform a polar lipid extraction from wet *Nannochloropsis* sp. biomass was developed and optimised. Different ratios of

ethanol to biomass ratio were studied to optimise the extraction. The corresponding results revealed that the ratio of 10 $mL.g^{-1}$ was capable to achieve higher polar lipid extraction efficiency (81% $w_{TFAextract}/w_{TFAbiomass}$). However, a techno-economic assessment revealed that scenario B (two-steps extraction with a solvent to biomass ratio of 1 $mL.g^{-1}$in the first step and 5 $mL.g^{-1}$in the second step of extraction) was able to produce a final product with the highest EPA concentration (17.3% w/w_{SFDW}). On the other hand, a sensitivity analysis to assess the impact of the solvent recovery percentage and the price of electricity on the production cost of the EPA revealed that scenario C (one-step extraction with a solvent to biomass ratio of 5 $mL.g^{-1}$) was the most advantageous one. Despite having a lower polar lipid extraction efficiency (71% $w_{TFAextract}/w_{TFAbiomass}$), scenario C was found to be the one with the lowest production cost, even with an increase of 50% in the electricity price (301.5 €/kg_{EPA}), or with a decrease in the solvent recovery percentage to 70% (319.7 €/kg_{EPA}).

Finally, a biorefinery to maximise the potential of EPA-rich *Nannochloropsis* sp. was proposed for the production of distinct fractions of soluble protein, EPA-rich polar lipids, and insoluble protein. It was demonstrated that the biomass purchase prices, as well as the biorefinery production scale, have a great impact on the project's estimated profitability. As for further optimization efforts, from an economic perspective, the ethanolic section of the biorefinery was found to be the costliest, both regarding investment and operating expenses, and therefore deserves to be paid special attention. It was also found that a multi-product biorefinery is economically more attractive than a single-product value chain biorefinery or a two-product value chain biorefinery. The baseline designed multi-product biorefinery resulted in estimated economic performance indicators that correspond to an IRR of 20.3%.

7.2. Future Work

A microalgae biomass biorefinery was proposed, designed and evaluated for the valorisation of *Nannochloropsis* sp. biomass. This biorefinery was studied under the broader scope of a multi-strain and multi-product biorefinery. *Nannochloropsis* sp. was selected as a role model for analysis in this thesis, but insights obtained can also be useful for other strains with the same morphological characteristics and the same types of products of interest. Further work may be conducted for addressing the possibilities of having in place a biorefinery that can process a variety of strains, rather than a single one, as assumed here.

The biorefinery proposed in this PhD thesis was designed for the recovery of three different compounds from *Nannochloropsis* sp. biomass: EPA-rich polar lipids extract (oleoresin) for food supplements, soluble protein for human food, and insoluble protein for animal feed. The *Nannochloropsis* sp. biorefinery includes biomass stabilisation followed by cellular disruption, and the fractionation and recovery of high-value fractions from *Nannochloropsis* sp., to reduce production costs and improve the techno-economic plant performance. Some additional work that may be carried out, addressing some of these process steps, will be enumerated next.

Regarding the biomass stabilisation step, the effect of the heat-treat on other types of enzymes (e.g., protease) should be analysed to evaluate if the degradation of other compounds, besides the lipids and the pigments (e.g., proteins), is avoided as well. Also, it seems to be important to evaluate the effect that the heat treatment itself could have on compounds such as proteins since the temperature is known to lead to protein denaturation. In order to validate this methodology for other possible applications in the microalgae industry, the heat treatment of other strains should also be studied, taking into account the strain's morphological characteristics as well as the compounds of interest.

Cellular disruption was optimised for a biomass suspension with a concentration of 100 $g_{SFDW}.L^{-1}$. The optimisation performed did not take into account the variation in the concentration of the fed biomass. To better understand the influence of the feed concentration on the performance of this unit operation, experiments should be performed to determine the optimal biomass concentration. An increase in the concentration could be reflected in the size of the downstream equipment, as the amount of water processed is reduced accordingly.

After the cellular disruption, centrifugation is proposed for the separation of the aqueous phase (soluble protein) and the solid phase (insoluble protein + lipids). An optimisation of this unit operation could be advantageous in terms of the amount of soluble protein recovered in the aqueous fraction. Experiments should be performed to evaluate if the resuspension of the pellet obtained in the first centrifugation,

followed by new centrifugation, increases the amount of soluble protein recovered in the aqueous supernatant.

To further validate this biorefinery for broader applications in the microalgae industry and within the global concept of a multi-strain and multi-product biorefinery, other strains should be studied and some process modifications may be necessary, taking into account the major compounds of each microalgae strain. Four different strains are suggested for future work, aligned with the multiple strain biorefinery design and operation: *Dunaliella* sp., *Lobosphaera* sp., *Haematococcus* sp., and *Arthrospira* sp..

Some exchanges in the aqueous centrifugation as well as in the polarity of the solvent used in *Nannochloropsis* sp. biorefinery (from a polar to a neutral solvent) might allow for the production of three different final products from the first three microalgae strains. The final products associated with these additional first three strains might be the following: a neutral lipid fraction rich in carotene (*Dunaliella* sp.), astaxanthin (*Haematococcus* sp.), or arachidonic acid (*Lobosphaera* sp.), a soluble protein fraction, and an insoluble and carbohydrates mix fraction. On the other hand, a more detailed study regarding the selected membrane cut-offs used in the recovery of soluble proteins at the *Nannochloropsis* sp. biorefinery might open the possibility to produce three different fractions from the last strain suggested – *Arthrospira* sp.. The final products connected with this strain might be an insoluble protein and a carbohydrates mix obtained after the aqueous centrifugation, and two distinct fractions obtained after the fractionation of the soluble proteins present in the aqueous fraction: phycocyanin and soluble proteins.

Finally, a more detailed techno-economic assessment for each strain, or combination of strains, together with the corresponding target products(e.g., specialty proteins or peptides), should be performed to compare the economic performances achieved and find optimal investment choices and operational policies for a multi-strain and multi-product biorefinery, comparing its performance and design with the ones studied here for the proposed *Nannochloropsis* sp. biorefinery that was assessed in this thesis.

BIBLIOGRAPHY

1. Safi, C.; Olivieri, G.; Campos, R.P.; Engelen-Smit, N.; Mulder, W.J.; Broek, L.A.M. Van Den; Sijtsma, L. Biorefinery of microalgal soluble proteins by sequential processing and membrane filtration. *Bioresour. Technol.* **2016**, *225*, 151–158, doi:10.1016/j.biortech.2016.11.068.

2. Figueiredo, A.R.P.; da Costa, E.; Silva, J.; Domingues, M.R.; Domingues, P. The effects of different extraction methods of lipids from *Nannochloropsis oceanica* on the contents of omega-3 fatty acids. *Algal Res.* **2019**, *41*, 101556, doi:10.1016/j.algal.2019.101556.

3. Mitra, M.; Mishra, S. A comparative analysis of different extraction solvent systems on the extractability of eicosapentaenoic acid from the marine eustigmatophyte *Nannochloropsis oceanica*. *Algal Res.* **2019**, *38*, 101387, doi:10.1016/j.algal.2018.101387.

4. Gouveia, L.; Batista, A.P.; Sousa, I.; Raymundo, A.; Bandarra, N.M. Microalgae in novel food products. In *Algae: Nutrition, Pollution Control and Energy Sources*; Konstantinos N. Papadopoulos, P., Ed.; 2008 Nova Science Publishers, Inc: Lisboa, 2009; pp. 265–300 ISBN 9781606920084.

5. Giraldo-Calderón, N.D.; Romo-Buchelly, R.J.; Arbeláez-Pérez, A.A.; Echeverri-Hincapié, D.; Atehortúa-Garcés, L. Microalgae biorefineries: applications and emerging technologies TT - Biorefinerías de microalgas: aplicaciones actuales y nuevas tecnologías en desarrollo. *Dyna* **2018**, *85*, 219–233.

6. Campbell, M.K.; Farrell, S.O. *Biochemistry*; Broyer, R., Ed.; 6th ed.; Thomson Brooks/Cole, 2006; ISBN 9780495390411.

7. Guil-Guerrero, J.L.; Navarro-Juárez, R.; López-Martínez, J.C.; Campra-Madrid, P.; Rebolloso-Fuentes, M.M. Functional properties of the biomass of three microalgal species. *J. Food Eng.* **2004**, *65*, 511–517, doi:10.1016/j.jfoodeng.2004.02.014.

8. Cavonius, L.R. Fractionation of lipids and proteins from the microalga *Nannochloropsis oculata* pH-shift process characterization and in vitro accessibility, PhD Thesis, Chalmers University of Thechnology, 2016.

9. Hess, S.K.; Lepetit, B.; Kroth, P.G.; Mecking, S. Production of Chemicals from Microalgae Lipids – Status and Perspectives. *Eur. J. Lipid Sci. Technol.* **2017**, doi:10.1002/ejlt.201700152.

10. Aishvarya, V.; Jena, J.; Pradhan, N.; Panda, P.K.; Sukla, L.B. Microalgae: Cultivation and Application. *Algal Res.* **2015**, *11*, 289–312, doi:10.1007/978-3-319-19018-1.

11. Kechasov, D. Biochemical and molecular analysis of LC-PUFA biosynthesis in the microalga *Nannochloropsis*, Master Thesis, University of Stavanger, 2013.

12. McMurry, J. *Organic Chemistry with Biological Applications*; 2nd ed.; Brooks/Cole, Cengage Learning ALL, 2011; ISBN 978-0-495-39144-9.

13. Dhanda, R.K. Fatty Acid Composition in Diverse Oat Germplasm, Master Thesis, University of Saskatchewan, 2011.

14. Islam, M.A. Microalgae : an alternative source of biodiesel for the compression ignition (CI) engine, PhD Thesis, Queensland University of Technology School, 2014.

15. Dominguez, L.J.; Barbagallo, M. Not All Fats Are Unhealthy. In *The Prevention of Cardiovascular Disease Through the Mediterranean Diet*; Elsevier Inc., 2018; pp. 35–58 ISBN 978-0-12-811259-5.

16. Francieli da Silva, G.; Rocha, L.W.; Quintão, N.L.M. 10. Nutraceuticals, Dietary Supplements, and Functional Foods as Alternatives for the Relief of Neuropathic Pain. In *Bioactive Nutraceuticals and Dietary Supplements in Neurological and Brain Disease*; Elsevier Inc., 2015; pp. 87–93 ISBN 9780124115293.

17. Zaytseva, A. Composition and quality of marine Omega-3 supplements on the Russian and Norwegian markets: a comparative study, Master Thesis, University of Nornay, 2014.

18. Venugopal, V. *Marine Products for Healthcare: Funtional and Bioactive Nutraceutical Compounds from the Ocean*; Press, C., Ed.; 1 ed.; 2009; ISBN 9781420052633.

19. Templeton, D.W.; Quinn, M.; Van Wychen, S.; Hyman, D.; Laurens, L.M.L. Separation and quantification of microalgal carbohydrates. *J. Chromatogr. A* **2012**, *1270*, 225–234, doi:10.1016/j.chroma.2012.10.034.

20. Markou, G.; Angelidaki, I.; Georgakakis, D. Microalgal carbohydrates: An overview of the factors influencing carbohydrates production, and of main bioconversion technologies for production of biofuels. *Appl. Microbiol. Biotechnol.* **2012**, *96*, 631–645, doi:10.1007/s00253-012-4398-0.

21. Pagels, F.; Salvaterra, D.; Amaro, H.M.; Guedes, A.C. *Handbook of Microalgae-Based Processes and Products, Pigments from microalgae*; Elsevier Inc., 2020; ISBN 9780128185360.

22. Masojdek, J.; Koblek, M.; Torzillo, G. Photosynthesis in Microalgae. *Handb. Microalgal Cult.* **2007**, 20–39, doi:10.1002/9780470995280.ch2.

23. Fernández, F.G.A.; Reis, A.; Wijffels, R.H.; Barbosa, M.; Verdelho, V.; Llamas, B. The role of microalgae in the bioeconomy. *N. Biotechnol.* **2021**, *61*, 99–107, doi:10.1016/j.nbt.2020.11.011.

24. Sahni, P.; Aggarwal, P.; Sharma, S.; Singh, B. Nuances of microalgal technology in food and nutraceuticals: a review. *Nutr. Food Sci.* **2019**, *49*, 866–885, doi:10.1108/NFS-01-2019-0008.

25. European Parliament and the Council of the European Union *Commission implementing Regulation (EU) 2017/2470 of 20 December 2017 establishing the Union list of novel foods in accordance with Regulation (EU) 2015/2283 of the European Parliament and of the Council on novel foods*; 2017; Vol. 351;.

26. Molino, A.; Iovine, A.; Casella, P.; Mehariya, S.; Chianese, S.; Cerbone, A.; Rimauro, J.; Musmarra, D. Microalgae characterization for consolidated and new application in human food, animal feed and nutraceuticals. *Int. J. Environ. Res. Public Health* **2018**, *15*, 1–21, doi:10.3390/ijerph15112436.

27. Cavonius, L.R. Fractionation of lipids and proteins from the microalga *Nannochloropsis oculata*, PhD Thesis, Chalmers University of Technology, 2016.

28. Christaki, E.; Bonos, E.; Florou-Paneri, P. Innovative Microalgae Pigments as Functional Ingredients in Nutrition. *Handb. Mar. Microalgae Biotechnol. Adv.* **2015**, 223–243, doi:10.1016/B978-0-12-800776-1.00014-5.

29. Camacho-Rodríguez, J.; Cerón-García, M.C.; Fernández-Sevilla, J.M.; Molina-Grima, E. The influence of culture conditions on biomass and high value product generation by *Nannochloropsis gaditana* in aquaculture. *Algal Res.* **2015**, *11*, 63–73, doi:10.1016/j.algal.2015.05.017.

30. Bondioli, P.; Della Bella, L.; Rivolta, G.; Chini Zittelli, G.; Bassi, N.; Rodolfi, L.; Casini, D.; Prussi, M.; Chiaramonti, D.; Tredici, M.R. Oil production by the marine microalgae *Nannochloropsis* sp. F&M-M24 and *Tetraselmis suecica* F&M-M33. *Bioresour. Technol.* **2012**, *114*, 567–572, doi:10.1016/j.biortech.2012.02.123.

31. Cecchin, M.; Berteotti, S.; Paltrinieri, S.; Vigliante, I.; Iadarola, B.; Giovannone, B.; Maffei, M.E.; Delledonne, M.; Ballottari, M. Improved lipid productivity in *Nannochloropsis gaditana* in nitrogen-replete conditions by selection of pale green mutants. *Biotechnol. Biofuels* **2020**, *13*, 1–14, doi:10.1186/s13068-020-01718-8.

32. Valente, L.M.P.; Custódio, M.; Batista, S.; Fernandes, H.; Kiron, V. Defatted microalgae (*Nannochloropsis* sp.) from biorefinery as a potential feed protein source to replace fishmeal in

European sea bass diets. *Fish Physiol. Biochem.* **2019**, *45*, 1067–1081, doi:10.1007/s10695-019-00621-w.

33. Hulatt, C.J.; Wijffels, R.H.; Bolla, S.; Kiron, V. Production of fatty acids and protein by *Nannochloropsis* in flat-plate photobioreactors. *PLoS One* **2017**, *12*, 1–17, doi:10.1371/journal.pone.0170440.

34. Grossmann, L.; Ebert, S.; Hinrichs, J.; Weiss, J. Production of protein-rich extracts from disrupted microalgae cells: Impact of solvent treatment and lyophilization. *Algal Res.* **2018**, *36*, 67–76, doi:10.1016/j.algal.2018.09.011.

35. Hibberd, D.J. Notes on the taxonomy and nomenclature of the algal classes Eustigmatophyceae and Tribophyceae (synonym Xanthophyceae). *Bot. J. Linn. Soc.* **1981**, *82*, 93–119, doi:10.1111/j.1095-8339.1981.tb00954.x.

36. Lubián, L.M.; Montero, O.; Moreno-Garrido, I.; Huertas, I.E.; Sobrino, C.; González-del Valle, M.; Parés, G. *Nannochloropsis* (Eustigmatophyceae) as source of commercially valuable pigments. *J. Appl. Phycol.* **2000**, *12*, 249–255.

37. Halim, R.; Hill, D.R.A.; Hanssen, E.; Webley, P.A.; Martin, G.J.O. Thermally coupled dark-anoxia incubation: A platform technology to induce auto-fermentation and thus cell-wall thinning in both nitrogen-replete and nitrogen-deplete *Nannochloropsis* slurries. *Bioresour. Technol.* **2019**, *290*, 121769, doi:10.1016/j.biortech.2019.121769.

38. Montalescot, V.; Rinaldi, T.; Touchard, R.; Jubeau, S.; Frappart, M.; Jaouen, P.; Bourseau, P.; Marchal, L. Optimization of bead milling parameters for the cell disruption of microalgae: Process modeling and application to *Porphyridium cruentum* and *Nannochloropsis oculata*. *Bioresour. Technol.* **2015**, *196*, 339–346, doi:10.1016/j.biortech.2015.07.075.

39. ResearchAndMarkets Algae Omega 3 Ingredients Market Assessment 2020-2027 Available online: https://www.businesswire.com/news/home/20200831005234/en/Algae-Omega-3-Ingredients-Market-Assessment-2020-2027-A-580-Million-Opportunity---ResearchAndMarkets.com (accessed on Dec 9, 2021).

40. Jong, E. De; Jungmeier, G. Biorefinery Concepts in Comparison to Petrochemical Refineries. In *Industrial Biorefineries and White Biotechnology*; 2015; pp. 3–33 ISBN 9780444634535.

41. Tredici, M.R. Photobiology of microalgae mass cultures : understanding the tools for the next green revolution. *Biofuels* **2010**, *1*, 143–162.

42. Molina Grima, E.; Belarbi, E.H.; Acién Fernández, F.G.; Robles Medina, A.; Chisti, Y. Recovery

of microalgal biomass and metabolites: Process options and economics. *Biotechnol. Adv.* **2003**, *20*, 491–515, doi:10.1016/S0734-9750(02)00050-2.

43. Barros, A.I.; Gonçalves, A.L.; Simões, M.; Pires, J.C.M. Harvesting techniques applied to microalgae: A review. *Renew. Sustain. Energy Rev.* **2015**, *41*, 1489–1500, doi:10.1016/j.rser.2014.09.037.

44. Balduyck, L.; Stock, T.; Bijttebier, S.; Bruneel, C.; Jacobs, G.; Voorspoels, S.; Muylaert, K.; Foubert, I. Integrity of the microalgal cell plays a major role in the lipolytic stability during wet storage. *Algal Res.* **2017**, *25*, 516–524, doi:10.1016/j.algal.2017.06.013.

45. Schokker, E.P. Kinetic Modelling of Enzyme: Inactivation Kinetics of heat inactivation of the extracellular proteinase from *Pseudomonas fluorescens* 22F, Wageningen University & Research, 1997.

46. Lehtinen, P.; Kiiliäinen, K.; Lehtomäki, I.; Laakso, S. Effect of heat treatment on lipid stability in processed oats. *J. Cereal Sci.* **2003**, *37*, 215–221, doi:10.1006/jcrs.2002.0496.

47. Doblado-Maldonado, A.F.; Pike, O.A.; Sweley, J.C.; Rose, D.J. Key issues and challenges in whole wheat flour milling and storage. *J. Cereal Sci.* **2012**, *56*, 119–126, doi:10.1016/j.jcs.2012.02.015.

48. Gong, M.; Hu, Y.; Yedahalli, S.; Bassi, A. Oil Extraction Processes in Microalgae Oil Extraction Processes in Microalgae. *Recent Adv. Renew. Energy* **2017**, *1*.

49. Scholz, M.J.; Weiss, T.L.; Jinkerson, R.E.; Jing, J.; Roth, R.; Goodenough, U.; Posewitz, M.C.; Gerken, H.G. Ultrastructure and Composition of the *Nannochloropsis gaditana* Cell Wall. *Eukaryot. Cell* **2014**, *13*, 1450–1464, doi:10.1128/EC.00183-14.

50. Lee, S.Y.; Cho, J.M.; Chang, Y.K.; Oh, Y. Cell disruption and lipid extraction for microalgal biorefineries : A review. *Bioresour. Technol.* **2017**, doi:10.1016/j.biortech.2017.06.038.

51. Dixon, C.; Wilken, L.R. Green microalgae biomolecule separations and recovery. *Bioresour. Bioprocess.* **2018**, *5*, doi:10.1186/s40643-018-0199-3.

52. Günerken, E.; D'Hondt, E.; Eppink, M.H.M.; Garcia-Gonzalez, L.; Elst, K.; Wijffels, R.H. Cell disruption for microalgae biorefineries. *Biotechnol. Adv.* **2015**, *33*, 243–260, doi:10.1016/j.biotechadv.2015.01.008.

53. Jiménez Callejón, M.J.; Robles Medina, A.; Macías Sánchez, M.D.; González Moreno, P.A.; Navarro López, E.; Esteban Cerdán, L.; Molina Grima, E. Supercritical fluid extraction and pressurized liquid extraction processes applied to eicosapentaenoic acid-rich polar lipid recovery

from the microalga *Nannochloropsis* sp. *Algal Res.* **2022**, *61*, 102586, doi:10.1016/J.ALGAL.2021.102586.

54. Geow, C.H.; Tan, M.C.; Yeap, S.P.; Chin, N.L. A Review on Extraction Techniques and Its Future Applications in Industry. *Eur. J. Lipid Sci. Technol.* **2021**, *123*, 1–10, doi:10.1002/ejlt.202000302.

55. Harrison, R.G.; Todd, P.; Rudge, S.R.; Petrides, D.P. *Bioseparations Science and Engineering, Second Edition*; 2015;

56. Sicaire, A.G.; Vian, M.; Fine, F.; Joffre, F.; Carré, P.; Tostain, S.; Chemat, F. Alternative bio-based solvents for extraction of fat and oils: Solubility prediction, global yield, extraction kinetics, chemical composition and cost of manufacturing. *Int. J. Mol. Sci.* **2015**, *16*, 8430–8453, doi:10.3390/ijms16048430.

57. Tanzi, C.D.; Vian, M.A.; Ginies, C.; Elmaataoui, M.; Chemat, F. Terpenes as Green Solvents for Extraction of Oil from Microalgae. *Molecules* **2012**, *17*, 8196–8205, doi:10.3390/molecules17078196.

58. Liu, S.X.; Mamidipally, P.K. First approach on rice bran oil extraction using limonene. *Eur. J. Lipid Sci. Technol.* **2004**, *106*, 122–125, doi:10.1002/ejlt.200300891.

59. Liu, S.X.; Mamidipally, P.K. Quality Comparison of Rice Bran Oil Extracted with d-Limonene and Hexane. *Cereal Chem.* **2005**, *82*, 209–215.

60. Chen, M.; Chen, X.; Liu, T.; Zhang, W. Subcritical Ethanol Extraction of Lipid from Wet Microalgae Paste of *Nannochloropsis* sp . *J. Biobased Mater. Bioenergy* **2011**, *5*, 385–389, doi:10.1166/jbmb.2011.1157.

61. Yang, F.; Xiang, W.; Sun, X.; Wu, H.; Li, T.; Long, L. A Novel Lipid Extraction Method from Wet Microalga *Picochlorum* sp. at Room Temperature. *Mar. Drugs* **2014**, *12*, 1258–1270, doi:10.3390/md12031258.

62. Wang, Z. Membrane Biotechnology. In *Encyclopedia of Membranes*; Drioli, E., Giorno, L., Eds.; Springer-Verlag Berlin Heidelberg, 2015.

63. Monte, J.; Ribeiro, C.; Parreira, C.; Costa, L.; Brive, L.; Casal, S.; Brazinha, C.; Crespo, J.G. Biorefinery of *Dunaliella salina*: Sustainable recovery of carotenoids, polar lipids and glycerol. *Bioresour. Technol.* **2020**, *297*, 122509, doi:10.1016/j.biortech.2019.122509.

64. Harvey, P.J.; Ben-Amotz, A. Towards a sustainable *Dunaliella salina* microalgal biorefinery for 9-cis β-carotene production. *Algal Res.* **2020**, *50*, 102002, doi:10.1016/j.algal.2020.102002.

65. Ashokkumar, V.; Chen, W.H.; Kumar, G.; Satjarak, A.; Chanthapatchot, W.; Ngamcharussrivichai, C. A biorefinery approach for high value-added bioproduct (astaxanthin) from alga *Haematococcus* sp. and residue pyrolysis for biochar synthesis and metallic iron production from hematite (Fe2O3). *Fuel* **2021**, *304*, 121150, doi:10.1016/j.fuel.2021.121150.

66. Koyande, A.K.; Chew, K.W.; Lim, J.W.; Lam, M.K.; Ho, Y.C.; Show, P.L. Biorefinery of *Chlorella sorokiniana* using ultra sonication assisted liquid triphasic flotation system. *Bioresour. Technol.* **2020**, *303*, 122931, doi:10.1016/j.biortech.2020.122931.

67. Chia, S.R.; Chew, K.W.; Show, P.L.; Xia, A.; Ho, S.H.; Lim, J.W. *Spirulina platensis* based biorefinery for the production of value-added products for food and pharmaceutical applications. *Bioresour. Technol.* **2019**, *289*, 121727, doi:10.1016/j.biortech.2019.121727.

68. Mendoza, Á.; Morales, V.; Sánchez-Bayo, A.; Rodríguez-Escudero, R.; González-Fernández, C.; Bautista, L.F.; Vicente, G. The effect of the lipid extraction method used in biodiesel production on the integrated recovery of biodiesel and biogas from *Nannochloropsis gaditana*, *Isochrysis galbana* and *Arthrospira platensis*. *Biochem. Eng. J.* **2020**, *154*, 107428, doi:10.1016/j.bej.2019.107428.

69. Taher, H.; Giwa, A.; Abusabiekeh, H.; Al-Zuhair, S. Biodiesel production from *Nannochloropsis gaditana* using supercritical CO_2 for lipid extraction and immobilized lipase transesterification: Economic and environmental impact assessments. *Fuel Process. Technol.* **2020**, *198*, 106249, doi:10.1016/j.fuproc.2019.106249.

70. Turkkul, B.; Deliismail, O.; Seker, E. Ethyl esters biodiesel production from *Spirulina* sp. and *Nannochloropsis oculata* microalgal lipids over alumina-calcium oxide catalyst. *Renew. Energy* **2020**, *145*, 1014–1019, doi:10.1016/j.renene.2019.06.093.

71. Cavonius, L.R.; Albers, E.; Undeland, I. pH-shift processing of *Nannochloropsis oculata* microalgal biomass to obtain a protein-enriched food or feed ingredient. *Algal Res.* **2015**, *11*, 95–102, doi:10.1016/j.algal.2015.05.022.

72. Wijffels, R.H.; Barbosa, M.J.; Eppink, M.H.M. Microalgae for the production of bulk chemicals and biofuels. *Biofuels, Bioprod. Biorefining* **2010**, 287–295, doi:10.1002/bbb.

73. Eppink, M.H.M.; Olivieri, G.; Reith, H.; van den Berg, C.; Barbosa, M.J.; Wijffels, R.H. From Current Algae Products to Future Biorefinery: A Review. *Adv. Biochem. Eng. Biotechnol.* **2017**.

74. Kassim, M.A.; Meng, T.K. Carbon dioxide (CO_2) biofixation by microalgae and its potential for biorefinery and biofuel production. *Sci. Total Environ.* **2017**, *584–585*, 1121–1129,

doi:10.1016/j.scitotenv.2017.01.172.

75. Balduyck, L.; Dejonghe, C.; Goos, P.; Jooken, E.; Muylaert, K.; Foubert, I. Inhibition of lipolytic reactions during wet storage of *T-Isochrysis lutea* biomass by heat treatment. *Algal Res.* **2019**, *38*, 101388, doi:10.1016/j.algal.2018.101388.

76. Li-Beisson, Y.; Thelen, J.J.; Fedosejevs, E.; Harwood, J.L. The lipid biochemistry of eukaryotic algae. *Prog. Lipid Res.* **2019**, *74*, 31–68, doi:10.1016/j.plipres.2019.01.003.

77. Mitra, M.; Patidar, S.K.; Mishra, S. Integrated process of two stage cultivation of *Nannochloropsis* sp. for nutraceutically valuable eicosapentaenoic acid along with biodiesel. *Bioresour. Technol.* **2015**, *193*, 363–369, doi:10.1016/j.biortech.2015.06.033.

78. Navarro López, E.; Robles Medina, A.; González Moreno, P.A.; Jiménez Callejón, M.J.; Esteban Cerdán, L.; Martín Valverde, L.; Castillo López, B.; Molina Grima, E. Enzymatic production of biodiesel from *Nannochloropsis gaditana* lipids: Influence of operational variables and polar lipid content. *Bioresour. Technol.* **2015**, *187*, 346–353, doi:10.1016/j.biortech.2015.03.126.

79. Batan, L.Y.; Graff, G.D.; Bradley, T.H. Techno-economic and Monte Carlo Probabilistic Analysis of Microalgae Biofuel Production System. *Bioresour. Technol.* **2016**, *219*, 45–52, doi:10.1016/j.biortech.2016.07.085.

80. Balduyck, L.; Bijttebier, S.; Bruneel, C.; Jacobs, G.; Voorspoels, S.; Van Durme, J.; Muylaert, K.; Foubert, I. Lipolysis in *T-Isochrysis lutea* during wet storage at different temperatures. *Algal Res.* **2016**, *18*, 281–287, doi:10.1016/j.algal.2016.07.003.

81. Jiménez Callejón, M.J.; Robles Medina, A.; González Moreno, P.A.; Esteban Cerdán, L.; Orta Guillén, S.; Molina Grima, E. Simultaneous extraction and fractionation of lipids from the microalga *Nannochloropsis* sp. for the production of EPA-rich polar lipid concentrates. *J. Appl. Phycol.* **2020**, *32*, 1117–1128, doi:10.1007/s10811-020-02037-z.

82. Swanson, D.; Block, R.; Mousa, S.A. Omega-3 fatty acids EPA and DHA: Health benefits throughout life. *Adv. Nutr.* **2012**, *3*, 1–7, doi:10.3945/an.111.000893.

83. Chua, E.T.; Schenk, P.M. A biorefinery for *Nannochloropsis*: Induction, harvesting, and extraction of EPA-rich oil and high-value protein. *Bioresour. Technol.* **2017**, *244*, doi:10.1016/j.biortech.2017.05.124.

84. Schneider, J.C.; Livne, A.; Sukenik, A.; Roessler, P.G. A mutant of *Nannochloropsis* deficient in eicosapentaenoic acid production. *Phytochemistry* **1995**, *40*, 807–814, doi:10.1016/0031-9422(95)00365-E.

85. Safafar, H.; Langvad, S.; Møller, P.; Jacobsen, C. Storage Conditions Affect Oxidative Stability and Nutritional Composition of Freeze-Dried *Nannochloropsis salina*. *Eur. J. Lipid Sci. Technol.* **2017**, *119*, 1–10, doi:10.1002/ejlt.201600477.

86. Kagan, M.L.; Levy, A.; Leikin-Frenkel, A. Comparative study of tissue deposition of omega-3 fatty acids from polar-lipid rich oil of the microalgae *Nannochloropsis oculata* with krill oil in rats. *Food Funct.* **2015**, *6*, 186–192, doi:10.1039/c4fo00591k.

87. Tang, X.; Li, Z.J.; Xu, J.; Xue, Y.; Li, J.Z.; Wang, J.F.; Yanagita, T.; Xue, C.H.; Wang, Y.M. Short term effects of different omega-3 fatty acid formulation on lipid metabolism in mice fed high or low fat diet. *Lipids Health Dis.* **2012**, *11*, 1–8, doi:10.1186/1476-511X-11-70.

88. Rossmeisl, M.; Macek Jilkova, Z.; Kuda, O.; Jelenik, T.; Medrikova, D.; Stankova, B.; Kristinsson, B.; Haraldsson, G.G.; Svensen, H.; Stoknes, I.; et al. Metabolic effects of n-3 PUFA as phospholipids are superior to triglycerides in mice fed a high-fat diet: Possible role of endocannabinoids. *PLoS One* **2012**, *7*, 1–13, doi:10.1371/journal.pone.0038834.

89. Basso, S.; Simionato, D.; Gerotto, C.; Segalla, A.; Giacometti, G.M.; Morosinotto, T. Characterization of the photosynthetic apparatus of the Eustigmatophycean *Nannochloropsis gaditana*: Evidence of convergent evolution in the supramolecular organization of photosystem i. *Biochim. Biophys. Acta - Bioenerg.* **2014**, *1837*, 306–314, doi:10.1016/j.bbabio.2013.11.019.

90. Ryckebosch, E.; Muylaert, K.; Eeckhout, M.; Ruyssen, T.; Foubert, I. Influence of drying and storage on lipid and carotenoid stability of the Microalga *Phaeodactylum tricornutum*. *J. Agric. Food Chem.* **2011**, *59*, 11063–11069, doi:10.1021/jf2025456.

91. Stephan, A.; Steinhart, H. Bitter taste of unsaturated free fatty acids in emulsions: Contribution to the off-flavour of soybean lecithins. *Eur. Food Res. Technol.* **2000**, *212*, 17–25, doi:10.1007/s002170000216.

92. Yilmaz, C.; Gökmen, V. Chlorophyll. In *Encyclopedia of Food and Health*; 2015; pp. 37–41 ISBN 9780123849533.

93. Schwartz, S.J.; Lorenzo, T. V. Chlorophylls in Foods. *Crit. Rev. Food Sci. Nutr.* **1990**, *29*, 1–17, doi:10.1080/10408399009527511.

94. Weemaes, C.A.; Ooms, V.; Van Loey, A.M.; Hendrickx, M.E. Kinetics of Chlorophyll Degradation and Color Loss in Heated Broccoli Juice. *J. Agric. Food Chem* **1999**, *47*, 2404–2409, doi:10.1021/JF980663O.

95. Aubourg, S.P. Fluorescence study of the pro-oxidant effect of free fatty acids on marine lipids.

J. Sci. Food Agric. **2001**, *81*, 385–390, doi:10.1002/1097-0010(200103)81:4<385::AID-JSFA821>3.0.CO;2-X.

96. Chen, L.; Liu, T.; Zhang, W.; Chen, X.; Wang, J. Biodiesel production from algae oil high in free fatty acids by two-step catalytic conversion. *Bioresour. Technol.* **2012**, *111*, 208–214, doi:10.1016/j.biortech.2012.02.033.

97. Esquivel, B.C.; Lobina, D.V.; Sandoval, F.C. The biochemical composition of two diatoms after different preservation techniques. *Comp. Biochem. Physiol. Part B Biochem.* **1993**, *105*, 369–373, doi:10.1016/0305-0491(93)90243-X.

98. Ramos, O.L.; Xavier Malcata, F. Food-grade enzymes. *Compr. Biotechnol.* **2019**, 587–603, doi:10.1016/B978-0-12-809633-8.09173-1.

99. Demir, B.S.; Tükel, S.S. Purification and characterization of lipase from *Spirulina platensis*. *J. Mol. Catal. B Enzym.* **2010**, *64*, 123–128, doi:10.1016/j.molcatb.2009.09.011.

100. Yong, S.K.; Lim, B.H.; Saleh, S.; Tey, L.H. Optimisation, purification and characterisation of extracellular lipase from *Botryococcus sudeticus* (UTEX 2629). *J. Mol. Catal. B Enzym.* **2016**, *126*, 99–105, doi:10.1016/j.molcatb.2016.02.004.

101. Schwartz, S.J.; Von Elbe, J.H. Kinetics of Chlorophyll Degradation to Pyropheophytin in Vegetables. *J. Food Sci.* **1983**, *48*, 1303–1306, doi:10.1111/j.1365-2621.1983.tb09216.x.

102. Canjura, F.L.; Schwartz, S.J.; Nunes, R. V. Degradation Kinetics of Chlorophylls and Chlorophyllides. *J. Food Sci.* **1991**, *56*, 1639–1643, doi:10.1111/j.1365-2621.1991.tb08660.x.

103. Schwartz, S.J.; Von Elbe, J.H.; Giusti, M.M. Colorants. In *Fennema's Food Chemistry*; 2008; pp. 571–638.

104. Hubert, F.; Poisson, L.; Loiseau, C.; Gauvry, L.; Pencréac'h, G.; Hérault, J.; Ergan, F. Lipids and lipolytic enzymes of the microalga *Isochrysis galbana*. *OCL - Oilseeds fats, Crop. Lipids* **2017**, *24*, doi:10.1051/ocl/2017023.

105. Budge, S.M.; Parrish, C.C. Lipid class and fatty acid composition of *Pseudo-nitzschia multiseries* and *Pseudo-nitzschia pungens* and effects of lipolytic enzyme deactivation. *Phytochemistry* **1999**, *52*, 561–566, doi:10.1016/S0031-9422(99)00241-1.

106. Berge, J.; Gouygou, J.; Dubacqt, J.; Durand, P. Reassessment of lipid composition of the diatom, *Skeletonema costatum*. **1995**, *39*, 1017–1021.

107. Meisner, H.; Tenney, K. pH as an indicator of free fatty acid release from adipocytes. *J. Lipid*

Res. **1977**, *18*, 774–776, doi:10.1016/s0022-2275(20)41596-2.

108. Ryckebosch, E.; Muylaert, K.; Foubert, I. Optimization of an analytical procedure for extraction of lipids from microalgae. *JAOCS, J. Am. Oil Chem. Soc.* **2012**, *89*, 189–198, doi:10.1007/s11746-011-1903-z.

109. Breuer, G.; Lamers, P.P.; Martens, D.E.; Draaisma, R.B.; Wijffels, R.H. The impact of nitrogen starvation on the dynamics of triacylglycerol accumulation in nine microalgae strains. *Bioresour. Technol.* **2012**, *124*, 217–226, doi:10.1016/j.biortech.2012.08.003.

110. León-Saiki, G.M.; Remmers, I.M.; Martens, D.E.; Lamers, P.P.; Wijffels, R.H.; van der Veen, D. The role of starch as transient energy buffer in synchronized microalgal growth in *Acutodesmus obliquus*. *Algal Res.* **2017**, *25*, 160–167, doi:10.1016/j.algal.2017.05.018.

111. Lepage, G.; Roy, C.C. Direct transesterification of all classes of lipids in a one-step reaction. *J. Lipid Res.* **1986**, *27*, 114–120, doi:10.1016/s0022-2275(20)38861-1.

112. Suarez Garcia, E.; Lo, C.; Eppink, M.H.M.; Wijffels, R.H.; van den Berg, C. Understanding mild cell disintegration of microalgae in bead mills for the release of biomolecules. *Chem. Eng. Sci.* **2019**, *203*, 380–390, doi:10.1016/j.ces.2019.04.008.

113. Delrue, F.; Setier, P.A.; Sahut, C.; Cournac, L.; Roubaud, A.; Peltier, G.; Froment, A.K. An economic, sustainability, and energetic model of biodiesel production from microalgae. *Bioresour. Technol.* **2012**, *111*, 191–200, doi:10.1016/j.biortech.2012.02.020.

114. Vanthoor-Koopmans, M.; Wijffels, R.H.; Barbosa, M.J.; Eppink, M.H.M. Biorefinery of microalgae for food and fuel. *Bioresour. Technol.* **2013**, *135*, 142–149, doi:10.1016/j.biortech.2012.10.135.

115. Kassim, M.A.; Rashid, M.A.; Halim, R. Towards Biorefinery Production of Microalgal Biofuels and Bioproducts: Production of Acetic Acid from the Fermentation of *Chlorella* sp. and *Tetraselmis suecica* Hydrolysates. *Green Sustain. Chem.* **2017**, *07*, 152–171, doi:10.4236/gsc.2017.72012.

116. Günerken, E.; D'Hondt, E.; Eppink, M.; Elst, K.; Wijffels, R. Influence of nitrogen depletion in the growth of *N. oleoabundans* on the release of cellular components after beadmilling. *Bioresour. Technol.* **2016**, *214*, 89–95, doi:10.1016/j.biortech.2016.04.072.

117. Gerde, J.A.; Montalbo-Lomboy, M.; Yao, L.; Grewell, D.; Wang, T. Evaluation of microalgae cell disruption by ultrasonic treatment. *Bioresour. Technol.* **2012**, *125*, 175–181, doi:10.1016/j.biortech.2012.08.110.

118. Skorupskaite, V.; Makareviciene, V.; Sendzikiene, E.; Gumbyte, M. Microalgae *Chlorella* sp. cell disruption efficiency utilising ultrasonication and ultrahomogenisation methods. *J. Appl. Phycol.* **2019**, *31*, 2349–2354, doi:10.1007/s10811-019-01761-5.

119. Buchmann, L.; Brändle, I.; Haberkorn, I.; Hiestand, M.; Mathys, A. Pulsed electric field based cyclic protein extraction of microalgae towards closed-loop biorefinery concepts. *Bioresour. Technol.* **2019**, *291*, 121870, doi:10.1016/j.biortech.2019.121870.

120. Postma, P.R.; Pataro, G.; Capitoli, M.; Barbosa, M.J.; Wijffels, R.H.; Eppink, M.H.M.; Olivieri, G.; Ferrari, G. Selective extraction of intracellular components from the microalga *Chlorella vulgaris* by combined pulsed electric field-temperature treatment. *Bioresour. Technol.* **2016**, *203*, 80–88, doi:10.1016/j.biortech.2015.12.012.

121. Postma, P.R.; Miron, T.L.; Olivieri, G.; Barbosa, M.J.; Wijffels, R.H.; Eppink, M.H.M. Mild disintegration of the green microalgae *Chlorella vulgaris* using bead milling. *Bioresour. Technol.* **2015**, *184*, 297–304, doi:10.1016/j.biortech.2014.09.033.

122. Iqbal, J.; Theegala, C. Microwave assisted lipid extraction from microalgae using biodiesel as co-solvent. *Algal Res.* **2013**, *2*, 34–42, doi:10.1016/j.algal.2012.10.001.

123. Rokicka, M.; Zieliński, M.; Dudek, M.; Dębowski, M. Effects of Ultrasonic and Microwave Pretreatment on Lipid Extraction of Microalgae and Methane Production from the Residual Extracted Biomass. *Bioenergy Res.* **2020**, doi:10.1007/s12155-020-10202-y.

124. Safi, C.; Cabas Rodriguez, L.; Mulder, W.J.; Engelen-Smit, N.; Spekking, W.; van den Broek, L.A.M.; Olivieri, G.; Sijtsma, L. Energy consumption and water-soluble protein release by cell wall disruption of *Nannochloropsis gaditana*. *Bioresour. Technol.* **2017**, *239*, 204–210, doi:10.1016/j.biortech.2017.05.012.

125. Maffei, G.; Bracciale, M.P.; Broggi, A.; Zuorro, A.; Santarelli, M.L.; Lavecchia, R. Effect of an enzymatic treatment with cellulase and mannanase on the structural properties of *Nannochloropsis* microalgae. *Bioresour. Technol.* **2018**, *249*, 592–598, doi:10.1016/j.biortech.2017.10.062.

126. Demuez, M.; Mahdy, A.; Tomás-Pejó, E.; González-Fernández, C.; Ballesteros, M. Enzymatic cell disruption of microalgae biomass in biorefinery processes. *Biotechnol. Bioeng.* **2015**, *112*, 1955–1966, doi:10.1002/bit.25644.

127. Zinkoné, T.R.; Gifuni, I.; Lavenant, L.; Pruvost, J.; Marchal, L. Bead milling disruption kinetics of microalgae: Process modeling, optimization and application to biomolecules recovery from

Chlorella sorokiniana. *Bioresour. Technol.* **2018**, *267*, 458–465, doi:10.1016/j.biortech.2018.07.080.

128. Kula, M. -R; Schütte, H. Purification of Proteins and the Disruption of Microbial Cells. *Biotechnol. Prog.* **1987**, *3*, 31–42, doi:10.1002/btpr.5420030107.

129. Balasundaram, B.; Skill, S.C.; Llewellyn, C.A. A low energy process for the recovery of bioproducts from cyanobacteria using a ball mill. *Biochem. Eng. J.* **2012**, *69*, 48–56, doi:10.1016/j.bej.2012.08.010.

130. Doucha, J.; Lívanský, K. Influence of processing parameters on disintegration of *Chlorella* cells in various types of homogenizers. *Appl Microbiol Biotechnol* **2008**, *81*, 431–440, doi:10.1007/s00253-008-1660-6.

131. Postma, P.R.; Suarez-Garcia, E.; Safi, C.; Olivieri, G.; Wijffels, R.H. Energy efficient bead milling of microalgae: Effect of bead size on disintegration and release of proteins and carbohydrates. *Bioresour. Technol.* **2017**, *224*, 670–679, doi:10.1016/j.biortech.2016.11.071.

132. Allard, B.; Templier, J. Comparison of neutral lipid profile of various trilaminar outer cell wall (TLS)-containing microalgae with emphasis on algaenan occurrence. *Phytochemistry* **2000**, *54*, 369–380, doi:10.1016/S0031-9422(00)00135-7.

133. Dunker, S.; Wilhelm, C. Cell wall structure of coccoid green algae as an important trade-off between biotic interference mechanisms and multidimensional cell growth. *Front. Microbiol.* **2018**, *9*, doi:10.3389/fmicb.2018.00719.

134. Quesada, S.; Azofeifa, G.; Jatunov, S.; Jiménez, G.; Navarro, L.; Gómez, G. Carotenoids composition, antioxidant activity and glycemic index of two varieties of *Bactris gasipaes*. *Emirates J. Food Agric.* **2011**, *23*, 482–489.

135. Gomes, T.A.; Zanette, C.M.; Spier, M.R. An overview of cell disruption methods for intracellular biomolecules recovery. *Prep. Biochem. Biotechnol.* **2020**, *50*, 635–654, doi:10.1080/10826068.2020.1728696.

136. Quesada-Salas, M.C.; Delfau-bonnet, G.; Willig, G.; Préat, N.; Allais, F.; Ioannou, I. Optimization and comparison of three cell disruption processes on lipid extraction from microalgae. *Processes* **2021**, *9*, 1–20, doi:10.3390/pr9020369.

137. Goldberg, S. Mechanical/physical methods of cell disruption and tissue homogenization. *Methods Mol. Biol.* **2008**, *424*, 3–22, doi:10.1007/978-1-60327-064-9_1.

138. Bunge, F.; Pietzsch, M.; Müller, R.; Syldatk, C. Mechanical disruption of *Arthrobacter* sp. DSM

3747 in stirred ball mills for the release of hydantoin-cleaving enzymes. *Chem. Eng. Sci.* **1992**, *47*, 225–232, doi:10.1016/0009-2509(92)80216-Y.

139. Kwade, A.; Schwedes, J. Breaking characteristics of different materials and their effect on stress intensity and stress number in stirred media mills. *Powder Technol.* **2002**, *122*, 109–121, doi:10.1016/S0032-5910(01)00406-5.

140. Fradique, Ḿonica; Batista, A.P.; Nunes, M.C.; Gouveia, L.; Bandarra, N.M.; Raymundo, A. Incorporation of *Chlorella vulgaris* and *Spirulina maxima* biomass in pasta products. Part 1: Preparation and evaluation. *J. Sci. Food Agric.* **2010**, *90*, 1656–1664, doi:10.1002/jsfa.3999.

141. Ansari, F.A.; Guldhe, A.; Gupta, S.K.; Rawat, I.; Bux, F. Improving the feasibility of aquaculture feed by using microalgae. *Environ. Sci. Pollut. Res.* **2021**, *28*, 43234–43257, doi:10.1007/s11356-021-14989-x.

142. Ashaolu, T.J.; Samborska, K.; Lee, C.C.; Tomas, M.; Capanoglu, E.; Tarhan, Ö.; Taze, B.; Jafari, S.M. Phycocyanin, a super functional ingredient from algae; properties, purification characterization, and applications. *Int. J. Biol. Macromol.* **2021**, *193*, 2320–2331, doi:10.1016/J.IJBIOMAC.2021.11.064.

143. Becker, E.W. Micro-algae as a source of protein. *Biotechnol. Adv.* **2007**, *25*, 207–210, doi:10.1016/j.biotechadv.2006.11.002.

144. Waghmare, A.G.; Salve, M.K.; LeBlanc, J.G.; Arya, S.S. Concentration and characterization of microalgae proteins from *Chlorella pyrenoidosa*. *Bioresour. Bioprocess.* **2016**, *3*, doi:10.1186/s40643-016-0094-8.

145. Lafarga, T. Effect of microalgal biomass incorporation into foods: Nutritional and sensorial attributes of the end products. *Algal Res.* **2019**, *41*, 101566, doi:10.1016/j.algal.2019.101566.

146. Schüler, L.; Greque de Morais, E.; Trovão, M.; Machado, A.; Carvalho, B.; Carneiro, M.; Maia, I.; Soares, M.; Duarte, P.; Barros, A.; et al. Isolation and Characterization of Novel *Chlorella vulgaris* Mutants With Low Chlorophyll and Improved Protein Contents for Food Applications. *Front. Bioeng. Biotechnol.* **2020**, *8*, 1–10, doi:10.3389/fbioe.2020.00469.

147. Qazi, W.M.; Ballance, S.; Uhlen, A.K.; Kousoulaki, K.; Haugen, J.E.; Rieder, A. Protein enrichment of wheat bread with the marine green microalgae *Tetraselmis chuii* – Impact on dough rheology and bread quality. *Lwt* **2021**, *143*, 111115, doi:10.1016/j.lwt.2021.111115.

148. Niggli, V. Structural properties of lipid-binding sites in cytoskeletal proteins. *Trends Biochem. Sci.* **2001**, *26*, 604–611, doi:10.1016/S0968-0004(01)01927-2.

149. Gong, Y.; Guo, X.; Wan, X.; Liang, Z.; Jiang, M. Triacylglycerol accumulation and change in fatty acid content of four marine oleaginous microalgae under nutrient limitation and at different culture ages. *J. Basic Microbiol.* **2013**, *53*, 29–36, doi:10.1002/jobm.201100487.

150. Gerardo, M.L.; Oatley-Radcliffe, D.L.; Lovitt, R.W. Integration of membrane technology in microalgae biorefineries. *J. Memb. Sci.* **2014**, *464*, 86–99, doi:10.1016/j.memsci.2014.04.010.

151. Crespo, J.G.; Brazinha, C. Membrane processing: Natural antioxidants from winemaking by-products. *Filtr. Sep.* **2010**, *47*, 32–35, doi:10.1016/S0015-1882(10)70079-3.

152. Ursu, A.V.; Marcati, A.; Sayd, T.; Sante-Lhoutellier, V.; Djelveh, G.; Michaud, P. Extraction, fractionation and functional properties of proteins from the microalgae *Chlorella vulgaris*. *Bioresour. Technol.* **2014**, *157*, 134–139, doi:10.1016/j.biortech.2014.01.071.

153. Field, R.W.; Wu, D.; Howell, J.A.; Gupta, B.B. Critical flux concept for microfiltration fouling. *J. Memb. Sci.* **1995**, *100*, 259–272, doi:10.1016/0376-7388(94)00265-Z.

154. Miller, D.J.; Kasemset, S.; Paul, D.R.; Freeman, B.D. Comparison of membrane fouling at constant flux and constant transmembrane pressure conditions. *J. Memb. Sci.* **2014**, *454*, 505–515, doi:10.1016/j.memsci.2013.12.027.

155. Monte, J.; Bernardo, J.; Sá, M.; Parreira, C.; Galinha, C.F.; Costa, L.; Casanovas, C.; Brazinha, C.; Crespo, J.G. Development of an integrated process of membrane filtration for harvesting carotenoid-rich *Dunaliella salina* at laboratory and pilot scales. *Sep. Purif. Technol.* **2020**, *233*, 116021, doi:10.1016/j.seppur.2019.116021.

156. Serra, M.; Weng, V.; Coelhoso, I.M.; Alves, V.D.; Brazinha, C. Purification of arabinoxylans from corn fiber and preparation of bioactive films for food packaging. *Membranes (Basel).* **2020**, *10*, 1–22, doi:10.3390/membranes10050095.

157. Teuling, E.; Wierenga, P.A.; Schrama, J.W.; Gruppen, H. Comparison of Protein Extracts from Various Unicellular Green Sources. *J. Agric. Food Chem.* **2017**, *65*, 7989–8002, doi:10.1021/acs.jafc.7b01788.

158. Cheryan, M. *Ultrafiltration and Microfiltration Handbook*; 2nd ed.; CRC Press: USA, 1998; ISBN 1566765986.

159. Tian, J. yu; Chen, Z. lin; Yang, Y. ling; Liang, H.; Nan, J.; Li, G. bai Consecutive chemical cleaning of fouled PVC membrane using NaOH and ethanol during ultrafiltration of river water. *Water Res.* **2010**, *44*, 59–68, doi:10.1016/J.WATRES.2009.08.053.

160. Walker, J.M. The bicinchoninic acid (BCA) assay for protein quantitation. *Walk. J.M. (eds)The*

Protein Protoc. Handb. **2009**, *32*, 5–8, doi:10.1385/0-89603-268-x:5.

161. Gomes, D. Extraction and characterization of microalgae proteins from the extremophile *Dunaliella*, Master Thesis, Instituto Superior Técnico, 2017.

162. Ritchie, R.J. Consistent sets of spectrophotometric chlorophyll equations for acetone , methanol and ethanol solvents. *Photosynth Res* **2006**, *89*, 27–41, doi:10.1007/s11120-006-9065-9.

163. Bogatcheva, N. V.; Machado, R.F. *Cytoskeletal Proteins*; 2nd ed.; Elsevier Inc., 2020; ISBN 9780128012383.

164. Crespo, J.P.S.G.; Trotin, M.; Hough, D.; Howell, J.A. Use of fluorescence labelling to monitor protein fractionation by ultrafiltration under controlled permeate flux. *J. Memb. Sci.* **1999**, *155*, 209–230, doi:10.1016/S0376-7388(98)00309-3.

165. Miller, D.J.; Paul, D.R.; Freeman, B.D. A crossflow filtration system for constant permeate flux membrane fouling characterization. *Rev. Sci. Instrum.* **2013**, *84*, doi:10.1063/1.4794909.

166. Balti, R.; Zayoud, N.; Hubert, F.; Beaulieu, L.; Massé, A. Fractionation of *Arthrospira platensis* (Spirulina) water soluble proteins by membrane diafiltration. *Sep. Purif. Technol.* **2021**, *256*, doi:10.1016/j.seppur.2020.117756.

167. Gifuni, I.; Lavenant, L.; Pruvost, J.; Masse, A. Recovery of microalgal protein by three-steps membrane filtration: Advancements and feasibility. *Algal Res.* **2020**, *51*, 102082, doi:10.1016/j.algal.2020.102082.

168. Vyas, H.K.; Bennett, R.J.; Marshall, A.D. Performance of crossflow microfiltration during constant transmembrane pressure and constant flux operations. *Int. Dairy J.* **2002**, *12*, 473–479, doi:10.1016/S0958-6946(02)00020-1.

169. Ryckebosch, E.; Bruneel, C.; Muylaert, K.; Foubert, I. Microalgae as an alternative source of omega-3 long chain polyunsaturated fatty acids. *Lipid Technol.* **2012**, *24*, 128–130, doi:10.1002/lite.201200197.

170. Khozin-Goldberg, I.; Iskandarov, U.; Cohen, Z. LC-PUFA from photosynthetic microalgae: Occurrence, biosynthesis, and prospects in biotechnology. *Appl. Microbiol. Biotechnol.* **2011**, *91*, 905–915, doi:10.1007/s00253-011-3441-x.

171. Meyer, B.J. Are we consuming enough long chain omega-3 polyunsaturated fatty acids for optimal health *Prostaglandins Leukot. Essent. Fat. Acids* **2011**, *85*, 275–280, doi:10.1016/j.plefa.2011.04.010.

172. Udayan, A.; Arumugam, M.; Pandey, A. Nutraceuticals From Algae and Cyanobacteria. *Algal Green Chem. Recent Prog. Biotechnol.* **2017**, 65–89, doi:10.1016/B978-0-444-63784-0.00004-7.

173. Li, Y.; Ghasemi Naghdi, F.; Garg, S.; Adarme-Vega, T.C.; Thurecht, K.J.; Ghafor, W.A.; Tannock, S.; Schenk, P.M. A comparative study: The impact of different lipid extraction methods on current microalgal lipid research. *Microb. Cell Fact.* **2014**, *13*, 1–9, doi:10.1186/1475-2859-13-14.

174. Bligh, E.G. and Dyer, W.J. A rapid method of total lipid extraction and purification. *Can. J. Biochem. Physiol.* **1959**, *37*.

175. Folch, J.; Lees, M.; Sloane Stanley, G.H. A simple method for the isolation and purification of total lipides from animal tissues. *J. Biol. Chem.* **1957**, *226*, 497–509, doi:10.1016/s0021-9258(18)64849-5.

176. Yao, L.; Gerde, J.A.; Lee, S.L.; Wang, T.; Harrata, K.A. Microalgae lipid characterization. *J. Agric. Food Chem.* **2015**, *63*, 1773–1787, doi:10.1021/jf5050603.

177. Molina-Grima, E.; González, J.I.; Giménez, A.G. Solvent extraction for micoalgae lipids. In *Algae for Biofuels and Energy*; Borowitzka, M.A., Moheimani, N.R., Eds.; Springer, 2013.

178. Abimbola, T.; Christodoulatos, C.; Lawal, A. Performance and optimization studies of oil extraction from *Nannochloropsis* spp. and *Scenedesmus obliquus*. *J. Clean. Prod.* **2021**, *311*, 127295, doi:10.1016/j.jclepro.2021.127295.

179. Lardon, L.; Hélias, A.; Sialve, B.; Steyer, J.P.; Bernard, O. Life-cycle assessment of biodiesel production from microalgae. *Environ. Sci. Technol.* **2009**, *43*, 6475–6481, doi:10.1021/es900705j.

180. Kwak, M.; Kim, D.; Kim, S.; Lee, H.; Chang, Y.K. Solvent screening and process optimization for high shear-assisted lipid extraction from wet cake of *Nannochloropsis sp.*; Elsevier Ltd, 2020; Vol. 149; ISBN 8242350884.

181. Yang, F.; Cheng, C.; Long, L.; Hu, Q.; Jia, Q.; Wu, H.; Xiang, W. Extracting lipids from several species of wet microalgae using ethanol at room temperature. *Energy and Fuels* **2015**, *29*, 2380–2386, doi:10.1021/ef5023576.

182. Balasubramanian, R.K.; Yen Doan, T.T.; Obbard, J.P. Factors affecting cellular lipid extraction from marine microalgae. *Chem. Eng. J.* **2013**, *215–216*, 929–936, doi:10.1016/j.cej.2012.11.063.

183. Ryckebosch, E.; Bermúdez, S.P.C.; Termote-Verhalle, R.; Bruneel, C.; Muylaert, K.; Parra-

Saldivar, R.; Foubert, I. Influence of extraction solvent system on the extractability of lipid components from the biomass of *Nannochloropsis gaditana*. *J. Appl. Phycol.* **2014**, *26*, 1501–1510, doi:10.1007/s10811-013-0189-y.

184. Jiménez Callejón, M.J.; Robles Medina, A.; Macías Sánchez, M.D.; Esteban Cerdán, L.; González Moreno, P.A.; Navarro López, E.; Hita Peña, E.; Grima, E.M. Obtaining highly pure EPA-rich lipids from dry and wet *Nannochloropsis gaditana* microalgal biomass using ethanol, hexane and acetone. *Algal Res.* **2020**, *45*, 101729, doi:10.1016/j.algal.2019.101729.

185. Christaki, E.; Bonos, E.; Giannenasa, I.; Florou-Paneria, P. Functional properties of carotenoids originating from algae. *J. Sci. Food Agric.* **2013**, *93*, 5–11, doi:10.1002/jsfa.5902.

186. Tribe, M.A. Scale Economies and the "0.6 rule." **1986**, *10*, 271–278.

187. Wieringa, E. Financial feasibility of using an electric steam boiler in a multifuel steam production set and providing grid flexibility, Master Thesis, Eindhoven University of Technology, 2015.

188. Spruijt, J.; Schipperus, R.; Kootstra, M.; de Visser, C. *Algae Economics: bio-economic production models of micro-algae and downstream processing to produce bio energy carriers, Public Output report of the EnAlgae project*; 2015;

189. Ferreira, A.; Gouveia, L. *Handbook of Microalgae-Based Processes and Products, Microalgal biorefineries*; Elsevier Inc.: Lisboa, 2020; ISBN 9780128185360.

190. Karemore, A.; Sen, R. Downstream processing of microalgal feedstock for lipid and carbohydrate in a biorefinery concept: a holistic approach for biofuel applications†. *RSC Adv.* **2016**, *6*, 29486–29496, doi:10.1039/c6ra01477a.

191. Chew, K.W.; Yap, J.Y.; Show, P.L.; Suan, N.H.; Juan, J.C.; Ling, T.C.; Lee, D.-J.; Chang, J.-S. Microalgae biorefinery: High value products perspectives. *Bioresour. Technol.* **2017**, *229*, 53–62, doi:10.1016/j.biortech.2017.01.006.

192. Nobre, B.P.; Villalobos, F.; Barragán, B.E.; Oliveira, A.C.; Batista, A.P.; Marques, P.A.S.S.; Mendes, R.L.; Sovová, H.; Palavra, A.F.; Gouveia, L. A biorefinery from *Nannochloropsis* sp. microalga - Extraction of oils and pigments. Production of biohydrogen from the leftover biomass. *Bioresour. Technol.* **2013**, *135*, 128–136, doi:10.1016/j.biortech.2012.11.084.

193. Bongiovani, N.; Popovich, C.A.; Martínez, A.M.; Constenla, D.; Leonardi, P.I. Biorefinery Approach from *Nannochloropsis oceanica* CCALA 978: Neutral Lipid and Carotenoid Co-Production Under Nitrate or Phosphate Deprivation. *Bioenergy Res.* **2020**, *13*, 518–529, doi:10.1007/s12155-019-10045-2.

194. Cui, Y.; Thomas-Hall, S.R.; Chua, E.T.; Schenk, P.M. Development of a *Phaeodactylum tricornutum* biorefinery to sustainably produce omega-3 fatty acids and protein. *J. Clean. Prod.* **2021**, *300*, 126839, doi:10.1016/j.jclepro.2021.126839.

195. Wood, L. Outlook on the Nannochloropsis Global Market to 2028 Available online: https://www.globenewswire.com/news-release/2022/01/18/2368121/28124/en/Outlook-on-the-*Nannochloropsis*-Global-Market-to-2028-Featuring-Reed-Mariculture-Lyxia-and-BlueBioTech-Among-Others.html (accessed on Mar 3, 2022).

196. Wood, L. Global *Nannochloropsis*-derived Lipids Market Research Report 2021 Available online: https://www.prnewswire.com/news-releases/global-*Nannochloropsis*-derived-lipids-market-research-report-2021-301459637.html (accessed on Mar 3, 2022).

197. Chouhan, N.; Vig, H.; Deshmukh, R. Fish Oil Market Size, Share and Industry Analysis Report, 2021-2027 Available online: https://www.alliedmarketresearch.com/fish-oil-market (accessed on Mar 4, 2022).

198. Kent, M.; Welladsen, H.M.; Mangott, A.; Li, Y. Nutritional evaluation of Australian microalgae as potential human health supplements. *PLoS One* **2015**, *10*, 1–14, doi:10.1371/journal.pone.0118985.

199. Paes, C.R.P.S.; Faria, G.R.; Tinoco, N.A.B.; Castro, D.J.F.A.; Barbarino, E.; Lourenço, S.O. Growth, nutrient uptake and chemical composition of *Chlorella* sp. and *Nannochloropsis oculata* under nitrogen starvation. *Lat. Am. J. Aquat. Res.* **2016**, *44*, 275–292, doi:10.3856/vol44-issue2-fulltext-9.

200. Schade, S.; Meier, T. Distinct microalgae species for food—part 1: a methodological (top-down) approach for the life cycle assessment of microalgae cultivation in tubular photobioreactors. *J. Appl. Phycol.* **2020**, *32*, 2977–2995, doi:10.1007/s10811-020-02177-2.

201. Fábregas, J.; Maseda, A.; Domínguez, A.; Otero, A. The cell composition of *Nannochloropsis* sp. changes under different irradiances in semicontinuous culture. *World J. Microbiol. Biotechnol.* **2004**, *20*, 31–35, doi:10.1023/B:WIBI.0000013288.67536.ed.

202. QYResearch Group Global Hydrolyzed Vegetable Protein Market Research Report 2021 Available online: https://www.marketresearch.com/QYResearch-Group-v3531/Global-Hydrolyzed-Vegetable-Protein-Research-30544723/ (accessed on Mar 4, 2022).

203. The Insight Partners Fishmeal Market to 2028 – Global Analysis and Forecast Available online: https://www.prnewswire.com/news-releases/fishmeal-market-to-reach-15-264-6--million-

globally-by-2028-at-8-3-cagr-the-insight-partners-301429022.html (accessed on Mar 4, 2022).

204. Khanra, S.; Mondal, M.; Halder, G.; Tiwari, O.N.; Gayen, K.; Bhowmick, T.K. Downstream processing of microalgae for pigments, protein and carbohydrate in industrial application: A review. *Food Bioprod. Process.* **2018**, *110*, 60–84, doi:10.1016/j.fbp.2018.02.002.

205. Topuz, O.K.; Kaya, A.; Alp, A.C. Effect of extraction variables on the omega-3 eicosapentaenoic acid (EPA) content of (*Nannochloropsis oculata*) microalga oil. *Sci. Bull. Ser. F. Biotechnol.* **2016**, *XX*, 172–177.

206. Ruiz, J.; Olivieri, G.; De Vree, J.; Bosma, R.; Willems, P.; Reith, J.H.; Eppink, M.H.M.; Kleinegris, D.M.M.; Wijffels, R.H.; Barbosa, M.J. Towards industrial products from microalgae. *Energy Environ. Sci.* **2016**, *9*, 3036–3043, doi:10.1039/c6ee01493c.

207. Branco-Vieira, M.; Mata, T.M.; Martins, A.A.; Freitas, M.A.V.; Caetano, N.S. Economic analysis of microalgae biodiesel production in a small-scale facility. *Energy Reports* **2020**, *6*, 325–332, doi:10.1016/j.egyr.2020.11.156.

208. Biondi, N.; Fonseca, D.; Sampietro, G.; Santos, E.; Costa, L.; Verdelho, V.; Carlini, D.; Mangini, S.; Bassi, N.; Rodolfi, L.; et al. BIOFAT: Cultivation of *Nannochloropsis oceanica* F&M M24 and *Tetraselmis suecica* F&M M33 in the two 0.5 ha BIOFAT Pilot Plants for biofuel production. In Proceedings of the Algae Europe 2016 Madrid, December 2016; 2016.

209. Slegers, P.M.; Olivieri, G.; Breitmayer, E.; Sijtsma, L.; Eppink, M.H.M.; Wijffels, R.H.; Reith, J.H. Design of Value Chains for Microalgal Biorefinery at Industrial Scale: Process Integration and Techno-Economic Analysis. *Front. Bioeng. Biotechnol.* **2020**, *8*, 1–17, doi:10.3389/fbioe.2020.550758.

210. Borowitzka, M.A. High-value products from microalgae-their development and commercialisation. *J. Appl. Phycol.* **2013**, *25*, 743–756, doi:10.1007/s10811-013-9983-9.

211. van der Voort, M.P.J.; Spruijt, J.; Potters, J.; de Wolf, P.L.; Elissen, H.J.H. Socio-economic assessment of Algae-based PUFA production. *Public Output Rep. PUFAChain Proj.* **2017**, 79.

212. Kaluzny, M.A.; Duncan, L.A.; Merritt, M. V.; Epps, D.E. Rapid separation of lipid classes in high yield and purity using bonded phase columns. *J. Lipid Res.* **1985**, *26*, 135–140, doi:10.1016/s0022-2275(20)34412-6.

213. Kim, H.Y.; Salem, N. Separation of lipid classes by solid phase extraction. *J. Lipid Res.* **1990**, *31*, 2285–2289, doi:10.1016/s0022-2275(20)42116-9.

214. Waibel, B.J.; Schonemann, H.; Krukonis, V.; Kagan, M. Eicosapentaenoic Acid (EPA)

Formulations 2017, *2*.

215. Zaripheh, S.; Erdman, J.W. Factors That Influence the Bioavailablity of Xanthophylls. *J. Nutr.* **2002**, 531–534.

216. Bosner, M.S.; Gulick, T.; Riley, D.J.S.; Spilburg, C.A.; Lange, L.G. Receptor-like function of heparin in the binding and uptake of neutral lipids. *Proc. Natl. Acad. Sci. U. S. A.* **1988**, *85*, 7438–7442, doi:10.1073/pnas.85.20.7438.

217. Wileman, A.; Ozkan, A.; Berberoglu, H. Rheological properties of algae slurries for minimizing harvesting energy requirements in biofuel production. *Bioresour. Technol.* **2012**, *104*, 432–439, doi:10.1016/j.biortech.2011.11.027.

218. PORDATA Electricity prices for domestic and industrial users (Euro/ECU) Available online: https://www.pordata.pt (accessed on Nov 15, 2021).

219. Market Research Engine Liquid Nitrogen Price Market Executive Data Report Available online: https://www.marketresearchengine.com/liquid-nitrogen-price-market (accessed on Nov 17, 2021).

220. Markets Insider Ethanol Price Available online: https://markets.businessinsider.com/commodities/ethanol-price/euro (accessed on Nov 16, 2021).

221. Carl Roth Tween-80 Price Available online: https://www.carlroth.com/com/en/detergents/tween-80 (accessed on Nov 16, 2021).

222. Ecolabel Partnership & Virebit Ltd *Overview of a selection of facilities for treatment and destruction of organic hazardous waste in the Barents and Baltic Sea region countries Environment*; 2013;

APPENDIX

A. Supplementary Material for the Biomass Stabilisation through heat treatment (Chapter 2)

A.1. Lipid fractionation through solid-phase extraction additional information

A.1.1. Introduction

Solid-phase extraction (SPE) is a relevant technique used to separate different classes of lipids, usually after total lipid extraction. It is a useful and rapid method for lipid isolation with a high yield and purity. Based on a chromatographic method sequencing, this technique includes creating selectivity in the isolation of compounds from a mixture by successively shifting either the solid phase support, the solvent, or both. In a biphasic solid/ support solvent system, a unique interaction exists between the compound to be isolated and the functional group of the solid phase. Therefore, by varying the solvent polarity, around the solid phase, or by changing the solid phase itself, compounds (in this case lipids) can be selectively isolated with a high degree of purity and recovery, maintaining throughout the process the integrity of the original lipid composition profile [212,213]

A.1.2. Materials and Methods

A.1.2.1. Material

For analytical procedures IWI® (EPA omega-3) capsules were obtained from IWI® (Houston, United States), Sep-Pak Silica Plus Long Cartridges (690 mg) were purchased from Waters (Massachusetts, United States), acetone 99.0% and methanol, 99.8% were obtained from JMGS (Odivelas, Portugal), chloroform and diethyl ether were obtained from Honeywell/ Riedel-de Haën (Seelze, Germany), n-hexane 99.0% was purchased from VWR Chemicals BDH® (Poole, United Kingdom), acetyl chloride 98% and 2,6-Di-tert-butyl-4-methylphenol (BHT) were obtained from Alfa Aesar (Karlsruhe, Germany), petroleum ether 60-80 ºC was purchased from Fisher Scientific (Leicestershire, United Kingdom), and the internal standard C17:0 was obtained from Dr. Ehrenstorfer GmbH (Augsburg, Germany).

A.1.2.2. Method development and validation

In this work, a methodology to fractionate lipids mixtures into two distinct fractions was tested and validated. In the first part of the experiment, a methodology to fractionate the lipids into a neutral lipid fraction and a polar lipid fraction was tested and validated. The second part of the experiments intends to evaluate the placement of the FFA fraction in both fractions: neutral lipids or polar lipids. Previous works demonstrated the difficulty to separate the free fatty acid fraction from the neutral lipid fraction (data not shown), therefore, a new approach to the fractionation assay was tested.

Lipid fractionation into NL fraction and PL fraction

In the first part of this experiment, the methodology proposed by Breuer *et al.* [109] and León-Saiki *et al.* [110] was performed and tested with the following modifications. The lipids present in the IWI® (EPA omega-3) capsule were washed with 20 mL of hexane. Hexane was evaporated under a N_2 stream and the lipid extract was dissolved in hexane: diethyl ether (7:1 v/v) in order to obtain a concentration of 25 ± 5 mg. mL^{-1}. The lipid extract was separated into neutral and polar lipids using a Sep-Pak Silica Plus Long Cartridge (690 mg, Waters). The silica cartridge was prewashed with 10 mL of hexane before loading the sample onto the column. The neutral lipid fraction was eluted with 7 mL of hexane: diethyl ether (7:1 v/v). The polar lipid fraction was eluted with 7 mL of methanol: acetone: diethyl ether (2:2:1 v/v/v). Both extracts were evaporated under a N_2 stream and then weighed in the analytical balance (Kern, ABJ 220, Kern, Germany). Afterwards, both extracts were submitted to transesterification and the fatty acids were quantified using gas chromatography (GC). The gas chromatography required for the analysis was performed by an external supplier. The pigment content of the IWI® (EPA omega-3) capsule was also analysed.

Table A.1. IWI® (EPA omega-3) capsule composition. Adapted from [214]

Free fatty acids (% w/w)	30.0%
Polar Lipids (% w/w)	31.0%
Neutral Lipids (% w/w)	15.0%
Chlorophyll *a* (% w/w)	11.0%
Others (% w/w)	10.0%
Sterols (% w/w)	2.0%
Carotenoids (% w/w)	1.0%

Lipid fractionation into NL + FFA fraction and PL fraction

In the second part of this experiment, and to test and validate the hypothesis proposed - fractionate the lipid fraction into a neutral lipid plus free fatty acids fraction, and a polar lipids fraction - a spiked sample was prepared. The lipids present in a new IWI® (EPA omega-3) capsule were washed with 20 mL of hexane. Hexane was evaporated under a N_2 stream and the lipid extract was dissolved in hexane: diethyl ether (7:1 v/v) in order to obtain a concentration of 5 ± 5 mg. mL^{-1}. Then, a known mass (20 mg) of a free fatty acid, palmitic acid (C16:0) was added to the previously prepared sample. The lipid extract was separated into a neutral lipid plus FFA fraction, and a polar lipids fraction using a Sep-Pak Silica Plus Long Cartridge (690 mg, Waters). The silica cartridge was prewashed with 10 mL of hexane before loading the sample onto the column. The neutral lipid fraction was eluted with 7 mL of hexane: diethyl ether (7:1 v/v). The polar lipid fraction was eluted with 7 mL of methanol: acetone: diethyl ether (2:2:1 v/v/v). Both extracts were evaporated under a N_2 stream and then weighed in the analytical balance (Kern, ABJ 220, Kern, Germany). Afterwards, both extracts were submitted to transesterification and the fatty acids were quantified using gas chromatography (GC). The gas chromatography required for the analysis was performed by an external supplier. The pigment content of the IWI® (EPA omega-3) capsule was also analysed.

A.1.2.3. Total fatty acids transesterification

The total fatty transesterification was carried out on samples before and after the lipid fractionation process. Before total fatty acids transesterification, a known volume of the lipid extract sample (3-4 mL) was evaporated in a glass tube (12 mL) under a N_2 stream. The glass tube (12 mL) with the dried lipid fraction was strictly weighed (Kern, ABJ 220, Kern, Germany), and the weight of the empty glass tube was subtracted. The lipid fraction previously obtained was mixed with 200 µL of internal standard C17:0 (standard heptadecanoic acid dissolved in petroleum ether 60-80 ºC with a concentration of 5 mg. mL^{-1}) before transesterification reaction. Finally, 4 mL of acetyl chloride/methanol solution with a 5:100 ratio (prepared with previously cold methanol) was added to the tube and vortexed. The mixture was heated at 100 ºC for 1 hour in a water bath to conduct a transesterification reaction. The samples were thoroughly mixed during heating. The reaction tube was slowly cooled down to room temperature. Then, 2 mL of n-hexane was added to the tubes and mixed through a vortex stirrer. To aid in phase separation, 2 mL of distilled water was added to the mixture and after centrifugation (for 3 min at 2,500 x g) the n-hexane layer that contained fatty acids methyl esters were collected and transferred to a glass vial passing through a cotton filter filled with sodium sulphate to prevent moisture and impurities. The gas chromatography (GC) required for the analysis was performed by an external supplier.

A.1.3. Results and Discussion

A.1.3.1. Lipid fractionation into NL fraction and PL fraction

The results of the fractionation of the lipids present in the IWI® (EPA omega-3) capsule through SPE are presented in **Table A.**2**.** The results obtained from the fractionation methodology are quite in agreement with the composition of the commercial capsule (**Table A.**1). The IWI® (EPA omega-3) supplier claims that the polar lipid fraction represents 31.0% (% w/w) of the product, however, the chlorophyll (11.0% w/w) is slightly more polar than carotenoids and it is eluted by more polar solvents. Therefore, the total polar fraction of the IWI® (EPA omega-3) might be 42.0% (% w/w), which is quite similar to the result obtained through the SPE fractionation (43.6% w/w). On the other hand, the IWI® (EPA omega-3) supplier claims that the neutral lipid fraction represents 15.0% (% w/w) of the product, however, FFA (30.0% w/w), carotenoids (1.0% w/w) [215], and sterols (2.0% w/w) are considered non polar compounds [216]. Therefore, the neutral fraction of the IWI® (EPA omega-3) may represent 48% (% w/w). The fractionation methodology result was 59.0% (% w/w) for the neutral lipid fraction, which seems somehow different from the value presented by the supplier. Though, the IWI® (EPA omega-3) capsule has also 10.0% (w/w) of other compounds, which might also exhibit non-polar properties. Also, the supplier claims that the IWI® (EPA omega-3) capsule has 11.0% (% w/w) of chlorophyll, however, the pigment analysis revealed that the sample no longer had chlorophyll in its composition, only the chlorophyll degradation products – pheophytin *a* equivalents (10.0% w/w). The chlorophyll might have degraded during the storage in the bottle, where the capsules were. was perfectly sealed before the experiments.

The fractionation of the IWI® (EPA omega-3) sample into a neutral fraction and a polar fraction through the methodology proposed by Breuer *et al.* [109] and León-Saiki *et al.* [110] was successfully validated.

Table A.2 Original IWI® sample fractionation into neutral lipid fraction and polar lipid fraction. Composition of the two distinct fractions (% w/w)

Neutral lipid fraction (% w/w)	**59.0%**
Neutral lipids (% w/w)	58.7%
Carotenoids (% w/w)	0.3%
Polar lipid fraction (% w/w)	**43.6%**
Polar lipids (% w/w)	33.6%
Pheophytin *a* equivalents (% w/w)	10.0%

After the lipid fraction into neutral lipids and polar lipids, the fatty acid profile of both fractions was performed through transesterification and GC analysis. The results are presented in **Table A.**3. The neutral lipid fraction possesses the majority (60%) of the total fatty acids present in the IWI® (EPA omega-3) sample. This result might indicate that the free fatty acids present in the sample were eluted onto the neutral lipid fraction as the FFA have non-polar characteristics [216]. Also, the EPA omega-3 was mainly eluted into the polar lipid fraction, as expected, since PUFAs are mainly present in the membrane lipids fraction.

Table A.3. Fatty acid profile of the fractionated original IWI® sample. The results are presented in mg of fatty acid and, they are based on 2 replicates for each sample fatty acid analysis.

Fatty Acid	Total lipid fraction (mg)	Neutral fraction (mg)	Polar fraction (mg)
C14:0	0.73 ± 0.08	0.56 ± 0.06	0.17 ± 0.02
C16:0	2.17 ± 0.11	1.57 ± 0.07	0.60 ± 0.04
C18:0	0.35 ± 0.03	0.35 ± 0.02	0.00 ± 0.00
ΣSFAs	**3.26 ± 0.21**	**2.49 ± 0.15**	**0.77 ± 0.06**
C16:1	1.89 ± 0.13	1.06 ± 0.08	0.83 ± 0.05
C18:1	0.67 ± 0.05	0.37 ± 0.01	0.30 ± 0.04
ΣMUFAs	**2.56 ± 0.18**	**1.43 ± 0.09**	**1.13 ± 0.09**
C18:2n6	0.37 ± 0.04	0.19 ± 0.01	0.18 ± 0.03
C18:3	0.10 ± 0.00	0.05 ± 0.00	0.05 ± 0.00
C20:4n6	0.64 ± 0.04	0.30 ± 0.02	0.34 ± 0.02
C20:5n3	3.58 ± 0.61	1.17 ± 0.06	2.40 ± 0.55
C22:5	0.28 ± 0.01	0.28 ± 0.01	0.00 ± 0.00
C22:6n3	1.55 ± 0.06	1.47 ± 0.03	0.08 ± 0.03
ΣPUFAs	**6.52 ± 0.76**	**3.47 ± 0.13**	**3.04 ± 0.63**
Total FA	**12.33 ± 1.15**	**7.39 ± 0.37**	**4.94 ± 0.78**

A.1.3.2. Lipid fractionation into NL + FFA fraction and PL fraction

The fractionation of the IWI® (EPA omega-3) sample into a neutral fraction and a polar fraction through the methodology proposed by Breuer *et al.* [109] and León-Saiki *et al.* [110] was successfully validated in the previous subchapter.

In the second part of this experiment, the fractionation of a spiked sample was performed to assess in which fraction the free fatty acids will be eluted. To test and validate the hypothesis proposed a spiked sample was prepared by adding 20 mg of palmitic acid (C16:0). The fatty acid profiles of both the original IWI® sample and the spiked IWI® sample are exhibited in **Table A.**4. The results revealed that 91% of the palmitic acid added to the sample was eluted into the neutral lipid fraction. The overlapping

in the polar lipid fraction was less than 10%. Therefore, it is possible to conclude that the free fatty acids are eluted along with the neutral lipids into the neutral lipid fraction.

Table A.4. Fatty acid profile of the fractionated original IWI® sample and the fractionated spiked IWI® sample. The results are presented in mg of fatty acid and, they are based on 2 replicates for each sample fatty acid analysis. *The spiked sample was prepared by adding 20 mg of palmitic acid (C16:0)

Fatty Acid	Original IWI® sample		Spiked IWI® sample*	
	Neutral fraction (mg)	Polar fraction (mg)	Neutral fraction (mg)	Polar fraction (mg)
C14:0	0.18 ± 0.04	0.05 ± 0.01	0.22 ± 0.03	0.05 ± 0.01
C16:0	**0.39 ± 0.03**	**0.15 ± 0.01**	**17.74 ± 0.05**	**1.84** ± 0.02
C18:0	0.11 ± 0.03	0.00 ± 0.00	0.14 ± 0.01	0.00 ± 0.00
ΣSFAs	**0.68 ± 0.10**	**0.20 ± 0.02**	**18.10 ± 0.09**	**1.89 ± 0.03**
C16:1	0.35 ± 0.08	0.21 ± 0.00	0.43 ± 0.05	0.21 ± 0.00
C18:1	0.11 ± 0.02	0.08 ± 0.01	0.13 ± 0.01	0.10 ± 0.01
ΣMUFAs	**0.46 ± 0.10**	**0.30 ± 0.01**	**0.56 ± 0.06**	**0.31 ± 0.01**
C18:2n6	0.07 ± 0.02	0.04 ± 0.00	0.08 ± 0.01	0.04 ± 0.01
C18:3	0.02 ± 0.01	0.01 ± 0.01	0.04 ± 0.01	0.00 ± 0.00
C20:4n6	0.11 ± 0.03	0.07 ± 0.01	0.14 ± 0.02	0.06 ± 0.01
C20:5n3	0.47 ± 0.18	0.55 ± 0.05	0.65 ± 0.10	0.50 ± 0.05
C22:5	0.08 ± 0.01	0.00 ± 0.00	0.08 ± 0.01	0.00 ± 0.00
C22:6n3	0.43 ± 0.06	0.01 ± 0.01	0.48 ± 0.04	0.00 ± 0.00
ΣPUFAs	**1.17 ± 0.31**	**0.68 ± 0.08**	**1.47 ± 0.50**	**0.60 ± 0.07**
Total FA	**2.32 ± 0.51**	**1.17 ± 0.11**	**20.13 ± 0.65**	**2.80 ± 0.11**

A.1.4. Conclusions

A methodology to fractionate lipids mixtures into two distinct fractions was tested and validated. In the first part of the experiment, the fractionation of the IWI® (EPA omega-3) sample into a neutral fraction and a polar fraction through the methodology proposed by Breuer *et al.* [109] and León-Saiki *et al.* [110] was successfully validated. The second part of the experiment evidenced that the free fatty acids are eluted along with the neutral lipids into the neutral lipid fraction when the methodology proposed by Breuer *et al.* [109] and León-Saiki *et al.* [110] is applied.

B. Supplementary Material for the *Nannochloropsis* sp. biorefinery: process design and techno-economic assessment (Chapter 6)

B.1. Process design and mass balance

B.1.1. Phase separation: centrifuge (cell debris/ aqueous fraction separation)

After the cellular disruption, a centrifugation step is required. This centrifugation step is used to separate the solid phase (cell debris) from the aqueous phase containing soluble proteins. This step also avoids a high membrane fouling in the subsequent ultrafiltration step. The input stream contains whole cells, disrupted cells, and the water–soluble intracellular components (released during cell disruption). It was assumed that the whole cells and the disrupted cells (containing membrane lipids, insoluble proteins, and other components) transfer during centrifugation to the solid phase. According to Slegers *et al.* [209], the critical size and density of cell debris to be separated should be set to 0.5 µm and 1500 $kg.m^{-3}$, respectively. The liquid viscosity was fixed at 4 cP based on an algae mixture at 10%$_{DW}$, according to the literature [217]. The typical electricity consumption was calculated automatically in SuperPro Designer®.

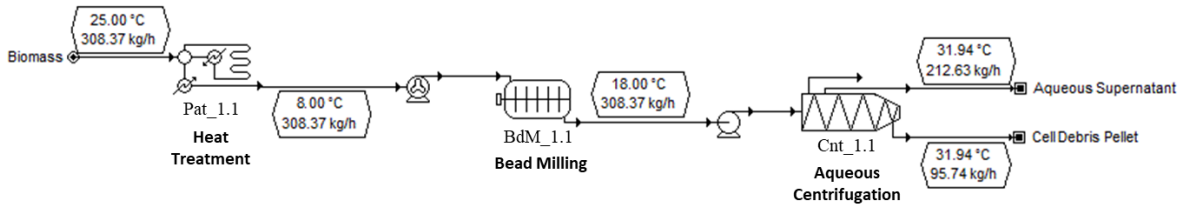

Figure B.1. Pre-treatment flow chart and streams characterisation using SuperPro Designer®.

B.1.2. Ultrafiltration/ Diafiltration

After the first ultrafiltration step, performed as reported in **Chapter 4**, a second ultrafiltration step was performed, aimed at purifying the soluble protein present in the permeate resulting from the first step of the membrane processing.

Tests were performed at a pilot scale using a ceramic membrane (Inopor®, Germany) with a molecular weight cut-off of 1 kDa. The membrane was composed of 19 channels, with a total filtration area of 0.251 m^2. Briefly, 5 L of soluble protein aqueous fraction (2.6 $g.L^{-1}$ soluble protein) were fed to the

membrane system. The ultrafiltration was performed in a concentration mode followed by diafiltration under controlled transmembrane pressure conditions (TMP 1.10 ± 0.11 bar). The volumetric flux during the experiment was 26.03 ± 5.18 $L.m^{-2}.h^{-1}$ (**Figure B.2**), the concentration factor was CF=2.5, and the membrane was capable to retain nearly 90% of the soluble protein present in the feed (**Table B.1**). Also, it was possible to remove 88% of salt present in the feed after four diafiltration volumes (**Figure B.3**). The typical electricity consumption was calculated automatically in SuperPro Designer®.

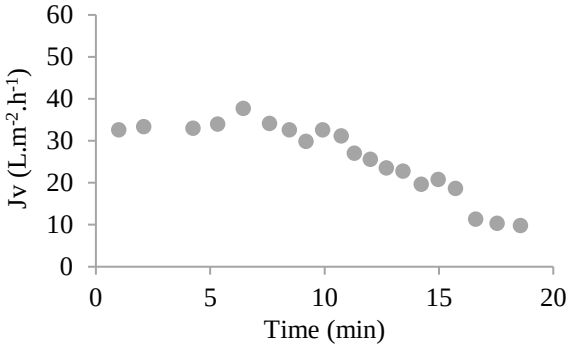

Figure B.2. Volumetric flux plotted against operating time during the concentration mode.

Table B.1. Mass balance of soluble proteins

	Mass $_{\text{soluble protein}}$ (g)	Recover $_{\text{soluble protein}}$ (%)
IN_{Feed}	13.00	-
$OUT_{Retentate}$	11.60	89.20 %
$OUT_{Permeate}$	1.17	9.00 %

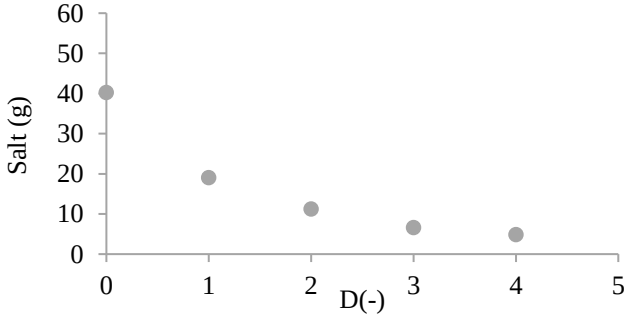

Figure B.3. Salt removal during the diafiltration mode. Salt quantity plotted against the diavolume D(-)

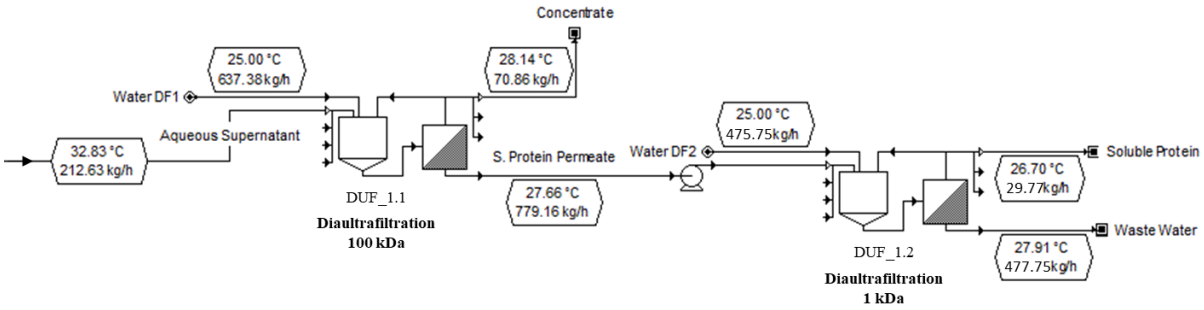

Figure B.4. Ultrafiltration flow chart and streams characterisation using SuperPro Designer®.

B.1.3. Spray Drying

After the ultrafiltration step, the soluble protein concentrate extract is fed to a drying step. On lab-scale freeze drying is often applied. Though, this is an expensive and arduous process at larger scales. On industrial scales, spray drying is the most effective drying technique. The residual water content after drying was fixed at 5%$_{DW}$. The typical electricity consumption was calculated automatically in SuperPro Designer®. An electrical resistance is used to warm the air up to an inlet temperature of 140 °C, while the outgoing temperature of the dry biomass is set to 85 °C.

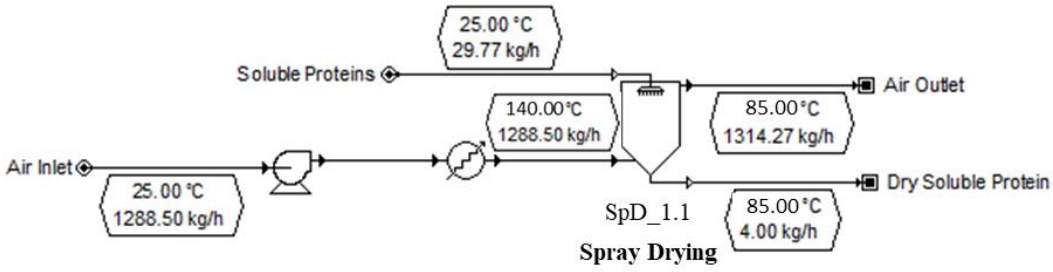

Figure B.5. Spray drying flow chart and streams characterisation in SuperPro Designer®.

B.1.3. Ethanolic phase separation

After the ethanolic extraction, a phase separation is required. A centrifugation step is used to separate the solid phase (defatted pellet) from the ethanolic extract (EPA-rich ethanolic extract). The input stream contains whole cells, defatted cell debris, and the lipids solubilized in ethanol (previously extracted). We assumed that the whole cells and the defatted cell debris (containing insoluble proteins, and other

components) transfer during centrifugation to the solid phase. The critical size and density of cell debris to be separated should be set to 0.5 µm and 1200 $kg.m^{-3}$, respectively. The typical electricity consumption was calculated automatically in SuperPro Designer®.

Tests were performed at an industrial scale using an ATEX centrifuge with automatic discharges every 2.5 minutes. A first centrifugation cycle was performed at a feed flow rate of 350 $L.h^{-1}$ and it was possible to remove 30% (% w/w) of the total solids present in the feed (solubilized + suspended solids). The supernatant obtained in the first cycle was fed to a second centrifugation cycle at a feed flow rate of 150 $L.h^{-1}$ and it was possible to remove 80% (% w/w) of the total solids present in the supernatant of the first cycle (solubilized + suspended solids). However, almost 45% of the solids present in the final ethanolic extract were suspended solids, which represent 1.25% (% w/v) of the ethanolic extract.

Therefore, an automatic pre-filter cartridge should be placed after the ATEX centrifuge. The pore size of the filter should be set to 0.1 µm, and it was assumed that suspended solid particles present in the ethanolic extract are retained by the filter. The typical electricity consumption was calculated automatically in SuperPro Designer®.

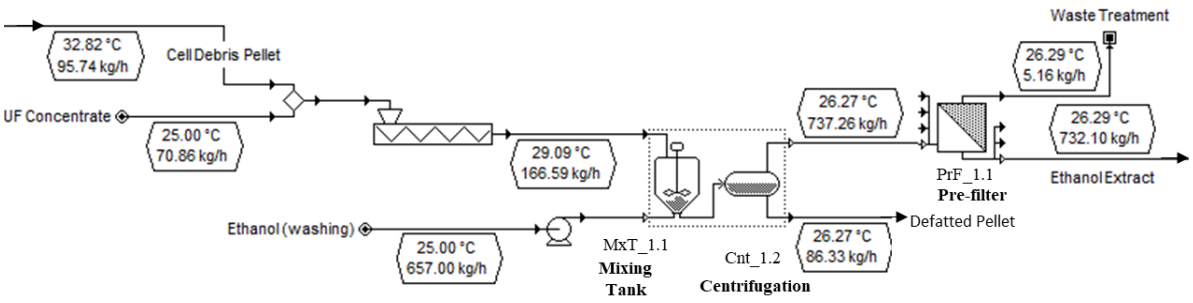

Figure B.6. Ethanolic extraction and phase separation flow chart and streams characterisation SuperPro Designer®.

B.1.4. Tween-80 Emulsification

After the production of an ethanolic EPA-rich extract free from suspended solids, the rheological properties (apparent viscosity) of the product obtained (oleoresin) after the evaporation of ethanol (+ water) under a N_2 stream was performed. Different sample dry weights (DW) were tested at 20 ºC, and the results are shown in **Figure B.**7. For the sample with 50% DW, a concentric cylinder geometry system was used, for the samples with 73% DW and 90% DW a cone-plate geometry system was applied, and for the sample with 100% DW, a parallel-plate geometry system was used.

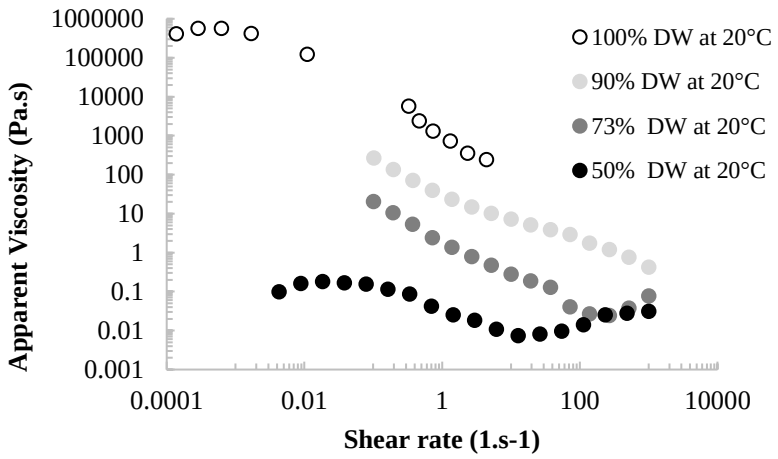

Figure B.7. Apparent viscosity of the product obtained after ethanol evaporation under a N_2 stream.

The results revealed that the apparent viscosity increase rapidly with increases of the sample dry weight. Therefore, tests were performed at a laboratory scale using Polysorbate 80 (Tween-80) as an excipient for the oleoresin formulation. Tween-80 is a non-ionic surfactant and emulsifier often used in foods and cosmetics. The results of this work revealed that it is possible to promote a stable emulsion with the addition of 0.1g $_{\text{tween-80}}$/g $_{\text{lipids present in the ethanol extract}}$. Also, the emulsion remained stable after the evaporation of nearly 90% of the initial ethanolic extract in a rotary evaporator.

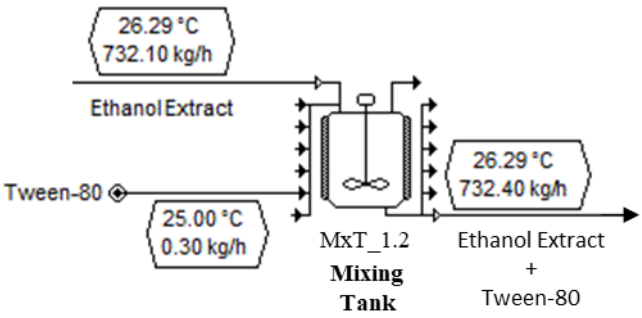

Figure B.8. Tween-80 emulsification flow chart and streams characterisation in SuperPro Designer®.

B.1.5. *Nutsche* Filter

After the ethanolic phase step, the defatted pellet (insoluble protein) is fed to a drying step. On lab-scale the defatted pellet was dried under a N_2 stream. However, this is an expensive process at larger scale. For as industrial scale the *Nutsche* filter was selected, due to its versatility. In the first cycle of the

Nutsche filter, previous to the drying step, it was assumed that the defatted pellet will be washed with ethanol (solvent to biomass ratio of 5 $mL.g^{-1}$) to minimize the EPA losses in this stream. The residual ethanol content after drying was fixed at $5\%_{DW}$. The typical electricity consumption was calculated automatically in SuperPro Designer®.

Tests were performed at a laboratory scale, re-extracting a previously extracted pellet (defatted pellet) with an ethanol to pellet ratio of 5 $mL.g^{-1}$. The initial defatted pellet still had 32% of total lipids present in the initial biomass. The results after the re-extraction revealed that it was possible to extract 62.5% of the lipids present in the initial defatted pellet. Hence, only 12% of the total lipids present in the initial biomass remained in the defatted pellet after the ethanol washing inside the *Nutsche* filter.

The second cycle of the Nutsche filter aims to concentrate the EPA rich extract after creating an emulsion with tween-80. The residual ethanol content after drying was assumed to be at $5\%_{DW}$. The typical electricity consumption was calculated automatically in SuperPro Designer®.

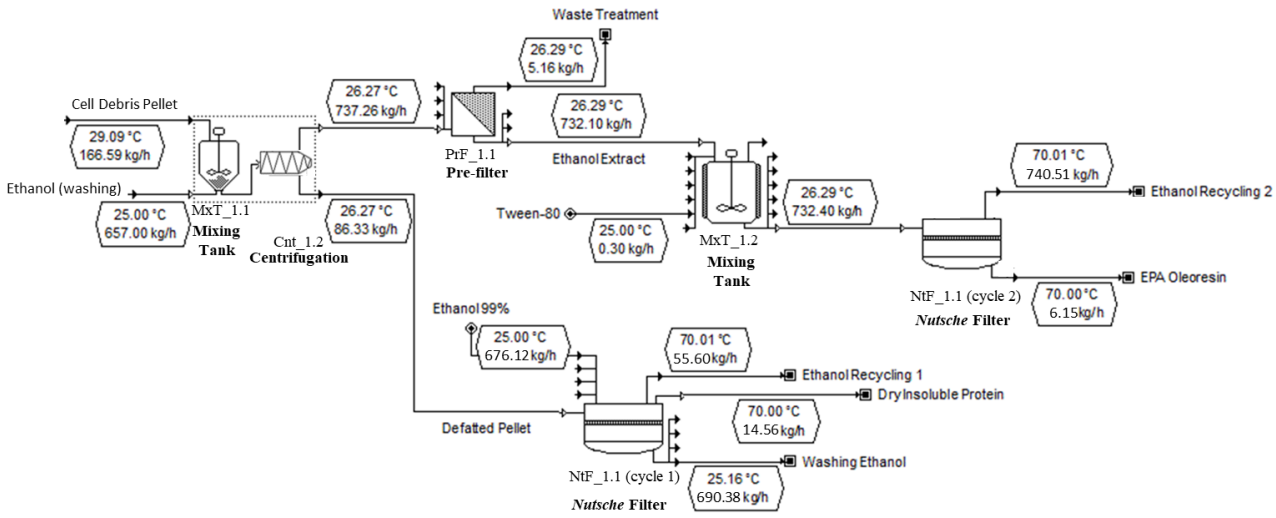

Figure B.9. *Nutsche* filter flow chart and streams characterisation in SuperPro Designer®.

B.2. Techno-Economic Assessment

The raw materials and utilities price information is presented in **Table B.**2.

Table B.2. Price for utilities and raw materials

Item	Price	Source
Electricity	1.130 €.kWh^{-1}	[218]
Steam	20.00 €.ton^{-1}	[187]
Water	0.48 €.m^{-3}	[209]
Nitrogen	1.50 €.L^{-1}	[219]
Ethanol	0.46 €.kg^{-1}	[209,220]
Tween-80	20.00 €.kg^{-1}	[221]

The estimated capital expenditures (CAPEX) and operational cost of a single product *Nannochloropsis* sp. biorefinery are presented in **Table B.**3, and **Table B.**6, respectively.

Table B.3. Capital Expenditures (CAPEX) regarding the main equipment of the single product *Nannochloropsis* sp. biorefinery

	Name	Description	Equipment cost (€)
Main Equipment	**Pat_1B**	Pasteurizer 1	*112,000*
	BdM_1B	Bead Mill 1	*184,500*
	Cnt_1B	Centrifuge 1	*241,000*
	MxT_1B	Mixing Tank 1	*80,000*
	Cnt_2B	Centrifuge 2	*260,000*
	PrF_1B	Pre-filter 1	*10,000*
	MxT_2B	Mixing Tank 2	*40,000*
	NtF_1B	Nutsche Filter 1	*295,200*
	Total Equipment Cost (€)		*1,222,700*
	Capital costs (€.year^{-1}) *depreciation over 10 years		*122,270*

Table B.4. Energy consumption (kWh/year) and steam consumption (ton/year) for a biorefinery with a single product. *The values were estimated in Super Pro Designer®.

	Name	Description	Energy* (kWh/year)	Steam* (ton/year)
Main Equipment	**Pat_1B**	Pasteurizer 1	70 700	1 500
	BdM_1B	Bead Mill 1	268 000	
	Cnt_1B	Centrifuge 1	101 000	
	MxT_1B	Mixing Tank 1	30 000	
	Cnt_2B	Centrifuge 2	120 000	
	PrF_1B	Pre-filter 1	15 000	
	MxT_2B	Mixing Tank 2	28 000	
	NtF_1B	Nutsche Filter 1	867 800	
	Total		1 498 486	1 500

Table B.5. Estimated total operational cost (OPEX) for the two products *Nannochloropsis* sp. biorefinery.

OPEX	
Human Resources (€.year^{-1}) *1	*210,000*
Operational Energy (kWh.year^{-1})	1 176 069
Energy price (€.year^{-1}) (0.129 €.kWh^{-1}) *2	*151,716*
Operational Steam (ton.year^{-1})	1 500
Steam price (€.year^{-1}) (20.0 €.ton^{-1}) [187]	*30 000*
Maintenance (€.year^{-1})	*61,135*
Consumables (€.year^{-1})	*24,454*
Solvents/Reagents (€.year^{-1})	*255,252*
Waste Water Treatment (m^3.year^{-1})	2300
Waste Water Treatment (€.year^{-1}) (0.45 €.m^{-3}) [209]	*1,035*
Biomass Purchase Cost (€.year^{-1}) (5.00 €.kg$_{SFDW}^{-1}$)	*1 090 000*
Total OPEX (€.year^{-1})	*1,823,589*

*1 HR = (number equipment -1) x 2500 €/employee
*2 source: www.pordata.pt

Table B.6. Estimated total operational cost (OPEX) for the single product *Nannochloropsis* sp. biorefinery.

OPEX	
Human Resources (€.year^{-1}) [*1]	*210,000*
Operational Energy (kWh.year^{-1})	1 498 486
Energy price (€.year^{-1}) (0.129 €.kWh^{-1}) [*2]	*193,305*
Operational Steam (ton.year^{-1})	1 500
Steam price (€.year^{-1}) (20.0 €.ton^{-1}) [187]	*30 000*
Maintenance (€.year^{-1})	*61,135*
Consumables (€.year^{-1})	*24,454*
Solvents/Reagents (€.year^{-1})	*335,725*
Waste Water Treatment (m^3.year^{-1})	1548
Waste Water Treatment (€.year^{-1}) (0.45 €.m^{-3}) [209]	*697*
Waste Treatment (ton.year^{-1})	204
Waste Treatment (€.year^{-1}) (200 €.ton^{-1}) [222]	*40,769*
Biomass Purchase Cost (€.year^{-1}) (5.00 €.kg$_{SFDW}^{-1}$)	*1 090 000*
Total OPEX (€.year^{-1})	*1,986,084*

[*1] HR = (number equipment -1) x 2500 €/employee
[*2] source: www.pordata.pt

2022

CLÁUDIA SOFIA MARTINS RIBEIRO

MICROALGAE BIOMASS BIOREFINERY: DEVELOPMENT AND IMPLEMENTATION OF PROCESSING STRATEGIES IN AN INDUSTRIAL UNIT IN PORTUGAL